UNIVERSITÀ
DEGLI STUDI
DI PADOVA

# Università degli Studi di Padova

Dipartimento di Tecnica e Gestione dei Sistemi Industriali

Scuola di Dottorato in Ingegneria Meccatronica e
dell'Innovazione Meccanica del Prodotto

Doctoral School in Mechatronics and
Product Innovation Engineering

XXVIII CYCLE

# *PROCESS PARAMETERS AFFECTING QUALITY OF HIGH-PRESSURE DIE CAST ALUMINIUM ALLOYS*

**School Director:** Prof. Alessandro Persona

**Supervisor:** Prof. Franco Bonollo

**Ph. D. Candidate:** Elena Fiorese

*Troppo spesso la saggezza è solamente la prudenza più stagnante,*

*e quasi sempre dietro la collina è il sole*

*Lucio Battisti*

# *Index*

# *Abstract*

High pressure die casting (HPDC) is a widely used process for manufacturing components with high production rate and complex geometries. However, high pressure die casting is still considered a “defect generating process”, since an amount of 5-10% of scrap is usually detected in castings. For this reason, the availability of new standards and tools for optimizing the process is one of the prominent needs of foundry field.

Both these issues are tackled in this Thesis. First, a new classification of defects and reference dies for estimating the static mechanical properties of aluminium alloys have been developed and then published as CEN Technical Reports, satisfying the need for new standards. Then, a novel and comprehensive methodology has been developed for optimizing HPDC process through the definition of meaningful behavioural models. Some newly defined process parameters have been hence introduced, by representing the most important physical phenomena affecting casting quality and the integral nature of HPDC, and an original approach is outlined. In particular, in order to provide an effective representation of the different process stages, the following parameters have been found to be more influential and effective in representing transmitted forces, mechanical energy exchange and heat removal: the root mean square acceleration in the second stage, the energy associated to the flow forces in the whole cycle, the work of the pressure forces in the third stage and the normalized thermal gradient. The first two parameters embody the plunger motion time-history, the third parameter represents the hydraulic pressure time-history, while the last one concentrates on some thermal aspects. These parameters take advantage from signal processing techniques of the measured position and pressure profiles. Four experimental campaigns (in the whole 210 castings) using different injection machines, different alloys and different geometries of the die have been carried out to validate the novel process parameters and to prove the general validity of the approach.

The statistical correlation with the measured static mechanical properties, density and percentage of porosity, as well as the metallographic analysis (percentage of oxides

on fracture surfaces, analysis of different kinds of internal defect) prove the soundness of the developed method.

Given the significance of the plunger motion profile in explaining the casting quality, analytical models for computing the root mean square acceleration and the energy associated to the flow forces have been developed. These analytical models permit selecting in advance the best plunger motion profile, which guarantees reliability and soundness of castings, thus satisfying the need expressed by foundries for effective optimization tools.

# *Sommario*

La pressocolata è un processo ampiamente utilizzato per produrre componenti con elevata produttività e geometria complessa. Comunque, la pressocolata è ancora considerata un "processo generatore di difetti", dal momento che una percentuale del 5-10% di scarto è rilevata di solito nei getti. Per questa ragione, la disponibilità di nuovi standard e strumenti per l'ottimizzazione di processo è uno dei bisogni più importanti del settore della fonderia.

Entrambe queste criticità sono affrontate in questa Tesi. Per prima cosa, è stata sviluppata e successivamente pubblicata come Report Tecnici riconosciuti dal CEN una nuova classificazione dei difetti e degli stampi di riferimento per stimare le proprietà meccaniche statiche delle leghe di alluminio, rispondendo al bisogno di nuovi standard. Poi, è stata sviluppata una metodologia nuova e completa per ottimizzare il processo di pressocolata attraverso la definizione di metamodelli significativi. Quindi, sono stati introdotti dei nuovi parametri di processo, che rappresentano i più importanti fenomeni fisici che influenzano la qualità dei getti e la natura integrale del processo di pressocolata, ed è stato delineato un approccio originale. In particolare, allo scopo di fornire una rappresentazione efficace delle diverse fasi del processo, si è dimostrato che i seguenti parametri sono i più influenti ed efficaci nel rappresentare le forze trasmesse, il flusso di energia meccanica e l'asportazione del calore: il valore quadratico medio dell'accelerazione in seconda fase, l'energia associata alle forze di flusso nell'intero ciclo, il lavoro delle forze di pressione nella terza fase e il gradiente termico normalizzato. I primi due parametri descrivono l'effetto del profilo di moto del pistone; il secondo è invece legato anche alla pressione esercitata dal pistone stesso, mentre l'ultimo rappresenta esclusivamente fenomeni di natura termica. Lo sviluppo ed il calcolo di questi parametri sfrutta le tecniche di elaborazione numerica dei segnali, al fine di estrarre le informazioni dai profili misurati di posizione e di pressione del pistone.

La validazione del metodo proposto è stata condotta attraverso quattro diverse campagne sperimentali, con un totale di 210 getti analizzati, nelle quali sono state

utilizzate diverse macchine di iniezione, diversi stampi e diverse leghe, al fine di ottenere risultati generali ed estendibili.

La correttezza del metodo proposto è confermata dalla correlazione statistica dei parametri proposti con la resistenza meccanica statica, con la densità, la porosità, e da alcune significative analisi metallografiche (percentuale di ossidi sulle superfici di frattura, analisi dei difetti interni).

Data l'efficacia dimostrata dei parametri proposti, ed in particolare di quelli legati al profilo di moto del pistone, l'approccio è stato esteso tramite lo sviluppo di alcune relazioni analitiche per calcolare i due parametri cinematici. Ciò rappresenta uno strumento efficace per sintetizzare a priori il profilo di moto ottimale del pistone che, nel rispetto dei vincoli di macchina, consenta di ottimizzare la qualità dei getti.

# *Chapter 1*

## *Introduction*

### *1.1. High Pressure Die Casting process*

High pressure die casting (HPDC) is a cost-effective process widely used to manufacture components with high productivity and dimensional accuracy for automotive and other industries.

HPDC can be basically described through the sequence of four stages, that can be easily recognized by analysing the plunger motion profile and the pressure exerted by the hydraulic actuator (see Figure 1.1).

- Stage 0, called initial speed blend. The stage 0 consists in a transient speed blend just before the stage 1.
- Stage 1, called slow shot stage. The stage 1 of the process requires usually constant and low speed for filling the shot sleeve and for avoiding turbulence and consequent generation of defects.
- Stage 2, called fast shot stage. The stage 2 of the process is the filling of the die cavity, which should be performed at higher speed in order to avoid premature solidification at the gate and incomplete castings.
- Stage 3, called upset pressure stage. The stage 3 consists in applying an upset pressure on the solidifying melt in order to prevent the formation of shrinkage defects and the expansion of previously entrapped air.

It is well-known that the main troubles of this process are air entrapment and oxide formation due to the highly turbulent flow of the molten metal. The entrapped air could remain in the casting in the form of gas porosity which hinders the casting suitability for conventional heat treatment and deteriorates the casting quality sometimes to such a degree that it must be rejected [1]. Meanwhile, oxides worsen the mechanical properties of the casting, causing its premature failure [2].

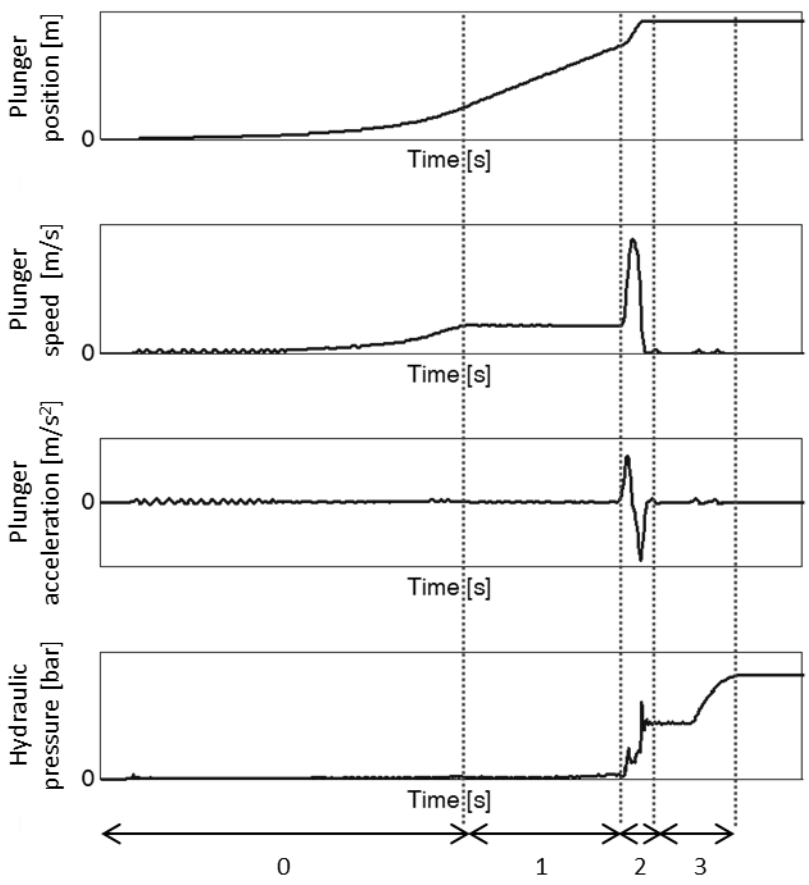


**Figure 1.1.** HPDC process: initial speed blend (0), slow shot stage (1), fast shot stage (2) and upset pressure stage (3).

## *1.2. Survey on needs of the European foundry*

With the aim of understanding the real needs of the foundry industry and thus focus the research activity of this Thesis, a survey based on an online questionnaire has been carried out in 2013 [3],[4]. More details on the structure of the questionnaire are reported in the Appendix A.

An overall number of 82 answers to the questionnaire were received from the whole supply chain, including foundries, material and service providers, die makers, end-users, universities and research centres. Several European countries contributed with their answers to the success of this survey, particularly Italy, Germany and Norway. The most interesting and significant results from this survey are here synthetized.

The annual production and the main categories of casting manufactured by the foundries, which were for the 70% HPDC foundries, are represented in Figure 1.2. Given the importance of housings and of thin wall components, which cover the 29% and the 21%, respectively, of the overall categories, the research activity of this

Thesis will be focused on this kind of castings, as it will be possible to see in the following Chapters.

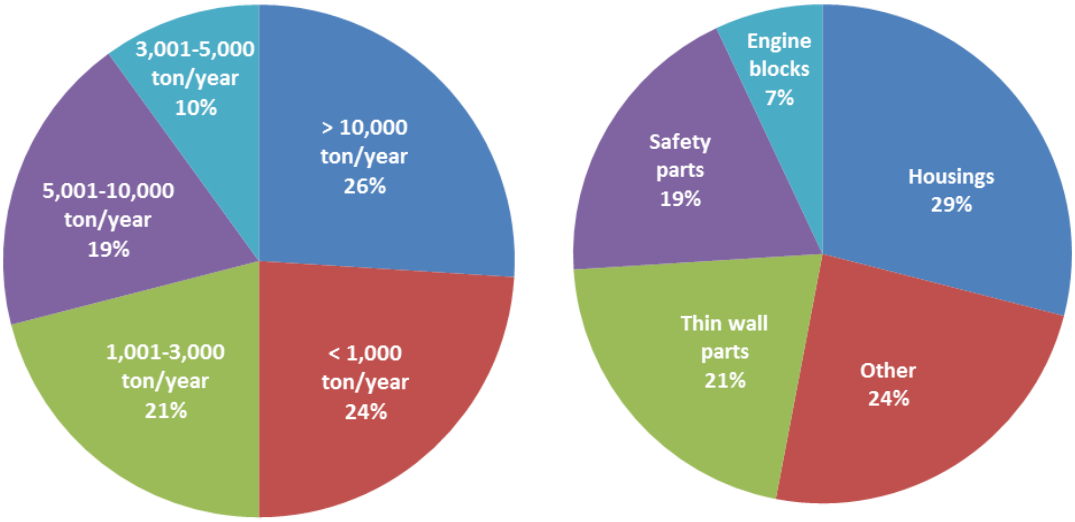


**Figure 1.2.** (a) Annual production and (b) main categories of casting manufactured by the foundries which answered to the questionnaire.

Some useful information about the most used alloys and the extent of defect quantification carried out by the foundries which answered to the questionnaire are reported in Figure 1.3. Starting from the results of the questionnaire, the research activity of this Thesis has been focused on some of the most used alloys, such as AlSi9Cu3(Fe), AlSi11Cu2(Fe) and AlSi12(Fe). Moreover, being the gas-related, shrinkage, filling-related defects and undesired phases the most measured kinds of defect, because of their persistent presence inside castings, the experimental campaigns of the following Chapters have been mainly oriented towards the deep investigation of this categories of defect.

Since in their answers to the questionnaire, the foundries expressed also the need for new standards about defects and static mechanical properties of aluminium alloys, two Technical Reports have been written in the frame of the doctoral programme and have been recently approved by the European Committee for Standardization (CEN):

- the CEN/TR 16749:2014 [5] about defects in aluminium alloys,
- the CEN/TR 16748:2014 [6] about reference dies and static mechanical properties of aluminium alloys.

A very concise synthesis of these Technical Reports is proposed in the following Sections 1.3 and 1.4, by highlighting just the topics which could be useful for the understanding of the core of this Thesis.

Finally, the questionnaire has also highlighted the necessity to develop some guidelines for optimizing the HPDC process, by correlating the main process variables to the final outcome leading to the desired "zero defect" condition. This one is the most important and challenging issue, which will be solved in this Thesis.

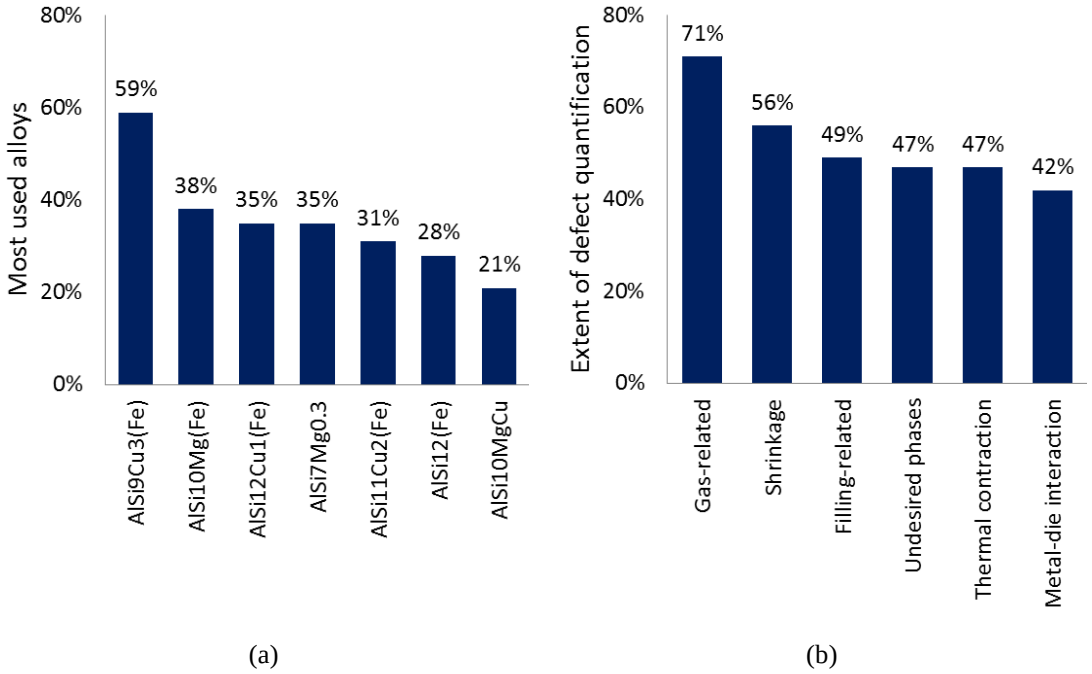


**Figure 1.3.** (a) Most used alloys and (b) extent of defect quantification for the foundries which answered to the questionnaire.

## *1.3. Classification of defects*

Defect is defined in the standard EN 12258-1:2012 [7] as a quality characteristic worse than the level or state foreseen, which does not allow the product to carry out the requested function when it is present in a certain amount depending on the final application of the casting.

In the frame of the doctoral programme, the CEN/TR 16749:2014 [5] on defects in die cast aluminium alloys has been written starting from the new classification previously introduced by Gariboldi et al. [8].

The classification of defects is based on a three-level approach [9]:

1. the first level refers to the position of defect in the casting, i.e. internal, external/surface or geometrical;
2. the second level refers to the metallurgical origin of defect, such as gas porosity, solidification shrinkage, etc.;
3. the third level refers to the specific type of defect, since the same metallurgical origin may generate different kinds of defect.

Some details on the three levels are provided below.

1. The first level distinguishes defects on the basis of their position in the casting and investigation techniques suitable for their detection, i.e. visual inspection and/or controls regarding the bulk material. In this level, internal and external/surface defects are contemplated and subsurface defects are accounted for as surface defects, since they usually affect the aesthetic quality of castings. In the first level, also geometrical defects are included, which imply non-compliance of a casting to its designed shape in terms of dimension and tolerances.
2. The second level is focused on the defect metallurgical origin. Defects are grouped into several categories, such as shrinkage defects, gas-related defects, filling-related defects, undesired phases, thermal contraction defects and metal-die interaction defects. The knowledge of the defect metallurgical origin is very important, because it could provide hints for developing and introducing some corrective actions to the process.
3. The third level contemplates the specific type of defect. Usually, the term adopted to identify a particular type of defect allows better understanding the metallurgical origin of it.

The overall classification of defects is schematically shown in Tables from 1.1 to 1.3.

In Sections from 1.3.1 to 1.3.4, just the most relevant kinds of defect (in accordance with the findings of the questionnaire) are described and shown. These defects will be those measured and investigated in Chapters 3 and 4. In contrast, all the other defects are not discussed here (the interested reader could refer to [9]). All the micrographs shown in the following Sections have been collected from the castings belonging to the experimental campaigns developed in this Thesis.

| 1st level | 2nd level | 3rd level |
|---|---|---|
| **Internal defects** | Shrinkage defects | Macro-shrinkage |
| | | Interdendritic shrinkage |
| | | Layer porosity |
| | Gas-related defects | Air entrapment porosity |
| | | Hydrogen porosity |
| | | Vapour entrapment porosity |
| | | Lubricant and/or die release agent entrapment porosity |
| | Filling-related defects | Cold joint |
| | | Lamination |
| | | Cold shot |
| | Undesired phases | Inclusion |
| | | Undesired structure |
| | Thermal contraction defects | Cold crack |
| | | Hot tear, hot crack |

| 1st level | 2nd level | 3rd level |
|---|---|---|
| **Surface defects** | Shrinkage defects | Sink |
| | Gas-related defects | Blister |
| | | Pinhole |
| | Filling-related defects | Cold joint, vortex |
| | | Lamination |
| | | Cold shot |
| | Undesired phases | Surface deposit |
| | | Contamination, inclusion |
| | Thermal contraction defects | Cold crack |
| | | Hot tear, hot crack |
| | Metal-die interaction defects | Erosion |
| | | Soldering |
| | | Thermal fatigue mark |
| | | Ejection mark |
| | | Corrosion of the die |

| 1st level | 2nd level | 3rd level |
|---|---|---|
| **Geometrical defects** | Lack of material | Incompleteness |
| | Excess material | Flash |
| | Out of tolerance | Deformation |

**Table 1.1.** Overall classification of defects, published as CEN/TR 16749:2014 [5].

### *1.3.1. Gas-related defects*

Gas-related defects are spherical or elongated cavities with smooth surface and are caused by entrapment of air, hydrogen, vapour or lubricant.

In HPDC, the most frequent kind of gas-related defects is the air entrapment porosity. This kind of defect appears as spherical or ellipsoidal cavities with smooth surface covered by a thin oxide layer (due to the interaction between the molten metal and the entrapped air). Air entrapment porosity is a consequence of the turbulent melt flow either in the shot sleeve or inside the cavity of the die, and its final distribution inside the casting usually reproduces the path of the molten metal. The size of an air entrapment porosity varies from 10 to 2000 μm. When air entrapment porosity is located just below the surface, a protrusion (called blister) occurs due to deformation of the skin of the casting as an effect of gas pressure.

Internal air entrapment porosity can be easily detected by means of X-rays or metallographic test, while blister could be also seen by visual inspection. Another investigation technique is for instance the measurement of density.

In Figure 1.4, examples of air entrapment porosity located in internal (Figure 1.4 (a)) and subsurface regions (Figure 1.4 (b)) of the casting are shown.

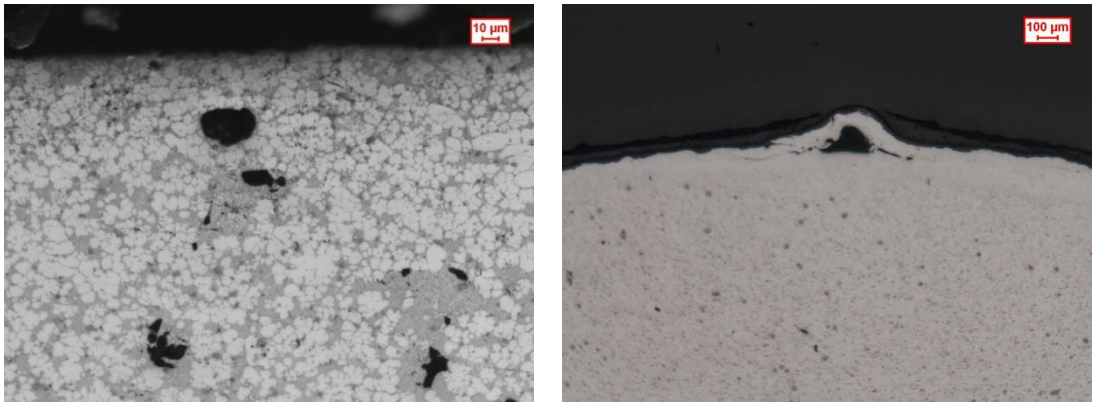


(a) (b)

**Figure 1.4.** Optical micrographs: (a) 200x magnification of internal porosity and (b) 25x magnification of a blister [10].

### *1.3.2. Filling-related defects*

The filling-related defects are caused by the interaction between different melt flows at different temperature. The most frequent kind of defect of this category is the cold joint. During the filling of the die cavity, a liquid and a partially solidified metal

veins (usually covered by an oxide film), can accidentally meet causing a metallurgical inhomogeneity, called cold joint. This defect is very detrimental, since the sample usually brakes along the oxide layer when relatively low tension stresses are applied.

Another kind of filling-related defects is the lamination, which is usually located in surface regions of the casting. Lamination originates when the molten metal comes into contact with the surface of the die and solidifies with higher cooling rate than the surrounding material. The filling-related defects can be detected by means of metallographic tests or by visual inspection when located on the surface of the casting. Another investigation technique is the ultrasonic testing.

In Figure 1.5, examples of a cold joint with related oxide film (Figure 1.5 (a)) and of a surface lamination (Figure 1.5 (b)) are shown.

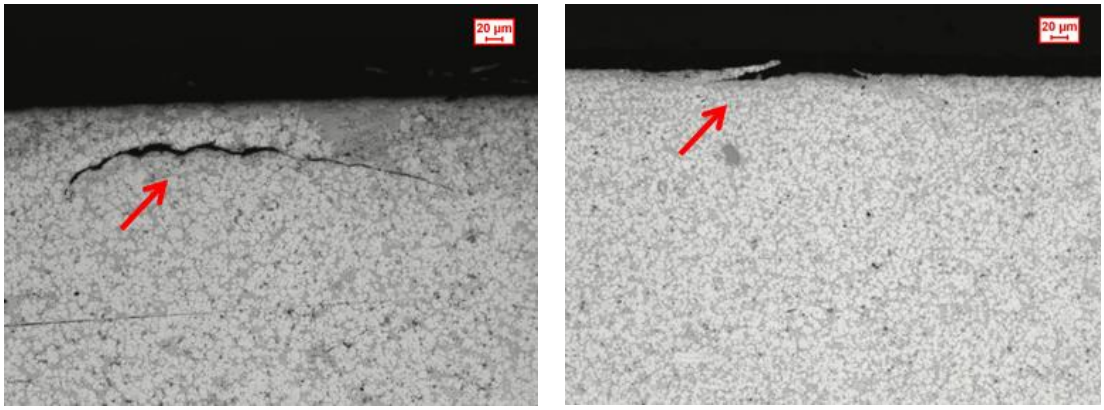


(a) (b)

**Figure 1.5.** Optical micrographs at 100x magnification of: (a) a cold joint with related oxide film and (b) a surface lamination.

### *1.3.3. Shrinkage defects*

Shrinkage defects are macroscopic or interdendritic cavities due to the volume contraction during solidification and occur in regions with insufficient or even absent feeding of molten metal. Such regions, called hot spots, are usually well inside the casting and solidify in the last stage of the process.

Shrinkage defect is characterized by rough and spongy surfaces for the presence of emerging dendrites as a consequence of their interrupted growth and can reach several millimetres in diameter. The generation of a shrinkage defect depends on

different factors, such as filling conditions and geometry of the die, solidification range of the alloy and process parameters adopted.

Shrinkage defects can be detected by means of radiographic and metallographic tests, or by density measurements.

In Figure 1.6, examples of a shrinkage defect (Figure 1.6 (a)) and of emerging dendrites from a shrinkage cavity (Figure 1.6 (b)) are shown.

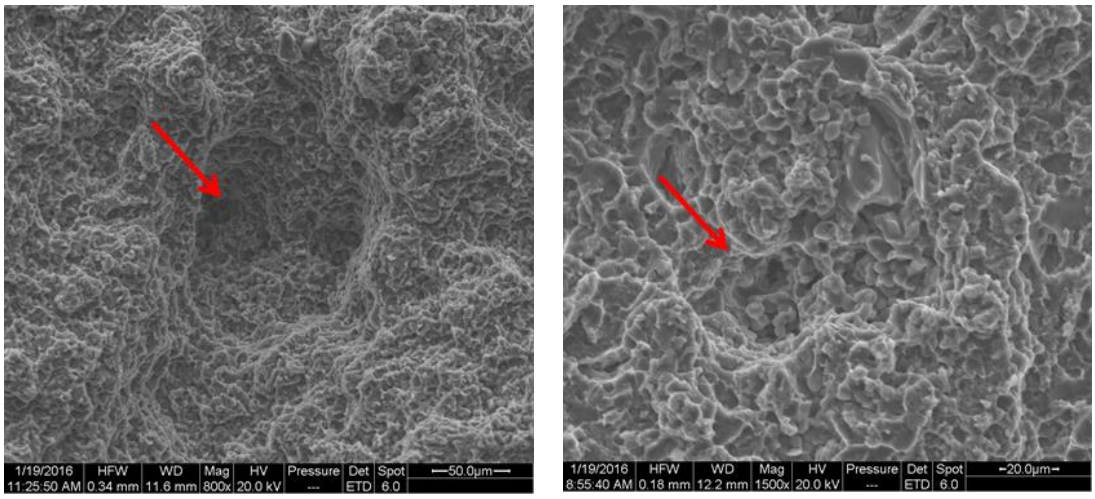


(a) (b)

**Figure 1.6.** SEM micrographs: (a) 800x magnification of a shrinkage defect and (b) 1500x magnification of emerging dendrites.

### *1.3.4. Undesired phases*

An undesired structure is an area of the casting with different microstructure with respect to the surrounding regions, which is undesired mainly for its high brittleness and for being the cause of a microstructural discontinuity. An undesired structure is detrimental because it could act as crack nucleation and propagation sites during cooling, finishing operations or in-service behaviour. However, the precise characteristics of an undesired structure cannot be uniquely described and its size is variable. For instance, segregation of eutectic phase can be considered as an undesired structure, because it hinders the molten metal feeding by frequently leading to porosity formation (see Figure 1.7).

Undesired phases can be easily detected by means of metallographic tests.

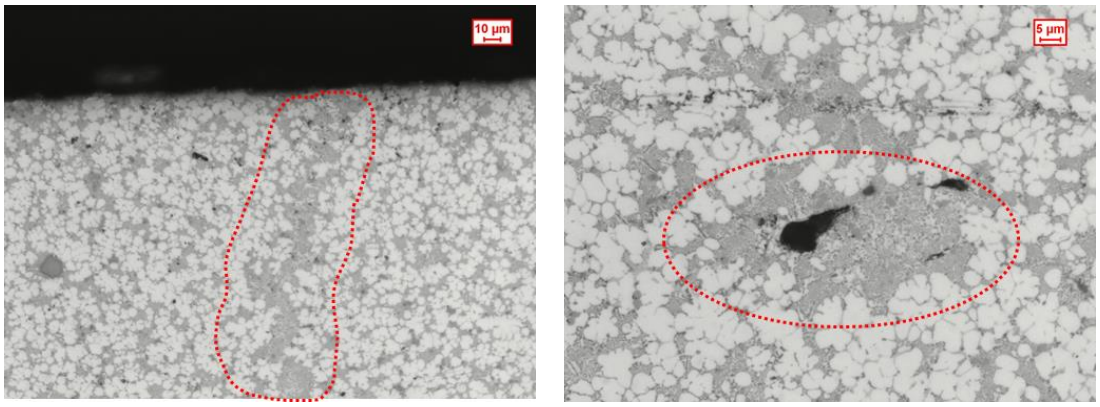


(a) (b)

**Figure 1.7.** Optical micrographs: (a) 200x magnification of an eutectic segregation and (b) 500x magnification of porosity associated to eutectic segregation.

## *1.4. Reference castings*

As already mentioned in Section 1.2, another CEN Technical Report (CEN/TR 16748:2014 [6]) has been written in the frame of the doctoral programme. This Technical Report describes the characteristics of reference dies and castings, which can be employed for estimating the static strength of aluminium alloys.

From this Technical Report, a reference casting has been properly chosen to execute the third experimental test of this Thesis (see Chapter 5). The die is the one designed, build and tested within the frame of NADIA project (New Automotive components Designed for and manufactured by Intelligent processing of light Alloys, EU IPs-SMEs, Contract n. 026563-2, 2006-2010). This casting, shown in Figure 1.8 (a), was carefully designed and optimized to maximize the process quality, by reducing the scrap percentage. Hence, this die leads to a reduced variance of the casting quality over a wide range of process parameters. In other terms, this die allows estimating the tensile strength of an alloy in the optimal case of minimized defects. More details about the casting are described in [6].

Another reference casting, which is subsequent to the Technical Report and therefore has not been included therein, is the horseshoe-shaped casting (Figure 1.8 (b)). This casting has been designed and developed at the foundry laboratory of Aalen University of Applied Sciences [11] in the frame of European Music project (MUlti-layers control & cognitive System to drive metal and plastic production line for Injected Components, N. 314145). The geometry of this casting has been designed in order to exacerbate the generation of defects and therefore to study the effect of the

process parameters on defects and on the overall casting quality. In other terms, this die allows evaluating the genesis of defects and estimating the static mechanical properties of an alloy as a function of the process parameters. This reference casting has been used in the first and second experimental campaigns of this Thesis (see Chapters 3 and 4).

Both these reference castings (except for some specific zones of the horseshoe-shaped casting) are representative of the category of thin wall components, since their thicknesses are very low in average.

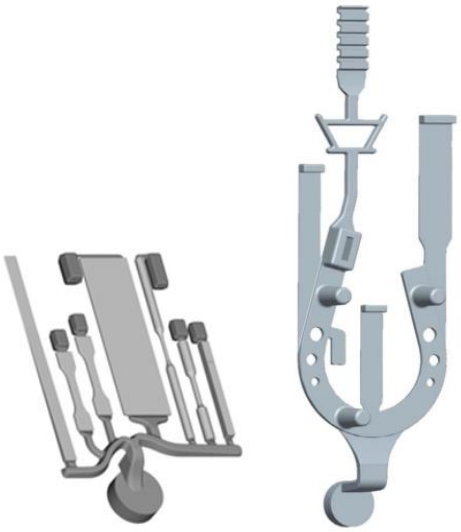

(a) (b)

**Figure 1.8.** Reference castings designed to: (a) minimize and (b) exacerbate the generation of defects as a function of the process parameters.

## *1.5. Literature review and motivations of the work*

### *1.5.1. Literature review*

The recent survey questionnaire addressed to the European foundries and the extensive literature review carried out in this dissertation have highlighted some critical issues that are yet unsolved.

On the one hand, there is the actual need to improve the HPDC technology, since an average of 5-10% scrap is typically manufactured by this process due to the presence of porosity and oxides, which deteriorate the quality of castings [3]. On the other hand, there are no reliable methods in the existing literature to overcome this trouble and the available results are sometimes fragmented and conflicting [12]. Several

works in the literature attempt to investigate these relevant issues, by examining the effect on the final outcome of different types of process characteristics.

Syrcos [13] conducted a study in which the die casting characteristics were divided into four categories:

- the alloy chemical composition, its delivery condition and temperature;
- the characteristics of the shot chamber, including its size, geometry, filling fraction and lubrication;
- the characteristics of the die, in terms of geometry, overflows, cooling and lubrication systems;
- the motion and pressure profiles of the plunger.

The optimization of the overall process would require tackling all these issues. Given the complexity of the HPDC process, the studies in the literature usually focus on just one or two of the abovementioned issues. Indeed, several physical phenomena related to different disciplines should be involved in the study such as physics, thermodynamics, fluid dynamic, chemistry, mechanics. Additionally, the ever increasing use of closed-loop control systems, for example to ensure correct execution of the plunger motion, to guarantee the desired temperature stability or to make the piston exert the correct pressure at the correct time instant, are requiring also to link the research with the mechatronic field.

Among the different critical process characteristics, several papers focus on the study of the so called "process parameters", that are the modifiable settings of the injection machines. This approach aims at optimizing the quality of the castings through the optimal selection of the machine settings, within those feasible, to ensure the best achievable performances given the melt chemical composition and the die geometry. This is the approach followed in this Thesis, which is specifically focused on this strategy. In practice, the selection of the optimal process parameters is an almost costless approach, that should boost the achievement of the theoretical expected properties of a casting.

Process parameters can be categorized on the basis of the type of the physical phenomena, by grouping them into:

- kinematic parameters of the plunger (position or speed) [14],[15],[16];
- pressure parameters (e.g. upset pressure) [14];

- thermal parameters related to the metal and die cavity (e.g. pouring temperature of the molten metal and thermoregulation system of the die) [17],[18].

This is the categorization followed in this Thesis, where Chapters 3 and 4 will be dedicated respectively to the kinematic parameters of the plunger and to pressure and thermal aspects. Detailed discussion on the literature of each class of parameter will be provided in the specific chapter. Here, only a brief overview is provided, to highlight the presence of some lacks in the literature, as well as to compare the traditional approach with the novel one proposed and validated in this Thesis.

Although the literature provides interesting results, there are still some limitations and many papers often supply partial information for achieving actual process optimization. In the following, it is provided a short description on these open issues.

- The focus on instantaneous values of the process parameters:
  many works in literature usually focus on studying the influence of the first stage constant speed, second stage maximum speed and third stage maximum upset pressure. They usually consider just set or measured values of these parameters which are sometimes not exhaustive in representing the process [14],[15],[16]. Indeed, by assuming instantaneous values it is neglected the integral nature of HPDC and the time-variability of speed and pressure during the process.
- The use of non-physical or high-order interpolation schemes:
  among the modelling approaches, attention has been often paid to non-physical schemes, such as neural networks, or to high order response-surfaces (see Chapter 2) to interpolate different combinations of some process parameters: e.g. constant or maximum injection speeds, maximum upset pressure, pouring temperature and die temperature [19],[20]. Nevertheless, these approaches are effective in the interpolation and useful for a specific case-study, but could not provide hints to understand the parameters affecting quality in HPDC and to optimize them.
- The focus on just some stages of the process:
  some papers focus on the first stage, by investigating the dynamic of the liquid metal flow as a function of the plunger speed and the possibility of air entrapment in the injection chamber of die casting machine [21],[22],[23]. Indeed,

the amount of air entrapped during the first stage is a considerable contribution on the overall trapped air that causes porosity in the casting. Nevertheless, the sole investigation of the first stage neglects the positive effects due to the forces exerted by the plunger to the melt in the second and third stages which may produce air bubble collapsing and oxide fragmentation, with a consequent improvement of the static properties.

- The use of simulation based studies:
  a different approach often adopted is the use of simulation models, formulated through complicate differential equations in numerical software, which provide accurate description of the phenomenon but could not explain the factors affecting quality of castings in a concise and effective way [24],[25].

All the cited works from the existing literature give interesting contributions to solve the issue. Nevertheless, the definition of reliable criteria for tuning the HPDC parameters, in order to obtain sound and reliable castings, is still an open and challenging issue, and should be solved with a more comprehensive approach.

### *1.5.2. Motivations of the work*

In this context, it is very promising the use of simplified behavioural models, which are abstract algebraic descriptions of HPDC representing the relation between some influential process parameters and quality of castings. To be effective, these simplified model should be, at the same time, capable of accounting for the physics and of integral nature of the process, and of its different stages.

The research proposed in this Thesis will introduce, therefore, a novel and comprehensive approach towards the optimization of HPDC through optimal selection of the process parameters. Some peculiar ideas and tools, that are new in the metallurgy field, will be exploited:

- the need of representing the integral nature of HPDC process (the time-history of the process), by means of parameters having a mathematical integral formulation;
- the need of representing the physical phenomena affecting the filling of the die cavity and the solidification of the casting, and dynamic behaviours that are responsible for quality;

- the possibility to employ physical quantities, such as forces, energy, work and heat, that are not just set or measured quantities;
- the possibility to employ numerical signal processing techniques (such as numerical derivation, integration, filtering, decimation) to enlarge the set of physical quantities obtained by a reduced set of measurements (e.g. just the position);
- the possibility to use the results obtained for an effective process planning, by selecting in advance the best parameter setting.

More details about the approach developed, and then validated, are described along the Thesis, which is structured as follows.

- Chapter 2 discusses the issue of model-based optimization of HPDC process, by outlining the steps, the methodologies, the tools and the goals that will be adopted in the subsequent chapters. The new approach is therefore set in this chapter. The following ones will implement it.
- Chapter 3 introduces the first set of the novel parameters adopted to describe, and hence optimize, HPDC. These parameters are denoted "kinematic", since they are just related to the plunger motion time-history. Experimental validation on a first experimental test will be done.
- Chapter 4 introduces other parameters accounting for pressure and temperature, by also studying the simultaneous effect of the plunger motion profile, pressure and temperature on quality of castings. Experimental validation will be done through a different test case.
- Chapters 5 and 6 focus on the analytical models for computing the most influential kinematic process parameters with the aim of optimizing a-priori the HPDC process. This chapters will involve the use of some concepts usually adopted in motion planning of mechatronic system, in the light of the ever growing integration of metallurgical processes. Both the chapters will present theoretical developments, as well as experimental application with two different test cases. An industrial test case is also adopted, in the light of the need of general and reliable methods suitable for both academic research and practitioners in foundries.
- Chapter 7 draws conclusion from this research activity, by summarizing the main results.

- Appendix A reports the questionnaire used for exploring the foundry needs, as discussed in this Chapter.
- Appendix B describes the main signal processing techniques adopted in the numerical elaboration of the data measured in the experimental activity. Attention and focus will be paid to some critical issues to be tackled in the metallurgy field.

# *Chapter 2*

## *Model-based optimization of HPDC*

### *2.1. Introduction to model-based design and optimization*

The increasing need of improving quality in HPDC, to overcome its defect-generating nature, has been boosting the use of model-based approaches to predict the final outcome and hence to optimize the process. Indeed, models provide a deeper insight into the main phenomena and allow investigating the relations with the process set-up parameters. This strategy is consistent with a general idea that is even more widespread in engineering, that is the model-based design and optimization, that is applied in a wide set of systems and processes [26] to overcome the limitations of traditional trial-and-error approaches.

### *2.2. The simulation approach*

Much of today's optimization of HPDC usually consists of performing extensive numerical simulations, by running complex computer codes through commercial software (such as MAGMASOFT®). The designer usually supplies a vector of independent input variables (here denoted $\boldsymbol{x}$), that are the modifiable process parameters, and computes a vector of responses (the simulation outputs, here denoted $\boldsymbol{y}$), that represent the casting properties of interest. Typical examples of input variables, as discussed later, are the plunger motion profile, the die and melting temperature, or the upset pressure. As for the output, attention should be usually paid to the mechanical strength (usually static) or to the so-called "internal properties", such as porosity or density.

Simulation through commercial software usually relies on the solution of high-order differential equations, that are often non-linear and implicit, to be solved through complicate numerical methods that simultaneously account for fluid flow, thermal

and chemical phenomena. Indeed, a foundry process is the resultant of several phenomena involving different disciplines, that should be accounted for in a coupled way. Hence, simulation of metallurgical processes requires modelling complicate fluid-dynamics equations (such as Navier-Stokes equations), the Fourier equation that governs the heat transfer, the solid state transformations related with thermodynamics and kinetics [27].

Numerical simulation can therefore provide detailed insights in microscopic or local phenomena as long as the model is correct and reliable, and accurate tuning of the model parameters is performed (i.e. correct boundary conditions, initial conditions, thermo-physical characteristics of the alloy, of the die and of their interaction should be adopted in the simulation). This is a first limitation in the use of numerical simulations for process optimization: the number of simulations that should be done to reach the correct model tuning may be very high, from several tens to several hundred [27].

## *2.3. The metamodeling approach in HPDC*

Despite advances in modelling accuracy and computational power, that allow reliable and fast simulations, this mode of "query-and-response" often leads to a trial and error approach to design [28], where the process designer may never discover the functional relationship between $\boldsymbol{x}$ and $\boldsymbol{y}$, and hence will hardly identify the best tuning for the process parameters values.

To address this issue, while ensuring a better understanding of the input-output relationship, statistical methods are widely used in engineering design [29]. The basic approach is to build simpler approximations of the actual process that yield insight into the functional relationship between $\boldsymbol{x}$ and $\boldsymbol{y}$. This type of model is often denoted metamodel [30], and consists in algebraic and explicit relations relating $\boldsymbol{x}$ and $\boldsymbol{y}$. This name is aimed at denoting a "model of the model" to stress the fact that it is a simplified representation of a more precise, but complicate, physical model.

This kind of models are, in practice, simplified behavioural models, that provide abstract descriptions of HPDC by representing the relation between some influential process parameters and quality. The insight is hence in macroscopic behaviour, that can be seen as the simultaneous effect of all the microscopic and local phenomena, and as the "cumulative" result of the whole process time-history. Metamodels drive

easily the process designer towards the suitable set of process parameters. Then, fine adjustment of these parameters can be done, in case, through numerical simulations just ranging in a narrow interval. The development of simplified and useful behavioural models is the essential first-step towards the set-up of a knowledge-based improvement of foundry efficiency and quality.

The idea of using simplified models is hence fully consistent with the recent paradigms of model-based design and optimization, as previously discussed, which suggest the use of simplified and reduced-order models aimed at describing the most relevant physical effects [26].

Since several disciplines and competencies are needed to understand the HPDC, another basic concept of model-based design is of interest for the optimization of HPDC, and will be therefore accounted for in this work. It is the need to integrate the model representing the metallurgical phenomena within other domains (disciplines) that are involved in the attainment of the final result. In particular, given the prominent role of the plunger motion in the casting final quality, the synthesized models relating quality of castings to process parameters should be extended towards the issues of planning and control of the injection machine.

## *2.4. The metamodeling technique*

### *2.4.1. Main phases*

The synthesis of effective metamodels involves usually three phases:

1. planning a proper experimental campaign, by choosing a design of experiments (DOE) for generating data;
2. choosing an algebraic mathematical model to represent the relation between input (also denoted as the design factors, the control factors, the process control parameters) and output variables (also denoted as the response variables, the casting quality), $\boldsymbol{y} = g(\boldsymbol{x})$;
3. fitting the model to the measured data.

In the case of HPDC, all the three phases have some specific critical issues. In particular, the second one imposes some theoretical and mathematical efforts, and an original solution is proposed in this work. Compared with traditional approaches, a slightly different strategy will be instead adopted, to overcome the difficulties of the abovementioned second phase, and the approach can be formalized as follows:

1. planning a proper experimental campaign, by choosing a design of experiments (DOE) through the definition of the independent variables $\boldsymbol{x}$, the process parameters, also in accordance with the common practice adopted in foundries;
2. transform the independent variables into a set of other independent variables, that are some novel process parameters, $\boldsymbol{z} = f(\boldsymbol{x})$, where the transformation may involve differentiation or integration. This stage is the crux in the development of the metamodels, since identifying the correct control factors $\boldsymbol{z}$ is not easy and requires effort in order to understand the parameters that actually affect the casting properties. This issue will be object of a thorough investigation in this Thesis in the Chapters 3 and 4;
3. choosing an algebraic mathematical model to represent the relation between input and output variables, $\boldsymbol{y} = h(\boldsymbol{z})$;
4. fitting the model to the measured data.

Figure 2.1 summarizes the metamodeling approach here proposed, by representing the main phases, their sequence, and the main factors and tools to be accounted for in each phase and the related issues to be carefully handled and solved to grant effective results.

There are several options for each of these steps (see [28] for an exhaustive categorization of all the metamodeling methods). In the following, a general discussion is provided, with regards to the possibility in the field of HPDC, by stressing the specific issues for this process. More detailed investigation on the suitable process parameters will be instead discussed in the following Chapters.

### *2.4.2. Design of the experiments (DOE)*

A proper definition of the experiments to be performed is essential, to provide an effective representation of the process while reducing the time and the cost of the experimental campaign. The design planning involves:

1. The selection of the factors to be varied, i.e. the design variables. This aspect deserves some comments. Indeed, the traditional approach relies on selecting these factors as the most influential parameters, that will be then correlated with the casting quality. This hypotheses is not assumed in this work, given the transformation $\boldsymbol{z} = f(\boldsymbol{x})$.

2. The selection of the upper and lower limits, and of the levels of the factors, that should cover a meaningful range to obtain models that are correct over a large domain, by accounting also for the limitation of the injection machine. A common choice is to select two levels ("low" and "high" levels) or three levels ("low", "intermediate", "high").
3. The selection of the combinations of the different values of the design variables, such as for instance full factorial (which tests all the combinations of design parameters) or fractional factorial design. The latter approach carefully chooses a subset (fraction) of the experimental of the full factorial design, so as to describe the main effects while using a fraction of the "effort" of a full factorial design in terms of experimental runs and resources. In this work, given the complexity of HPDC process and given the need to get a deep knowledge into the problem, large sampling techniques are adopted. The use of full factorial approaches, indeed, allows to understand the interaction between the factors. In practice, however, some set of parameters should be sometimes discarded since they are infeasible (e.g. due to machine limitations or to premature solidification in the case of long process duration).
4. The number of experiments for each set of process parameters, to account for external disturbances, process uncertainty and variability and phenomena that cannot be modelled or expected, and hence ensuring adequate "signal-to-noise ratio" and hence statistical significance of the experiment.
5. The selection of the response variables, that are the casting properties to be measured (such as porosity, density, mechanical strength, as already discussed). These variables are those of interest for the process optimization, and allow discriminating between "good" and "scrap" castings, and hence between "correct" and "incorrect" process parameter settings. They should be measurable with adequate accuracy and precision, to allow a proper comparison between castings, and ensure an adequate range of variation, so that the difference between castings is related to the control process parameters, rather than exogenous and random disturbance effects.

   Clearly, the property variability is strongly affected by the geometrical shape of the die, that can be designed to ensure quasi-uniform casting properties, over a large variation of process parameters. This issue will be handled in this work,

by testing the models developed both with industrial dies, with defect-generating dies, and with optimized dies.

### *2.4.3. Selection of the mathematical relation of the metamodel*

After selecting the suitable experimental design, performing the casting and measuring the response properties, next step is to choose the approximating model, $\boldsymbol{y} = f(\boldsymbol{x})$ in the traditional approach, or $\boldsymbol{y} = h(\boldsymbol{z})$ in the novel one here proposed. Several options exist and have been proposed in engineering for the synthesis of metamodeling. In the field of HPDC, attention has been usually paid to two approaches: response surfaces and neural networks.

#### *2.4.3.1.Method 1: response surfaces*

Given the measured response vector $\boldsymbol{y}$, and a vector of independent control factors $\boldsymbol{x}$ (or $\boldsymbol{z}$), a response surface ($\boldsymbol{y} = f(\boldsymbol{x})$ or $\boldsymbol{y} = h(\boldsymbol{z})$) is the function approximating the relation between input and output variables. This is the most "natural" and intuitive way to intend metamodeling. The use of response surface is the most well-established metamodeling technique, because of its ease of use and interpretation, and its capability to reveal the physical phenomena effectively to the designers, once that the design parameters have been properly chosen. Hence, it is well suited for being employed in model-based design or optimization of metallurgical processes, also whenever the final users of the model are intended to be practitioners. Under a mathematical point of view, it is well suited for applications with random error, and with less than 10 factors adopted as the design independent variables [28]. Both these features meet the characteristics of HPDC.

To ensure reliability, great attention should be paid in the selection of the mathematical formulation of the approximating functions. Generally speaking, with reference to arbitrary scientific disciplines, the most widely used response surface approximating functions are linear functions, bilinear functions or low-order polynomials.

Metallurgical engineers and foundry practitioners often look for linear relations between the process parameters and the casting properties:

$$y = \alpha_0 + \sum_i \alpha_i \, x_i \qquad [2.1]$$

where $y$ denotes one of the response variables, $x_i$ (for proper indexes $i$) are the process parameters and $\alpha_i$ are real numbers representing the model coefficients, usually computed through least-square fitting of the measured data. Obvious extension in the case of the novel approach, where $y$ is related to $z_i$.

These models dictate that the well-known superposition principle works also in representing a very complex phenomenon, like HPDC is. Clearly, in accordance with the Taylor's theorem, linear relations hold in the case of small parameter variation about a certain configuration. In contrast, when analysing the factors ranging in a large interval, it should be expected a-priori that linear models would fail. Additionally, these linear models neglect any two-factor interaction.

The use of bilinear models allows representing two-factor interaction, by means of this formulation (with $\alpha_{ij}$ the coupling coefficients):

$$y = \alpha_0 + \sum_i \alpha_i \, x_i + \sum_i \sum_j \alpha_{ij} \; x_j \, x_i \qquad [2.2]$$

The extension to account for three-factor interactions (or even more) is trivial. These nonlinear models, although they are an improvement compared with the linear ones, are still not adequate to represent correctly the physical phenomena. As for the bilinear terms, they often do not correctly represent the actual interaction between different parameters, which could be instead governed by more complicate algebraic relations (see Chapters 5 and 6 with the analytical models on the novel parameters). In this work, this complicate interaction will be mainly accounted for through the proper definition of the transformation $h$ from the independent variables adopted for planning the DOE, $\boldsymbol{x}$, and those adopted for modelling, $\boldsymbol{z}$.

As for polynomial, a common approach [28] is using models including the second or third power of the design variables, together with bilinear terms:

$$y = \alpha_0 + \sum_i \alpha_i \, x_i + \sum_i \alpha_{ii} x_i^2 + \sum_i \sum_j \alpha_{ij} \; x_j \, x_i \qquad [2.3]$$

Clearly, the higher the number of coefficients and the degree of the polynomial, the more close is the capability of the model to fit the measured data within the domain of the experimental test performed. However, high-order function, of the type in Equation [2.3], are usually significantly affected by measurement noise and have oscillatory behaviour outside the domain of the measured data. Hence they are not useful for both extrapolation or for providing useful hints for process optimization.
Compared with these traditional approaches, this work suggests the use of power, exponential or logarithmic fitting models, such as for instance:

$$exp(y) = \alpha_0 + \sum_i \alpha_i \, x_i \qquad [2.4]$$

The use of this kind of models often accounts for non-linear behaviour without leading to oscillatory behaviour, and allows modelling "less than linear" or "more than linear" rate of growth (or of decrease) of the dependent parameters with respect to the independent ones.
As often done in other fields of engineering, a power relation between dependent and independent variables can be assumed:

$$y = \alpha_0 \, x_i^{\alpha_i} \, x_j^{\alpha_j} \qquad [2.5]$$

As for the need to represent the two-factor effect, a different and effective approach is here proposed. Once that the most relevant among the design variables are identified, their regression coefficients are written as parametric function of the other less relevant parameters. With reference to the previous model, and by assuming for instance two main process parameters denoted $x_h$ and $x_k$ (with $\alpha_h$ and $\alpha_k$ their regression coefficients), the following representation is obtained:

$$exp(y) = \alpha_0 + x_h \left( \alpha_{h0} + \sum_{i \neq h,k} \alpha_{hi} x_i \right) + x_k \left( \alpha_{k0} + \sum_{i \neq h,k} \alpha_{ki} x_i \right) \qquad [2.6]$$

Besides these general comments, detailed description of the formulation adopted will be provided in each Chapter where these models will be employed.

Once that the model has been chosen, least-square fitting is performed to compute the coefficients, by minimizing the sum of the squared difference between the measured response $\boldsymbol{y}$ and the one predicted by the model $\hat{\boldsymbol{y}}$. Weight can be also adopted to ponder the importance of the difference points (through a weight matrix, denoted $\boldsymbol{W}$ in the following Equation), to boost the model correctness in a specified region or to trust more some measurements than others:

$$\alpha_i \mid min\{\|\boldsymbol{W}(\boldsymbol{y} - \hat{\boldsymbol{y}})\|\} \qquad [2.7]$$

In the case that there are many outliers, robust linear least-square fitting method should be used, to give less concern to the outliers in the norm minimization. Typical algorithms, that are for instance provided in commercial software, are the "LAR" algorithm (least absolute residual method) and the "Bisquare methods" (which specifies the bisquare weighing method) [31].

#### *2.4.3.2. Method 2: neural networks*

A second approach that deserves some comments, among the dozen quoted in [28], is the use of neural networks, as already provided by some papers in the recent literature on HPDC. It is an alternative to the response surface approach adopted in this work with some advantages, but also many disadvantages, that often threat its effectiveness for the purpose of this work.

Neural networks contain some mathematical equations that are used to simulate biological processes, such as learning and memory, for predicting the process response on the basis of the values of the independent variables. They are not constrained by an assumed and predefined mathematical relationship between dependent and independent variables, as done in the previous Section for the response surface, and therefore have the ability to model any arbitrarily complicate nonlinear relationship, even without any theoretical knowledge on the process and of the physical phenomena affecting it [32]. In practice, this kind of models maps accurately the nonlinear relation between a very large number of process parameters (more than 10000 parameters [28]) and the investigated ones. However, they work well whenever application is almost deterministic.

If, on the one hand, this totally black-box approach could be seen as advantage, since neural networks could synthesize models that fit well the experimental data, some criticisms could be done, by taking advantage of the explanations proposed in the seminal work [33]:

- neural networks, in practice, do not explain the relationship between the process design variables and the output, by neglecting any physical relation. The model is, in practice, just a numerical model;
- it is difficult to understand which are the most important input variables, as it is instead easily provided by the statistical tools adopted for surface response;
- it is usually not clear the internal logic of the neural networks;
- neural networks are computationally expensive and difficult to be used in the field;
- the models obtained are usually effective only in interpolating the training set of $\boldsymbol{x}$ and $\boldsymbol{y}$, within their domains, but fail significantly in extrapolation;
- given the excellent capability to map the input-output relations of the training data, neural networks are not very robust to random disturbances, as those usually affecting HPDC processes.

In practice, in the light of the needs revealed by foundries (and discussed in the Chapter 1), these approaches do not provide hints to understand the parameters affecting HPDC and hence are not practical tools to optimize it.
Similar approaches, such as genetic algorithms, have similar drawbacks.

### *2.4.4. Model validation*

Validation should be done by taking advantage of rigorous statistical methods, to draw conclusions that are meaningful and reliable under a statistical point of view. This is ensured by paying attention to the following issues:

- a proper planning of the experiments (see the previous discussion in Section 2.4.2), which should involve a significant number of castings in accordance with the statistical sampling theory;
- the use of both exploratory and confirmatory statistical methods:
    - boxplots,
    - t-tests,
    - correlation coefficients,

    - residual plots,
    - least-square fitting,
    - quantile-quantile plots;
- the application of the method developed to different test cases, involving
    - different alloys,
    - different geometries of the die,
    - different injection machines.

## *2.5. Transformation of the process design variables*

### *2.5.1. Mathematical reasons*

As previously described, this work proposes a different modelling approach, compared with both the traditional metamodeling techniques in engineering and the literature on HPDC investigating the correlation between process parameters and casting quality. Indeed, in this work the behavioural models developed will employ some variables that are not those directly employed for planning the DOE. The set of experiments is usually planned by defining the first stage speed, the second stage maximum speed, the switching position between the two stages, the maximum upset pressure, as well as some thermal properties. This way of planning the process is basically related to practice in foundries, rather than scientific basis.

In contrast, in order to synthesize effective models that provide an algebraic approximation of a complicate phenomenon governed by differential equations, it is necessary introducing some different parameters, which should represent and summarize the main physical phenomena affecting HPDC, in particular the filling of the die and the solidification of the casting.

This need is also boosted by the requirement, posed by the least-square fitting, to keep low the order of the algebraic functions adopted, for avoiding overfitting or oscillating behaviours of the models. As a matter of fact, a few parameters $\boldsymbol{z}$ combining those in $\boldsymbol{x}$ on the basis of physical considerations (through the suitable definition of the transformation $f$) replace high-order polynomial in $\boldsymbol{x}$, as well as products of the type $x_i\, x_j\, x_k$, without causing dangerous overfitting.

The definition of these influential parameters is therefore the most critical issue to be tackled, and is one of the major contribution of this Thesis.

### *2.5.2. Criteria for defining the influential parameters*

Four criteria are adopted to define the most influential parameters. All these ideas and tools, summarized in Figure 2.2, are new in the metallurgy field, and also the overall approach proposed, described in this Chapter, is a novelty in this field. Detailed insights and comparison with the existing literature will be provided in the Chapters 3 and 4.

#### *2.5.2.1. Relation with the physical phenomena*

The definition of the most influential parameters should account for some physical considerations, although simplified. Their conception will be based on investigating the most relevant macroscopic phenomena and by translating them in some simple and concise scalar values that allow revealing them. This is, for sure, the most critical issue to be solved.

The following Chapters will handle separately the novel parameters proposed, by discussing:

- the forces applied to oxides and air bubbles;
- the main effects due to the melt flow;
- the effect of pressure;
- the thermal flux during solidification.

#### *2.5.2.2. The integral nature*

Being the filling of the die and the solidification of the casting an "integral process" (in the mathematical sense), these novel parameters should represent the time-history of the phenomenon, rather than just some instants, as it is in contrast usually done in the literature. In particular, to account for the integral nature of the HPDC process, whose final outcome is expected to depend on the whole process or on some time intervals, integral values of some parameters computed over different time intervals are considered. Parameters that represent energy, work, as well as mean values over some time intervals of forces, heat flux, are expected to be suitable for the purpose.

#### *2.5.2.3. The use of signal processing techniques*

On the basis of the two mentioned criteria, it is expected that a correct description of the physical phenomenon could rely on some physical quantities that are not directly

measured. Indeed, the possibility to employ numerical signal processing techniques (such as numerical derivation, integration, filtering, decimation) allows enlarging the set of physical quantities obtained by a reduced set of measurements (e.g. just the position, in the case of study of the effect of the plunger motion, see Chapter 3). Therefore, the novel parameters will deeply exploit numerical derivatives or integration of the measured signals to provide a more effective explanation of HPDC process. Appendix B will provide an exhaustive explanation of the methodologies and of the issues for exploiting such a numerical tool in the analysis of metallurgical processes.

#### *2.5.2.4. The possibility to employ these parameters for optimal process planning*

In the light of the idea of model-based optimization of the process, the proposed parameters should be useful for being employed in two different ways to improve the process. By translating two terms usually adopted in control theory, these two ideas can be categorized as:

1. "Feedforward control" (*a priori*), through optimal setting of the process parameters.

   This first type of control relies on the possibility to trace back the most relevant parameters to those adopted in planning the process (e.g. for selecting and planning the plunger motion profile), by choosing in advance the best set-up of the machine parameters to optimize the final outcome. Constraints on the feasible machine performances (e.g. speed or force limitations of the injection machine) should be also accounted for. Then, once that these parameters are properly chosen, process control can be performed through the injection machine real-time controller by taking advantage of the ever growing performances of closed-loop motion controller of hydraulic actuators, that operates to ensure accurate tracking of the motion and the pressure reference profiles.

   Clearly, the possibility to perform this control depends on the possibility of relating the injection machine set-up parameters through analytical models, by following a multidisciplinary approach, as discussed in Chapters 5 and 6.

2. “Feedback control” (*a posteriori*), by checking if the parameters differ significantly from the expected values, due to machine fault or unexpected exogenous factors.

   On the other hand, once that the model coefficients are well tuned, the availability of effective behavioural models allows the real-time monitoring and control of the process, by forecasting fault whenever the actual parameters differ from the nominal ones. This feature is allowed by the simple and low-computational-effort formulations due to the use of algebraic models and signal processing techniques. In contrast, the use of numerical simulation as a mean for real-time control is not feasible in practice, because of the high computational effort required and of the much higher complexity in tuning the model parameters.

   This idea recalls one of the challenges of HPDC recently quoted in the review provided in [34], where it is mentioned the ever increasing need of employing Statistical Process Control techniques or Control Charts, that are, in practice, similar to fault detection techniques employed in control theory, to see whether the process is performing correctly, in accordance with the reference values set a-priori to boost quality attainment.

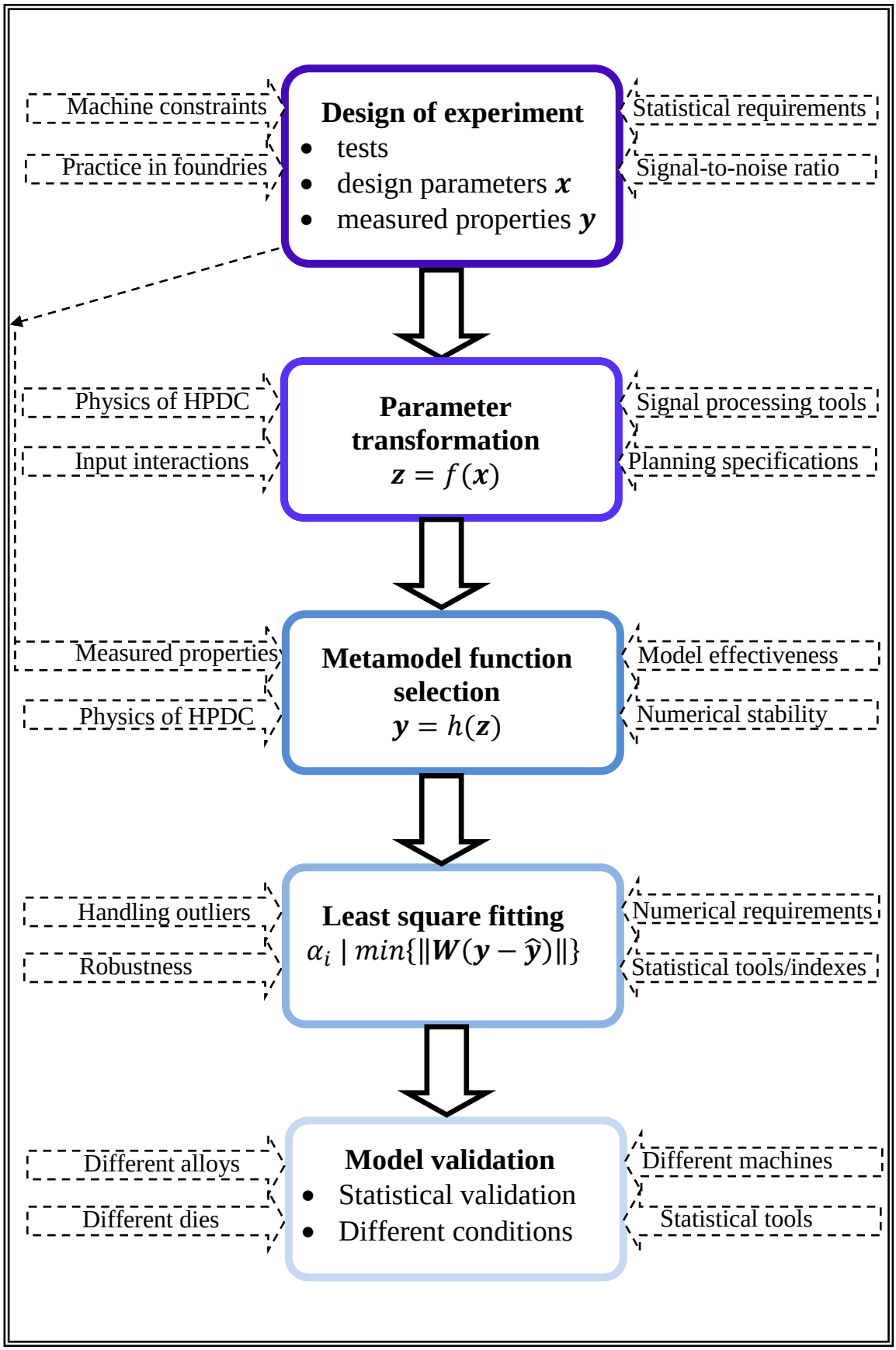


**Figure 2.1.** The proposed metamodeling approach.

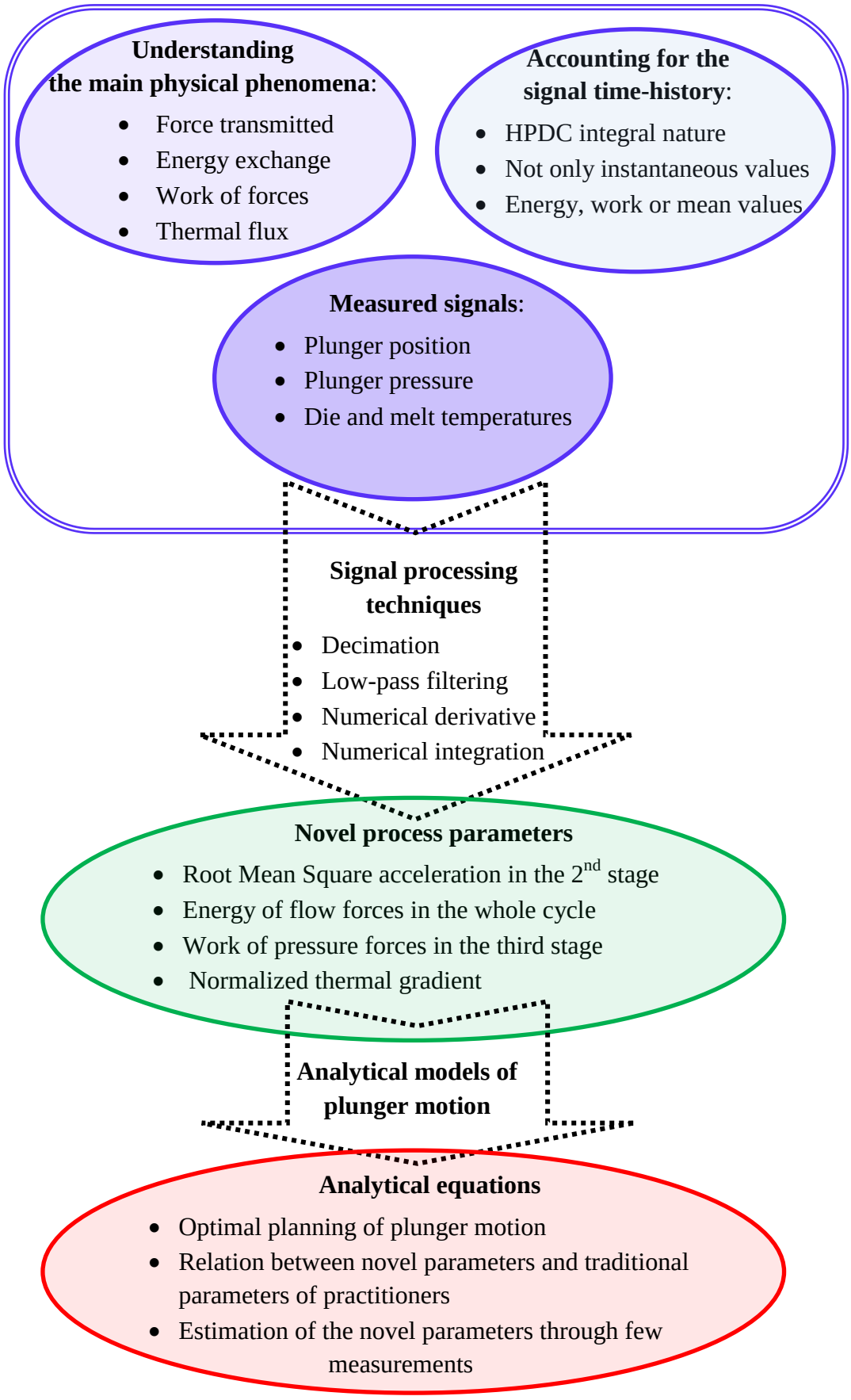


**Figure 2.2.** Conception of the novel influential process parameters.

# *Chapter 3*

## *Plunger kinematic parameters*

### *3.1. Plunger kinematic parameters in literature*

Among the HPDC process parameters investigated in literature, particular attention has been paid to the so called kinematic parameters, i.e. those related to the plunger motion. On the one hand, modifying the motion profile of the plunger is simple and costless, given the increasing use of highly automated and servo-controlled injection machines which are capable of tracking desired motion profiles with high repeatability [35]. On the other, the plunger motion allows explaining several relevant phenomena such as air entrapment, bubble collapsing, as well as the forces exerted to the melt, that are responsible for the casting quality, as it will be discussed in this Chapter. An overview of the most important papers is proposed in the following, to review the state-of-the-art and to highlight the open issues.

Verran et al. [14] discussed the influence of two injection parameters, i.e. slow shot and fast shot speeds, on the internal quality of die cast Al12Si1.3Cu alloy. They have shown that the best results in terms of density were related to low speed of slow (corresponding to 0.14 m/s) and fast (corresponding to 1.33 m/s) shots. They demonstrated that the use of high speed for the slow shot, as well as for the fast shot, increased turbulence in liquid metal, thus causing air entrapment by the filling front and formation of porosity in the castings. Dargusch et al. [36] examined the effects of different process parameters on the quality of castings in Al13Si0.3Cu and Al9Si4Cu alloys. By investigating the influence of casting velocity, porosity was found to increase with increasing this parameter (in the range 1–3.8 m/s). Nevertheless, they underlined that the variability in the data was large and more data was required to accurately demonstrate this trend.

Conversely, in the work of Gunasegaram et al. [15], analysis of tensile specimens of Al8Si3Cu made using HPDC process at three different melt flow velocities (in the range 26–82 m/s) has revealed that by increasing melt velocity resulted in a finer microstructure and a reduced pore volume fraction and, consequently, better mechanical properties. Lumley et al. [16] investigated the influence of melt velocity at the gate in die cast Al9Si3Cu alloy. They demonstrated that by increasing the melt velocity at the gate (in the range 26–82 m/s), the probability of failure decreased due to less amount of pores and oxides on the tensile bar fracture surfaces.

This brief introduction to the state-of-the-art shows that some correlations between plunger kinematic parameters and quality of castings already exist in the previous literature, although the available results are sometimes fragmented and conflicting, as also highlighted by an earlier literature review published by the Author [12]. The major limit of the previous works is that they usually take into account instantaneous values of the speed, such as the maximum value. In contrast, they neglect the analysis of the time-history of the speed and of its rate of variation. The definition of reliable criteria for tuning the injection parameters, in order to obtain sound and reliable castings, is therefore still an open and challenging issue.

The aim of this Chapter is to identify the plunger kinematic parameters affecting quality of high pressure die cast Al–Si alloys. In Section 3.2, a novel approach based on numerical processing of signals is proposed for computing some novel kinematic parameters. In Section 3.3, this approach is validated through experimental activity and thorough statistical analysis, which permits identifying some significant correlations between the novel kinematic parameters and quality of the castings. In Section 3.4, conclusions from this Chapter are drawn.

## *3.2. Novel plunger kinematic parameters*

To solve the issue, a new approach has been developed in this Thesis (see also references [37],[38]), by overcoming the limitations of the use of either the slow shot speed or the fast shot maximum instantaneous speed. The novel kinematic parameters, proposed in this work, take origin from some basic requirements that are consistent with the general ideas described in Chapter 2.

First of all, the parameters should represent the main physical phenomena affecting the filling of the die and the solidification of the casting. Therefore, being the filling

of the die and the solidification of the casting an "integral process" (in the mathematical sense), whose final outcome is expected to depend on the whole process or on some time intervals, the parameters should represent the time-history of the phenomenon, rather than just some instants. Hence, integral values of some signals computed over different time intervals are considered. Energy, as well as mean values over some time intervals, are expected to be suitable for the purpose.

Finally, it is expected that a correct description of the physical phenomenon could rely on some parameters, related to the plunger motion, that go beyond the simple measured position. Therefore, the signals to be integrated will not belong to just the set of physical parameters that are directly measured by the sensors, i.e. the position. In contrast, numerical derivatives of the displacement profiles will be employed to estimate speed and accelerations, as well as other related physical quantities that are meaningful.

The use of signal processing is an effective tool to enlarge the set of data available and to provide a more exhaustive explanation of the phenomena, as discussed in Chapter 2. Clearly, the availability of effective and reliable numerical schemes to perform signal processing is of primary importance and allows reducing the number of sensors to be employed, e.g. by avoiding speed or acceleration direct measurements. In order to perform accurate estimation of these parameters, by reducing the high-frequency noise usually introduced by numerical derivation [39], improved low-noise differentiators have been adopted, in accordance with the recommendations and the schemes reported in Appendix B. As an example, Figure 3.1 shows the measured plunger position and the computed speed and acceleration signals, taken from a sample casting among those analysed.

Starting from the speed and acceleration estimations and from the careful identification of the most relevant physical phenomena (and their representation through algebraic models), two meaningful parameters have been finally defined and then validated through a rigorous statistical analysis reported in Section 3.3.2. As discussed in Chapter 2, this transformation from the set including the "rough" design variables adopted to plan the DOE and the measured data, to the new set of influential process parameters (the one denoted $\boldsymbol{z}$), is the crux of the method development. The two parameters proposed, which are novel in the metallurgy field, are the Root Mean Square acceleration in the second stage, and the integral of the

cubic speed in the first and second stages. The mathematical and physical explanation of these parameters is provided and justified in Sections 3.2.1. and 3.2.2.

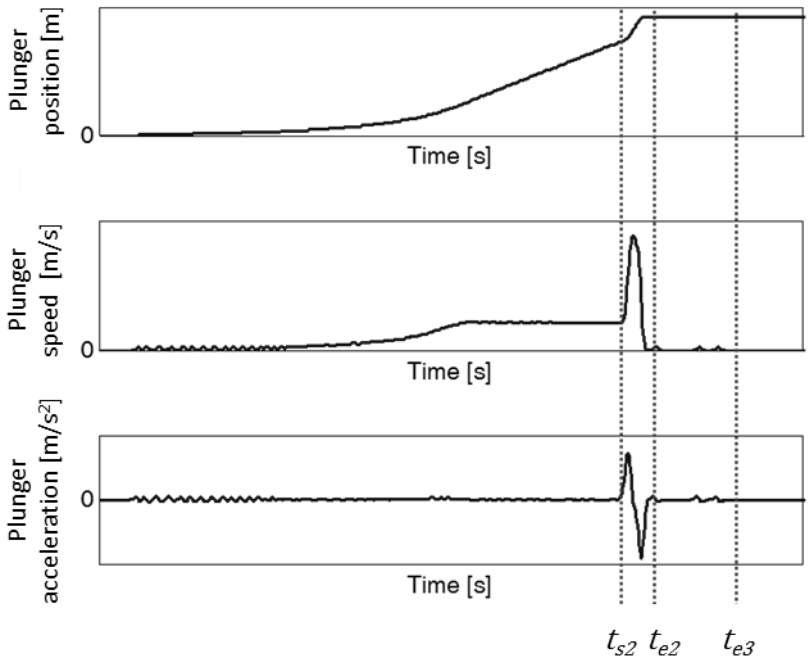


**Figure 3.1.** Example of measured position and estimated speed and acceleration of the plunger during the process.

### *3.2.1. Root Mean Square acceleration: $a_{RMS}$*

Since acceleration measurements are usually not provided, the effect of acceleration is rarely accounted for in the literature, except for vibrocasting processes [40] or in some works focusing on the effect of the transient acceleration on flow before the slow shot stage [23] (the so called stage 0, mentioned in Chapter 1).

On the one hand, speed is not constant during the second stage and therefore the knowledge of its rate of variation is of interest and provides more information than just the knowledge of the maximum instantaneous speed (see also Chapter 5). On the other hand, acceleration sets the plunger inertial force and therefore it represents the force transmitted to the melt by the plunger. These reasons justify that acceleration should be considered.

In order to account for the whole second stage, the Root Mean Square acceleration in the second stage is assumed as a representative parameter to describe and forecast the casting quality:

$$a_{RMS} = \sqrt{\frac{\int_{t_{s2}}^{t_{e2}} \ddot{x}(t)^2 dt}{t_{e2} - t_{s2}}} \qquad [3.1]$$

In Equation [3.1], $t$ is the time, $x(t)$ denotes the plunger displacement (and hence $\ddot{x}(t)$ the acceleration), $t_{e2} - t_{s2}$ is the duration of the second stage (also represented in Figure 3.1), which begins at $t = t_{s2} = t_{SW}$ (i.e. the switching time), when the plunger reaches the switching position between first and second stages, and ends when it reaches almost the final position at $t = t_{e2}$ (i.e. the instant in which the second stage ends and the third stage starts). Equation [3.1] highlights also the integral nature of the parameter.

Physically, $a_{RMS}$ represents the average value of the inertial forces (with unitary mass) of the plunger over the interval of integration. In practice, by expressing the Newtonian equilibrium of the plunger, it is also a measure of the force transmitted to the melt by the plunger during the second stage, which has been often recognized in the literature as the stage most affecting the final outcome [41].

### *3.2.2. Parameter representative of the energy associated to the flow forces: $E_f$*

The second influential factor assumed to explain and predict the casting quality is a parameter representative of the energy associated to the flow forces, exchanged between the melt and the wall of the die/chamber, or exerted to solid particles, such as oxides or inclusions, which are known to be preferential nucleation sites for porosity. Since flow forces are proportional to the square velocity [42], the energy (i.e. the integral over time of the power) is proportional to the integral of the cubic velocity. To account for the whole motion time of the plunger, integration of the cubic velocity has been performed over both the first and the second stages, i.e. from time 0 to time $t_{e2}$, by leading to the following formulation:

$$E_f = \int_0^{t_{e3}} \dot{x}(t)^3 \, dt \cong \int_0^{t_{e2}} \dot{x}(t)^3 \, dt \qquad [3.2]$$

In Equation [3.2], $t$ is the time, $\dot{x}(t)$ denotes the plunger speed, $t_{e3}$ and $t_{e2}$ are the instants in which the plunger reaches the end of the third and second stages,

respectively (also shown in Figure 3.1). The two proposed formulations are almost equivalent, because the speed in the third stage approaches to zero.

The computation of the integrals has been performed numerically in accordance with the recommendations and the scheme reported in Appendix B.

A second physical interpretation can be given to this parameter, according to Bernoulli principle. Indeed, $E_f$ can be seen as a meaningful measure of the energy associated to the pressure forces in the whole cycle, since the pressure variation is related to the square velocity.

Besides having two different and significant physical interpretations, this parameter deserves also a mathematical interpretation, in accordance with some works proposed in the literature showing that the second stage speed has more influence compared with the one of the first stage [41]. The presence of the cubic exponent in the integral, as assumed in the novel parameter here proposed, gives higher importance to the higher speed values. The proposed parameter is therefore significantly affected by the peak speed and by the second stage speed, but also accounts for the first stage.

While the parameter $a_{RMS}$ represents the average value of the force resultant in just the second phase, which is usually recognized in the literature as the most influential one, $E_f$ represents the overall energy exerted by the flow forces inside the chamber/cavity, in the whole process. The two parameters represent therefore two slightly different phenomena and both should be accounted for to explain the final outcome of HPDC process.

## *3.3. Validation of the novel plunger kinematic parameters*

### *3.3.1. Experimental procedure of the test 1*

For research purposes, a die for manufacturing horseshoe-shaped castings of aluminium alloy has been designed and developed at the foundry laboratory of Aalen University of Applied Sciences in the frame of European Music project (MUlti-layers control & cognitive System to drive metal and plastic production line for Injected Components, N. 314145). The geometry of the casting has been designed in order to exacerbate the generation of defects and therefore to study the effect of the process parameters on defects and on the overall casting quality (see Figure 3.2). This reference casting (except for some specific zones which were not analysed) is

representative of the category of thin wall components, since its thicknesses are very low in average. More details on the horseshoe-shaped casting are given in [11].


**Figure 3.2.** Horseshoe-shaped casting designed to exacerbate the generation of defects.

The manufacture process of the castings was realized at an industrial plant (Saen S.r.l., Italy) in a die casting cell, comprising a 7355 kN cold chamber die casting machine (shot chamber length 0.482 m and diameter 0.080 m), as well as a furnace and an automatic lubrication system for cooling down the die material and aiding the release of the casting. The furnace was set to 705 °C, while the pouring temperature was approximately 45 °C lower. The temperature of the die was kept constant by a thermoregulation system. The temperature of the oil cooling channels was set to 245 °C for the moving half of the die, and to 235 °C for the fixed half.

An Al9Si3Cu(Fe) alloy was cast, corresponding to the EN AB-46000 aluminium alloy (European designation, equivalent to the US designation A380). A number of 15 to 20 castings were scrapped after start up to obtain a quasi-steady state temperature in the shot sleeve and the die.

Design of the experiment has been planned, and then applied, by changing the slow and maximum fast shot speeds, the switching position between first and second stages, and the maximum upset pressure. These independent process parameters have been selected because they are simple to manipulate and to control, in accordance with those usually adopted by practitioners in planning the process. Each of the mentioned independent variable of the experiment, called control factor, has been varied within a feasible range, as large as possible, in accordance with the guidelines given in Chapter 2. The values assumed by the four control factors are given in Table

3.1 by means of their lower and upper levels of observation, together with the discretization values. Only the first three parameters affect the motion profile of the plunger, and will be therefore accounted for in this investigation. The fourth one will be only considered as a disturbance factor.

**Table 3.1.** Control factors with their lower and upper levels of observation, and discretization values.

| Control factor | Low level | High level | Discretization |
|---|---|---|---|
| Slow shot speed [m/s] | 0.2 | 0.9 | 0.1 |
| Max fast shot speed [m/s] | 1.5 | 4.5 | 0.5 |
| Switching position [m] | 0.30 | 0.35 | 0.01 |
| Max upset pressure [bar] | 500 | 1000 | 100 |

The machine was instrumented with a position sensor recording the plunger displacement with sample time $\Delta t = 0.5e^{-3}s$, and each casting is documented with its shot profile representing the plunger actual displacement curve. The motion of the servo-controlled plunger recalls the typical displacement curve described in Chapter 1, with an initial transient before reaching the constant speed of the first stage, and then a second stage which follows a polynomial displacement profile. In contrast, no measurement of the time-history of the pressure was performed. Therefore, the upset pressure cannot be effectively investigated through an approach consistent with those proposed for studying the motion profile, since, in practice, just the set point value was available rather than the complete time-history of the actual value.

A total amount of 32 different combinations of the control factors were tried, and each combination was manufactured with a number of repetitions ranging from 3 to 7. This set leads to a statistically significant sample (around 90 castings).

As for the dependent response variables, i.e. the measured variables representing the casting quality (which should be correlated to the process parameters), both the peak load (representative of static mechanical properties) and the porosity percentage of the castings have been identified.

Bending test specimens were trimmed from the flat appendixes of the casting (Figure 3.3). Four specimens for each casting were drawn (with 0.04 m width, 0.002 m thickness and 0.06 m length). The three-point bending test has been carried out with displacement control with a 4 mm/min rate and a rating force of 10 kN.

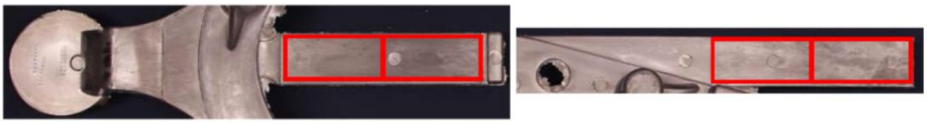

**Figure 3.3.** Position of specimens for bending testing in the appendixes of the casting.

Moreover, the stepped wedge of the casting has been chosen for porosity measurements, as it was the most critical zone and emphasized the difference in quality level between castings obtained by different process parameters. The stepped wedge is a zone of the casting with the following dimensions: 0.059 m width, thickness ranging from 0.001 m to 0.003 m, and 0.2 m length (Figure 3.4). The stepped wedges have been analysed by a macro-focus X-ray equipment, whose settings were 60 kV and 1.5 mA, and the percentage of porosity has been then estimated by means of an image analysis software.

**Figure 3.4.** Position of specimen for radiographic testing in the stepped wedge of the casting.

As a further proof, the fracture surfaces of some selected castings have been also analysed by scanning electron microscope (SEM) and their percentage of oxide has been estimated by means of an image analysis software. Finally, the zone near the fracture surface has been analysed by optical microscope in order to see which kinds of defect were present.

The rigorous application of statistical concepts, methods and models, as well as the execution of thorough microscopic analyses, have been employed in the following Section to demonstrate that the novel kinematic parameters allow explaining and forecasting both the static mechanical properties and the overall quality of the castings. The coherence between exploratory and confirmatory analyses has also been assessed, to prove the reliability of the results obtained.

### *3.3.2. Correlation between plunger kinematic parameters and quality*

#### *3.3.2.1. Correlation with the static peak load*

In order to find some statistically significant correlations between the novel plunger kinematic parameters and mechanical properties measured in the appendixes of the castings (see Figure 3.3), both exploratory and confirmatory analyses have been carried out, and their coherence has been proven.

The exploratory analysis includes summary statistics (i.e. minimum, maximum, median, 25$^{th}$ percentile, 75$^{th}$ percentile, mean and standard deviation) and graphical displays of the data, such as boxplots, without making any assumption on distributions or models [43].

The castings have been discriminated in two groups on the basis of their peak load, to analyse the summary statistics of the plunger kinematic parameters for two groups. The first group collects the castings with peak load greater than 1.1 kN (see Table 3.2), while the second one those with peak load lower or equal to this value (see Table 3.3). The threshold of 1.1 kN corresponds to the median value of all the measured peak loads.

**Table 3.2.** Summary statistics of the kinematic parameters for castings with peak load greater than 1.1 kN.

| Parameter | Min | 1$^{st}$ Qu. | Median | 3$^{rd}$ Qu. | Max | Mean | St. dev. |
|---|---|---|---|---|---|---|---|
| $a_{RMS}$ $[m/s^2]$ | 29.78 | 51.32 | 65.73 | 71.46 | 80.59 | 60.23 | 14.70 |
| $E_f$ $[m^3/s^2]$ | 0.36 | 0.75 | 1.21 | 1.39 | 2.09 | 1.14 | 0.45 |

**Table 3.3.** Summary statistics of the kinematic parameters for castings with peak load lower or equal to 1.1 kN.

| Parameter | Min | 1$^{st}$ Qu. | Median | 3$^{rd}$ Qu. | Max | Mean | St. dev. |
|---|---|---|---|---|---|---|---|
| $a_{RMS}$ $[m/s^2]$ | 17.11 | 21.84 | 36.09 | 46.36 | 64.57 | 34.80 | 12.50 |
| $E_f$ $[m^3/s^2]$ | 0.20 | 0.46 | 0.55 | 0.83 | 1.66 | 0.61 | 0.28 |

The boxplots of the two proposed parameters for the two groups of castings are represented in Figure 3.5. This figure highlights that both $a_{RMS}$ and $E_f$ affect the

peak load of the castings (referred to as $F_{max}$), since the interquartile ranges of the two groups are distinct. This is in particular true for $a_{RMS}$, where there is no overlap between the two groups. In contrast, the interquartile ranges are slightly overlapped in the case of $E_f$.

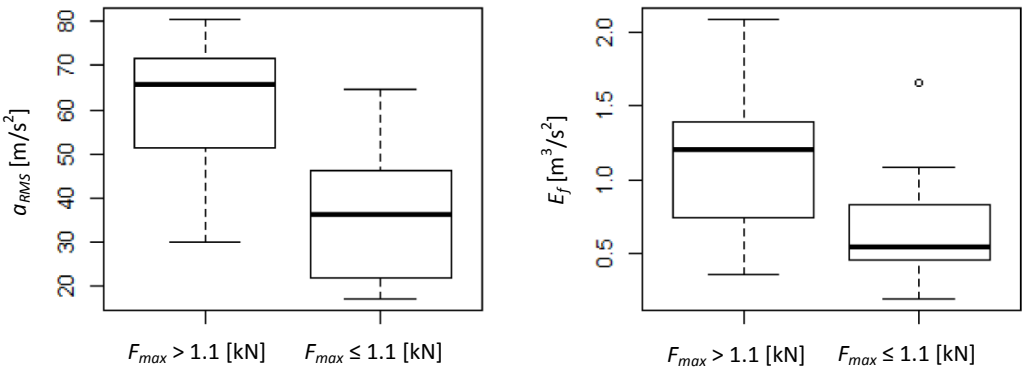


**Figure 3.5.** Boxplots of $a_{RMS}$ and $E_f$ parameters for the two groups of castings, discriminated on the basis of bending peak load.

The results of the exploratory analysis have been also confirmed through the application of the formal statistical methods performed through the confirmatory analysis. Indeed the t-tests executed on $a_{RMS}$ and $E_f$ confirm that there is true difference in means between the two groups of castings with 95% confidence interval and the p-values are $8.4e^{-15}$ and $6.0e^{-10}$, respectively. The p-value measures the evidence that there is true difference in means between the two groups of castings: the smaller the p-value (particularly less than 0.05), the stronger the evidence [43].

On the basis of the analysis of the boxplots and of the p-value, and given the weak correlation between $a_{RMS}$ and $E_f$ in this specific set of data (although it is not true in the general case, since these two parameters are mathematically different and represent two different physical phenomena), the fitting model has been developed by just assuming $a_{RMS}$ as the sole independent variable. The correlation between such a parameter and the mechanical strength is corroborated by Figure 3.6 which plots the exponential of the median peak load (denoted $F_{max}$) against this parameter, by means of the following fitting model (see the discussion provided in Section 2.4.3.1):

$$\exp(F_{max}) = \alpha_0 + \alpha_1 a_{RMS} \quad [3.3]$$

where $\alpha_0$ and $\alpha_1$ are the scalar coefficients to be identified through least square fitting [44]. The fitted coefficients for the alloy and geometry investigated are the following ones: $\alpha_0 = 2.40$ and $\alpha_1 = 0.01$. Clearly, the coefficients of the proposed metamodel are related to the specific test case investigated. The result is however representative of the general case, and reveals that quality improvement can be obtained by pushing the accelerations towards the highest feasible values. Whenever the proposed metamodel should be employed for different geometries or alloys for process control or prediction, a preliminary model tuning would allow estimating the correct model coefficients and hence accomplishing the task.

Figure 3.6 confirms that $a_{RMS}$ affects the quality of the castings and allows explaining the static mechanical properties: the higher $a_{RMS}$, the higher is the bending peak load. This result can be reasonably justified, by considering that higher accelerations mean higher forces transmitted by the plunger to the melt, that strive against oxides and fragment them (as demonstrated in Section 3.3.2.3).

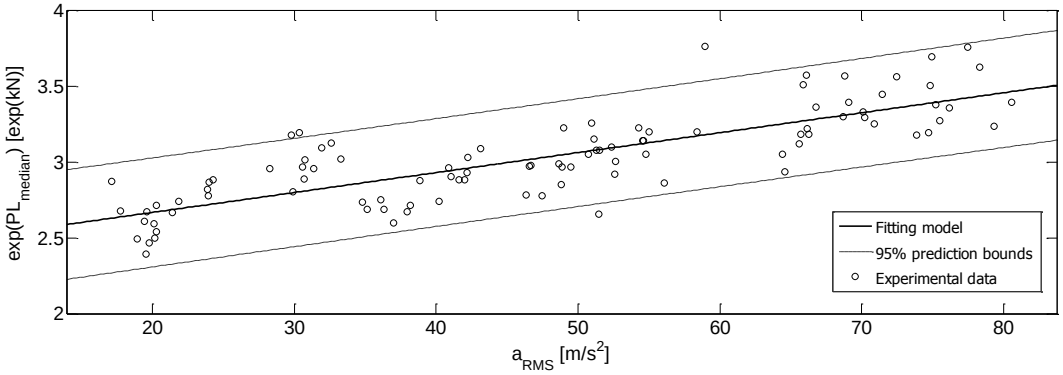


**Figure 3.6.** Bending peak load of the castings as a function of $a_{RMS}$.

The median value has been calculated between the peak loads of the four bending test specimens obtained from each casting. Indeed, the median value is more representative than the mean in the presence of outliers, due to random and uncontrolled exogenous factors. As for the fitting function, a logarithmic model has been assumed, to set a rate of growth that is "less than linear", so as to represent a decreasing rate of growth for high values of $a_{RMS}$, as it is reasonable. This assumption makes more reasonable the metamodel proposed for being used in

extrapolation. The resulting fitting model for $a_{RMS}$ approximates the data distribution with correlation coefficient equal to 0.66, which is a very satisfactory value.

The diagnostic plots (see Figure 3.7) highlight that this model fits the experimental data well: indeed, the residual plot does not show any pattern, and the quantile-quantile plot shows normality since its points do not deviate from a straight-line [45]. The conclusions are reliable and convincing, as the results from exploratory and confirmatory analyses agree.

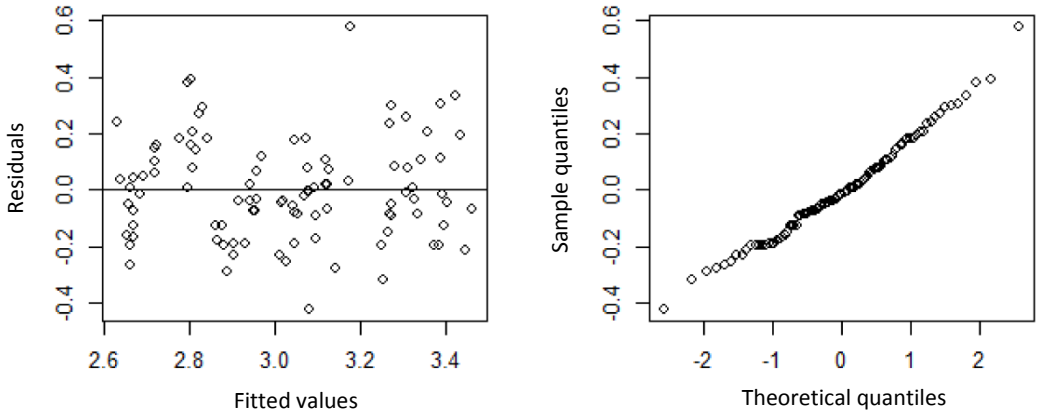


**Figure 3.7.** Residual plot and quantile-quantile plot of the model in Equation [3.3].

It is also worth mentioning that assuming a power relation between dependent and independent variables, of the type $F_{max} = \alpha_0 {a_{RMS}}^{\alpha_1}$ (as often done in other fields of engineering) leads to a 0.64 correlation coefficient. Hence, both the models can be adopted effectively.

Although the values of correlation obtained do not approach the ideal target of 1, they should be assumed as very satisfactory, since they have been computed through a relevant number of samples (around 90 castings) and in the presence of the unavoidable uncertainty and disturbance of exogenous factors, affecting the HPDC process. Among the disturbance factors, it should be accounted for the role of the upset pressure, as discussed in Section 3.3.1, which is not uniform between the castings. The effect of this parameter, which cannot be regarded as a kinematic parameter, will be object of the following Chapter through a different set of castings, where the time-history of the upset pressure will be available to provide a more rigorous discussion.

### *3.3.2.2. Correlation with the percentage of porosity*

The same approach proposed in Section 3.3.2.1 has been applied in order to find some statistically significant correlations between the novel plunger kinematic parameters and the percentage of porosity.

The castings have been discriminated in two groups on the basis of their percentage of porosity, to analyse the summary statistics of the two proposed parameters for two groups. The first group collects the castings with percentage of porosity lower or equal to 2%, while the second one those with porosity greater than this value. Based on a common practice, a reasonable and conservative threshold of 2% porosity has been chosen to discriminate sound and poor castings [46]. However, the choice of the suitable threshold depends on the final application of the casting.

The boxplots of the two proposed parameters for the two groups of castings are represented in Figure 3.8. This figure highlights that both the proposed parameters significantly affect the porosity of the castings (referred to as *Porosity*), since the interquartile ranges of the two groups are markedly distinct.

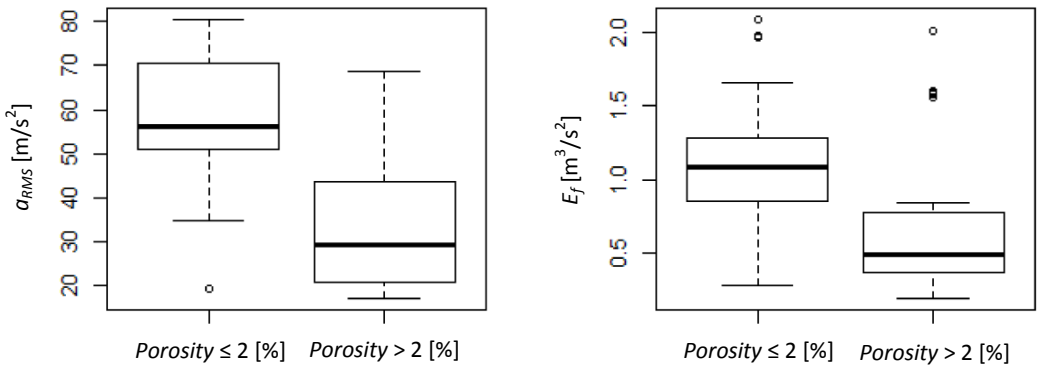


**Figure 3.8.** Boxplots of $a_{RMS}$ and $E_f$ parameters for the two groups of castings, discriminated on the basis of percentage of porosity.

The results of the exploratory analysis have been also confirmed through the application of the formal statistical methods performed through the confirmatory analysis. The t-tests performed on $a_{RMS}$ and $E_f$ demonstrate that there is true difference in means between the sound and poor castings with 95% confidence interval and the p-values are $2.8e^{-8}$ and $5.4e^{-4}$, respectively. Once again, $a_{RMS}$ is the parameter most influencing the casting quality. However, with respect to the peak

load, the boxplots are completely separated for both the parameters, and hence multivariable models can be developed.

If a fitting model relating the natural logarithm of the porosity against $a_{RMS}$ is assumed, an effective prediction is provided:

$$\log(Porosity) = \alpha_0 + \alpha_1 a_{RMS} \qquad [3.4]$$

The fitted coefficients for the alloy and geometry investigated are the following ones: $\alpha_0 = 4.42$ and $\alpha_1 = -0.08$. The fitting model approximates the data distribution with correlation coefficient equal to 0.63, which is highly satisfactory. Indeed, porosity is often significantly affected by casual exogenous factors that cannot be monitored or predicted. Hence, castings having the same combination of the three control factors in the DOE, and almost identical time-histories of the measured signal, sometimes had remarkably different values of porosity.

Figure 3.9 confirms that $a_{RMS}$ positively affects also the porosity of the castings: the higher $a_{RMS}$, the lower is the porosity, since higher accelerations mean higher forces that make previous formed air bubbles collapse.

It is worth mentioning that porosity was measured in a different region of the casting with respect to the one used for measuring the static peak load. Hence, the proposed parameter provides a meaningful explanation of the overall casting quality.

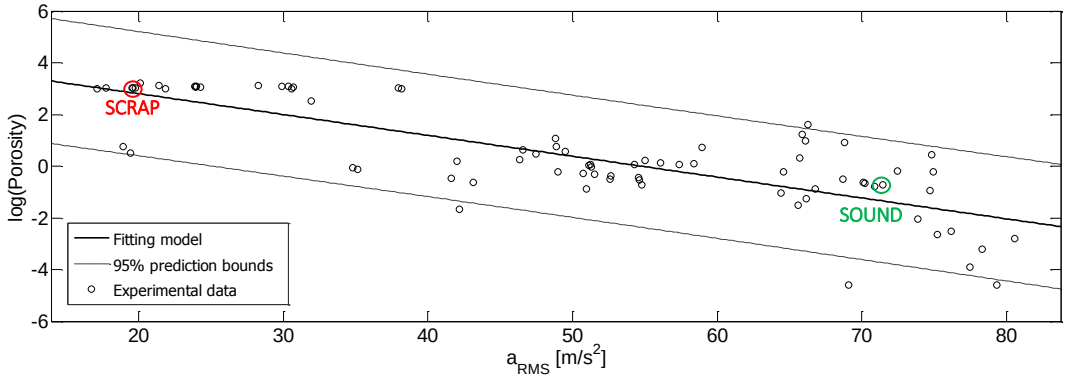


**Figure 3.9.** Porosity of the castings as a function of $a_{RMS}$.

Examples of radiographic images of a scrap (the one with $a_{RMS} = 20.25$ m/s$^2$) and a sound (the one with $a_{RMS} = 71.46$ m/s$^2$) castings are also shown in Figure 3.10 to corroborate the discussion provided. It is possible to see that both the amount and the

size of porosity in the casting in (a) are higher than those in (b), which is the sample with an higher value of $a_{RMS}$.

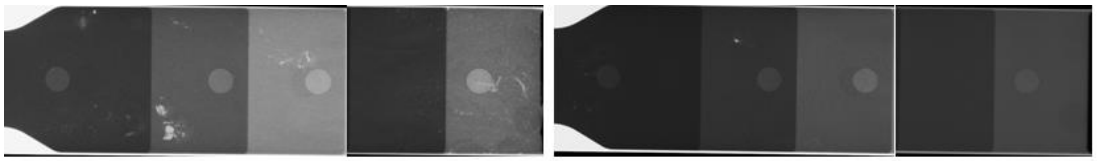

(a) (b)

**Figure 3.10.** Radiographic images of the stepped wedge of: (a) a scrap casting ($a_{RMS} = 20.25$ m/s$^2$) and (b) a sound casting ($a_{RMS} = 71.46$ m/s$^2$).

If both $a_{RMS}$ and $E_f$ are taken into account in a multivariable model, a significant improvement is obtained, by leading to a 0.72 correlation coefficient and highlighting the influence also of the first stage, besides the second one, on the porosity. The final model proposed is the following one:

$$\log(Porosity) = \alpha_0 + \alpha_1 a_{RMS} + \alpha_2 E_f \qquad [3.5]$$

The diagnostic plots of this model (which have been omitted for brevity) are similar to those in Figure 3.7, and show that this model fits, once again, the experimental data well. Since the results from exploratory and confirmatory analyses agree, the conclusions are reliable and convincing.

The fitting model obtained is represented in Figure 3.11. It can be seen that the plane of the regression model fits effectively the experimental data.

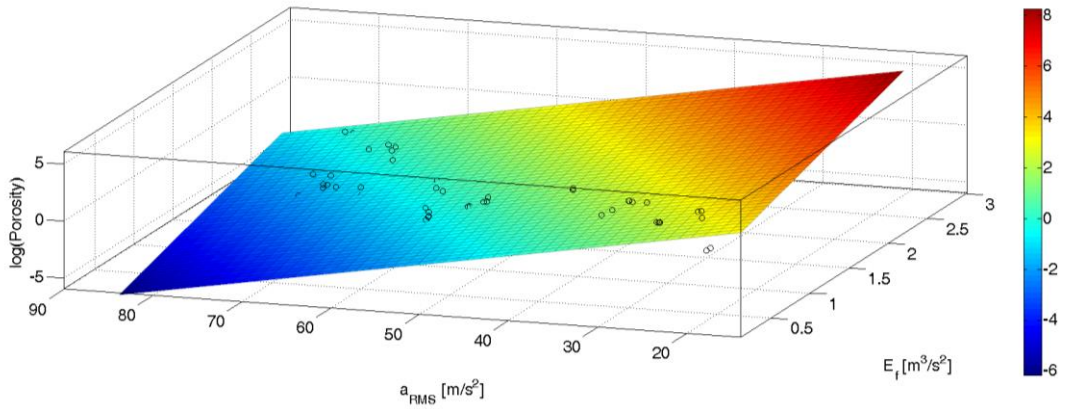


**Figure 3.11.** Three-dimensional representation of the model in Equation [3.5].

### *3.3.2.3. Analysis of internal and subsurface defects*

As a further evidence of the correctness of the proposed approach in explaining the overall casting quality, the fracture surfaces of some selected castings have been analysed by scanning electron microscope (SEM) and their percentage of oxide has been estimated by means of an image analysis software. The aim of this analysis is to show the effect on the percentage of oxide of an increase of $a_{RMS}$ and $E_f$, by analyzing some castings with increasing values of these parameters, and therefore of increasing values of $F_{max}$. The analysis reveals that by increasing $a_{RMS}$ and $E_f$, then the percentage of oxide decreases, as shown in Table 3.4. The marked lines of Table 3.4 correspond to the marked castings in Figure 3.12. The correlation is justified by the fact that higher accelerations imply higher forces that fragment the oxides, thus promoting their partial dissolution and avoiding premature failure of castings. As for the other parameter, being the flow forces exchanged between the melt and the wall of the die/chamber, or exerted to solid particles, the energy associated to these forces is an influent parameter on destabilizing the preferential nucleation sites for defects.

**Table 3.4.** Percentage of oxide and bending peak load as a function of $a_{RMS}$ and $E_f$.

| $a_{RMS}$ [m/s$^2$] | $E_f$ [m$^3$/s$^2$] | $F_{max}$ [kN] | Oxide [%] |
|---|---|---|---|
| 20.25 | 0.45 | 0.93 | 9.12 |
| 36.33 | 0.56 | 0.99 | 4.75 |
| 46.55 | 0.93 | 1.09 | 1.69 |
| 50.73 | 1.04 | 1.12 | 0.88 |
| 71.46 | 1.41 | 1.24 | 0.18 |

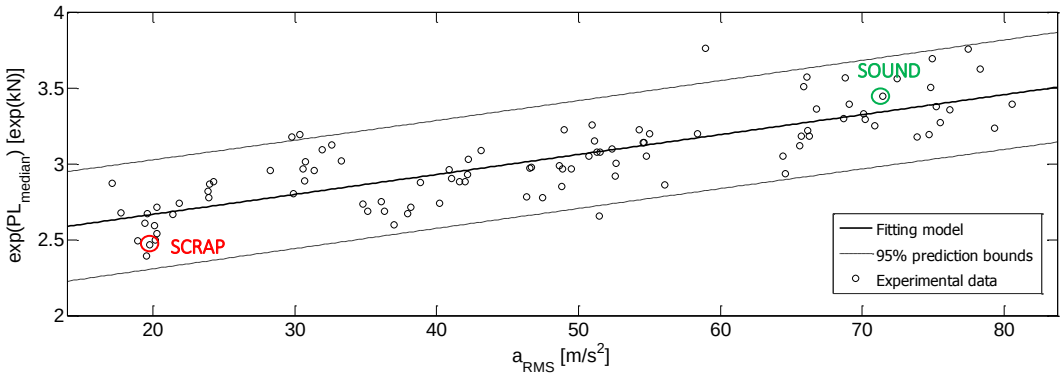


**Figure 3.12.** Bending peak load of the castings as a function of $a_{RMS}$.

In Figures 3.13 and 3.14, SEM micrographs of the fracture surfaces of a scrap casting (the one in the first line of Table 3.4, with $a_{RMS} = 20.25$ m/s$^2$) and a sound casting (the one in the last line of Table 3.4, with $a_{RMS} = 71.46$ m/s$^2$), respectively, are shown. Both secondary electron and back-scattered electron images are represented for comparison. Magnifications of the marked zones of the abovementioned Figures 3.13 and 3.14 are then shown in Figures 3.15 and 3.16.

SEM micrographs from 3.13 to 3.16 highlight that the amount and the size of defects on the fracture surface are higher in the case of a scrap casting, justifying its lower bending peak load. Moreover, very large and detrimental oxides are usually located in sub-surface regions in the case of the scrap casting (see Figures 3.13 and 3.15), facilitating crack nucleation. In contrast, the fracture surface is more homogeneous and little defects are usually found in internal regions in the case of the sound casting with a consequent positive effect on the mechanical behaviour (see Figures 3.14 and 3.16).

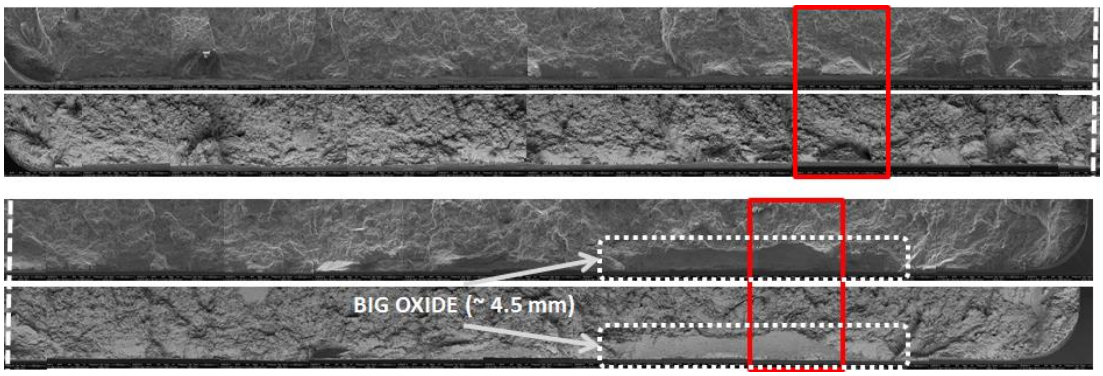


**Figure 3.13.** SEM micrograph of the fracture surface of a scrap casting ($a_{RMS} = 20.25$ m/s$^2$).

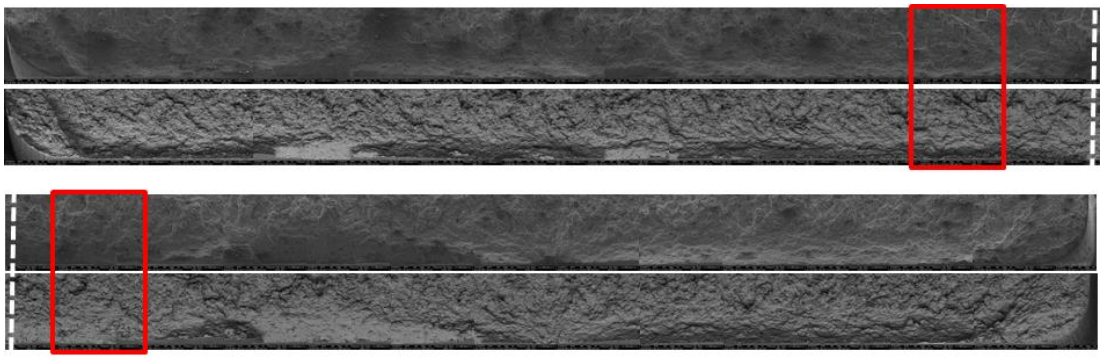

**Figure 3.14.** SEM micrograph of the fracture surface of a sound casting ($a_{RMS} = 71.46$ m/s$^2$).

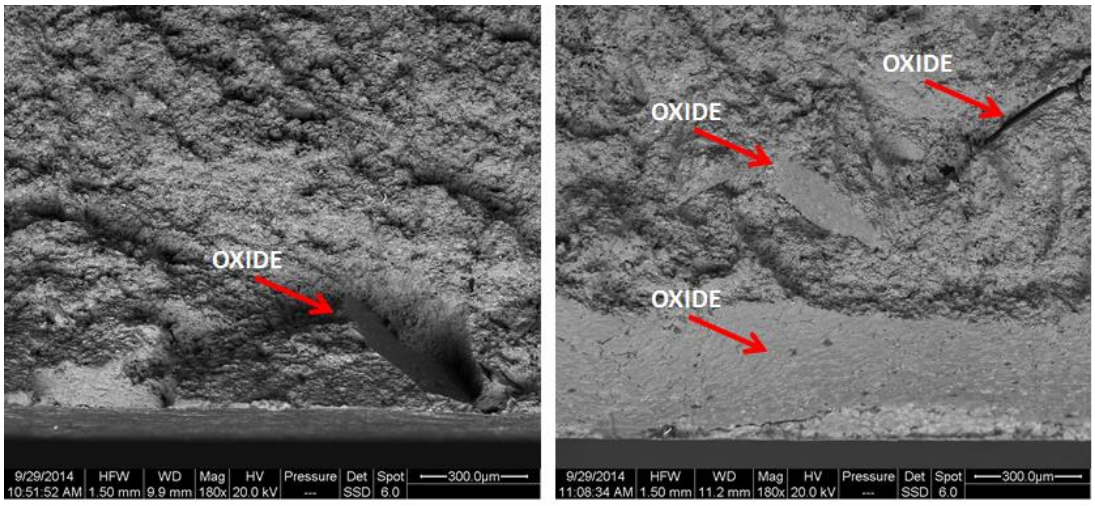


**Figure 3.15.** 180x magnification of the marked zones of a scrap casting ($a_{RMS} = 20.25$ m/s$^2$).

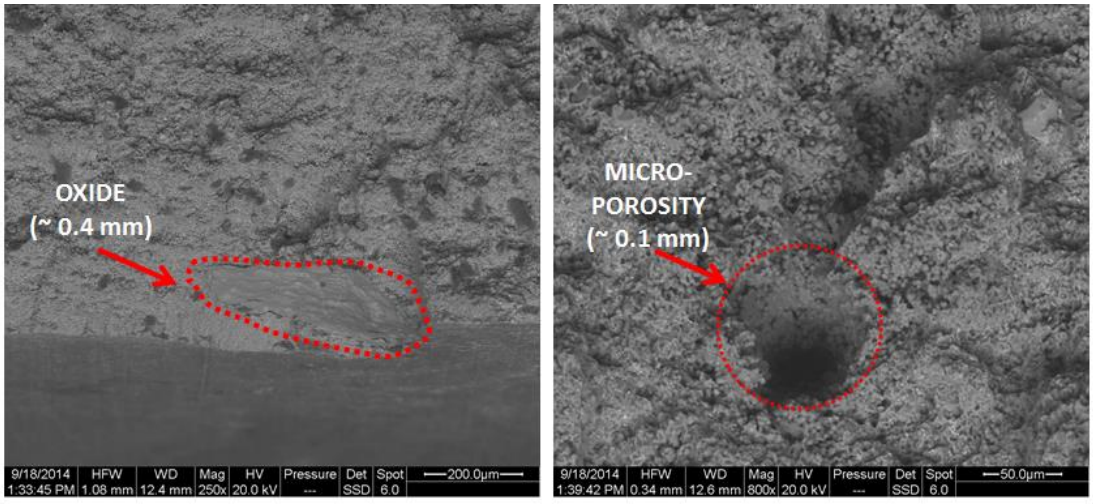


(a) (b)

**Figure 3.16.** Marked zones of a sound casting ($a_{RMS} = 71.46$ m/s$^2$) at:
(a) 250x and (b) 800x magnification.

Finally, optical micrographs of Figure 3.17 confirm that the microstructure of a sound casting is more uniform than the one of a scrap casting. Moreover, Figure 3.17 (a) highlights that a lot of very dangerous defects, such as porosity and oxides, are concentrated just below the surface of the scrap casting, compromising its mechanical behaviour.

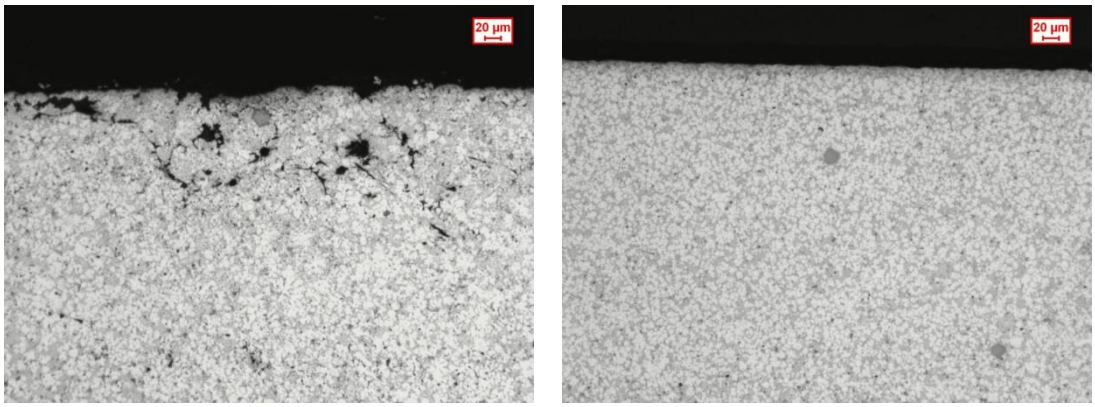


(a) (b)

**Figure 3.17.** Optical micrographs at 100x magnification of the zone near the fracture surface of: (a) a scrap casting ($a_{RMS} = 20.25$ m/s$^2$) and (b) a sound casting ($a_{RMS} = 71.46$ m/s$^2$).

## *3.4. Concluding remarks*

Starting from the concepts and the ideas proposed in the previous discussions provided in the Thesis, this Chapter has been focused to the identification and the definition of some parameters affecting the casting quality, by just analysing the plunger motion. The meaningful parameters obtained through a systematic approach and by taking advantage of numerical processing of the plunger displacement time-history are denoted kinematic parameters and are:

- the Root Mean Square plunger acceleration in the second stage, $a_{RMS}$, which represents the average value of inertial forces related to the plunger motion;
- the integral of the cubic speed in the first and in the second stages, $E_f$, which deserves two different physical interpretations. On the one hand, it represents the energy associated to the flow forces due to the contact between the melt and the wall of the die/chamber or some solid particles (such as oxides or inclusions), that are proportional to the square speed; on the other, in accordance with Bernoulli principle, it approximates the energy of the fluid pressure forces.

Given the integral nature of the HPDC process, the experimental analysis has confirmed that the two parameters having an integral mathematical nature (and hence accounting for the whole process or for some significant time intervals), are meaningful. As a matter of fact, they explain both the static mechanical property and the percentage of porosity, measured in different regions of the castings, as demonstrated by the application of statistical concepts, methods and models. The

fitting models synthesized in this Chapter permit obtaining good correlation coefficients with the measured data, i.e. 0.66 and 0.72 for, respectively, the peak load and the porosity. Although these values do not approach the ideal target of 1, they are satisfactory, since they have been computed through a relevant number of samples (around 90 castings), whose large size exacerbates the process variance, due to the unavoidable uncertainty and disturbance of the uncontrollable and casual exogenous factors usually affecting the HPDC process. Additionally, the effect of variation in the upset pressure has been treated as a disturbance factor, since it has been not accounted for. Finally, the microscopic analysis reveals that by increasing $a_{RMS}$ and $E_f$, then the percentage of oxide decreases.

Overall, the results obtained clearly show that the casting quality is affected, in a complicate and nonlinear way, by all the process parameters discussed in the previous literature and that their influence can be traced back to the two parameters suggested, which explain effectively the effect of the plunger motion on bending peak load, percentage of porosity and percentage of oxide.

Further improvement of the model, to include pressure and temperature parameters, as well as the development of the analytical models for the a-priori optimization of the HDPC process, will be proposed in the following Chapters of this Thesis.

# *Chapter 4*

## *Simultaneous effect of plunger motion profile, pressure and temperature*

## *4.1. Effect of pressure and temperature: literature analysis and theoretical concepts*

### *4.1.1. Motivations*

As discussed in the Introduction, a comprehensive study on the effect of process parameters should account also for the effect of pressure and temperature, whose relevance has been already shown in the literature. In particular, two issues are often discussed: the effect of the upset pressure exerted during the third stage of HPDC when the plunger control is switched to force control, and the thermal flux.

This Chapter aims at further improving the novel approach introduced in Chapter 3 by including two other significant parameters, describing the abovementioned effects of pressure and temperature on the final quality of castings. In Section 4.1.2 and 4.1.3, literature review is provided to highlight the most important theoretical concepts on the issue. In Section 4.2, two novel parameters accounting for the influence of the upset pressure and temperature on the casting quality are proposed. In Section 4.3, the experimental validation is presented. Moreover, statistical and metallurgical analyses are reported to prove the correctness of both the previous introduced plunger kinematic parameters and the newly defined ones. Finally, concluding remarks and further developments are discussed in Section 4.4.

### *4.1.2. Effect of the upset pressure*

It is well-known in literature, and also recognized by practitioners, that the application of high upset pressure has positive effects on the internal quality of

castings. Indeed, high upset pressure prevents the formation of shrinkage porosity and the expansion of previously entrapped air during the casting solidification. This concept is similar to the one represented by the two novel kinematic parameters introduced in the previous Chapter, which, however, focus also on the second stage, where the plunger is still in position-control operating mode.

Several experimental works corroborate the need of higher upset pressure. For example, Dargusch et al. [36] examined the effects of the upset pressure (in the range 30–90 MPa ) in castings obtained with Al13Si0.3Cu and Al9Si4Cu alloys . Porosity was found to decrease with increasing upset pressure. Verran et al. [47] analysed the influence of the upset pressure on the internal quality of die cast Al12Si1.3Cu alloy in the range 15–30 MPa, by confirming once again the theoretical expectations.

Although the influence of the upset pressure on porosity has been widely discussed, the feeding mechanisms by which material is forced through the gate and into the die cavity have not been studied in detail. Otarawanna et al. [48] studied this issue by focusing on the relation between such a mechanism, the upset pressure and the gate thickness. They discovered that shear banding does not occur when a low upset pressure (studied in the range 0–61 MPa) is combined with a thin gate. Hence, feeding is less effective under these conditions, by resulting in higher porosity in the castings. Indeed, shear banding reduces the resistance to shear by creating weak shear zones of increased liquid fraction that aid in transporting the material in the central region of the cross section forward through the gate.

A slightly different focus, and explanation of the results, was adopted by Chiang et al. [17] who studied the influence of the upset pressure on the density of Al-Si alloy castings. They demonstrated that, by increasing the upset pressure, the mean particle size of primary silicon was smaller as a consequence of the higher compression and compaction of the casting into the die, which promoted a higher heat transfer.

Several works among those employing response surface methodology with high-order models or neural networks also studied the effect of the upset pressure, by including it among the design (independent) parameters (see e.g. [49],[50]). However, it is difficult to obtain general results from the complex metamodels proposed, which in practice neither explain nor reveal the relationship between the process design variables and the output.

### *4.1.3. Effect of the temperature*

As for the effect of the temperature, several studies have been devoted to investigating either the effect of thermal flux on the casting quality or the parameters affecting and representing the flux itself.

Chiang et al. [17] studied the influence of the die temperature on the primary silicon of Al-Si alloy castings. They demonstrated that the grain and the mean particle size of the primary silicon increase by increasing the die temperature, due to the slower heat transfer and smaller cooling rate during solidification.

Given the importance of the thermal flux during the cooling, in order to improve the casting quality, some studies investigate the interfacial heat transfer coefficient (IHTC). The IHTC is the heat flux per unit area at the metal/die interface (denoted $q$), divided by the difference in interface temperature between the alloy and the die:

$$IHTC = \frac{q}{T_m - T_{die}} \qquad [4.1]$$

where $T_m$ and $T_{die}$ are the melt temperature and die surface temperature, respectively.

By using a large sample of Al17Si4Cu castings, Cao et al. [18] demonstrated that the initial die surface temperature has the most dominant influence on the peak value of the IHTC among all the processing parameters. In particular, they have shown that with increased initial die surface temperature, the IHTC decreases. By considering the IHTC as a function of the temperature gap at the interface (characterizing the thermal resistance between the melt and the die), the effect of the initial die surface temperature can be easily understood.

## *4.2. Proposed pressure and temperature parameters*

The approach suggested in Chapter 3 has been here extended by including two other meaningful parameters affecting quality of castings, that have been defined on the basis of the theoretical concepts previously defined:

- work of the pressure forces in the third stage, denoted $L_i$;
- normalized thermal gradient, denoted $r_T$.

### *4.2.1. Work of the pressure forces: $L_i$*

The existing literature takes into account the set or maximum value of the upset pressure for investigating its influence on the casting quality, neglecting two important aspects. First of all, this approach does not account for the time-variability of such a parameter, which may reach its peak value just for a few time instants. Secondly, it neglects the actual capability of pressure to compact the solidifying melt. Indeed, once the gate becomes fully solid, the pressure from the machine hydraulic system can no longer be transmitted to the metal in the die cavity. Moreover, the degree of compaction of the solidifying melt due to the applied pressure depends also on the freezing range width of the alloy, as highlighted in the work of Dargusch [36] et al. Indeed, when the solid fraction of the casting is not too high, a pressure-transfer path exists inside the casting, through which the upset pressure can be effective, maintaining a close contact between the molten metal and the die [18]. This fact is also confirmed in the work of Hamasaiid et al. [51].

Therefore, such traditional approach may be ineffective in finding statistically significant correlations between process and quality of castings, whenever the upset pressure, though high, is applied when the gate is almost completely solidified. This could happen whenever the switching from the position-controlled stages (first and second stages) to the pressure-controlled one (the third one) requires a long transient (delay), in order to avoid water-hammer effects or discontinuous control actions [35]. The use of closed-loop effective control systems, that manage fast and bumpless switching between the two different types of control, allows reducing such a delay and hence improves the effectiveness and the repeatability of the upset pressure exerted [35],[52]. These considerations enforce the need of a multidisciplinary approach in process optimization, as discussed in Chapter 2, as one of the challenges in HPDC. Figure 4.1 shows the measured static property and density against the maximum upset pressure. It is evident that no statistical correlation can be found in the explanation of $F_{max}$. In contrast, a trend is visible in the relation with the density.

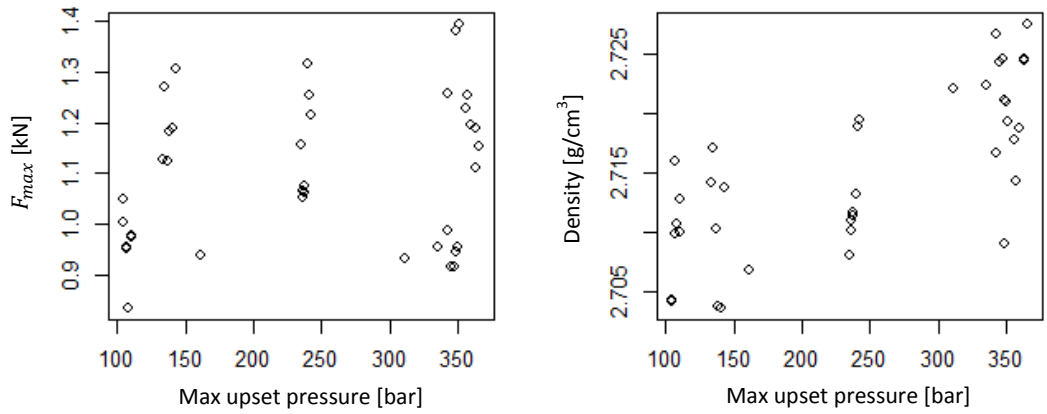


**Figure 4.1.** Traditional approach in finding correlations between process and quality of the castings.

The capability of the upset pressure to compact the solidifying material can be revealed by observing if it is capable of producing displacements of the plunger. If the pressure is ineffective in making the bubbles collapse, then no plunger displacement occurs. This may happen because of small values of the upset pressure, or because of excessive delay introduced by the control switching. This consideration suggests to account for the plunger displacement caused in the third stage by the upset pressure. In practice, it should be evaluated the work of the pressure forces, which is defined as follows:

$$L_i = \int_{t_{e2}}^{t_{e3}} p(t)\, dx = \int_{t_{e2}}^{t_{e3}} p(t)\, \dot{x}(t)\, dt \qquad [4.2]$$

In Equation [4.2], $t$ is the time, $x(t)$ denotes the plunger displacement, $p(t)$ denotes the plunger hydraulic pressure, $t_{e2}$ and $t_{e3}$ are the instants in which the plunger reaches the end of the second and third stages, respectively. In Figure 4.2, examples of measured position and hydraulic pressure of the plunger, taken from a sample casting among those analysed, are shown and the interval of integration is marked.

This approach is a generalization of the traditional approach based on investigating the maximum upset pressure. The results provided by the two approaches almost coincide whenever the upset pressure is correctly applied, before the gate is solidified. However, this approach is consistent with those proposed for studying the motion profile, since it accounts for an excerpt of the pressure time-history.

The work of the pressure forces is positive if the gate is still hot and pressure is high enough to determine displacement of the solidifying melt (as shown in Figure 4.2)

and thus to compact the previously entrapped air. The concept of work of pressure forces is novel in the metallurgical literature, since the existing papers only account for the maximum upset pressure, regardless it produces or not any displacement, and hence regardless of the work exerted.

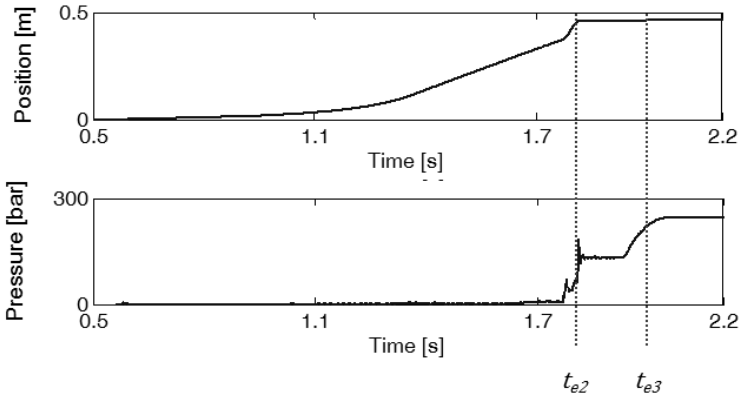


**Figure 4.2.** Examples of measured position and hydraulic pressure of the plunger and interval of integration.

Some issues affect the computation of the work of the pressure forces, which can rely on the techniques explained in Appendix B.

Whenever pressure measurements are less affected by noise, compared with position (which is often roughly discretized), Equation [4.2] can be transformed through part integration as follows, to provide another way to compute $L_i$:

$$L_i = \int_{t_{e2}}^{t_{e3}} p(t)\, dx = [p(t_{e3})\, x(t_{e3}) - p(t_{e2})\, x(t_{e2})] - \int_{t_{e2}}^{t_{e3}} \dot{p}\,(t) x(t)\, dt \qquad [4.3]$$

It is also worth providing an approximate method for computing $L_i$ through the average speed in the third stage $\left(\dot{x}_{mean} = \frac{\Delta x}{\Delta t}\right)$ as follows:

$$L_i = \int_{t_{e2}}^{t_{e3}} p(t)\, dx = \int_{t_{e2}}^{t_{e3}} p(t)\dot{x}(t)\, dt \cong \dot{x}_{mean} \int_{t_{e2}}^{t_{e3}} p(t)\, dt \qquad [4.4]$$

The definition of this approximate method is justified by the problems caused by the numerical derivation of the slowly-varying position in the third stage, where small displacements lead to speeds approaching zero (see the discussion proposed in

Appendix B). The problem is exacerbated by the low resolution of the position sensors sometimes employed in less recent injection machines. Fortunately, the development of closed-loop effective control schemes has been boosting the use of high resolution sensors, that allow improving the estimation of the speed even in the third stage [35]. In contrast, in the experimental investigation proposed in this Chapter, the approximate method of Equation [4.4] has been applied for computing the work, since it has led to more uniform results within the castings obtained through the same combination of factors and thus it has been proved to be more reliable.

A final, and more approximate formulation can be obtained by replacing the time-varying pressure with the constant value of the set upset pressure $p_{set}$:

$$L_i \cong \dot{x}_{mean} \, (t_{e3} - t_{e2}) \, p_{set} \qquad [4.5]$$

### *4.2.2. Normalized thermal gradient: $r_T$*

After the filling of the cavity, the heat should be removed from the high temperature molten alloy to allow solidification. The literature analysis has proved that the optimization of the thermal flux and the consequent quick and uniform cooling improve the internal quality of castings. High heat removal rates are obtained either in the presence of high temperature gradients between the hotter melt and the die, or in the presence of high interfacial heat transfer coefficients. Both these conditions boost the achievement of fine microstructure. The time-history of the temperature within the cavity is governed by the initial conditions (i.e. the melt and the die initial temperature), by the heat transfer coefficient and the thermal properties of the complete system, and by the plunger motion profile, which sets the melt flow and hence the temperature rise. Since the latter contribution is already accounted for in the model, and also on the basis of the aim of synthesizing metamodels that can be employed at the process planning stage, the model should be augmented for representing the effect of the initial thermal condition and of the heat transfer coefficient. This suggests that the die temperature before the injection and the melting temperature could be important parameters to be taken into account as a synthesis of the missing information.

Given the definition of the initial melt-die thermal gradient $\Delta T = T_{melt} - T_{die}$ (where the initial temperatures are assumed), and given the decreasing relation

between the IHTC and $T_{die}$, as proposed in the quoted literature, the following parameter is introduced in the model:

$$r_T = \frac{\Delta T}{T_{die}} \qquad [4.6]$$

It is defined as the thermal gradient between the melt and the die normalized on the initial temperature of the die. By increasing the thermal gradient, the heat removal improves with an expected positive effect on the microstructure of castings. Moreover, by decreasing the initial die temperature, the interfacial heat transfer coefficient increases with a consequent favourable effect on the heat flux [18]. For metallurgical evidence of these considerations, with reference to the experimental application of the method, see Section 4.3.2.3.

Such a normalized thermal gradient has the advantage that it can be easily used for planning and optimizing the process, being a very simple and intuitive parameter that just relies on some process setting parameters.

## *4.3. Validation of the proposed pressure and temperature parameters*

### *4.3.1. Experimental procedure of the test 2*

In this Chapter, the horseshoe-shaped casting introduced in the previous Chapter (see Figure 3.2) has been once again employed, and a different experimental campaign has been carried out. In order to investigate the effect of temperature and pressure, the DOE has involved the modification of an higher number of independent parameters: the slow and maximum fast shot speeds, the switching position between the two stages, the maximum upset pressure, the melt and the die temperature before the injection. The selected factors and their lower and upper levels of observation are shown in Table 4.1.

As in the previous test, these factors have been selected because they are simple to manipulate and control, in accordance with those usually adopted by practitioners in foundry. A total amount of 15 different combinations have been planned, and from 2 to 3 castings for each combination have been manufactured and analysed (overall 40 castings). This set of castings leads to a statistically significant sample for

investigating the effect of pressure and temperature, being the plunger kinematic parameters already validated through 90 additional castings.

**Table 4.1.** Control factors with their lower and upper levels of observation.

| Control factor | Low level | High level |
|---|---|---|
| Slow shot speed [m/s] | 0.2 | 0.9 |
| Max fast shot speed [m/s] | 0.9 | 3.4 |
| Switching position [m] | 0.29 | 0.37 |
| Max upset pressure [bar] | 104 | 364 |
| Pouring temperature [°C] | 677 | 727 |
| Die temperature [°C] | 120 | 220 |

The experiments were conducted at the foundry laboratory of Aalen University of Applied Sciences (Germany) in a die casting cell, comprising a 7355 kN die casting machine (shot chamber length 0.482 m and diameter 0.070 m), as well as a holding furnace, and automatic lubrication and pouring systems. The machine was instrumented with a position sensor recording the plunger displacement with sample time $\Delta t = 0.5e^{-3}s$, and each casting is documented with its shot profile representing the time-history of the plunger actual displacement curve. The motion of the servo-controlled plunger recalls the typical displacement curve described in Chapter 1, with an initial transient before reaching the constant speed of the first stage, and then a second stage.

An Al9Si3Cu(Fe) alloy was cast, corresponding to the EN AB-46000 aluminium alloy (European designation, equivalent to the US designation A380).

For the assessment of the casting quality both three-point bending tests and density measurements by the Archimedes's principle have been carried out. Bending test specimens were trimmed from the flat appendixes of the casting (Figure 3.3). As in the previous experimental campaign (see Chapter 3), four specimens for each casting were drawn (with 0.04 m width, 0.002 m thickness and 0.06 m length). The three-point bending test has been carried out with displacement control with a 4 mm/min rate and a rating force of 10 kN. Conversely, density measurements have been executed on the whole casting by the Archimedes's principle. As a further proof,

cross sections and fracture surfaces of some selected castings have been also analysed through optical and scanning electron microscopes.

### *4.3.2. Simultaneous effect of plunger motion profile, pressure and temperature on the quality*

#### *4.3.2.1. Correlation with the static peak load*

The castings have been discriminated in two groups on the basis of their peak load to analyse the summary statistics of the two proposed parameters for the two groups. The first group collects the castings with peak load greater than 1.1 kN, while the second one those with peak load lower or equal to this value. The threshold of 1.1 kN corresponds, approximately, to the mean value of all the measured peak loads.

As expected, the boxplots in Figure 4.3 highlight that $a_{RMS}$ primarily affects the peak load, referred to as $F_{max}$, since the interquartile ranges of the two groups are markedly distinct. The other kinematic parameter, i.e. $E_f$, shows a slightly weaker correlation, but provides useful information about the first stage of the process and will be useful in the multivariable model. As for the newly introduced parameters, i.e. $L_i$ and $r_T$, their effect is significant when combined with $a_{RMS}$, as shown in Figure 4.4 where the products $a_{RMS}\,L_i$ and $a_{RMS}\,r_T$ are investigated.

The results of the exploratory analysis have been confirmed by the application of t-tests and regression models, in order to draw conclusions about the population. The t-tests demonstrate that there is true difference in means between the two groups of castings with 95% confidence interval and the p-values are adequately small ($1.85e^{-8}$ and $1.72e^{-5}$ for $a_{RMS}$ and $E_f$, while $2.87e^{-6}$ and $3.51e^{-8}$ for $a_{RMS}\ L_i$ and $a_{RMS}\,r_T$ respectively).

Least-square regression models have been developed, by progressively including all the four parameters discussed in order to evaluate the model improvements due to the increasing number of parameters.

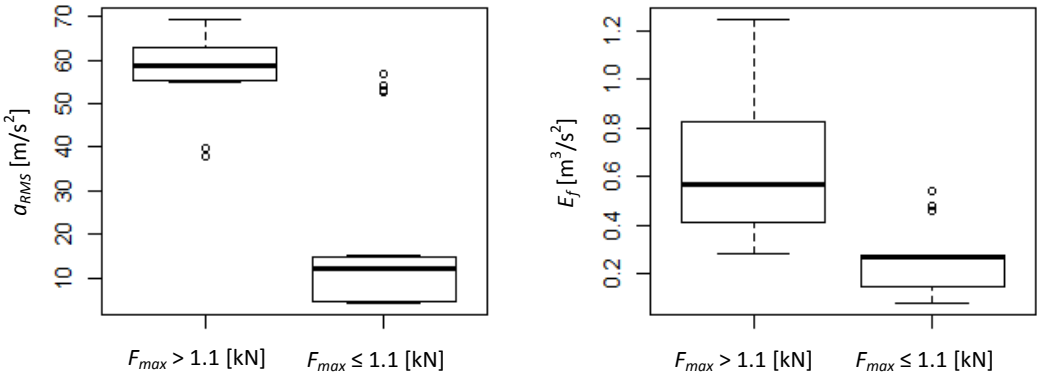


**Figure 4.3.** Boxplots of $a_{RMS}$ and $E_f$ parameters for the two groups of castings, discriminated on the basis of bending peak load.

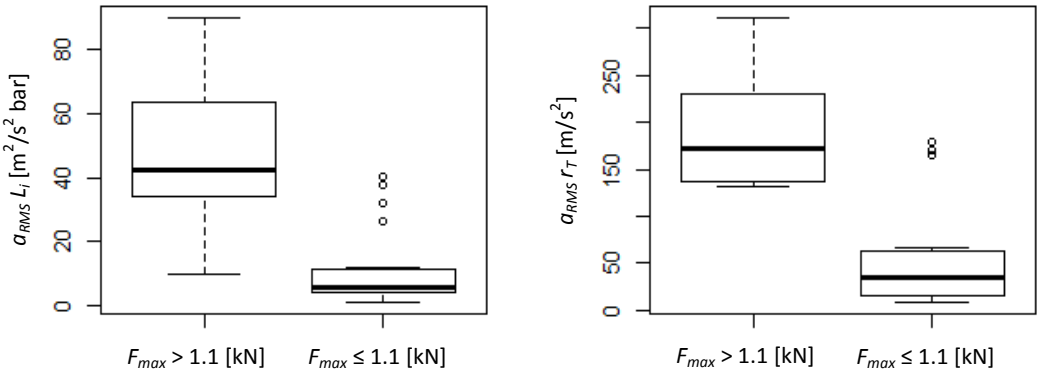


**Figure 4.4.** Boxplots of $a_{RMS}$ $L_i$ and $a_{RMS}$ $r_T$ parameters for the two groups of castings, discriminated on the basis of bending peak load.

It should be noticed that these values are very close to those obtained in the previous Chapter (i.e. $\alpha_0 = 2.41$; $\alpha_1 = 0.01$), where the same geometry and the same alloy were cast with a different machine. The correlation is corroborated by Figure 4.5 which plots the exponential of the average peak load (denoted $F_{max}$) against the RMS acceleration: the central line is the fitting model, while the upper and lower bound lines are the 95% confidence interval.

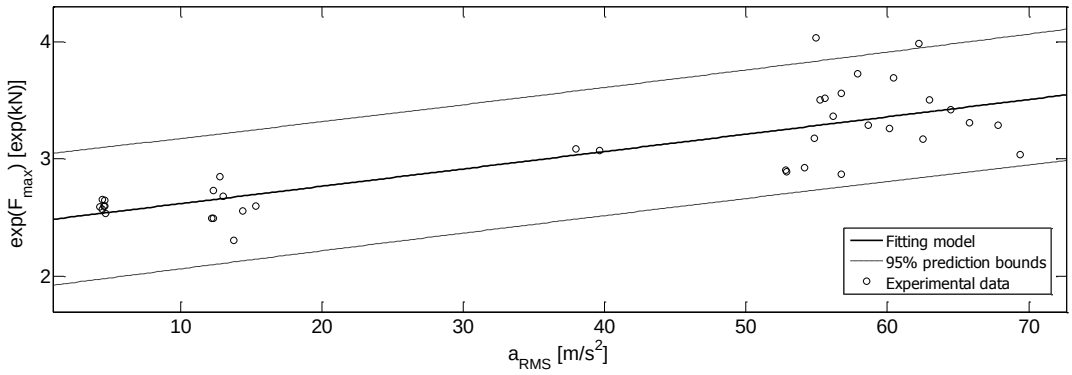


**Figure 4.5.** Bending peak load of the castings as a function of $a_{RMS}$.

If a multivariable regression model is developed, by including simultaneously the two kinematic parameters as the predictors, an appreciable improvement is obtained, by leading to a 0.70 correlation coefficient. The model employed is the following one:

$$exp(F_{max}) = \alpha_0 + \alpha_1 a_{RMS} + \alpha_2 E_f \qquad [4.7]$$

The fitted coefficients for the alloy and the geometry investigated are: $\alpha_0 = 2.43$; $\alpha_1 = 0.01$; $\alpha_2 = 0.44$. Compared with the previous Chapter, the introduction of $E_f$ in the model is reasonable, since such a parameter is significantly independent from $a_{RMS}$, as it is proved by Figure 4.6. Additionally, the boxplots are completely separated for both the parameters (see Figure 4.3). These facts justify the noticeable improvement provided by the multivariable model.

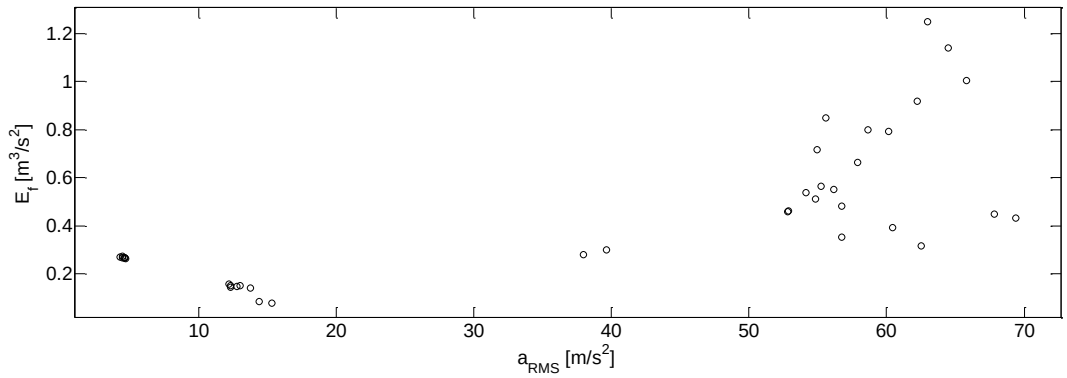


**Figure 4.6.** Independence between $a_{RMS}$ and $E_f$ parameters.

With the aim of improving the models developed so far, by accounting for all the main physical phenomena affecting casting quality, the simultaneous effect of plunger motion profile, pressure and temperature has been evaluated. The inclusion of the two parameters proposed in this Chapter, i.e. $L_i$ and $r_T$, allows further improving the model correctness, by leading to overall 0.89 correlation coefficient. The model has been represented by including $L_i$ and $r_T$ within the coefficients multiplying the two kinematic parameters, as follows:

$$exp(F_{max}) = \alpha_0 + (\alpha_1 + \alpha_3 L_i + \alpha_5 r_T)\, a_{RMS} + (\alpha_2 + \alpha_4 L_i + \alpha_6 r_T)\, E_f \qquad [4.8]$$

This representation has been assumed since the work of the pressure forces and the normalized thermal gradient have a significant influence on the casting quality when combined with the plunger kinematic parameters. The fitted coefficients for the alloy and the geometry investigated are the following ones: $\alpha_0 = 2.40$; $\alpha_1 = -0.02$; $\alpha_2 = 1.54$; $\alpha_3 = 0.02$; $\alpha_4 = -0.88$; $\alpha_5 = 0.01$; $\alpha_6 = -0.11$. It is worth noticing that resulting coefficients multiplying $a_{RMS}$ and $E_f$ are positive, as it was expected. The correlation coefficient obtained is highly satisfactory, since it has been computed through a relevant number of castings (approximately 40 castings), whose large size exacerbates the process variance, due to the uncertainty and disturbance of the uncontrollable and casual exogenous factors usually affecting the HPDC process.
In Figure 4.7, a clear graphical representation of the effect of the two pressure and temperature parameters is proposed, by relating the peak load with the product $a_{RMS}\, L_i\, r_T$ , and then performing fitting:

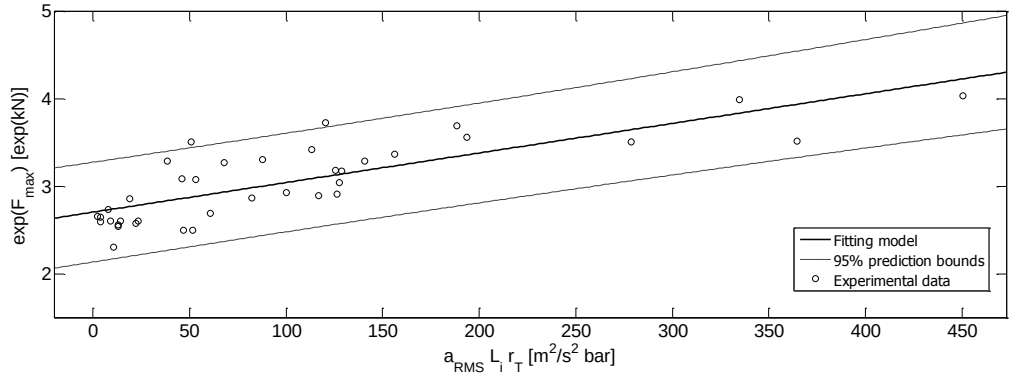


**Figure 4.7.** Correlation between $a_{RMS}\, L_i\, r_T$ and bending peak load.

The proposed parameters are also meaningful if the power model is adopted. Only mono-dimensional or bi-dimensional models are here shown for clarity of representation of the models. In Figure 4.8, the model $F_{max} = \alpha_0 {a_{RMS}}^{\alpha_1}$ with a correlation coefficient of 0.64 is shown.

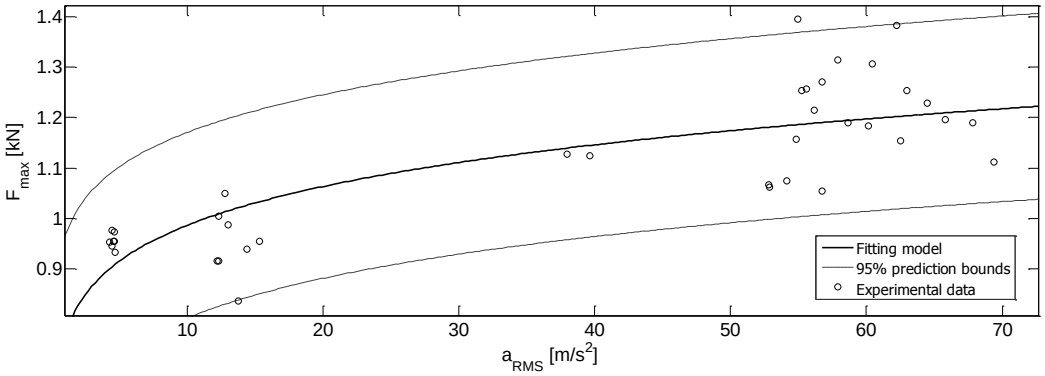


**Figure 4.8.** Power model relating bending peak load of the castings to $a_{RMS}$.

In Figure 4.9, the model $F_{max} = \alpha_0 {E_f}^{\alpha_1}$ with a correlation coefficient of 0.61 is shown.

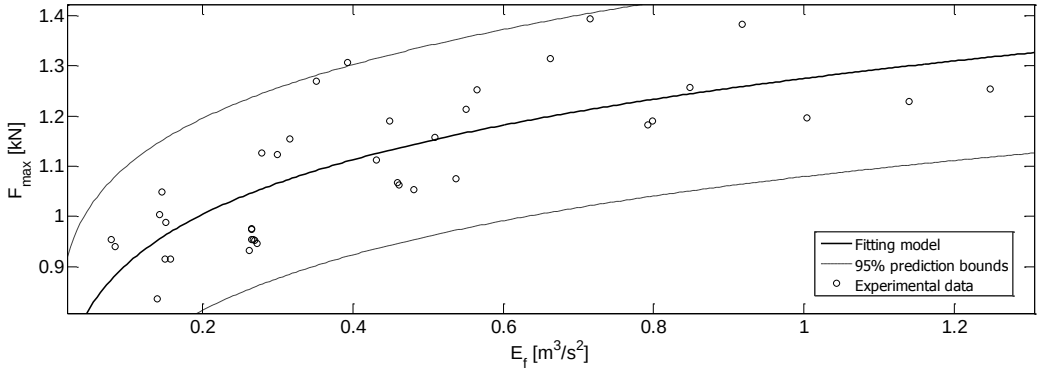


**Figure 4.9.** Power model relating bending peak load of the castings to $E_f$.

Finally, the bi-dimensional model $F_{max} = \alpha_0 {a_{RMS}}^{\alpha_1} E_f^{\alpha_2}$ is represented in Figure 4.10 and the correlation coefficient is 0.76.

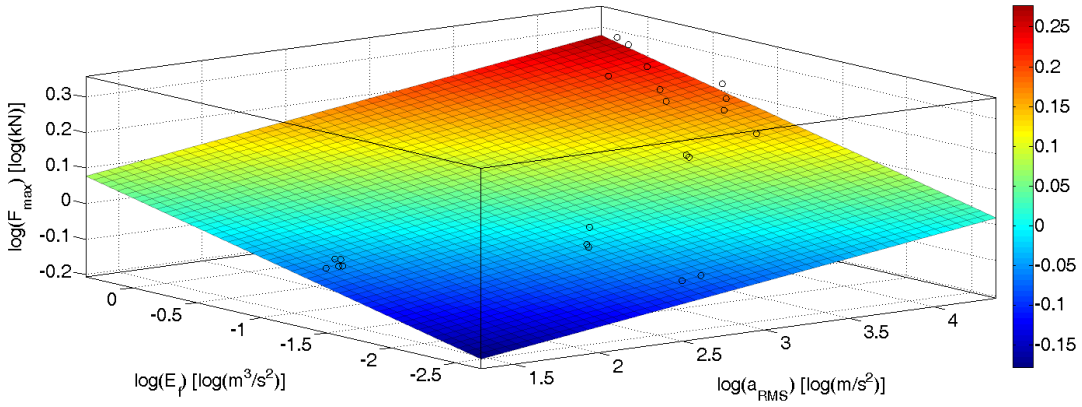


**Figure 4.10.** Power model relating bending peak load of the castings to $a_{RMS}$ and $E_f$.

### *4.3.2.2. Correlation with the density*

In order to find some statistically significant correlations between the proposed parameters and density, the castings have been discriminated in two groups on the basis of their overall density. The first group collects the castings with a density greater than 2.716 g/cm$^3$, while the second one those with an overall density lower or equal to this value. The threshold of 2.716 g/cm$^3$ corresponds to the mean value of all the measured densities, and approaches the theoretical value of density for the used alloy.

The most important boxplots are represented in Figure 4.11. This figure highlights that the work of the pressure forces and the normalized thermal gradient affect the overall density of the castings (referred to as *Density*), since the interquartile ranges of the two groups are evidently distinct.

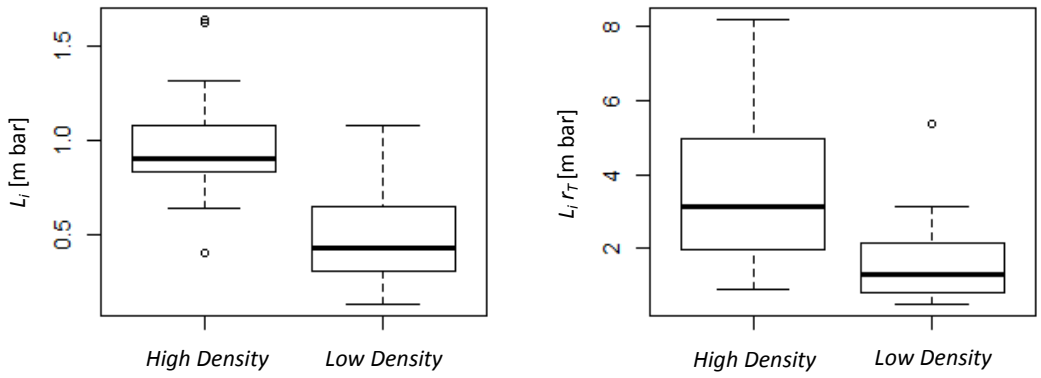


**Figure 4.11.** Boxplots of $L_i$ and $L_i\ r_T$ parameters for the two groups of castings, discriminated on the basis of overall density.

The results of the exploratory analysis have been also confirmed through the t-tests performed on $L_i$ and $L_i\, r_T$, which demonstrate that there is true difference in means between sound and poor castings with 95% confidence interval and p-values are, respectively, $5.26e^{-6}$ and $1.09e^{-3}$. In this case, $L_i$ is the parameter most influencing the overall density of the castings. If a fitting model is assumed, by relating the overall density against the sole work of the pressure forces, a visible correlation is provided (see Figure 4.12). The fitting model acceptably approximates the data distribution, by considering the very low variability of the density values of castings obtained with different process combinations. Indeed, the standard deviation of this measured parameter, between the 40 castings, is 0.0068 g/cm$^3$, that is just the 0.25% of the mean value, while the maximum difference with the mean is just 0.0124 g/cm$^3$.

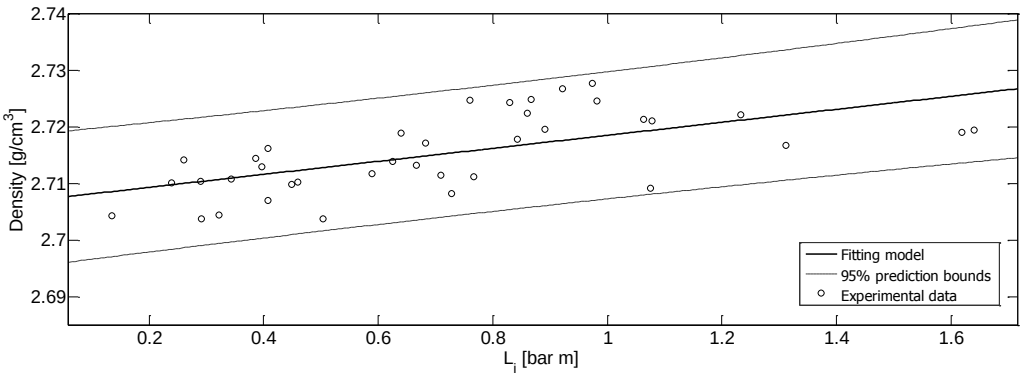


**Figure 4.12.** Overall density of the castings as a function of $L_i$.

If all the four proposed parameters are taken into account in a multivariable model, a significant improvement of the model is obtained, by leading to a 0.67 correlation coefficient. The final model proposed is the following one:

$$log(Density) = \alpha_0 + (\alpha_1 + \alpha_5 r_T)\, a_{RMS} + (\alpha_2 + \alpha_6 r_T)\, E_f + (\alpha_3 + \alpha_4 r_T)\log(L_i) \qquad [4.9]$$

The fitted coefficients for the alloy and the geometry investigated are the following ones: $\alpha_0 = 9.99e^{-1};\ \alpha_1 = 1.43e^{-5};\ \alpha_2 = 3.62e^{-3};\ \alpha_3 = 3.67e^{-3};\ \alpha_4 = 3.43e^{-5};$ $\alpha_5 = -3.64e^{-6};\ \alpha_6 = -2.20e^{-3}$.

The diagnostic plots (Figure 4.13) highlight that this model fits the data well, because the residual plot does not show any pattern, and the quantile-quantile plot shows

normality since its points do not markedly deviate from a straight-line [45]. The conclusions are reliable and convincing, as the results from exploratory and confirmatory analyses agree.

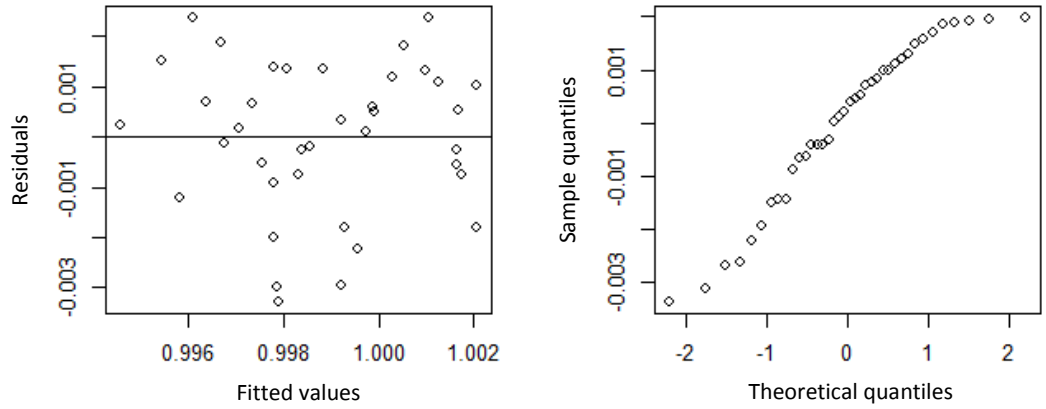


**Figure 4.13.** Residual plot and quantile-quantile plot of the model in Equation [4.9].

### *4.3.2.3. Analysis of the internal and subsurface defects*

As a further evidence of the correctness of the proposed approach in explaining the overall quality of castings, the cross sections along the thickness and the fracture surfaces of some meaningful sample castings have been analysed by optical and scanning electron microscopes (SEM). The aim of this microscopic analysis is to show the simultaneous effect of all the parameters introduced on the presence and severity of defects, by comparing three different combinations of these parameters.

In Table 4.2, the values assumed by the process parameters and the bending peak load of three different castings have been summarized. The marked coloured lines of Table 4.2 correspond to the marked castings in Figure 4.14. The "scrap" and the "sound" castings will be more thoroughly analysed, while just the most important results, providing other insights, will be provided for the "intermediate" one.

**Table 4.2.** Static mechanical property as a function of the novel parameters.

| $a_{RMS}$ [m/s$^2$] | $E_f$ [m$^3$/s$^2$] | $L_i$ [bar m] | $r_T$ [ - ] | $F_{max}$ [kN] |
|---|---|---|---|---|
| 13.73 | 0.14 | 0.34 | 2.26 | 0.84 |
| 62.24 | 0.92 | 1.08 | 5.00 | 1.38 |
| 69.40 | 0.43 | 0.87 | 2.12 | 1.11 |

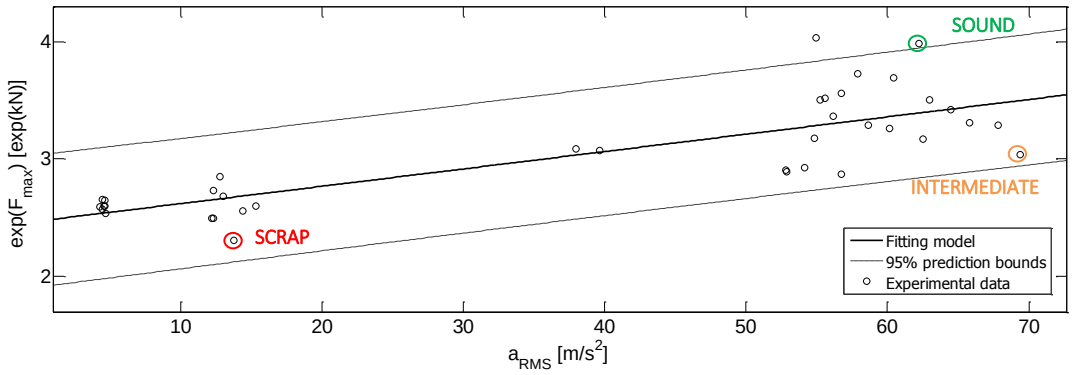


**Figure 4.14.** Bending peak load of the castings as a function of $a_{RMS}$.

In Figure 4.15, optical micrographs of the cross section along the thickness near the fracture surface of a scrap casting (the one in the first line of Table 4.2, with $a_{RMS} = 13.73$ m/s$^2$) and a sound casting (the one in the second line of Table 4.2, with $a_{RMS} = 62.24$ m/s$^2$), respectively, are shown. The microscopic analysis has highlighted that the sound casting shows an uniform microstructure with a low amount of porosity, while the scrap casting shows detrimental porosity (in this case with an average size of 755 μm$^2$), which covers a consistent fraction of the thickness. Magnification of porosity detected in the scrap casting is shown in Figure 4.16.

(a) (b)

**Figure 4.15.** Optical micrographs of the zone near the fracture surface of: (a) a scrap casting ($a_{RMS} = 13.73$ m/s$^2$) and (b) a sound casting ($a_{RMS} = 62.24$ m/s$^2$).

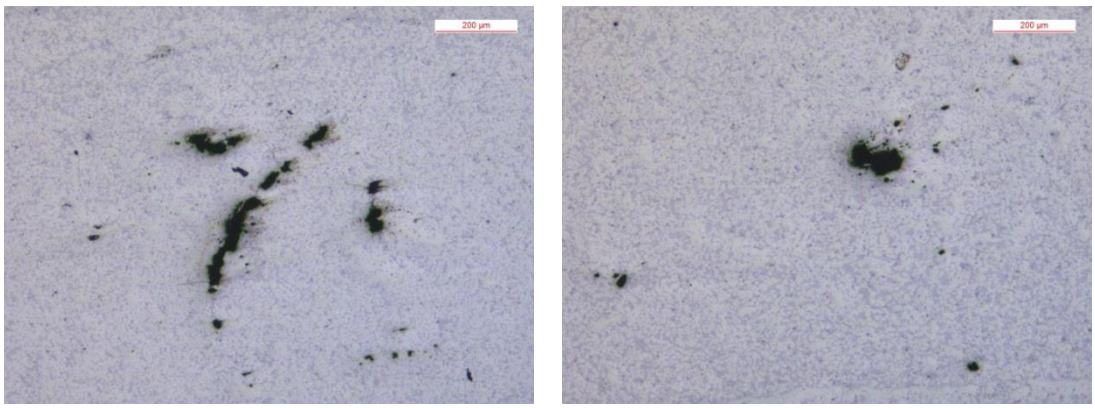

**Figure 4.16.** Optical micrographs at 10x magnification of a scrap casting ($a_{RMS} = 13.73$ m/s$^2$).

SEM micrographs in Figures from 4.17 to 4.19 reveal that the amount and the size of defects on the fracture surface are higher in the case of a scrap casting, justifying its lower bending peak load. Moreover, very large and detrimental oxides are usually located in sub-surface regions in the case of the scrap casting (see Figure 4.18 (a)), by causing its premature failure. In contrast, the fracture surface is more homogeneous and very little defects are usually found in internal regions in the case of the sound casting with a consequent positive effect on the mechanical behaviour (see Figure 4.19).

These findings are consistent with the ideas expressed in the previous Chapter: by increasing $a_{RMS}$ and $E_f$, the overall quality of the castings improves for the same reasons exhaustively explained before.

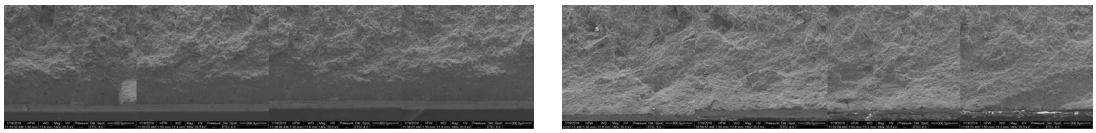

(a) (b)

**Figure 4.17.** SEM micrographs of the fracture surface of: (a) a scrap casting ($a_{RMS} = 13.7$ m/s$^2$) and (b) a sound casting ($a_{RMS} = 62.2$ m/s$^2$).

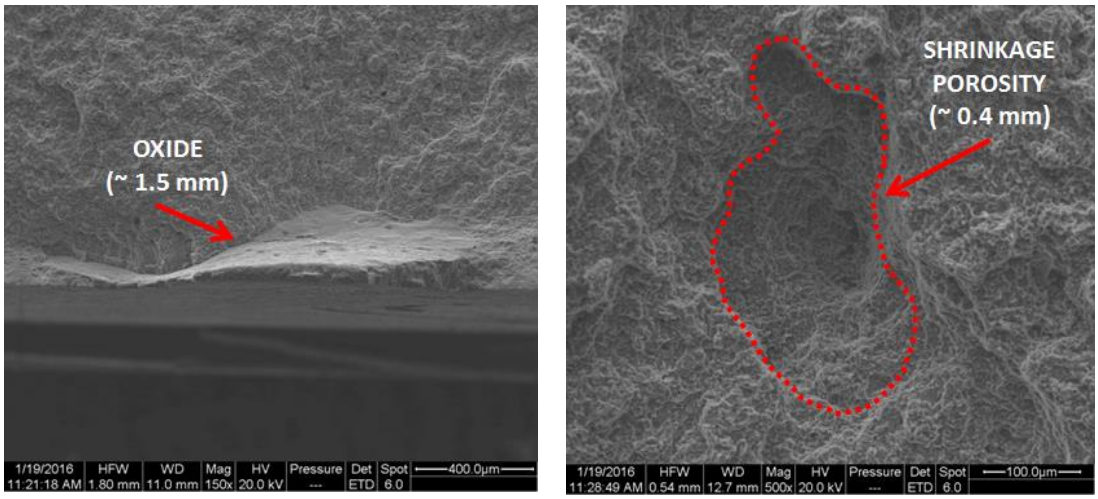


(a) (b)

**Figure 4.18.** SEM micrographs of the fracture surface of a scrap casting ($a_{RMS} = 13.73$ m/s$^2$): (a) 150x magnification of a subsurface oxide and (b) 500x magnification of a shrinkage porosity.

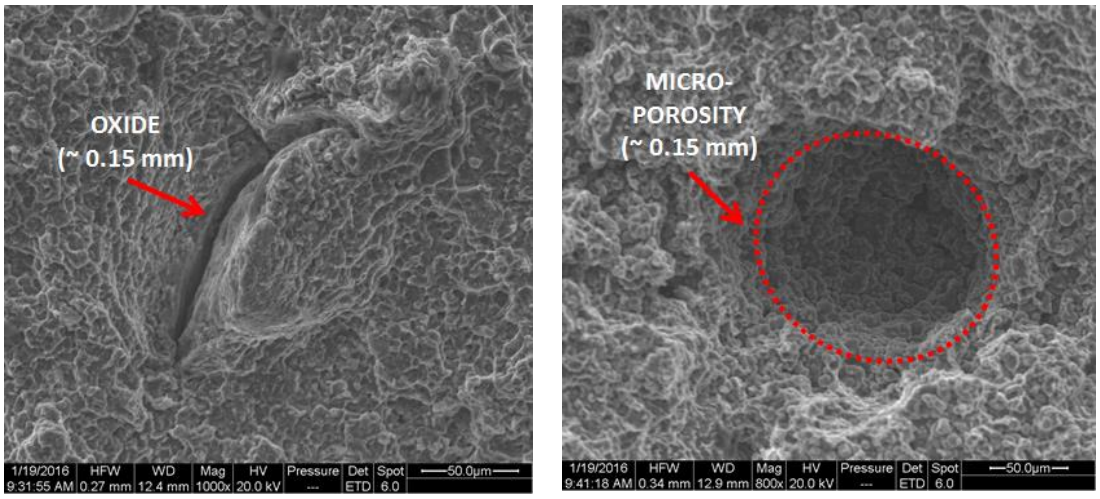


(a) (b)

**Figure 4.19.** SEM micrographs of the fracture surface of a sound casting ($a_{RMS} = 62.2$ m/s$^2$): (a) 1000x magnification of a small internal oxide and (b) 800x magnification of a micro-porosity.

Besides providing a confirmation of the correctness of the plunger kinematic parameters, the further contribution of this Section is to understand the influence of the work of the pressure forces $L_i$ and of the normalized thermal gradient $r_T$ on the internal quality of the analysed castings. For completeness, the thermal parameters of the three castings have been also reported in Table 4.3. In Figure 4.20 (a), the optical micrograph of the scrap casting reveals the presence of evident segregation bands along the subsurface regions of the specimen. These segregation bands are due to the low value of $r_T$ and thus are the consequence of a slow and non-uniform heat removal from surface to internal regions of the casting. As already mentioned before, these segregation bands could inhibit the feeding mechanism of the molten metal, in turns negatively affecting the transmission of the upset pressure.

Another consequence of a low $r_T$ (and hence of an inadequate heat removal) is the risk of hot spots, which determine the formation of shrinkage porosity in the internal regions of the casting, as shown in Figure 4.20 (b) in the case of an intermediate casting (the one in the last line of Table 4.2, with $a_{RMS} = 69.40$ m/s$^2$). However, shrinkage porosity can be avoided by reducing the heat to be removed (and thus reducing the temperature of the melt while keeping high gradient, that means also reducing the temperature of the die within feasible and reasonable values) or partially compensated for high levels of $L_i$. Indeed, shrinkage porosity of the scrap casting is

evidently bigger than the one of the intermediate casting (compare Figures 4.18 (b) and 4.20 (b)).

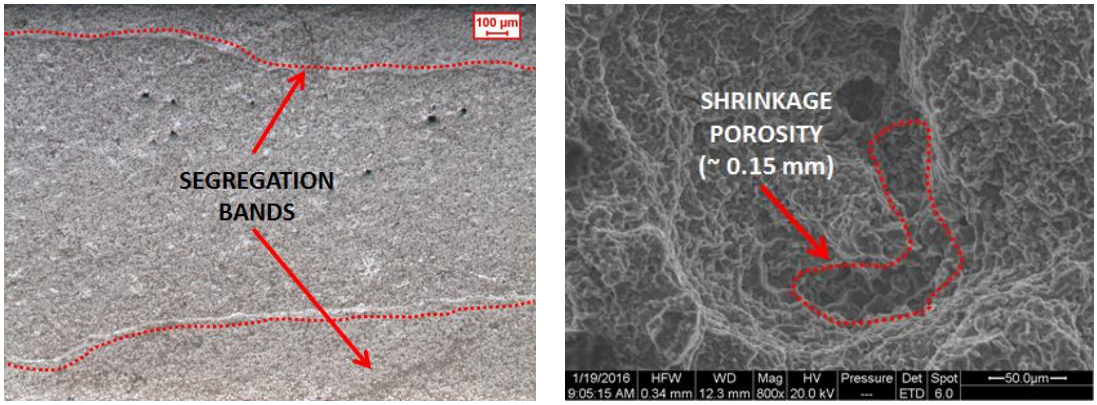


(a) (b)

**Figure 4.20.** (a) Optical micrograph at 25x magnification of a scrap casting showing segregation bands and (b) SEM micrograph at 800x magnification of an intermediate casting showing shrinkage.

**Table 4.3.** Static mechanical property as a function of $a_{RMS}$ and thermal parameters.

| $a_{RMS}$ [m/s$^2$] | $T_{melt}$ [°C] | $T_{die}$ [°C] | $r_T$ [ - ] | $F_{max}$ [kN] |
|---|---|---|---|---|
| 13.73 | 716 | 220 | 2.26 | 0.84 |
| 62.24 | 720 | 120 | 5.00 | 1.38 |
| 69.40 | 687 | 220 | 2.12 | 1.11 |

To summarize, by increasing $L_i$ the upset pressure applied during the third stage is effective in compacting air bubbles and shrinkage porosity, as shown in the cases of the sound and intermediate castings. As for $r_T$, by increasing this parameter both segregation bands and shrinkage porosity are usually limited or absent, as it is the case of the sound casting. Obviously, the simultaneous interaction between all the four parameters proposed has to be taken into account, because the variation of just one of these could significantly influence the microstructural features. However, the most influential parameter is confirmed to be $a_{RMS}$, followed by $E_f$. As already mentioned, the other parameters $L_i$ and $r_T$ play a compensative role in adjusting the prominent effect of the plunger kinematic parameters.

## *4.4. Concluding remarks*

In this Chapter, two relevant pressure and thermal parameters affecting quality of castings have been identified by taking advantage of numerical processing of the plunger hydraulic pressure time-history and by knowing the temperature of the melt and of the die.

The existing literature takes into account the set or maximum value of the upset pressure for investigating its influence on casting quality, neglecting two important aspects. First of all, this approach does not consider the time-variability of such a parameter, which may reach its peak value just for a few time instants. Secondly, it neglects the actual capability of pressure to compact the solidifying melt. Indeed, once the gate becomes fully solid, the pressure from the machine hydraulic system can no longer be transmitted to the metal in the die cavity.

As for thermal aspects, when the molten alloy is in the die cavity, the heat in the alloy should be removed to allow solidification and consequent cooling to occur. This suggests that the die temperature before the injection and the melting temperature can be important parameters to be taken into account when investigating quality of castings.

On the basis of these considerations, the model proposed in Chapter 3 has been further improved by including two other meaningful parameters, describing the effect of the upset pressure and temperature on the final quality of castings.

- The work of the pressure forces in the third stage of the process, $L_i$, which accounts for the actual capability of pressure to compact the solidifying melt. This approach is a generalization of the traditional approach based on investigating the maximum upset pressure. The results provided by the two approaches almost coincide whenever the upset pressure is correctly applied by using closed-loop effective control systems with negligible delay time.
- The normalized thermal gradient, $r_T$, which embodies the concepts of heat removal from the melt and heat flux.

Both the static mechanical property and the overall density of the castings have been related to these novel parameters, which have never been used in literature before. Both the fitting models developed show that the simultaneous use of the four parameters $a_{RMS}$, $E_f$, $L_i$ and $r_T$ as the predictors permits obtaining good correlation coefficients with the experimental data, i.e. 0.89 and 0.67. Although these values do

not approach the ideal target of 1, they are satisfactory, since they have been computed through a relevant number of samples (around 40 castings in this second experimental campaign), whose large size exacerbates the process variance, due to the unavoidable uncertainty and disturbance of the uncontrollable and casual exogenous factors usually affecting the HPDC process.

However, the most influential parameter is confirmed to be $a_{RMS}$, followed by $E_f$. As already mentioned, the other parameters $L_i$ and $r_T$ play a compensative role in adjusting the prominent effect of the plunger kinematic parameters.

# Chapter 5

## Analytical computation of the RMS acceleration

### 5.1. Analytical developments

#### 5.1.1. Motivations

Starting from the results proposed in Chapters 3 and 4, where numerical signal processing was performed on the measured plunger position, the aim of the present Chapter is to propose an analytical method for computing, and hence predicting, the RMS acceleration of the plunger in the fast shot stage, through the plunger displacement curve or just some notable points. The availability of an analytical method to compute such a relevant parameter would allow optimizing the process by selecting in advance the best motion profile of the plunger, to improve the casting properties. This possibility allows accomplishing the last goal of metamodels, as stated in Chapter 2 (see also Figure 2.2), that is the model-based a-priori control of the process.

The theoretical explanation of the method adopted to get the analytical expression of the RMS acceleration, as well as the resulting formulas, are proposed and thoroughly explained in Section 5.1. In Section 5.2, sensitivity analysis provides useful hints to understand the result and to apply this method. The inclusion of limits, due to the characteristics of the injection machine, the alloy and the die, is discussed in Section 5.3. Experimental validation of the method is then described in Section 5.4, to prove its correctness and applicability. Compared with the previous experimental campaigns, different alloy, geometry of the die and injection machine are employed, to show further experimental evidence of the correctness of the proposed parameter. Finally, concluding remarks are discussed in Section 5.5.

### *5.1.2. General hypotheses*

The analytical model for computing the RMS acceleration constitutes another innovative result of this Thesis (see also the papers of the Author [53],[54]).

In order to obtain an analytical expression of the RMS acceleration in the second stage, the typical HPDC process cycle is considered, which includes the constant-speed stage and the high-speed stage. Additionally, in order to provide a more accurate description of the cycle, the initial transient stage for reaching the constant speed is also accounted for (denoted stage 0). In particular, the following motion primitives are assumed for the plunger displacement curve: a parabolic blend (i.e. a speed ramp) in stage 0, a ramp (i.e. constant speed) in stage 1, and finally a $5^{th}$ degree polynomial in stage 2.

Several considerations justify and corroborate the use of a $5^{th}$ degree polynomial displacement curve. First of all, it is in practice frequently adopted in HDPC processes, because of its ease of implementation in the motion controllers driving the injection machine. Secondly, it represents a motion profile that is feasible and consistent with the physic nature of the system, with continuous speed and acceleration curves (contrary with other primitives with discontinuous acceleration, such as for instance the $3^{rd}$ degree polynomial, which do not represent the actual motion). Finally, a $5^{th}$ degree polynomial displacement curve can also effectively approximate other motion profiles, such as sinusoidal ones. As for the primitive adopted in stage 0, although this choice does not affect the final outcome, it is reasonable since speed ramps are usually adopted for this kind of transients.

This cycle should be hence regarded as the "standard cycle", being representative of the vast majority of the cold chamber HDPC processes [55]. A sample curve is also shown in Figure 5.1, with the main definitions adopted for developing the analytical method. In the case slight modifications of the cycle occur, the proposed approach keeps on representing correctly the relative ranking of the RMS acceleration between different sets of process parameters, with just an approximation of the absolute magnitude. Nonetheless, the analytical approach herein suggested can be easily developed for arbitrary processes using other motion profiles (see e.g. those reviewed in [56]). The method should be therefore regarded as a general approach.

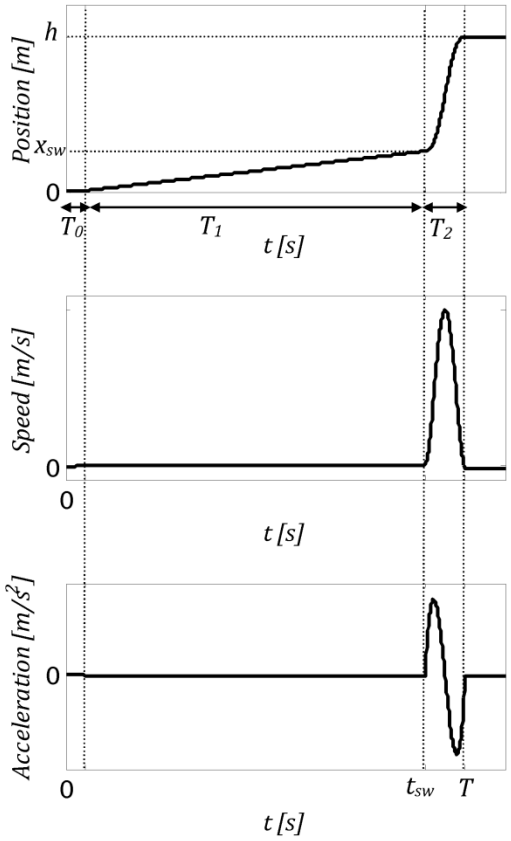


**Figure 5.1.** Position, speed and acceleration of the plunger during the HPDC process: nomenclature used in the analytical model is indicated.

### *5.1.3. Motion primitives and boundary conditions*

The following equations represent the motion model in the three stages, where $T_0$, $T_1$ and $T_2$ are the duration of the three stages ($T_0 + T_1 + T_2 = T$):

$$\begin{cases} x(t) = \frac{1}{2}a_0 t^2 & \dot{x}(t) = a_0 t \quad \ddot{x}(t) = a_0 \quad t \in [0, T_0] \end{cases} \quad [5.1]$$

$$\begin{cases} x(t) = \frac{1}{2}v_1 T_0 + v_1(t - T_0) & \dot{x}(t) = v_1 \quad \ddot{x}(t) = 0 \quad t \in [T_0, T_0 + T_1] \end{cases} \quad [5.2]$$

$$\begin{cases} x(t) = \beta_0 + \beta_1 t_s + \beta_2 {t_s}^2 + \beta_3 {t_s}^3 + \beta_4 {t_s}^4 + \beta_5 {t_s}^5 \\ \dot{x}(t) = \beta_1 + 2\beta_2 t_s + 3\beta_3 {t_s}^2 + 4\beta_4 {t_s}^3 + 5\beta_5 {t_s}^4 \\ \ddot{x}(t) = 2\beta_2 + 6\beta_3 t_s + 12\beta_4 {t_s}^2 + 20\beta_5 {t_s}^3 \quad t \in [t_{SW}, T] \end{cases} \quad [5.3]$$

where $t_s = t - t_{SW}$ is the second-stage shifted time, $t_s \in [0, T - t_{SW}]$.

In Equations [5.1], [5.2] and [5.3], $a_0$ is the constant acceleration during stage 0, $v_1$ is the constant speed during stage 1, $t_{SW} = T_0 + T_1$ denotes the switching time (i.e. the beginning of stage 2). Finally, the unknown scalars $\beta_0, \dots, \beta_5$ are the polynomial coefficients, to be computed on the basis of the following boundary conditions of Equations [5.4], where $h$ is the overall plunger displacement (by neglecting the very exiguous displacement during the third stage of the process):

$$\begin{cases} x(t = t_{SW}) = v_1\left(\frac{T_0}{2} + T_1\right) & \dot{x}(t = t_{SW}) = v_1 & \ddot{x}(t = t_{SW}) = 0 \\ x(t = T) = h & \dot{x}(t = T) = 0 & \ddot{x}(t = T) = 0 \end{cases} \quad [5.4]$$

The solution of the linear system set by the boundary conditions leads to the final analytical computation of the polynomial law ensuring the desired displacement in the desired time $T_2$, with continuous speed and acceleration profiles:

$$\begin{cases} \beta_0 = v_1\left(\frac{T_0}{2} + T_1\right) & \beta_3 = -\frac{v_1}{T_2^3}\left(5T_0 + 10T_1 + 6T_2 - \frac{10h}{v_1}\right) \\ \beta_1 = v_1 & \beta_4 = \frac{v_1}{2T_2^4}\left(15T_0 + 30T_1 + 16T_2 - \frac{30h}{v_1}\right) \\ \beta_2 = 0 & \beta_5 = -\frac{3v_1}{T_2^5}\left(T_0 + 2T_1 + T_2 - \frac{2h}{v_1}\right) \end{cases} \quad [5.5]$$

### *5.1.4. Computation of the RMS acceleration*

The analytical integration of the squared acceleration, obtained by Equations [5.3] and [5.5], and the algebraic manipulation of the results, lead to three equivalent formulations of $a_{RMS}$. Each formulation is suitable for different applications or evaluations.

The first formulation highlights the absolute value of the duration of the three stages, namely $T_0$, $T_1$ and $T_2$, on $a_{RMS}$:

$$a_{RMS} = \sqrt{\frac{30(T_0 v_1 + 2T_1 v_1 - 2h)^2}{7T_2^4} + \frac{60v_1(T_0 v_1 + 2T_1 v_1 - 2h)}{7T_2^3} + \frac{192v_1^2}{35T_2^2}} \quad [5.6]$$

A different formulation can be obtained by using the normalized time of each stage (denoted $\lambda_0$, $\lambda_1$ and $\lambda_2$, with $\lambda_i = T_i/T$) to emphasize how the relative partitioning between the three stages affects the final outcome. Additionally, it is clearly shown the effect of the overall motion time $T$. The new representation is therefore:

$$a_{RMS} = \sqrt{\frac{30}{7}\frac{1}{(\lambda_2 T)^4}[(\lambda_0 + 2\lambda_1)Tv_1 - 2h]^2 + \frac{60}{7}\frac{v_1}{(\lambda_2 T)^3}[(\lambda_0 + 2\lambda_1)Tv_1 - 2h] + \frac{192}{35}\frac{v_1^2}{(\lambda_2 T)^2}} \quad [5.7]$$

The second formulation proposed is typical of the field of motion planning in mechatronic systems and automatic machines [57], and is useful for the practical implementation of the profile in the motion controller of the die casting machine.
Finally, the exact RMS acceleration can be also computed by making explicit the switching position $x_{SW}$ in Equation [5.7]:

$$a_{RMS} = \sqrt{\frac{120(h - x_{SW})^2}{7(\lambda_2 T)^4} - \frac{120v_1(h - x_{SW})}{7(\lambda_2 T)^3} + \frac{192v_1^2}{35(\lambda_2 T)^2}} \quad [5.8]$$

This formulation is suitable for being used by practitioners in foundries, where $x_{SW}$ is usually adopted to plan the plunger motion. Additionally, it allows also getting rid of the lack of information on stage 0 and of any approximation in modelling such a stage.
Equation [5.8] can be further manipulated to obtain an approximate equation, by making explicit the maximum speed in stage 2, which is often denoted $v_2$ and assumed in foundries as a relevant and known parameter. The analytical computation of the maximum speed leads to the following relation:

$$v_2 = \frac{(5T_0v_1 + 10T_1v_1 + 4T_2v_1 - 10h)^3(15T_0v_1 + 30T_1v_1 + 16T_2v_1 - 30h)}{-2000T_2(T_0v_1 + 2T_1v_1 + T_2v_1 - 2h)^3} \quad [5.9]$$

Equation [5.9] can be very precisely approximated through the following simplified relation, with just a negligible error:

$$v_2 \cong \frac{3750(h - x_{SW})}{2000(\lambda_2 T)} - \frac{875 v_1}{2000} \qquad [5.10]$$

On the basis of Equations [5.8] and [5.10], some algebraic manipulations lead to the following approximate formulation of the RMS acceleration:

$$a_{RMS} \cong \sqrt{\frac{512}{105}\frac{v_2^2}{(\lambda_2 T)^2} - \frac{120 v_1 (h - x_{SW})}{7(\lambda_2 T)^3} + \left(\frac{14}{15} + \frac{192}{35}\right)\frac{v_1^2}{(\lambda_2 T)^2}} \qquad [5.11]$$

Equation [5.11] reveals that $a_{RMS}$ is clearly related to the second stage maximum instantaneous speed. However, $v_2$ does not entirely explain the acceleration because of the effect of the duration of the second stage and of the contribution of the term $\frac{120 v_1 (h - x_{SW})}{7(\lambda_2 T)^3}$ which is relevant in the case of very short second stage. This fact allows justifying the conflicting results of the existing literature. Whenever different values of $v_2$ but with similar values of $T_2$ are compared, it is expected that good correlations are obtained also by using $v_2$.

## *5.2. Formula explanation and sensitivity analysis*

On the one hand, all these analytical equations are a powerful and practical tool for optimizing the HPDC process by choosing in advance the best plunger motion profile to improve the quality of castings. On the other, they allow better understanding how the parameter $a_{RMS}$, numerically calculated in previous Chapters 3 and 4, is related in a complicate and non-linear way to the well-known parameters usually adopted in foundries by practitioners, such as $v_1$, $v_2$, $x_{SW}$ and $T$.

In accordance with the notation introduced in Chapter 2, the parameter $a_{RMS}$, which belongs to the set of the transformed one $\boldsymbol{z}$, combines those in $\boldsymbol{x}$ (i.e. the traditional ones, adopted for planning the DOE) in a non-linear and non-intuitive way, on the basis of physical considerations. This transformation replaces high-order fitting functions, which usually cause dangerous overfitting.

Finally, these analytical equations permit easily predicting $a_{RMS}$ and therefore the casting quality by reconstructing plunger motion curves from some notable points or simple information, without the need of additional sensors recording the time-history of the displacement.

Sensitivity analysis of the RMS acceleration formula allows better understanding the complicate relation and proves that just one of the aforementioned "conventional" parameters is not sufficient to explain the casting quality. This fact justifies the presence of conflicting results in the literature, whenever just one of these parameters is accounted for to explain the quality of castings, as discussed in Section 3.1 of this Thesis.

In this Section, a sensitivity analysis is carried out, by taking advantage also of some straightforward graphical representations. The figures proposed show the impact of the modification of one or two parameters in the resulting RMS acceleration. Obviously, the modification of just one or two parameters is not sufficient to explain the final outcome, since the mutual effect of all the parameters should be considered. Indeed, different combinations of all these parameters may lead to the same casting quality since they may determine the same value of $a_{RMS}$.

As it can be noticed in Equation [5.7] and in Figure 5.2, reducing the overall motion time $T$, by keeping the same partitioning between the three stages (i.e. the same $\lambda_0$, $\lambda_1$ and $\lambda_2$), makes $a_{RMS}$ increase approximately with a quadratic behaviour.

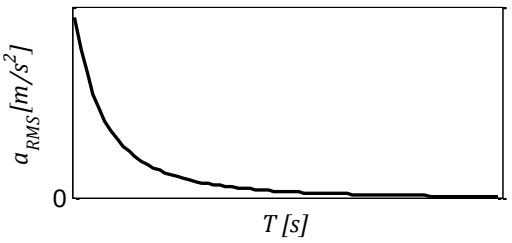


**Figure 5.2.** Effect of $T$ on $a_{RMS}$.

As for the effect of the sole variation of the slow shot speed, $a_{RMS}$ decreases by increasing $v_1$ due to the reduced residual space to cover during stage 2 (see Figure 5.3 (a)). Since $da_{RMS}/dv_1$ is approximately constant, if the other parameters remain unchanged, a quasi-linear relation is established.

The same reason justifies the quasi-linear relation between $a_{RMS}$ and $x_{SW}$, shown in Figure 5.3 (b) (where $x_{SW}$ is normalized with respect to the overall plunger displacement $h$, which is instead a feature of the injection system). Such a figure highlights that by decreasing $x_{SW}$, i.e. by anticipating the switching position between stages 1 and 2, $a_{RMS}$ increases almost linearly, due to the increased residual space to cover in the second stage.

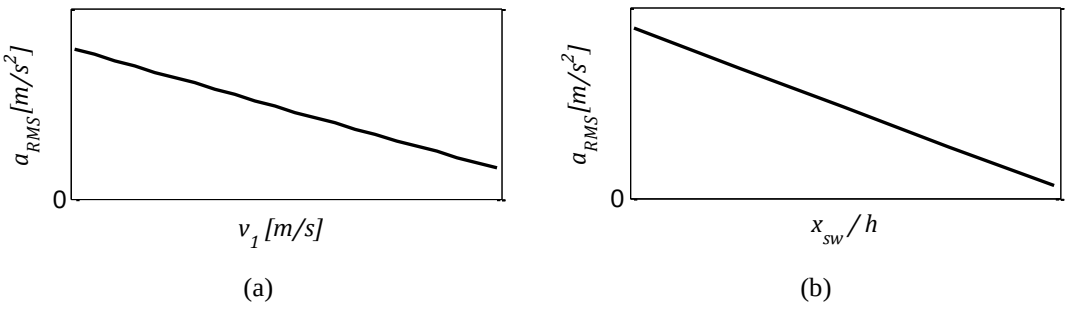


(a) (b)

**Figure 5.3.** (a) Effect of $v_1$ on $a_{RMS}$ and (b) effect of $x_{SW}$ on $a_{RMS}$.

As far as the effect of a variation of the duration of stage 2, expressed in terms of a variation of its normalized value $\lambda_2$, Equations [5.7] and [5.8] reveal that $a_{RMS}$ almost quadratically increases by decreasing $\lambda_2$ (i.e. increasing $\lambda_1$), since the time for performing the displacement in the second stage is smaller. This effect is shown in Figures 5.4 (a) and 5.4 (b), where the curves $a_{RMS}(\lambda_2)$ are respectively parameterized with respect to $v_1$ and $x_{SW}$, by keeping constant all the other parameters.

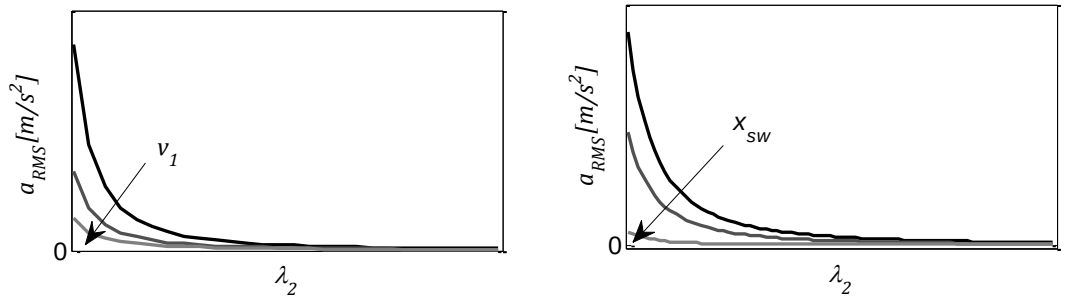


(a) (b)

**Figure 5.4.** (a) Simultaneous effect of $\lambda_2$ and $v_1$ on $a_{RMS}$ and (b) simultaneous effect of $\lambda_2$ and $x_{SW}$ on $a_{RMS}$.

## *5.3. Introduction of constraints*

The sensitivity analysis shows that the time devoted to the second stage, $T_2$ (or equivalently $\lambda_2$) should be reduced to improve the casting quality. Ideally, it should approach the unfeasible value of zero. In practice, it exists a lower bound on the feasible $\lambda_2$, henceforth denoted $\lambda_{2min}$, which depends on different factors due to the injection machine characteristic, the fluid properties (density and viscosity of the alloy), the shape and the size of the die. All these limitations can be summarized in

terms of speed, acceleration and bandwidth (i.e. dynamic response) constraints. The explicit evaluation of maximum feasible speed, acceleration and bandwidth, as functions of the characteristic of the machine, the alloy and the die, goes beyond the aims of this Thesis, and will be subject of future developments. Nonetheless, since these values are often known by practitioners on the basis of the acquired experience, this Section explains how to account explicitly for these constraints.

### *5.3.1. Maximum speed constraint*

Let $v_{LIM}$ be the maximum feasible speed of the injection machine, due to flow limitation of the hydraulic actuator [58]. Then the following constraint should be ensured:

$$v_2 = max\{\dot{x}(t)\} < v_{LIM} \quad [5.12]$$

Equations [5.12] and [5.10] set therefore the following lower bound on $\lambda_2$:

$$\lambda_2 > \frac{3750(h - x_{SW})}{T(2000v_{LIM} + 875v_1)} \quad [5.13]$$

### *5.3.2. Maximum acceleration constraint*

Limits on the maximum force that can be exerted by the plunger define the maximum feasible acceleration $a_{LIM}$:

$$a_{max} = max\{|\ddot{x}(t)|\} < a_{LIM} \quad [5.14]$$

The exact value of the maximum acceleration can be very precisely approximated through the simplified relation [5.15], just providing a small overestimation of the actual maximum acceleration with minor error, thus slightly increasing the safety margin in the computation of the constraint:

$$a_{max} \cong \frac{10}{\sqrt{3}} \frac{(h - x_{SW})}{(\lambda_2 T)^2} \quad [5.15]$$

The following additional lower bound on $\lambda_2$ is set in Equation [5.16]:

$$\lambda_2 > \frac{1}{T}\sqrt{\frac{10(h - x_{SW})}{a_{LIM}\sqrt{3}}} \quad [5.16]$$

### *5.3.3. Bandwidth constraint*

Besides speed and force limitations, dynamic performances of hydraulic servo-controlled actuators are limited by the system bandwidth [58]. Additionally, the underdamped behaviour of the actuator often prevents too fast settling to the desired position. Therefore, the time devoted to the second stage should be greater than the minimum time required to reach and to settle about the target position, which can be estimated in accordance with the control theory as $4.6/(\omega_p \xi_p)$ [s], with $\omega_p$ [rad/s] the minimum bandwidth and $\xi_p$ the minimum damping coefficient of the controlled actuator. The bandwidth constraint can be therefore written through the following inequality:

$$\lambda_2 > \frac{4.6}{T\omega_p \xi_p} \quad [5.17]$$

### *5.3.4. First stage speed constraint*

The result proposed in this Chapter focuses on the second stage, since it has been proved, with a significant statistical analysis, that it is the most influential process stage. Nonetheless, although no statistical correlation has been found between the static mechanical properties and the first stage speed $v_1$ (see [37],[38]), the method here suggested can account also for constraints on $v_1$ that have already appeared in the literature.

The first constraint is related to the existence of an upper bound on $v_1$ [21],[22],[23]. As demonstrated in the work of Zamora et al. [22], if the plunger reaches a speed higher than a certain optimum value during the first stage, the wave of the molten metal will reflect against the chamber ceiling and its forward face might roll over.

On the other hand, $v_1$ should not be reduced excessively, as shown by Nikroo et al. [23], otherwise the maximum wave height will not reach the shot sleeve ceiling and, as a result, some air will remain between the top of the wave and the ceiling. At the later stage in the slow shot stage, the air will change to discrete bubbles mixed with the fluid. A second effect that might occur in the case of too long duration of the

slow shot stage, due to excessively small speed and ineffective feeding of the chamber, is the premature solidification of the melt, which could cause incomplete filling or internal defects [59].

Hence, by introducing the upper and lower bounds on the feasible first stage speed, denoted $v_{1,max}$ and $v_{1,min}$ the following inequalities are posed:

$$v_{1,min} < v_1 < v_{1,max} \qquad [5.18]$$

### *5.3.5. Inclusion of the constraints*

The minimum feasible value of $\lambda_2$ should satisfy simultaneously Equations [5.13], [5.16] and [5.17], whose intersection sets $\lambda_{2min}$. Such a lower bound depends on both the machine limits $(v_{LIM}, a_{LIM}, \omega_p, \xi_p)$ and the cycle parameters $(h, T, x_{SW}, v_1)$. Since the relation between $\lambda_2$ and $a_{RMS}$ is monotonic, the inclusion of the condition $\lambda_2 \geq \lambda_{2min}$ is straightforward and can be also represented graphically (the equality is included in the constraint by assuming that a reasonable safety margin is considered in defining $\lambda_{2min}$).

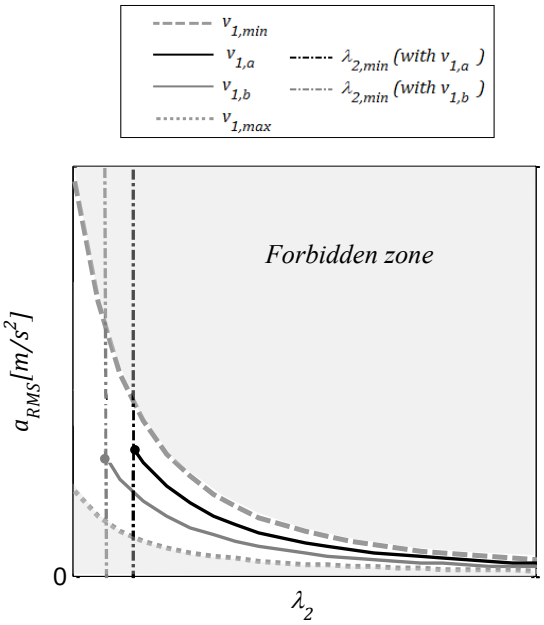


**Figure 5.5.** Graphical inclusion of the constraints.

This is explained in Figure 5.5, where $a_{RMS}(\lambda_2)$ is parameterized as a function of $v_1$, by showing two different sample values of $v_1$ ($v_{1,a} < v_{1,b}$); $T$ and $x_{SW}$ are in contrast assumed as fixed parameters. This representation allows also including the constraint

in Eq. [5.18], by defining two forbidden zones due to $v_{1,min}$ and $v_{1,max}$. The lower bounds on $\lambda_2$ are represented through the dashed-dotted vertical lines. The intersection between $a_{RMS}(\lambda_{2min})$ and the constraint $\lambda_{2min}$ defines the optimal feasible values of $a_{RMS}$ for different first stage speeds, represented through circles in Figure 5.5.

## *5.4. Experimental application of the method*

### *5.4.1. Experimental procedure of the test 3*

In the experimental campaign aimed at applying the method and further validating the effectiveness of the proposed parameter, an Al12Si(Fe) Sr-modified alloy (corresponding to the EN AC-44300 modified aluminium alloy, European designation according to EN 1706:2010) was cast. The die employed was the one designed, build and tested within the frame of NADIA project (New Automotive components Designed for and manufactured by Intelligent processing of light Alloys, EU IPs-SMEs, Contract n. 026563-2, 2006-2010), and has been recently included in CEN/TR 16748 [6] as a reference die. This casting, shown in Figure 5.6, was carefully designed and optimized to maximize the process quality, by reducing the scrap percentage. Hence, this die leads to a reduced variance of the casting quality over a wide range of process parameters, which makes its use a very challenging test to assess the correctness and effectiveness of both the parameter $a_{RMS}$ and of the analytical method proposed in this Chapter. As the horseshoe-shaped casting of Chapters 3 and 4, also this one is representative of the category of thin wall components, since its thicknesses are very low in average.

The castings were manufactured at an industrial plant (Saen S.r.l., Italy) using a 3000 kN cold chamber die-casting machine with shot chamber length 0.3 m and diameter 0.07 m. The furnace was set to 765 °C, while the pouring temperature was approximately 45 °C lower. The shot sleeve and the die were preheated before the experimental campaign until a quasi-steady state temperature of about 200 °C was reached. The temperature of the die was kept constant by a thermoregulation system. Moreover, automatic spraying and blowing processes were performed in order to properly cool down the die material and aid the release of the casting after its complete solidification.

**Figure 5.6.** Reference casting designed to minimize the generation of defects.

Castings were manufactured in accordance with a planned Design of Experiments, based on ensuring a wide range of feasible values of the parameter $a_{RMS}$ from about 20 to 180 m/s$^2$, by changing the constant plunger velocity of the first stage $v_1$, the maximum plunger velocity of the second stage $v_2$, and the switching position between two stages $x_{SW}$. Each independent parameter, called factor, has been analysed within a specific range of variation. The factors, with their lower and upper levels of observation, and respective discretization steps, are given in Table 5.1. The intensification pressure was kept approximately constant at 38 MPa, because this factor is not accounted for in the proposed model. A statistically significant sample was manufactured, i.e. from 5 to 6 repetitions for each combination of parameters (in the whole 60 castings).

**Table 5.1.** Control factors with their lower and upper levels of observation, and discretization values.

| Factor | Low level | High level | Discretization |
|---|---|---|---|
| $v_1$ [m/s] | 0.08 | 0.42 | 0.17 |
| $v_2$ [m/s] | 2.00 | 3.20 | 0.60 |
| $x_{SW}$ [m] | 0.215 | 0.230 | 0.015 |

Tensile test bars with circular cross section, 0.006 m diameter and 0.0325 m gauge length were extracted from the castings and tested without machining. The tests were carried out on a tensile testing machine with a crosshead speed of 2 mm/min. Experimental data have been collected to provide yield strength and ultimate tensile strength of the castings.

### *5.4.2. Results of the method application*

The computation of the RMS acceleration has been performed through the Equation [5.8], i.e. the one based on $v_1$, $x_{SW}$ and $T_2$, which are the values provided in the control and interface panel of the HPDC machine used. In accordance with the model described in Chapters 3 and 4, the following relation has been assumed to fit the experimental data:

$$\sigma = \alpha_0 + \alpha_1 \, log(a_{RMS}) \qquad [5.19]$$

where $\sigma$ denotes the measured tensile properties (namely the yield strength and the ultimate tensile strength), $\alpha_0$ and $\alpha_1$ are two scalar coefficients computed through least-square fitting [44], while the function $log$ denotes the natural logarithm. The use of the logarithm is justified by the decreasing rate of growth of $\sigma$ for increasing accelerations, compared with that of a linear model which is constant. This assumption is evidently reasonable.

The results of the application of the least-square fitting model are shown in the semi-logarithmic plots in Figures 5.7 and 5.8 for, respectively, the yield strength and the ultimate tensile strength of the same specimens. The central lines are the fitting models, while the upper and lower bound lines are the 95% confidence intervals. If a power model is assumed, similar results can be obtained.

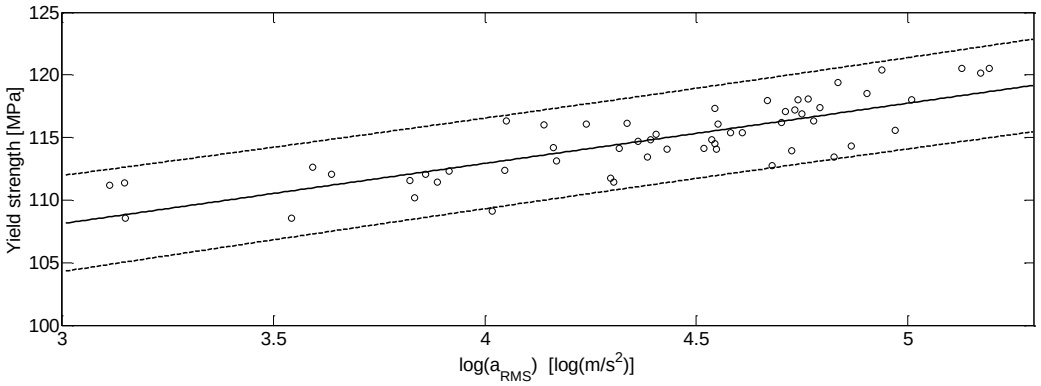


**Figure 5.7.** Correlation between RMS acceleration and yield strength of the castings.

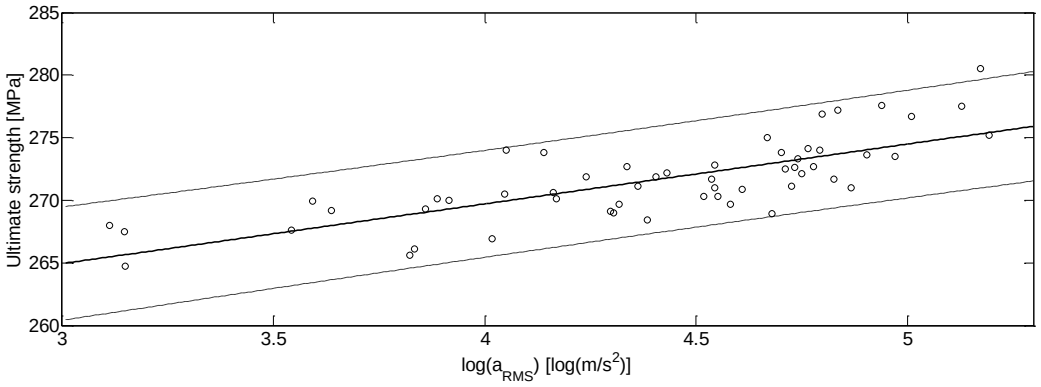


**Figure 5.8.** Correlation between RMS acceleration and ultimate strength of the castings.

Even though the overall range of variation of the tensile properties is not so large, as expected as a consequence of the optimized geometry of the die, the figures clearly show that the models fit accurately the experimental data, and the data trend is evident: the higher $a_{RMS}$, the higher is the static strength. In particular, the fitting models for these two properties approximate the data distribution with correlation coefficients equal to 65% and 58%, respectively. Also the power models confirm these coefficients of correlation. Once again, these values are highly satisfactory, since they have been computed through a relevant number of samples, and in the presence of the unavoidable uncertainty and disturbance of exogenous factors, that affect the HPDC process. Additionally, the mentioned small range of variation of the mechanical properties, due to the particular design of the die, boosts the achievement of correlation coefficients smaller than one. Indeed, as a further proof, small RMS values of the estimation error (i.e. the difference between the fitting model and the measured properties) are obtained, namely 1.78 and 2.09 MPa for, respectively, the yield strength and the ultimate strength. These values correspond to just the 1.5% and 0.7% of the mean measured values of the dependent variables.

Hence, the RMS acceleration in the second stage, computed through the analytical model suggested in this Chapter, allows explaining and predicting effectively the static mechanical properties of the castings.

## *5.5. Concluding remarks*

Given the effectiveness of the parameter $a_{RMS}$, which has been demonstrated to be the most influential one, this Chapter proposes and experimentally validates a method for explaining and predicting the quality of castings as a function of the

plunger displacement curve, thus overcoming the limitations of the traditional approaches based on the extraction of some instantaneous values of directly measured process parameters.

Besides further proving the correctness of the use of the RMS acceleration in the second stage to represent the static mechanical properties, some analytical formulations of such an effective parameter are proposed.

On the one hand, these equations explain the relation with all those parameters usually adopted by practitioners in foundries and suggested in the existing literature, by showing the complicate, and not intuitive, mathematical relation between them and the novel parameter $a_{RMS}$.

On the other hand, they provide an effective and straightforward tool to optimize the process by selecting in advance the set of feasible parameters of the plunger motion profile, that assure higher accelerations and therefore higher tensile strength. Moreover, the availability of analytical equations allows computing the RMS acceleration through just a few information, even in the absence of sensors recording the whole time-history of the plunger.

Sensitivity analysis of the RMS acceleration formula has allowed better understanding the complicate relation and has proved that just one of the "conventional" parameters is not sufficient to explain the casting quality. This fact justifies the presence of conflicting results in the literature, whenever just one of these "conventional" parameters is accounted for to explain the quality of castings, as discussed in Section 3.1 of this Thesis. Indeed, different combinations of all these "conventional" parameters may lead to the same casting quality since they may determine the same value of $a_{RMS}$.

The experimental results of this Chapter corroborate the correctness and the ease of implementation of the proposed method. Compared with the previous experimental campaigns, different alloy, geometry of the die and injection machine are employed, to show further experimental evidence of the correctness and of the general validity of the RMS acceleration.

# *Chapter 6*

## *Analytical computation of the energy of flow forces, and final validation*

## *6.1 Analytical developments*

### *6.1.1. Motivations*

By taking advantage of the possibility to develop analytical relations, as previously proved, this Chapter extends the models developed in Chapter 5 for estimating the parameter denoted $E_f$, which represents the energy of the flow forces proportional to the cubic speed in the whole cycle. These forces are exerted by the liquid melt to solid particles, such as oxides or inclusions, which are known to be preferential nucleation sites for porosity. Hence, it has been proved that higher flow forces, that strive against the nucleation sites for porosity along the whole cycle, would eliminate air bubbles giving reduced porosity.

Once again, the availability of analytical models is a powerful tool for both computing this second influential parameter even in the absence of sensors recording the whole time-history, and for also planning in advance the optimal process parameters.

A second relevant issue is tackled in this Chapter, that is the final stage of the research developed in this Thesis. Since the whole research has been targeted to both the scientific community and practitioners in foundries, the final experimental validation is here proposed through an industrial test case. On the one hand, assessment of the analytical equation is proposed, given the presence of a sensor recording the whole time-history of the plunger position, which was not instead available in the previous Chapter. On the other hand, the novel plunger kinematic parameters developed in this Thesis are again validated through a different test,

involving a different injection machine, a different alloy and a different geometry of the die, having industrial relevance.

In Section 6.1, the main assumptions of the model, the computation and approximate formulation of $E_f$ are described. The experimental validation of the analytical model is reported in Section 6.2, by using a different alloy and the geometry of an industrial casting.

### *6.1.2. Process model*

In order to get the analytical expression of $E_f$, the four stages of a standard (typical) HPDC process are modelled as in previous Chapter. Compared with the previous Chapter, however, the whole cycle will be taken into account in the following developments. In the first three stages, the same motion profiles of previous Chapter have been assumed. In contrast, no motion profile is assumed to model the upset pressure stage, where the controller of the injection machine is switched in pressure control mode to exert the desired pressure after reaching the final position [35].

On the one hand, its contribution is negligible in the computation of $E_f$, since speed approaches zero. On the other, the motion model cannot be predicted a-priori, since the plunger is under pressure (force) control, and hence the speed depends on the resistant forces due to the melt.

### *6.1.3. Computation of $E_f$*

The analytical integration of the cubic speed in the four process stages allows establishing the formulation of $E_f$:

$$E_f = \int_0^{T_0} \dot{x}(t)^3 \, dt + \int_{T_0}^{T_0+T_1} \dot{x}(t)^3 \, dt + \int_{T_0+T_1}^{T_0+T_1+T_2} \dot{x}(t)^3 \, dt + \int_{T_0+T_1+T_2}^{T_3} \dot{x}(t)^3 \, dt \qquad [6.1]$$

where $T_0$, $T_1$, $T_2$ and $T_3$ are the duration of the four stages (see Figure 6.1).

The latter term of the sum in Equation [6.1] can be neglected, since speed in the upset pressure stage approaches zero. In order to make easier the numerical integration, it is employed the shifted time, by taking advantage of this relation:

$$\int_{T_{in}}^{T_{fin}} \dot{x}(t)^3 \, dt = \int_{0}^{T_{fin}-T_{in}} \dot{x}(t+T_{in})^3 \, dt \qquad [6.2]$$

where $T_{in}$ and $T_{fin}$ denote the initial and final time instants of an arbitrary stage, among those in Equation [6.1].

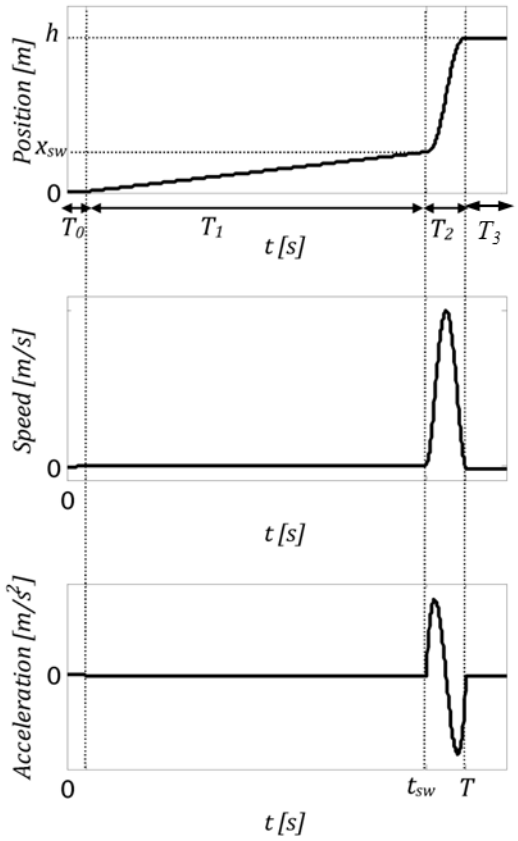


**Figure 6.1.** Position, speed and acceleration of the plunger during the HPDC process: nomenclature used in the analytical model is indicated.

The less relevant contribution of stage 0, $E_{f0}$, is computed as follows:

$$E_{f0} = \int_{0}^{T_0} (a_0 t)^3 \, dt = \frac{a_0^3 {T_0}^4}{4} = v_1^3 \frac{T_0}{4} \qquad [6.3]$$

The contribution of stage 1, $E_{f1}$, is computed as follows:

$$E_{f1} = \int_{0}^{T_1} v_1^3 \, dt = v_1^3 T_1 \qquad [6.4]$$

Finally, the most important contribution of stage 2, $E_{f2}$, is evaluated through the method proposed in Equation [6.2], by integrating the 4th order polynomial representing the speed time-history (see also Equation [5.3]). The solution of the linear system set by the boundary conditions (see [5.4]) leads to the final analytical computation of the polynomial law. Compared with the results in Chapter 5, a slightly different representation of the coefficients is adopted, to make easier the development of the analytical expression of $E_f$, by introducing the displacement required in the second stage $d = h - x_{SW}$:

$$\begin{cases} \beta_0 = x_{SW} & \beta_3 = \dfrac{10d - 6T_2 v_1}{T_2^3} \\ \beta_1 = v_1 & \beta_4 = \dfrac{-15d + 16T_2 v_1}{T_2^4} \\ \beta_2 = 0 & \beta_5 = \dfrac{6d - 3T_2 v_1}{T_2^5} \end{cases} \quad [6.5]$$

By adopting the obtained coefficients, the following integration should be computed:

$$E_{f2} = \int_0^{T_2} \left( v_1 + \frac{30d - 18T_2 v_1}{T_2^3} t^2 + \frac{-60d + 64T_2 v_1}{T_2^4} t^3 + \frac{30d - 15T_2 v_1}{T_2^5} t^4 \right)^3 dt \quad [6.6]$$

The development of Equation [6.6], together with Equations [6.3] and [6.4], leads to the final result:

$$E_f = v_1^3 \left( T_1 + \frac{T_0}{4} \right) + \frac{1}{5005} \left( 11250 \frac{d^3}{T_2^2} - 6150 \frac{v_1 d^2}{T_2} + 2425\, d\, v_1^2 + 452\, T_2 v_1^3 \right) \quad [6.7]$$

A different formulation can be obtained by using the normalized duration of each stage (denoted $\lambda_0$, $\lambda_1$ and $\lambda_2$, with $\lambda_i = T_i/T$) to emphasize how the relative partitioning between the three stages affects the final outcome. Additionally, it is shown the effect of the overall motion time $T$:

$$E_f = v_1^3 \left( T\lambda_1 + \frac{T\lambda_0}{4} \right) + \frac{11250 \dfrac{d^3}{(T\lambda_2)^2} - 6150 \dfrac{v_1 d^2}{T\lambda_2} + 2425\, d\, v_1^2 + 452\, T\lambda_2 v_1^3}{5005} \quad [6.8]$$

As already mentioned in Chapter 3, besides the meaningful physical interpretations discussed, this parameter deserves also a mathematical interpretation that is in accordance with some works proposed in the literature showing that the second stage speed has more influence compared with the one of first stage [41]. Indeed, the presence of the cubic exponent of the speed, gives higher importance to the higher speed values. The proposed parameter is therefore more affected by the second stage speed, and in particular by the peak speed. Nonetheless, in contrast with the traditional methods relying on instantaneous values, it also accounts for the whole time-history of the speed profile.

### *6.1.4. Approximated formulation*

The previous considerations suggest providing an approximate formulation of $E_f$ as a function of the maximum speed in stage 2, which is often denoted $v_2$, and assumed in foundries as a relevant and known parameter. The analytical and exact value of the maximum speed is given by:

$$v_2 = \frac{(2T_2v_1 - 5d)^3(8T_2v_1 - 15d)}{500T_2(-T_2v_1 + 2d)^3} \quad [6.9]$$

Equation [6.9] can be very precisely approximated through the following simplified relation, based on the first-order Taylor's approximation of $T_2v_2$ (with $o(T_2^2)$ as the negligible remainder term):

$$v_2 = \frac{1}{T_2}\left(\frac{\partial(T_2v_2)}{\partial T_2}T_2 + o(T_2^2)\right) \cong 1.875\frac{d}{T_2} - \frac{7}{16}v_1 \quad [6.10]$$

By neglecting $T_2v_1^3$ in Equation [6.7] (since often $T_2 < 1$ s, $v_1 < 1$ m/s and therefore $T_2v_1^3 \ll 1$) and the contribution of the stages 0 and 1, the following approximate formulation is obtained from Equations [6.7] and [6.10]:

$$E_f \approx 0.341\,T_2v_2^3 + 0.344\frac{v_1d^2}{T_2} + 0.117\,v_1^2d \approx 0.341\left(T_2v_2^3 + \frac{v_1d^2}{T_2} + 0.341\,v_1^2d\right) \quad [6.11]$$

This formulation is also useful for practitioners working in foundries, which often plan the motion (or the Design of Experiment) by thinking in terms of peak speed of the second stage.

## *6.2. Experimental application to an industrial case-study*

### *6.2.1. Description of the test case 4*

The experimental campaign proposed in this Chapter has two goals. First, it aims at assessing the method for estimating $E_f$ and $a_{RMS}$, by taking advantage of the recording provided by the position sensor placed on the plunger. Secondly, the correlation with the static mechanical strength measured through tensile test allows further validating the effectiveness of the proposed approach, based on the ideas developed in the previous Chapters with a different alloy, a different injection machine and a different geometry of the die. The latter feature is another add-on of this Chapter, since castings are made through an industrial die, employed for manufacturing the boxes covering the electric motor and the gear in automatic gates. This industrial casting is representative of the category of housings, in accordance with the targets expressed in Chapters 1 and 2. A picture of the casting with evidenced the zones for tensile test is shown in Figure 6.2. Two flat bars with rectangular cross section were drawn in the middle zone of the castings and ultimate tensile strength (UTS) has been measured. The tensile specimens were 87 mm long, 15 mm wide, and 2.6 mm thick, with a gage length of 40 mm and a width of 12 mm.

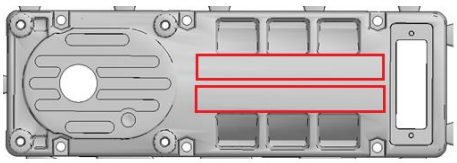

**Figure 6.2.** Geometry of the casting manufactured during the experimental campaign with evidenced the zones for tensile test.

As for the material adopted, it was an Al11Si2Cu(Fe) alloy (corresponding to the EN AB-46100 aluminium alloy, European designation according to EN 1706:2010).

The castings were manufactured at an industrial plant (Rds Moulding Technology S.p.a., Italy) using a 3138 kN cold chamber die-casting machine with shot chamber length 0.380 m and diameter 0.070 m. The initial temperatures of the melt in the

furnace and of the die were around 690 °C and 200 °C, respectively. The pouring temperature of the melt was approximately 40 °C lower.

Castings were manufactured by changing the constant plunger velocity of the first stage $v_1$, the maximum plunger velocity of the second stage $v_2$, and the switching position between two stages $x_{SW}$. Each independent variable has been varied to ensure that $a_{RMS}$, i.e. the most influential among the process parameters, ranges from 25 to 50 m/s$^2$.

### *6.2.2. Parameter computation*

The application of Equation [6.7] has led to the computation of $E_f$, by means of the values of $T_1$, $T_2$, $v_1$, $x_{SW}$. It is worth noticing that these values can be easily extracted by the plunger position time-history, even if they are sometimes available in the control PC (or PLC) panel, without the need of additional sensors. The computation of the RMS acceleration has been performed through the analytical Equation [5.8] proposed in the previous Chapter, by adopting the substitution $d = h - x_{SW}$:

$$a_{RMS} = \sqrt{\frac{120d^2}{7{T_2}^4} - \frac{120v_1 d}{7{T_2}^3} + \frac{192v_1^2}{35{T_2}^2}} \qquad [6.12]$$

Both the results are compared with the numerical values, computed through numerical derivatives and integration. Given the presence of noise in the measured data, in particular because of the rough quantization of the position signal, whose resolution is 1 mm, low-pass filtering has been performed in the numerical derivative. The filtering has caused a slight underestimation of the two parameters computed through numerical signal processing, compared with the ones calculated through analytical equations, because of the smoothing of the speed and acceleration peaks (see also Appendix B for more details on this topic). Nonetheless, the analytical and the numerical values are in excellent agreement, as shown in Figure 6.3. Just a couple of outliers are present, due to noisy measurements.

Even in this experimental campaign, the correlation between the two plunger kinematic parameters and the tensile strength (calculated as mean value between the two specimens) is confirmed, by leading to an overall 0.80 correlation coefficient if the model $exp(UTS) = \alpha_0 + \alpha_1 a_{RMS} + \alpha_2 E_f$ is employed. In contrast, if just the

mono-dimensional model relating the $exp(UTS)$ with $a_{RMS}$ is adopted, as reported in Figure 6.4, the correlation coefficient is 0.75.

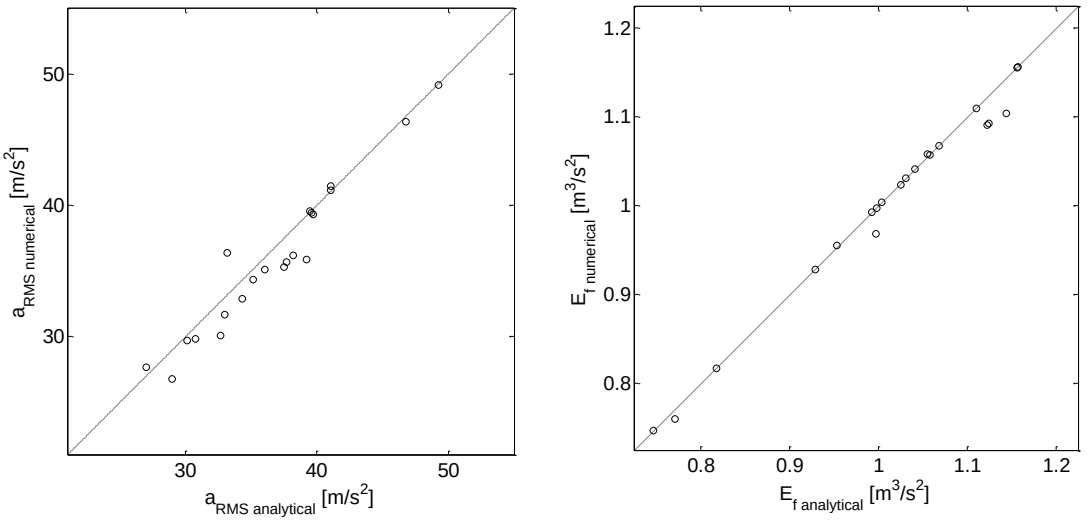


(a) (b)

**Figure 6.3.** Correlation between analytical and numerical $a_{RMS}$ (a) and $E_f$ (b).

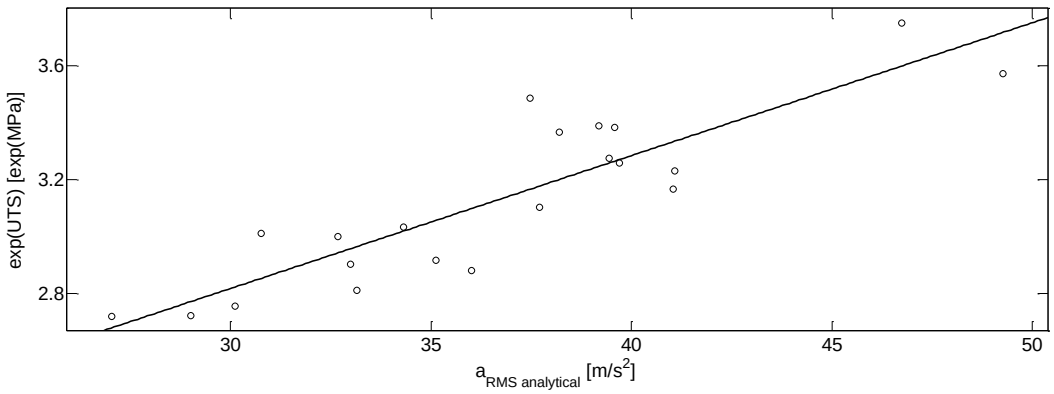


**Figure 6.4.** Correlation between $a_{RMS}$ and ultimate tensile strength (UTS) of the castings.

## *6.3. Concluding remarks*

With the aim of improving the analytical model developed in Chapter 5, some analytical formulations of the energy associated to the flow forces are here developed and exhaustively explained. Indeed, it has been demonstrated in Chapters 3 and 4 that $a_{RMS}$ and $E_f$ are the most influential parameters on the casting quality. Hence, this Chapter proposes and experimentally validates a method for explaining and predicting the quality of castings as a function of the plunger displacement curve,

thus overcoming the limitations of the traditional approaches based on the extraction of some instantaneous values of directly measured process parameters.

Besides explaining the relation with all those parameters usually adopted by practitioners in foundries and suggested in the existing literature, the equations proposed are an effective tool to optimize the process by selecting in advance the best motion profile, which guarantees sound castings. Moreover, the availability of analytical equations allows computing the kinematic parameters through just a few information, even in the absence of sensors recording the whole time-history of the plunger.

The experimental campaign described in this Chapter corroborates the correctness and the ease of implementation of the analytical models, and the significance of the plunger kinematic parameters. Compared with the previous experimental campaigns, different alloy, geometry of the die and injection machine are employed, to show further experimental evidence of the general validity of the developed approach. It is worth noticing that the geometry used in this Chapter corresponds to an industrial housing, which demonstrates the correctness and the validity of the proposed methodology even in the presence of more complicate and real dies.

# *Chapter 7*

## *Conclusions*

The in-field survey questionnaire addressed to European foundries and the literature review carried have highlighted that HPDC still needs both new standards and effective tools for improving and optimizing its outcomes. A thorough study and approach have been carried out in this Thesis to tackle both these issues.

The starting point to tackle the problem is the deep knowledge of the metallurgical origin of the main kinds of defects. For this reason, new and systematic classifications of defects and of reference dies have been firstly developed, and then published as CEN Technical Reports, to satisfy the need of foundry for new standards.

The main contribution of this Thesis is the subsequent development of an original and comprehensive methodology for representing the complicate relations between process parameters and casting quality, as a response to the second requirement for HPDC improvement. A new path for the synthesis of effective behavioural models (metamodels) has been outlined and experimentally validated. Hence, some novel process parameters have been defined and extracted from the measured signals, by taking advantage of either signal processing techniques or of analytical equations. The identification of the most relevant physical phenomena affecting the final casting quality and their translation into scalar representative parameters, has been the crux of the research. In particular, an effective representation of the process has been proved to be achieved through four meaningful parameters defined as follows:

- the root mean square acceleration of the plunger in the second stage;
- the energy associated to the flow forces in the whole cycle;
- the work of the pressure forces in the third stage;
- the normalized thermal gradient.

These parameters are representative of different and relevant physical phenomena all along the injection cycle, such as forces exerted, mechanical energy exchange, heat removal, and also account for the integral nature of the HPDC process.

With the aim of validating thoroughly the developed process parameters, four experimental campaigns have been executed, by using different injection machines, different alloys and different geometries of the die. In particular, an optimized die, a defect-generating die and an industrial one have been employed in order to evaluate the quality of castings over remarkably different conditions. The quality of the castings have been assessed through bending peak load, tensile strength, percentage of porosity, density, percentage of oxides and internal defects. Property measurements and metallographic analysis corroborate the proposed method. Additionally, rigorous statistical concepts allow drawing conclusions about the population, by taking advantage of the large size of the sample investigated (overall 210 castings).

Given the prominent role of the plunger motion in affecting the casting quality, analytical models of the plunger kinematic parameters have been suggested and experimentally validated to extended the process optimization towards the issues of planning and control of the injection machine. These analytical models permit selecting in advance the best plunger motion for obtaining sound and reliable castings, by also accounting for the feasibility constraints posed by the injection machine. Moreover, these analytical models allow explaining the relationship between the traditional kinematic parameters, usually used in foundries by practitioners and proposed in the previous literature, and the newly defined parameters, which represent the most influential physical phenomena and the integral nature of HPDC. The analytical models demonstrate that the simultaneous interaction between the traditional kinematic parameters should be accounted for, because the investigation of just one parameter is not enough in explaining and predicting the casting quality.

# *Appendix A*

## *European foundry questionnaire*

This appendix encloses the text of the survey questionnaire carried out for investigating the needs of the foundry industries, as discussed in Chapter 1.

# Questionnaire on use and possible introduction of EU Standards in Al alloys foundries

***SECTION ADDRESSED TO FOUNDRIES***

NOTE:

All the information implemented will be anonymously processed in view of the targets of StaCast Project. The results of statistics elaboration from data will be made available to all persons which answered to the questionnaire.

## *1 - Company Information and Profile*

1.1) Company name

1.2) Contact name

1.3) E-mail

1.4) Phone number

1.5) Company type : O SME O IND

*SME: <250* employees; turnover < 50 million Euro/year

*IND: > 250* employees; turnover > 50 million Euro/year

## *2 - General Data on Production*

2.1) Annual production (ton/year)

O <1000 O 1001 to 3000 O 3001 to 5000 O 5001 to 10.000 O >10.000

2.2) Which is the main production process in your foundry?

O HPDC O Gravity / LPDC

2.3) Alloys used

- O EN AC-42100 [Al-Si7-Mg0,3]
- O EN AC-42200 [Al-Si7-Mg0,6]
- O EN AC-43200 [Al-Si10-Mg(Cu)]
- O EN AC-43400 [Al-Si10-Mg(Fe)]
- O EN AC-44300 [Al-Si12(Fe)]
- O EN AC-44400 [Al-Si9]
- O EN AC-46000 [Al-Si9-Cu3(Fe)]
- O EN AC-46100 [Al-Si11-Cu2(Fe)]
- O EN AC-46200 [Al-Si8-Cu3]
- O EN AC-46500 [Al-Si9-Cu3(Fe)(Zn)]
- O EN AC-47100 [Al-Si12-Cu1(Fe)]
- O EN AC-51200 [Al-Mg9]
- O EN AB-44000 [Al-Si11]
- O EN AB-44100 [Al-Si12]
- O EN AB-46300 [Al-Si7-Cu3-Mg]
- O EN AB-48000 [Al-Si12-Cu-Ni-Mg]
- O EN AB-71100 [Al-Zn10-Si8-Mg]
- O Other (specify)

2.4) Other alloys : _____

2.5) Applications: *(Max 2 choices)*

O Automotive O Mechanical Engineering O Electronics O Architecture and Design O Other

2.6) Casting Categories

Main category:

- O Thin wall components
- O Safety components
- O Housings
- O Engine blocks
- O Other_____

Secondary category:

- O Thin wall components
- O Safety components
- O Housings
- O Engine blocks
- O Other_____

## *3- CEN Standards*

CEN Standards adopted and used in your company:

- O EN 1559-1 Founding - Technical conditions of delivery - Part 1: General
- O EN 1559-4 Founding - Technical conditions of delivery - Part 4: Additional requirements for aluminium alloy castings
- O EN 1676 Al and Al alloys - Alloyed aluminium ingots for remelting - Specifications
- O EN 1706 Aluminium and aluminium alloys - Castings - Chemical composition and mechanical properties
- O EN 1780-1 Aluminium and aluminium alloys - Part 1: Numerical designation system
- O EN 1780-2 Aluminium and aluminium alloys - Part 2: Chemical symbol based designation system
- O EN 1780-3 Aluminium and aluminium alloys - Part 3: Writing rules for chemical composition
- O EN 12258-1 Aluminium and aluminium alloys - Terms and definitions - Part 1: General terms
- O EN 12258-2 Aluminium and aluminium alloys - Terms and definitions - Part 2: Chemical analysis
- O EN 12681 Founding - Radiographic examination
- O EN 14361 Aluminium and aluminium alloys - Chemical analysis - Sampling from metal melts
- O None of the abovementioned ones

## *4 - Need for new European Standards*

Please specify your interest for having new European Standards in the field of Aluminium alloys cast products:

- New CEN Standard about Classification of casting defects

O Very High O High O Average O Low O No interest

- New CEN Standard about mechanical properties of Al-based casting alloys

O Very High O High O Average O Low O No interest

- New CEN Standard about mechanical properties of Al-based castings

O Very High O High O Average O Low O No interest

- New CEN Standard and/or Guidelines on Al-based cast products design

O Very High O High O Average O Low O No interest

## *5 – Defect analysis*

For each type of defect, tick the applied methods of control specifying if they are carried out on 100% of castings or on a statistical basis.

Main categories of defects:

**5.1) Gas/Air Porosity (air, hydrogen, vapour, lubricant entrapment)**

| | | | |
|---|---|---|---|
| *Visual control (non-destructive testing)* | O 100% of the production | O Statistical sample | O Not used |
| *X Ray inspection (X-ray inspection, CT scan)* | O 100% of the production | O Statistical sample | O Not used |
| *Leak tightness* | O 100% of the production | O Statistical sample | O Not used |
| *Density* | O 100% of the production | O Statistical sample | O Not used |
| *Liquid penetrant (Dye or fluorescent penetrant)* | O 100% of the production | O Statistical sample | O Not used |
| *Ultrasonic testing* | O 100% of the production | O Statistical sample | O Not used |
| *Destructive testing (machining, sawing, metallography, fractography)* | O 100% of the production | O Statistical sample | O Not used |

Is this type of defect measured and/or quantified ? O Yes O No

**5.2) Inclusions (oxide skins, refractory, ...)**

| | | | |
|---|---|---|---|
| *Visual control (non-destructive testing)* | O 100% of the production | O Statistical sample | O Not used |
| *X Ray inspection (X-ray inspection, CT scan)* | O 100% of the production | O Statistical sample | O Not used |
| *Leak tightness* | O 100% of the production | O Statistical sample | O Not used |
| *Density* | O 100% of the production | O Statistical sample | O Not used |
| *Liquid penetrant (Dye or fluorescent penetrant)* | O 100% of the production | O Statistical sample | O Not used |
| *Ultrasonic testing* | O 100% of the production | O Statistical sample | O Not used |
| *Destructive testing (machining, sawing, metallography, fractography)* | O 100% of the production | O Statistical sample | O Not used |

Is this type of defect measured and/or quantified ? O Yes O No

**5.3) Shrinkage (macro-shrinkage, micro-shrinkage/interdendritic)**

| | | | |
|---|---|---|---|
| *Visual control (non-destructive testing)* | O 100% of the production | O Statistical sample | O Not used |
| *X Ray inspection (X-ray inspection, CT scan)* | O 100% of the production | O Statistical sample | O Not used |
| *Leak tightness* | O 100% of the production | O Statistical sample | O Not used |
| *Density* | O 100% of the production | O Statistical sample | O Not used |
| *Liquid penetrant (Dye or fluorescent penetrant)* | O 100% of the production | O Statistical sample | O Not used |
| *Ultrasonic testing* | O 100% of the production | O Statistical sample | O Not used |
| *Destructive testing (machining, sawing, metallography, fractography)* | O 100% of the production | O Statistical sample | O Not used |

Is this type of defect measured and/or quantified ? O Yes O No

**5.4) Cracks (Hot tears, cracks)**

| | | | |
|---|---|---|---|
| *Visual control (non-destructive testing)* | O 100% of the production | O Statistical sample | O Not used |
| *X Ray inspection (X-ray inspection, CT scan)* | O 100% of the production | O Statistical sample | O Not used |
| *Leak tightness* | O 100% of the production | O Statistical sample | O Not used |
| *Density* | O 100% of the production | O Statistical sample | O Not used |
| *Liquid penetrant (Dye or fluorescent penetrant)* | O 100% of the production | O Statistical sample | O Not used |
| *Ultrasonic testing* | O 100% of the production | O Statistical sample | O Not used |
| *Destructive testing (machining, sawing, metallography, fractography)* | O 100% of the production | O Statistical sample | O Not used |

Is this type of defect measured and/or quantified ? O Yes O No

**5.5) *Filling-related* (cold joint, lamination, cold shot)**

| | | | |
|---|---|---|---|
| *Visual control (non-destructive testing)* | O 100% of the production | O Statistical sample | O Not used |
| *X Ray inspection (X-ray inspection, CT scan)* | O 100% of the production | O Statistical sample | O Not used |
| *Leak tightness* | O 100% of the production | O Statistical sample | O Not used |
| *Density* | O 100% of the production | O Statistical sample | O Not used |
| *Liquid penetrant (Dye or fluorescent penetrant)* | O 100% of the production | O Statistical sample | O Not used |
| *Ultrasonic testing* | O 100% of the production | O Statistical sample | O Not used |
| *Destructive testing (machining, sawing, metallography, fractography)* | O 100% of the production | O Statistical sample | O Not used |

Is this type of defect measured and/or quantified ? O Yes O No

**5.6) *Metal-die interaction* (soldering, ejection mark, thermal fatigue...)**

| | | | |
|---|---|---|---|
| *Visual control (non-destructive testing)* | O 100% of the production | O Statistical sample | O Not used |
| *X Ray inspection (X-ray inspection, CT scan)* | O 100% of the production | O Statistical sample | O Not used |
| *Leak tightness* | O 100% of the production | O Statistical sample | O Not used |
| *Density* | O 100% of the production | O Statistical sample | O Not used |
| *Liquid penetrant (Dye or fluorescent penetrant)* | O 100% of the production | O Statistical sample | O Not used |
| *Ultrasonic testing* | O 100% of the production | O Statistical sample | O Not used |
| *Destructive testing (machining, sawing, metallography, fractography)* | O 100% of the production | O Statistical sample | O Not used |

Is this type of defect measured and/or quantified ? O Yes O No

## *6 – Specify the frequency of the defects*

| | | | | |
|---|---|---|---|---|
| Porosity | O Never | O Occasionally | O Frequently | O Very frequently |
| Inclusions | O Never | O Occasionally | O Frequently | O Very frequently |
| Shrinkage | O Never | O Occasionally | O Frequently | O Very frequently |
| Cracks | O Never | O Occasionally | O Frequently | O Very frequently |
| Filling defects | O Never | O Occasionally | O Frequently | O Very frequently |
| Metal-die interaction | O Never | O Occasionally | O Frequently | O Very frequently |

# *Appendix B*

## *Fundamentals of signal processing in metallurgical data analysis*

### *B.1. Motivations*

As discussed along the Thesis, the possibility to exploit signal processing techniques allows enlarging the set of parameters adopted to predict the casting quality and hence to optimize and to monitor the process. The traditional approaches, both used in foundry and proposed in the quoted literature, do not exploit such a tool since they basically rely on instantaneous values of measured variables, as already discussed. In contrast, the original approach proposed and validated in this Thesis takes advantage of numerical signal processing in order to:

- compute physical signals that are not directly measured, such as speed and acceleration, although it could be done by employing additional sensors (such as accelerometers);
- compute the "integral" physical quantities that cannot be measured, such as the root mean square acceleration, the energy of flow forces and the work of pressure forces.

This Appendix briefly describes the main methodologies and algorithms to perform such a computation, to provide the reader useful hints to apply effectively the method.

### *B.2. Causal vs. non-causal processing*

A scheme for signal processing (such as for filtering or differentiating a signal) is said to be "causal" if the output values of the algorithm depend only on the past and

the present input values, while do not depend on the future input values (i.e. of the measured signal). Hence, a causal system is non-anticipative.

In contrast, a numerical scheme is said to be "non-causal" if the output values depend also on some future input values. Thus, a non-causal algorithm is anticipative.

In real-time signal processing, future input values are not yet known. Therefore, real-time computation must thus be causal. However, in the case of off-line post-processing of the measured and stored data, it is possible to use future signal values together with current and past values to compute an output signal. This opportunity allows taking advantage of the negligible time delay introduced through the use of non-causal schemes, which provide therefore more reliable results for the purpose of the work. In contrast, causal schemes introduce delay since they just account for past samples.

This Appendix will focus, therefore, on some non-causal signal processing schemes. The extension to causal schemes, for instance whenever the proposed method would be adopted for on-line real-time control, as suggested in Chapter 2, is quite easy.

## *B.3. Data filtering*

### *B.3.1. Overview*

The measured signals provided by the sensors installed to monitor HPDC process are usually affected by noise, due to both electrical disturbances and, in particular, to round-off and truncation errors caused by quantization in the analog-to-digital conversion or due to sensor resolution. The latter problem has been shown to be not negligible in the measurements adopted in this work, in particular for the position whose resolution is 1 mm in most of the experimental campaigns.

High noise-to-signal ratio can negatively affect the numerical computation of the proposed parameters, by introducing error in their values. The problem is exacerbated because of the need to further numerical processing of the measured data, in particular in the case of numerical derivative (as discussed in the related Section B.4). It is therefore necessary adopting some techniques to improve the numerical analysis and to get rid of noise. Several tools are available, and have been therefore applied, as described in the following Sections.

### *B.3.2. Decimation and issues related to the sample time*

Digital data provided by the sensor measurement are usually recorded with high frequency rates, to represent correctly the "fast" dynamics, and hence fast variation of the measured signal. On the other hand, in the case of "slow" variations of the physical quantity to be measured, the presence of rough measurement resolution may lead to visible step variations of the measured signal. Indeed, the sensors cannot detect a variable changing unless it is bigger than its resolution. Therefore, the slow-varying digital measured signals will have a lot of repeated samples, followed by a step. Whenever these sharp signal changes are numerically differentiated, some spikes will appear in the derivative signal.

To reduce this problem occurring because of the simultaneous presence of high-frequency and low-resolution measurements, the measured data should be decimated, by reducing in practice the sample rate of the signals to be processed. Indeed, as proved in [60] the quantization error of the derived signal is proportional to the sampling frequency. Hence, doubling the step size doubles the attenuation of the noise by halving the noise magnitude.

The application of this concept in HPDC analysis should account for two conflicting requirements. On the one hand, the sample time should be small enough to represent correctly the rapid changes in speed and in acceleration in the second stage. In particular, acceleration rises quickly from zero (at the end of the first stage) to its positive peak value (at about one quarter of the second stage), and then decreases quickly to reach its negative peak. On the other, the third stage would require low frequency sampling, to represent correctly the slow motion. It is worth noticing that the approximation adopted in Equation [4.4] to compute the work of the pressure forces in such a stage, i.e. parameter $L_i$, is aimed at overcoming such an issue without excessively reducing the sample time.

A similar issue would arise if temperature measurements are of interest, e.g. for an estimation of thermal gradients, cooling rate, which are however not investigated in this Thesis. Given the high thermal time constant of the system, the rate of change of temperature is low, and therefore it is useless reducing excessively the sampling time.

### *B.3.3. Low-pass filters*

Low-pass filtering has been performed to remove high frequency noisy components in the signal to be numerically differentiated. In practice, low-pass filters retain the part of signal of interest, such as for example the dynamics related to the actual plunger motion, while remove noise components.

Among the different techniques that are proposed in the literature on signal processing, the moving average is the most common low-pass filter, because of its simple formulation, intuitive tuning, and also effectiveness [61].

Basically, the moving average filter operates by averaging a number $N+1$ of samples from the original (input) signal $x$ to compute the filtered signal $x^F$ (output) at each time step. By assuming a non-causal formulation, and by weighing the different components with a set of non-negative and normalized weights $w$ ($\sum_{i=k-N/2}^{k-N/2} w_i = 1$), the following numerical scheme has been adopted and implemented:

$$x_k^F = \sum_{i=k-N/2}^{k-N/2} x_i \, w_i \qquad \text{[B.1]}$$

In Equation [B.1], $x_k^F$ denotes the $k^{th}$ sample of the filtered signal, i.e. the one at time $k\,\Delta t$ (that is the current instant), while $x_i$ denotes the $i^{th}$ sample of the input signal $x$, i.e. the one at time $i\,\Delta t$.

As an effective choice, the weight can define a rectangular window (i.e. identical weights for all the samples), as well as a trapezoidal and symmetric window. The latter approach has been followed in this work, as often done in practice, since better noise smoothing capability, together with less distortion of the part of signal of interest are obtained.

As for the number of samples to be averaged, the higher $N$ is, the more the noise is filtered. At the same time, however, increasing $N$ causes underestimation of the signal peaks and smooths the signal edges, such as step-like variation, even when these fast changes are real. The selection of $N$ should be therefore carefully performed, with a trial-and-error tuning.

### *B.3.4. Median filters*

A different tool adopted for reducing noise in the measured data is the use of median filters to remove spikes and sharp peaks, as those due to numerical derivatives of step-like signals, that can negatively affect the computation of the process parameters. Median filters replace the samples of the signal to be filtered with the median value within of a set of $N$ values. This set includes an odd number of samples (both past and future samples, centred about the current sample) including the current sample itself. This kind of non-causal filter is more suitable than low pass-filters for removing signal outliers. Indeed, a median filter removes noise, while the low-pass filter just spreads it around [62].

## *B.4. Numerical derivatives*

Both the speed, adopted to estimate the flow force energy, and the acceleration, to which RMS value is then computed, are calculated through first and second numerical derivatives of the measured position, whose signal is assumed to be sampled with the sample time $\Delta t = 1/f_s$ ($f_s$ is the sampling frequency).

Numerical differentiation is the numerical estimation of derivatives of an unknown function from some discrete, and usually noisy, measurement data. It has attracted a lot of attention in the literature on signal processing because of two main critical issues that impose particular attention in its implementation:

- the computed numerical derivative may be delayed, compared with the "actual" (the "exact") derivative;
- numerical differentiation is ill-posed, since small high-frequency noise components in the measured data usually induce large errors in the approximate derivatives.

To overcome the first issue, as stated in Section B.2, the use of non-causal schemes, also denoted "centred schemes" is suggested in the case of post-processing, as developed in this Thesis. As for the second issue, a proper selection of the numerical algorithm should be instead done, in accordance with the characteristics of the measured data and with the aim of the computation.

Among the several approaches proposed in the literature for numerical derivative, at least two families of techniques should be mentioned:

- finite difference techniques and
- smooth noise-robust differentiators.

Finite difference techniques (also denoted central difference) are the classical approach. These schemes are simple approximations of the definition of time-derivative, and aim at approximating the exact derivate in the low frequency range. Therefore, they are not suitable for smoothing the high frequency noise. For this reason, they are not suitable for the purpose of this Thesis, since the data measured in the experimental campaigns were affected by significant noise (mainly due to the low sensor resolution, and hence to the quantization noise).
Their main formulations are briefly recalled in Equation [B.2] for different number of points (i.e. the number of samples adopted to compute the derivative):

$$\dot{x}_k = \frac{x_{k+1} - x_{k-1}}{2\Delta t}$$

$$\dot{x}_k = \frac{-x_{k+2} + 8x_{k+1} - 8x_{k-1} + x_{k-2}}{12\Delta t} \qquad \text{[B.2]}$$

$$\dot{x}_k = \frac{x_{k+3} - 9x_{k+2} + 45x_{k+1} - 45x_{k-1} + 9x_{k-2} - x_{k+3}}{60\Delta t}$$

In Equation [B.2], $x_k$ denotes the $k^{th}$ sample, i.e. the one at time $k\,\Delta t$, that is the present (current) instant.

In contrast with finite difference techniques, smooth noise-robust differentiators are aimed at being as close as possible to the response of an ideal differentiator in the low frequency region, while providing noise smoothing (filtering) in the high frequency. Therefore, they are more suitable for the purpose of this research. Among the different algorithms, the 5$^{th}$ and 7$^{th}$ order Lanczos low-noise differentiators have been found to be effective [63].
Their main formulations are briefly recalled in Equation [B.3] for different number of points:

$$\dot{x}_k = \frac{2x_{k+2} + x_{k+1} - x_{k-1} - 2x_{k-2}}{10\Delta t}$$

$$\dot{x}_k = \frac{3x_{k+3} + 2x_{k+2} + x_{k+1} - x_{k-1} - 2x_{k-2} - 3x_{k-3}}{28\Delta t} \quad \text{[B.3]}$$

$$\dot{x}_k = \frac{4x_{k+4} + 3x_{k+3} + 2x_{k+2} + x_{k+1} - x_{k-1} - 2x_{k-2} - 3x_{k-3} - 4x_{k-4}}{60\Delta t}$$

Among the different schemes proposed, the selection should account for the fact that higher number of points provides better noise filtering, and therefore the numerical scheme behaves also as a low-pass (non-causal) filter. However, for the purpose of the work, it should be considered that much high number of points causes two drawbacks, that may negatively affect the result:

- peaks may be smoothed, by leading to a slight underestimation of their values. This is of interest for the computation of both $a_{RMS}$ and $E_f$. Indeed, peak values are magnified by the power in the formulation of both the parameters (respectively the second and the third power);
- in the acceleration signal, computed through the second derivative of the position, the second stage of HPDC process may apparently begin earlier than its actual start (because of the causal terms in the derivation schemes), while it may apparently end later than its actual end (because of the non-causal terms). This can be revealed through a slight shift between position, speed and acceleration signals. The main effect is that the second stage duration $T_2$ may be slightly overestimated (unless it is compensated), by introducing errors in the computation of $a_{RMS}$ through the analytical equations.

In this Thesis, in order to trade-off between the conflicting requirements of noise filtering and peak preservation, it has been employed the improved 7$^{th}$ order Lanczos low-noise differentiator in the first three tests (see Chapters 3, 4 and 5). Indeed, this scheme allows an excellent trade-off between several requirements, and is also often adopted in the literature (see e.g. [39]). In contrast, the fourth test (see Chapter 6) employs the 5$^{th}$ order scheme, which has showed to provide more effective computation for such a test case.

## *B.5. Numerical integrations*

Numerical integration has been employed in this research to compute the novel parameters introduced. The main issue in performing this computation is that numerical integration may cause unrealistic drifts in the integrated signal, in the case of long-lasting and noisy signal (i.e. the introduction of a fictitious trend in the integral). In contrast with the numerical derivative, numerical integration introduces low frequency errors, that affect the final value of the computed signal.

Hence, the selection of the most suitable integration schemes is often challenging.

In this work, since short time intervals are considered in the computation of integrals, it has been verified through extensive analysis that numerical integration is a much more well-posed problem than numerical differentiation. The selected algorithm is therefore the trapezoidal rule, which merges good performances and low computational effort, in accordance with the following recursive scheme:

$$I_k = I_{k-1} + \Delta t \frac{x_k + x_{k-1}}{2} \qquad [B.4]$$

where $I_k$ is the integral value at time $k\ \Delta t$, while $x_k$ is the integrand, i.e. the signal to be integrated. In practice, such a method performs a straight-line interpolation between two consecutive samples of the integrand, to approximate the actual continuous signal.

# *References*


[1] Wang, L., Turnley, P., & Savage, G. (2011). Gas content in high pressure die castings. Journal of Materials Processing Technology, 211(9), 1510-1515.

[2] Francis, J. A., & Cantin, G. D. (2005). The role of defects in the fracture of an Al–Si–Mg cast alloy. Materials Science and Engineering: A, 407(1), 322-329.

[3] Bonollo, F., Fiorese, E., Timelli, G., Arnberg, L., & Adamane, A. R. (2014). StaCast Project: from a Survey of European Aluminium Alloys Foundries to New Standards on Defect Classification and on Mechanical Potential of Casting Alloys. 71st World Foundry Congress, 19-21 May 2014, Bilbao (Spain).

[4] Bonollo, F., Fiorese, E., Timelli, G., Arnberg, L., & Adamane, A.R. (2014). StaCast: linee guida per la progettazione di getti in lega di alluminio. La Metallurgia Italiana: 10, 63-71.

[5] PD CEN/TR 16749: 2014. Aluminium and aluminium alloys. Classification of defects and imperfections in high pressure, low pressure and gravity die cast products, 1-41.

[6] PD CEN/TR 16748: 2014. Aluminium and aluminium alloys. Mechanical potential of Al-Si alloys for high pressure, low pressure and gravity die casting. 1-24.

[7] BS EN 12258-1:2012. Aluminium and aluminium alloys. Terms and definitions. General terms.

[8] Gariboldi, E., Bonollo, F., & Parona, P. (2010). Handbook of Defects in HPDC, 1st ed. (Milano: Associazione Italiana di Metallurgia).

[9] Fiorese, E., Bonollo, F., Timelli, G., Arnberg, L., & Gariboldi, E. (2015). New classification of defects and imperfections for aluminum alloy castings. International Journal of Metalcasting, 9(1).

[10] Fiorese, E., Bonollo, F., Battaglia, E., & Cavaliere, G. (2016). Improving die casting processes through optimization of lubrication. Paper accepted for publication in International Journal of Cast Metals Research.

[11] Winkler, M., Kallien, L., & Feyertag, T. (2015). Correlation between process parameters and quality characteristics in aluminum high pressure die casting. NADCA Die Casting Congress and Exposition.

[12] Adamane, A. R., Arnberg, L., Fiorese, E., Timelli, G., & Bonollo, F. (2015). Influence of injection parameters on the porosity and tensile properties of high-pressure die cast Al-Si alloys: a review. International Journal of Metalcasting, 9(1), 43-53.

[13] Syrcos, G. P. (2003). Die casting process optimization using Taguchi methods. Journal of materials processing technology, 135(1), 68-74.

[14] Verran, G. O., Mendes, R. P. K., & Dalla Valentina, L. V. O. (2008). DOE applied to optimization of aluminum alloy die castings. Journal of materials processing technology, 200(1), 120-125.

[15] Gunasegaram, D. R., Finnin B. R., & Polivka, F. B. (2007). Melt flow velocity in high pressure die casting: Its effect on microstructure and mechanical properties in an Al-Si alloy. Materials Science and Technology, 23(7), 847-856.

[16] Lumley, R., Deeva, N., & Gershenzon, M. (2011). An evaluation of quality parameters for high pressure die castings. International Journal of Metalcasting, 37-56.

[17] Chiang, K. T., Liu, N. M., & Tsai, T. C. (2009). Modeling and analysis of the effects of processing parameters on the performance characteristics in the high pressure die casting process of Al–SI alloys. The International Journal of Advanced Manufacturing Technology, 41(11-12), 1076-1084.

[18] Cao, Y., Guo, Z., & Xiong, S. (2012, July). Determination of the metal/die interfacial heat transfer coefficient of high pressure die cast B390 alloy. In IOP Conference Series: Materials Science and Engineering (Vol. 33, No. 1, p. 012010). IOP Publishing.

[19] Krimpenis, A., Benardos, P. G., Vosniakos, G. C., & Koukouvitaki, A. (2006). Simulation-based selection of optimum pressure die-casting process parameters using neural nets and genetic algorithms. The International Journal of Advanced Manufacturing Technology, 27(5-6), 509-517.

[20] Zheng, J., Wang, Q., Zhao, P., & Wu, C. (2009). Optimization of high-pressure die-casting process parameters using artificial neural network. The International Journal of Advanced Manufacturing Technology, 44(7-8), 667-674.

[21] Garber, L. W. (1982). Theoretical analysis and experimental observation of air entrapment during cold chamber filling. Die Casting Engineer, 26(3), 14-15.

[22] Zamora, R., Faura, F., López, J., & Hernández, J. (2007). Experimental verification of numerical predictions for the optimum plunger speed in the slow phase of a high-pressure die casting machine. The International Journal of Advanced Manufacturing Technology, 33(3-4), 266-276.

[23] Nikroo, A. J., Akhlaghi, M., & Najafabadi, M. A. (2009). Simulation and analysis of flow in the injection chamber of die casting machine during the slow shot stage. International Journal of Advanced Manufacturing Technology, 41, 31-41.

[24] Cleary, P. W., & Ha, J. (2002). Three-dimensional smoothed particle hydrodynamics simulation of high pressure die casting of light metal components. Journal of Light Metals, 2(3), 169-183.

[25] Yi, H. E., Zhou, Z. Y., Cao, W. J., & Chen, W. P. (2011). Simulation of mould filling process using smoothed particle hydrodynamics. Transactions of Nonferrous Metals Society of China, 21(12), 2684-2692.

[26] Hehenberger, P., Follmer, M., Geirhofer, R., & Zeman, K. (2013). Model-based system design of annealing simulators. Mechatronics, 23(3), 247-256.

[27] Anglada, E., Meléndez, A., Vicario, I., Arratibel, E., & Cangas, G. (2015). Simplified models for high pressure die casting simulation. Procedia Engineering, 132, 974-981.

[28] Simpson, T. W., Poplinski, J. D., Koch, P. N., & Allen, J. K. (2001). Metamodels for computer-based engineering design: survey and recommendations. Engineering with computers, 17(2), 129-150.

[29] Wang, G. G., & Shan, S. (2007). Review of metamodeling techniques in support of engineering design optimization. Journal of Mechanical Design, 129(4), 370-380.

[30] Kleijnen, J. P. (1986). Statistical tools for simulation practitioners. Marcel Dekker, Inc..

[31] The Mathworks, Matlab’s Curve Fitting Toolbox User's Guide, The MathWorks Inc., USA.

[32] White, H. (1989). Learning in artificial neural networks: A statistical perspective. Neural computation, 1(4), 425-464.

[33] Tu, J. V. (1996). Advantages and disadvantages of using artificial neural networks versus logistic regression for predicting medical outcomes. Journal of clinical epidemiology, 49(11), 1225-1231.

[34] Bonollo, F., Gramegna, N., & Timelli, G. (2015). High-Pressure Die-Casting: Contradictions and Challenges. JOM, 67(5), 901-908.

[35] Thibault, C., & Funke, M. (2000). Closed-loop control improves die-casting performance. Hydraulics & pneumatics, 53(10), 51-54.

[36] Dargusch, M. S., Dour, G., Schauer, N., Dinnis, C. M., & Savage, G. (2006). The influence of pressure during solidification of high pressure die cast aluminium telecommunications components. Journal of materials processing technology, 180(1), 37-43.

[37] Fiorese, E., & Bonollo, F. (2015). Process parameters affecting quality of high-pressure die-cast Al-Si alloy. Proceedings of 8th European Metallurgical Conference 2015, 14-17 June 2015, Düsseldorf (Germany).

[38] Fiorese, E., & Bonollo, F. Plunger kinematic parameters affecting quality of high pressure die cast Al-Si alloy. Paper submitted to Metallurgical and Materials Transactions A.

[39] Palomba, I., Richiedei, D., & Trevisani, A. (2014). In: P. Sas, H. Denayer and D. Moens (Eds.), Proceedings of 26th International Conference on Noise and Vibration Engineering (ISMA), 2014, Leuven, Belgium, 2899-2914.

[40] Wu, S., Xie, L., Zhao J., & Nakae, H. (2008). Formation of non-dendritic microstructure of semi-solid aluminum alloy under vibration. Scripta Materialia, 58, 556-559.

[41] Dour, G., Dargusch, M., Davidson, C., & Nef, A. (2005). Development of a non-intrusive heat transfer coefficient gauge and its application to high pressure die casting: effect of the process parameters. Journal of Materials Processing Technology, 169(2), 223-233.

[42] Merritt, H. E. (1967). Hydraulic control systems. John Wiley & Sons.

[43] Montgomery, D. C., & Runger, G. C. (2010). Applied statistics and probability for engineers. John Wiley & Sons.

[44] Faraway, J. J. (2014). Linear models with R. CRC Press.

[45] Wu, L. (2009). Mixed effects models for complex data. CRC Press.

[46] VDG Specification (2010). Examples of microstructures with different pore contents. BDG-Reference Sheet, 1-24.

[47] Verran, G. O., Mendes, R. P. K., & Rossi, M. A. (2006). Influence of injection parameters on defects formation in die casting Al12Si1,3Cu alloy: Experimental results and numeric simulation. Journal of materials processing technology, 179(1), 190-195.

[48] Otarawanna, S., Laukli, H. I., Gourlay, C. M., & Dahle, A. K. (2010). Feeding mechanisms in high-pressure die castings. Metallurgical and Materials Transactions A, 41(7), 1836-1846.

[49] Kittur, J. K., Choudhari, M. N., & Parappagoudar, M. B. (2015). Modeling and multi-response optimization of pressure die casting process using response surface methodology. The International Journal of Advanced Manufacturing Technology, 77(1-4), 211-224.

[50] Tsoukalas, V. D. (2008). Optimization of porosity formation in AlSi 9 Cu 3 pressure die castings using genetic algorithm analysis. Materials & Design, 29(10), 2027-2033.

[51] Hamasaiid, A., Dour, G., Dargusch, M. S., Loulou, T., Davidson, C., & Savage, G. (2008). Heat-transfer coefficient and in-cavity pressure at the casting-die interface during high-pressure die casting of the magnesium alloy AZ91D. Metallurgical and Materials Transactions A, 39(4), 853-864.

[52] Natchtwey, Peter E. (2009). Fluid Power Motion Control – A Guide to Practical Design, Delta Computer Systems 2nd Edition.

[53] Fiorese, E., Richiedei, D., & Bonollo, F. (2015). Analytical computation of the plunger kinematic parameters affecting quality in HPDC. Proceedings of International CAE Conference 2015, 19-20 October 2015, Pacengo del Garda (Italy).

[54] Fiorese, E., Richiedei, D., & Bonollo, F. Improving the quality of die castings through optimal plunger motion planning: analytical computation and experimental validation. Paper submitted to International Journal of Advanced Manufacturing Technology.

[55] Jiang, J. F., Ying, W. A. N. G., & Qu, J. J. (2014). Effect of process parameters on microstructure and properties of AM50A magnesium alloy parts formed by double control forming. Transactions of Nonferrous Metals Society of China, 24(2), 321-333.

[56] Gasparetto, A., Boscariol, P., Lanzutti, A., & Vidoni, R. (2015). Path Planning and Trajectory Planning Algorithms: A General Overview. In Motion and Operation Planning of Robotic Systems (pp. 3-27). Springer International Publishing.

[57] Caracciolo, R., & Richiedei, D. (2014). Optimal design of ball-screw driven servomechanisms through an integrated mechatronic approach. Mechatronics, 24(7), 819-832.

[58] Richiedei, D. (2012). Synchronous motion control of dual-cylinder electrohydraulic actuators through a non-time based scheme. Journal of Control Engineering and Applied Informatics, 14(4), 80-89.

[59] Cleary, P. W., Ha, J., Prakash, M., & Nguyen, T. (2010). Short shots and industrial case studies: Understanding fluid flow and solidification in high pressure die casting. Applied mathematical modelling, 34(8), 2018-2033.

[60] Zhu, W. H., & Lamarche, T. (2007). Velocity estimation by using position and acceleration sensors. Industrial Electronics, IEEE Transactions on, 54(5), 2706-2715.

[61] Hussain, Z. M., Sadik, A. Z., & O'Shea, P. (2011). Digital signal processing: an introduction with MATLAB and applications. Springer Science & Business Media.

[62] Little, J. N., & Shure, L. (2015). Signal Processing Toolbox User's Guide. The MathWorks Inc, Copyright 1988-2015 by The MathWorks, Inc.

[63] Lanczos, C. (1988). Applied analysis. Courier Corporation.

# *List of publications*

*Publications strictly related to the core of this Ph. D. Thesis:*

- E. Fiorese, F. Bonollo, "Plunger kinematic parameters affecting quality of high pressure die cast Al-Si alloy", paper submitted to Metallurgical and Materials Transactions A.
- E. Fiorese, D. Richiedei, F. Bonollo, "Improving the quality of die castings through optimal plunger motion planning: analytical computation and experimental validation", paper submitted to International Journal of Advanced Manufacturing Technology.
- E. Fiorese, F. Bonollo, L. Kallien, "Simultaneous effect of plunger motion profile, pressure and temperature on the quality of high-pressure die-cast Al-Si alloy", paper under preparation to be submitted to an International Journal.
- E. Fiorese, D. Richiedei, F. Bonollo, "Analytical computation of the plunger motion parameters affecting internal quality and static mechanical properties in high-pressure die-casting: experimental application to an industrial case-study", paper under preparation to be submitted to an International Journal.
- E. Fiorese, F. Bonollo, "Process parameters affecting quality of high-pressure die-cast Al-Si alloy", Proceedings of 8$^{th}$ European Metallurgical Conference 2015, 14-17 June 2015, Düsseldorf (Germany).
- E. Fiorese, D. Richiedei, F. Bonollo, "Analytical computation of the plunger kinematic parameters affecting quality in HPDC", Proceedings of International CAE Conference 2015, 19-20 October 2015, Pacengo del Garda (Italy).
- E. Fiorese, D. Richiedei, F. Bonollo, "Improved metamodels for the optimization of high-pressure die casting process", abstract accepted for High Tech Die Casting 2016, 22-23 June 2016, Venezia (Italy).

*Publications related to the drawing up of the cited CEN Technical Reports:*

- A.R. Adamane, E. Fiorese, G. Timelli, F. Bonollo, L. Arnberg, "Reference dies for the evaluation of tensile properties of gravity cast Al-Si alloys: an overview", Materials Science Forum Vols. 794-796 pp 71-76 (2014).
- F. Bonollo, E. Fiorese, G. Timelli, L. Arnberg, A.R. Adamane, "StaCast: linee guida per la progettazione di getti in lega di alluminio", La Metallurgia Italiana Vol. 10 pp 63-71 (2014).
- A.R. Adamane, L. Arnberg, E. Fiorese, G. Timelli, F. Bonollo, "Influence of injection parameters on the porosity and tensile properties of high-pressure die cast Al-Si alloys: a review", International Journal of Metalcasting Vol. 9, Issue 1 pp 43-53 (2015).
- E. Fiorese, F. Bonollo, G. Timelli, L. Arnberg, E. Gariboldi, "New classification of defects and imperfections for aluminum alloy castings", International Journal of Metalcasting Vol. 9, Issue 1 pp 55-66 (2015).
- F. Bonollo, E. Fiorese, G. Timelli, L. Arnberg, A.R. Adamane, "StaCast Project: New Standards on defect classification and on mechanical properties of casting alloys", International CAE Conference 2013, 21-22 october 2013, Pacengo del Garda (Italy).
- F. Bonollo, E. Fiorese, G. Timelli, L. Arnberg, A.R. Adamane, "StaCast project: from a survey of european aluminium alloys foundries to new standards on defect classification and on mechanical potential of casting alloys", 71$^{st}$ World Foundry Congress, 19-21 May 2014, Bilbao (Spain).
- A.R. Adamane, E. Fiorese, G. Timelli, F. Bonollo, L. Arnberg, "Reference dies for the evaluation of tensile properties of gravity cast Al-Si alloys: an overview", 14$^{th}$ International Conference on Aluminium Alloys, 15-19 June 2014, Trondheim (Norway).
- F. Bonollo, E. Fiorese, G. Timelli, L. Arnberg, A.R. Adamane, "StaCast: linee guida per la progettazione di getti in lega di alluminio", 35° Convegno Nazionale AIM, 5-7 November 2014, Roma (Italy).

*Other publications:*

- E. Fiorese, F. Bonollo, E. Battaglia, G. Cavaliere, "Improving die casting processes through optimization of lubrication", paper accepted for publication in International Journal of Cast Metals Research.
- E. Fiorese, G. Timelli, L. Kallien, W. Leis, B. Tonn, "Hypereutectic Al alloys die-cast at semi-solid state", 8th International Congress Aluminium Two Thousand, 14-18 May 2013, Milano (Italy).
- E. Battaglia, F. Bonollo, G. Timelli, E. Fiorese, G. Kral, "Correlation between process, microstructure and properties in High Pressure Die Casting Aluminum-Silicon alloys", Advances in Materials and Processing Technologies conference, 14-17 December 2015, Madrid (Spain).
- E. Battaglia, F. Bonollo, I. Tonello, E. Fiorese, "Correlations between defect content, mechanical properties and fractographic investigation of AlSi9Cu3(Fe) alloy Reference Castings", Thermec 2016 International Conference on processing and manufacturing of advanced materials, 29 May-3 June 2016, Graz (Austria).

# *Selected papers*

*This section collects the published versions of the following papers, whose topics are consistent with the issues developed in the Thesis:*

- E. Fiorese, F. Bonollo, G. Timelli, L. Arnberg, E. Gariboldi, "New classification of defects and imperfections for aluminum alloy castings", International Journal of Metalcasting Vol. 9, Issue 1 pp 55-66 (2015).
- A.R. Adamane, L. Arnberg, E. Fiorese, G. Timelli, F. Bonollo, "Influence of injection parameters on the porosity and tensile properties of high-pressure die cast Al-Si alloys: a review", International Journal of Metalcasting Vol. 9, Issue 1 pp 43-53 (2015).
- E. Fiorese, F. Bonollo, "Process parameters affecting quality of high-pressure die-cast Al-Si alloy", Proceedings of 8$^{th}$ European Metallurgical Conference 2015, 14-17 June 2015, Düsseldorf (Germany).
- E. Fiorese, D. Richiedei, F. Bonollo, "Analytical computation of the plunger kinematic parameters affecting quality in HPDC", Proceedings of International CAE Conference 2015, 19-20 October 2015, Pacengo del Garda (Italy).

Starting from the conference versions here enclosed, the last two conference papers have been extensively improved and are currently under submission in international journals.

# NEW CLASSIFICATION OF DEFECTS AND IMPERFECTIONS FOR ALUMINUM ALLOY CASTINGS

**Elena Fiorese, Franco Bonollo and Giulio Timelli**
Department of Management and Engineering (DTG), University of Padova, Vicenza, Italy

**Lars Arnberg**
Department of Materials Science and Engineering,
Norwegian University of Science and Technology (NTNU), Trondheim, Norway

**Elisabetta Gariboldi**
Department of Mechanics, Polytechnic of Milano, Milano, Italy



## Abstract

*In recent years, aluminum alloys have become more and more relevant because of their low density, coupled with good mechanical and corrosion properties. Different processes are available for the production of aluminum alloy components, such as rolling, extrusion, and powder metallurgy, but a significant role is played by foundry processes. Defects and imperfections are physiologically generated by different casting techniques as a result of the process stages, alloy properties and die or mold design.*

*In the present work, a multi-level classification of structural defects and imperfections in Al alloy castings is proposed. The first level distinguishes defects on the basis of their location (internal, external, or geometrical), the second level distinguishes on the basis of their metallurgical origin, while the third level refers to the specific type of defect, because the same metallurgical phenomenon may generate various defects.*

***Keywords:*** *aluminum alloys, casting defects, casting imperfections, casting defects classification, quality, permanent mold*

## Introduction

The final properties and in-service behavior of castings are determined by the microstructure and defects, which are the result of process stages, alloy properties and die/mold design. For instance, in high-pressure diecasting, extreme conditions are prevailing: complex components lead to complicated dies, and the required high production rates (up to 120 castings/hour) require high filling velocities of the molten alloy up to 40 m/second (131 ft./second) with significant turbulence in the flow. Solidification takes place in a few seconds, and the die is first in contact with a molten alloy at a temperature higher than 700°C (1,292°F) and, after 30-40 seconds, sprayed with a die release agent at room temperature. For these reasons high-pressure diecasting, as well as other foundry processes for Al alloys, can be considered a "*defects generating process.*" Not only is an average of 5-10% scrap typically generated, but the type, size and severity of defects also vary. The analysis of defects could provide foundries with useful correlations between defects type/distribution and their origin, which can be used for process adjustments for improving product quality.

Three main approaches for defects classification in cast components are proposed in literature or currently adopted by foundries: Cocks' approach based on defect geometry/location,[1] Campbell's approach based on defect metallurgical origin/causes,[2,3] and North American Die Casting Association's (NADCA) approach based on defect morphology.[4]

The first approach, proposed by Cocks, discerns between surface and internal defects. Surface defects are visible by the naked eye and impact both the product aesthetics and functionality. On the other hand, internal defects influence only the in-service behavior of the component.[1] The second route, suggested by Campbell, classifies defects on the basis of their metallurgical origin/causes (casting geometry, alloy, die characteristics, lubrication, process parameters, etc.). The main advantage of this classification is the opportunity to design and adopt strategies for improving the product quality. Nevertheless, the origin/causes of defects are discovered concurrently to defect identification and the same defect can be due to several factors. Furthermore, this approach is less suitable for application in foundries with respect to the previous geometry/position-based techniques, in which specific inspections can be used to reveal different defect groups.[2,3]

The third approach has been proposed by NADCA and is based on defect morphology. NADCA suggests seven defects categories that are indicated by a letter. Each category is divided into groups that are in turn divided into different

subgroups.[4] In this paper, a new terminology is presented, together with a classification of defects and imperfections with the purpose of helping die casting facilities address defects-related issues with increased confidence and ability in order to assure quality and reliability of their products.

## A Multi-Level and Hybrid Classification of Defects and Imperfections

The Standard EN 12258-1:2012[5] defines "defect" as a quality characteristic which does not allow the product to carry out the requested function. This European Standard (EN 12258-1:2012) defines general terms relating to products made from aluminum alloys such as processing, sampling, testing and overall characteristics. On the contrary, the presence of an imperfection does not necessarily mean the product is not suitable for use. An imperfection should be evaluated by means of a proper scale, based on the related specifications, to decide if the product has the necessary level of quality to make it suitable for use.

In this paper, the word "defect" is used mainly for simplicity. The new classification of defects and imperfections is based on three-level approach:[6]

I) morphology/location of defects (internal, external, geometrical);
II) metallurgical origin of defects (e.g. gaseous porosity, solidification shrinkage, etc.);
III) specific type of defects (the same metallurgical phenomenon may generate various defects).

Level I distinguishes defects on the basis of their location and investigation techniques suitable for their detection (visual inspections and controls including the bulk material). In this level, internal and external (i.e. surface) defects are included, while sub-surface defects (i.e. so close to the surface that they affect external aspect of casting) are accounted for as surface defects. Finally, geometrical defects imply non-compliance of a casting to the designed shape in terms of dimension and tolerances.[6]

Level II is focused on the metallurgical origin of defects. Defects are grouped into several categories, such as shrinkage defects, gas-related defects, filling-related defects, undesired phases, thermal contraction defects and metal-die interaction defects.

As previously mentioned, the knowledge of metallurgical origin supplies a starting point for corrective actions on the process.[6]

Level III identifies the specific type of defect. Usually, the term adopted to describe a particular type of defect allows a better explanation of the metallurgical origin mentioned in Level II.[6]

The present classification of defects and imperfections is hybrid and multi-level, as schematically shown in Tables 1, 2 and 3. This proposal refers to metallurgical defects arising in permanent mold cast products. In contrast, defects related to handling, finishing and machining operations following the ejection from the die are excluded from this classification, even if they could be possible causes for product rejection.

## Internal/Surface Defects and Imperfections

### Shrinkage Defects

Shrinkage defects are metal discontinuities resulting from volume contraction during solidification and occur in regions with insufficient or even absent feeding. Such regions are the last to solidify (*hot spots*) and are normally well inside the casting, but sometimes they are sufficiently close to the casting surface to give rise to surface defects.

*Macro-shrinkage* (A1.1 in Table 1) is a relatively large (with respect to casting thickness) cavity formed inside a hot spot due to volume contraction during solidification.

As shown in Figure 1, macro-shrinkage is characterized by rough and spongy surfaces due to the interrupted growth of emerging dendrites.[1-3,7-12]

*Interdendritic shrinkage* (A1.2 in Table 1) forms when liquid metal cannot adequately feed the interdendritic regions to counterbalance shrinkage during solidification (Figure 2). The resulting small discontinuities are interconnected and can affect pressure tightness.[1-3,7-23]

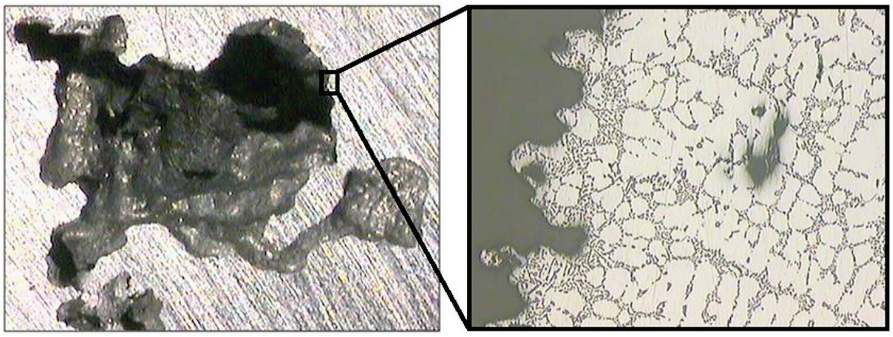

***Figure 1. Macrograph of a macro-shrinkage (left) and corresponding micrograph (right).[12]***

*Table 1. Classification of Internal Defects and Imperfections*

| 1st Level | 2nd Level | | 3rd Level | |
|---|---|---|---|---|
| **A**<br>**Internal Defects and Imperfections** | A1 | Shrinkage defects and imperfections | A1.1 | Macro-shrinkage |
| | | | A1.2 | Interdendritic shrinkage |
| | | | A1.3 | Layer porosity |
| | A2 | Gas-related defects and imperfections | A2.1 | Air entrapment porosity |
| | | | A2.2 | Hydrogen porosity |
| | | | A2.3 | Vapor entrapment porosity |
| | | | A2.4 | Lubricant and/or die release agent entrapment porosity |
| | A3 | Filling-related defects and imperfections | A3.1 | Cold joint |
| | | | A3.2 | Lamination |
| | | | A3.3 | Cold shot |
| | A4 | Undesired phases | A4.1 | Inclusion |
| | | | A4.2 | Undesired structure |
| | A5 | Thermal contraction defects and imperfections | A5.1 | Cold crack |
| | | | A5.2 | Hot tear, hot crack |

*Table 2. Classification of Internal Defects and Imperfections*

| 1st Level | 2nd Level | | 3rd Level | |
|---|---|---|---|---|
| **B**<br>**Surface Defects and Imperfections** | B1 | Shrinkage defects and imperfections | B1.1 | Sink |
| | B2 | Gas-related defects and imperfections | B2.1 | Blister |
| | | | B2.2 | Pinhole |
| | B3 | Filling-related defects and imperfections | B3.1 | Cold joint, vortex |
| | | | B3.2 | Lamination |
| | | | B3.3 | Cold shot |
| | B4 | Undesired phases | B4.1 | Surface deposit |
| | | | B4.2 | Contamination, inclusion |
| | B5 | Thermal contraction defects and imperfections | B5.1 | Cold crack |
| | | | B5.2 | Hot tear, hot crack |
| | B6 | Metal-die interaction defects and imperfections | B6.1 | Erosion |
| | | | B6.2 | Soldering |
| | | | B6.3 | Thermal fatigue mark |
| | | | B6.4 | Ejection mark |
| | | | B6.5 | Corrosion of the die |

*Table 3. Classification of Geometrical Defects and Imperfections*

| 1st Level | 2nd Level | | 3rd Level | |
|---|---|---|---|---|
| **C**<br>**Geometrical Defects and Imperfections** | C1 | Lack of material | C1.1 | Incompleteness |
| | C2 | Excess material | C2.1 | Flash |
| | C3 | Out of tolerance | C3.1 | Deformation |

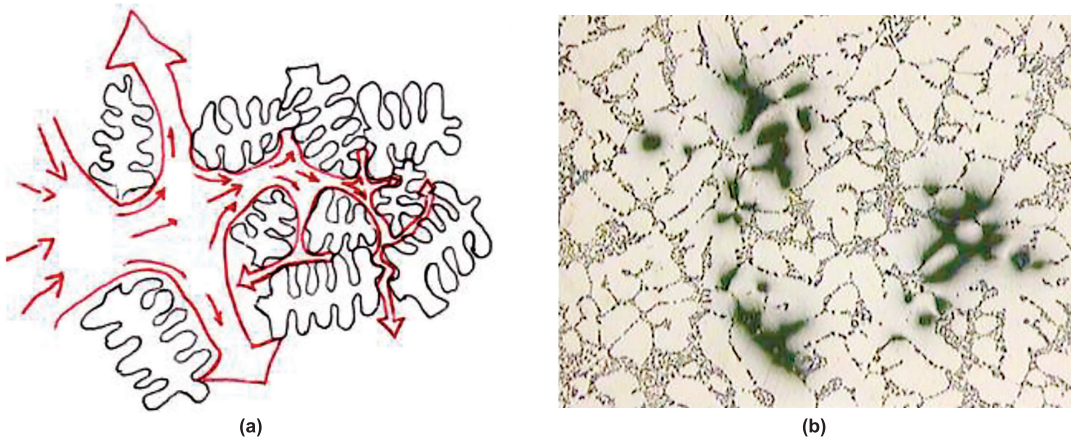


*Figure 2. (a) Schematic view of metal flow around dendrites and (b) micrograph of a region with interdendritic porosity.*[12]

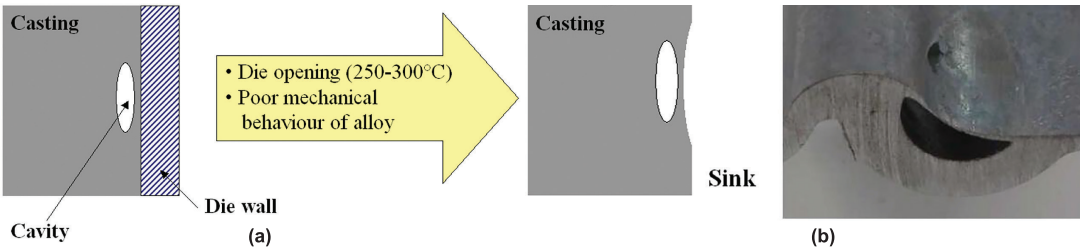


*Figure 3. (a) Draft of sink formation and (b) sink appearance on the external surface of casting.*[12]

Formation of both macro- and interdendritic shrinkage depends on mold-filling conditions, alloy physical properties (e.g. solidification range- and shrinkage), geometry of the casting and process parameters.

*Layer porosity* (A1.3 in Table 1) consists of a set of shrinkage defects typically aligned along the neutral thermal axis/surface of the casting. The neutral thermal axis/surface is located in sections of the castings where the thermal gradient is lower than adjacent points.[2,3,11,13]

*Sink* (B1.1 in Table 2) is a surface depression related to the presence of a sub-surface shrinkage porosity. This kind of defect occurs during the casting solidification, when a hot spot is localized close to the metal/die interface. The skin layer, formed as a consequence of melt contact with the die, is not able to sustain the atmospheric pressure and plastically deforms (Figure 3). Sinks are typically found in components with relatively wide plane surfaces or sharp cross section changes.[1,12]

## Gas-Related Defects

Gas-related defects are small cavities due to entrapment of air, or gas mixture, inside the die cavity.

*Air entrapment porosity* (A2.1 in Table 1) forms as a consequence of air entrapment in the liquid metal. As shown in Figure 4a, air porosity appears as spherical or ellipsoidal cavities characterized by relatively smooth surfaces on which a thin oxide layer, due to the interaction between air and liquid metal at high temperature, can be found. Air porosity is the most frequent gas-related defect in high-pressure diecasting: air bubbles can form in the turbulent metal vein in the shot sleeve, in the runners and gates or inside the die cavity.[1-4,12,19,20,22,24-36]

*Hydrogen porosity* (A2.2 in Table 1) consists of spherical or elongated cavities characterized by a smooth and non-oxidized surface (Figure 4b). Such cavities are small and distributed almost homogeneously within the casting. Humidity in the die cavity or air causes the presence of monoatomic hydrogen in the liquid metal at high temperature. Due to the abrupt reduction of hydrogen solubility in the solid phase, the solidifying metal rejects the hydrogen, which forms bubbles near the liquid/solid interface. In high-pressure diecasting, hydrogen porosity is far less frequent than air entrapment porosity. This is due to the high pressure on solidifying melt increasing the solubility of nascent hydrogen in the remaining melt, drastically reducing the size of forming molecular gas pores.[2,3,12,13,16,35,37-41]

*Vapor entrapment porosity* (A2.3 in Table 1) is due to residual humidity on the die surface, which becomes vapor when it comes into contact with the molten metal. The presence of humidity on the die surface could result from an excess of water-based lubricant and/or die release agent.

*Lubricant and/or die release agent entrapment porosity* (A2.4 in Table 1) forms when gases resulting from decomposition of shot sleeve lubricant and/or die release agent remain trapped as bubbles in the liquid metal. The surface of these bubbles appears darker than the other gas-related defects due to the presence of combustion products.

Superficial gas-related defects are commonly known as blisters and pinholes.

*Blisters* (B2.1 in Table 2) consist of small surface areas that protrude from the surface when the internal pressure of subsurface gas-related porosity plastically deforms the skin of the casting (Figure 5a). The layer deformation usually happens at relatively high temperatures, when castings are ejected from the die or during subsequent heat treatments.[1,12]

*Pinhole* (B2.2 in Table 2) is a smooth-walled cavity approximately spherical and located in sub-surface regions, as shown in Figure 5b. Pinholes are caused by gas entrapment in the metal during solidification. Such gases arise from moisture, binders and additives (containing hydrocarbons, blacking and washes) from sand cores.[36]

## Filling-Related Defects

Filling-related defects are caused by anomalous melt flow. During the die cavity filling, liquid and solidified metal veins at different temperatures and sometimes covered by oxide films can accidentally meet, causing a metallurgical inhomogeneity.

*Cold joint* (A3.1 in Table 1 and B3.1 in Table 2) forms when a relatively cold metal flow, partially solidified and in some cases covered by an oxide film, meets another warmer metal vein that can flow around it (Figure 6a). A particular cold joint defect is the *vortex* (B3.1 in Table 2) which occurs on a casting surface and shows a characteristic spiral distribution of oxide films and microstructures. Cold joint and vortex usually cause fracture at relatively low stresses.[1,3,12,22,24,26,27- 29,31-33,35,42-48]

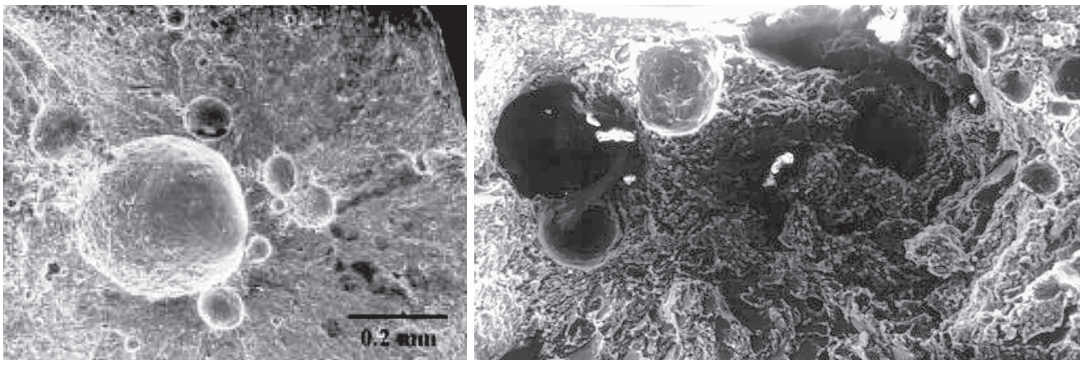


(a) (b)

***Figure 4. SEM image of (a) air porosity and (b) hydrogen porosity.[12,26]***

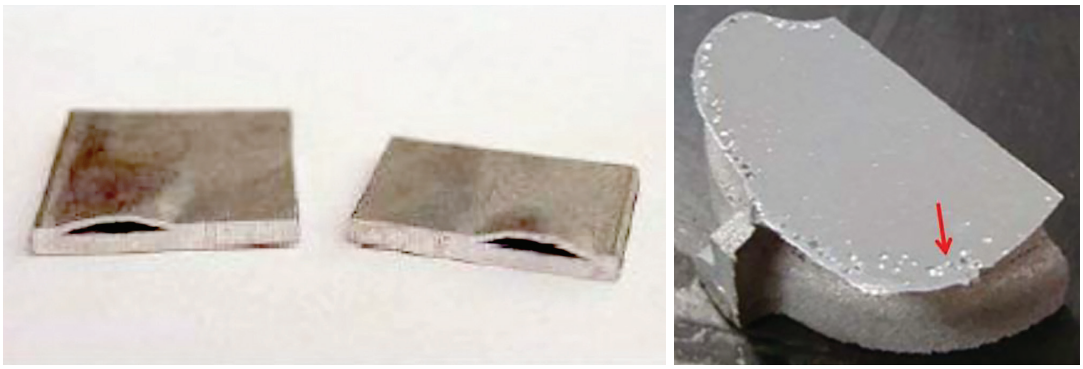

(a) (b)

***Figure 5. Examples of (a) blisters and (b) pinholes.[12,36]***

*Lamination* (A3.2 in Table 1 and B3.2 in Table 2) is a typical surface defect (Figure 6b), but can sometimes also be considered as internal defect. This is a type of thin metallic layer/skin with different microstructure from the surrounding material and partly separated by an oxide film. Lamination forms when metal comes into contact with the die surface and solidifies with a higher rate.[1,3,12,22,26-29,31-33,35,42-46,48]

*Cold shot* (A3.3 in Table 1 and B3.3 in Table 2) is a small amount of metal characterized by finer microstructure than surrounding regions and separated by a thin oxide layer, as shown in Figure 7b. It forms when the melt flows turbulently with a front characterized by the presence of droplets (*spray effect*) and comes into contact with the surface of the die (Figure 7a). Under such conditions, the molten metal solidifies rapidly.[1,3,12,22,26-29,31-33,35,42-46,48]

## Undesired Phases

Some phases are undesired for their high hardness, stiffness, brittleness and because they create microstructural discontinuities resulting in crack nucleation and propagation sites. Intermetallics sometimes can be identified as undesired phases.

*Inclusions* (A4.1 in Table 1 and B4.2 in Table 2) are typically non-metallic phases and include oxides (Figure 8a), pieces of refractories (often silicon carbide) and dross. In Al alloys, the most frequent type of inclusion is aluminum oxide, $Al_2O_3$.[1,3,12,22,26,32,33,35,41-46,49-51]

*Undesired structure* (A4.2 in Table 1) consists of local unsuitable structure characterized by low strength or higher values of dendrite arm spacing than surrounding microstruc-

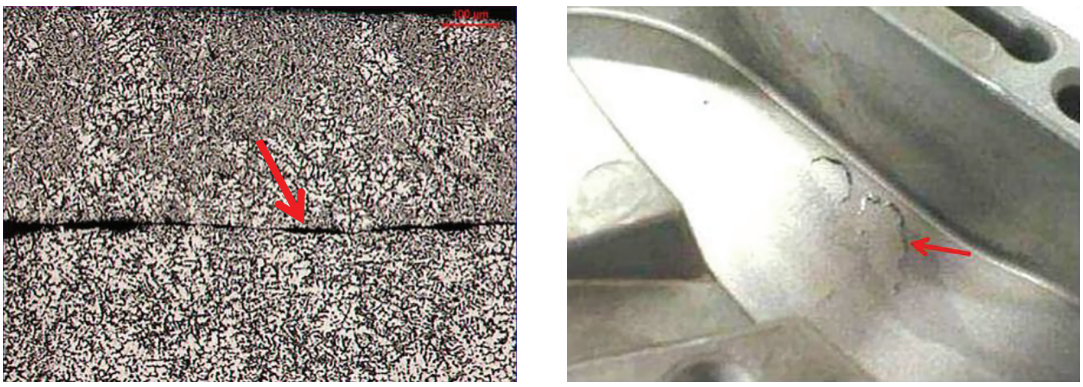

(a) (b)

***Figure 6. Examples of (a) cold joint and (b) surface lamination.***

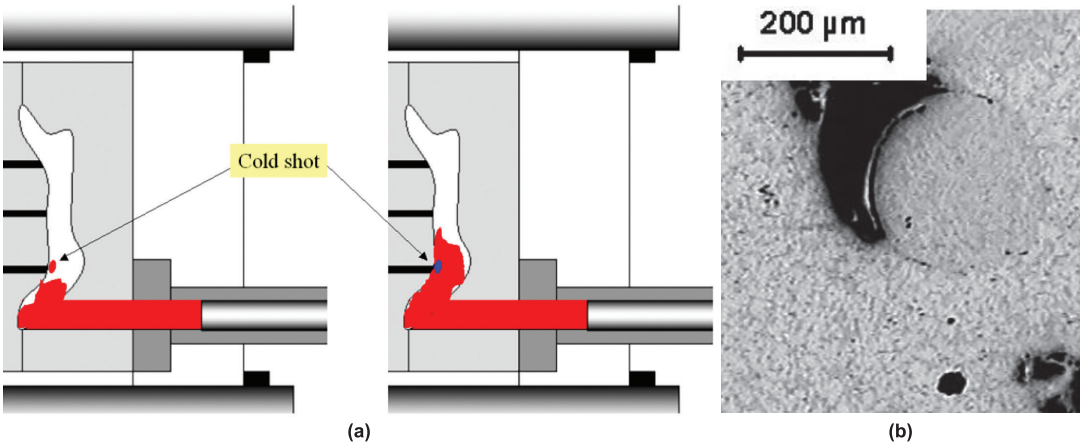


(a) (b)

***Figure 7. (a) Scheme of cold shot formation and (b) micrograph showing a cold shot associated with air entrapped porosity.***

ture (Figure 8b).[1,3,51-53] Undesired phases also can be located on the surface of castings, such as surface deposits and contamination defects.

*Surface deposit* (B4.1 in Table 2) is a layer of varying chemical composition, thickness, distribution and adhesion, which deposits on the surface of casting (Figure 9a). The formation of surface deposit can be caused by lubricant and/or die release agent excess.

*Contamination defects* (B4.2 in Table 2) are the result of interaction between metal and environment. When a contaminant defect occurs, part of the casting surface has a different color than other regions, as shown in Figure 9b.

### Thermal Contraction Defects

Thermal contraction defects consist of cracks formed during solidification or cooling to room temperature, when tensile stresses, arising from material contraction, exceed the ultimate tensile strength at local metal temperature.

*Cold crack* (A5.1 in Table 1 and B5.1 in Table 2) is a geometrical discontinuity characterized by one dimension far smaller than the two others, as shown in Figure 10a. The surfaces of a cold crack often show transcrystalline failure mode. In high-pressure diecasting such defects occur at relatively low temperatures, far below the solidification range. At these temperatures thermal contraction of casting is prevented by the die.[1,3]

*Hot tear* or *hot crack* (A5.2 in Table 1 and B5.2 in Table 2) is a crack formed in liquid portions of the mushy zone during the final stages of solidification. The surface of a hot tear displays a dendritic morphology (Figure 10b), heavily oxidized since it formed at high temperature. This defect usually occurs in alloys characterized by a wide solidification range and in hot spot areas at stresses far below the tensile stress of the alloy.[1-3,12,54-56]

Both cold cracks and hot tears often occur in regions of stress, either due to macroscopic geometrical reasons or to the presence of microstructural defects, such as gas-related

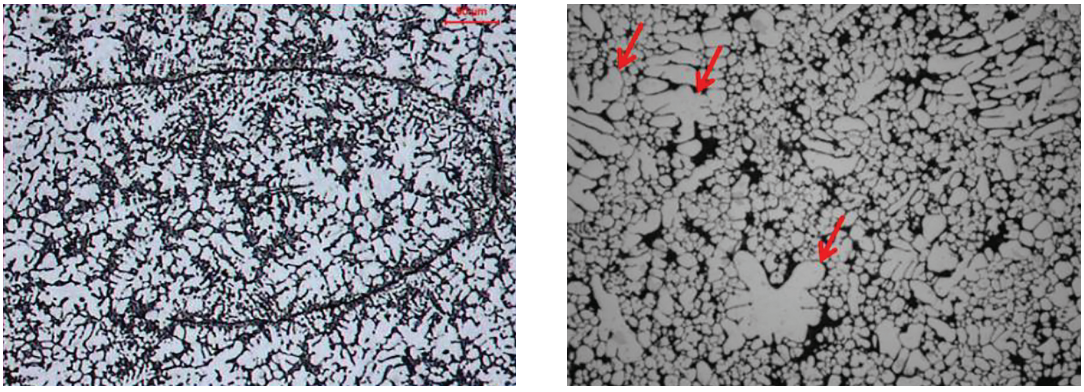

(a) (b)

***Figure 8. Micrograph of (a) an oxide bi-film and (b) a region with large dendrites surrounded by fine dendrites.[12,52]***

(a) (b)

***Figure 9. (a) Macrograph of a deposit and (b) example of contamination.***

or interdendritic porosity. Since the thermal contraction defects can extend throughout the casting, they are accounted for both as internal and surface defects.

## Surface Defects and Imperfections

### Metal-Die Interaction Defects

Metal-die interaction defects are surface defects and result from unsuitable surface conditions caused by the interaction between metal and die. Since most of these defects are consequences of geometry modifications of the die surface, they are named according to the degradation phenomenon occurring in the die itself, i.e. erosion, soldering, thermal fatigue, ejection marks and corrosion. These defects are often located in regions of the die that are exposed to melt at relatively high temperature and flow rate. For this reason, they can be found frequently in high-pressure diecasting.

*Erosion* (B6.1 in Table 2) consists of excess material on the casting due to steel removal from the die for erosive wear. Erosion depends on the inclination angle between the melt flow and die surface and on the presence of particles, or bubbles in cavitation, in the liquid metal.[1,12,54,58-60]

*Soldering* (B6.2 in Table 2) appears as roughness or localized lack of material on the casting. The metallurgical origin of soldering is the formation of intermetallic phases on the die surface (Figure 11) and following adhesion of Al alloy onto these phases. Soldering can take place easily in zones of the die where thermal fatigue or erosion phenomena have previously occurred.[1,12,54,57-70]

*Thermal fatigue marks* (B6.3 in Table 2) result in a set of narrow reliefs on the surface of the casting, sometimes called "crocodile skin" (Figure 12). As the service time of the die increases, small cracks can form on its edges and surface, due to the thermal stress cycles. Subsequently the melt fills these cracks and gives rise to the relieves on the surface of casting.[1,6,12,54,58-61,65,66,71]

*Ejection mark* (B6.4 in Table 2) appears as a plastic deformation of the casting that extends along the direction of the die ejection, as shown in Figure 13a. This defect is related to the presence of an undercut in the die, which could be a result of die-geometry modifications due to one of the previously described phenomena.

*Corrosion of the die* (B6.5 in Table 2) results in surface roughness of the casting due to a corresponding surface roughness of the die caused by corrosion (Figure 13b).

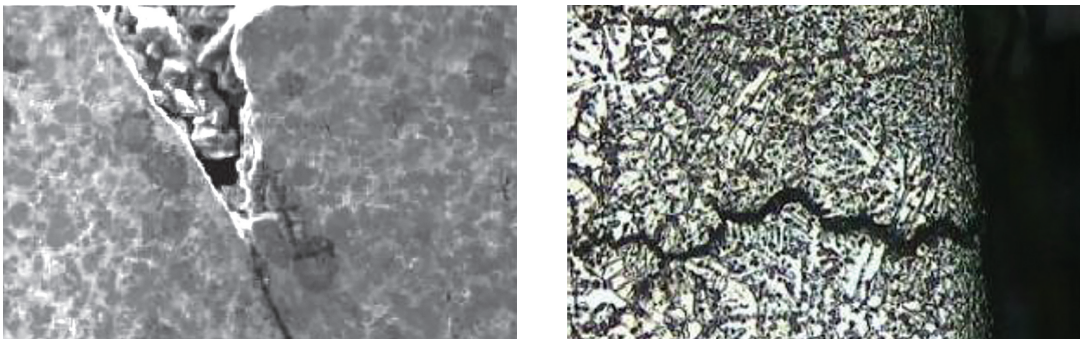

(a) (b)

***Figure 10. Micrographs of (a) cold crack and (b) hot crack.[12]***

(a) (b)

***Figure 11. (a) Example of a die affected by soldering and (b) die damage after soldering.[12]***

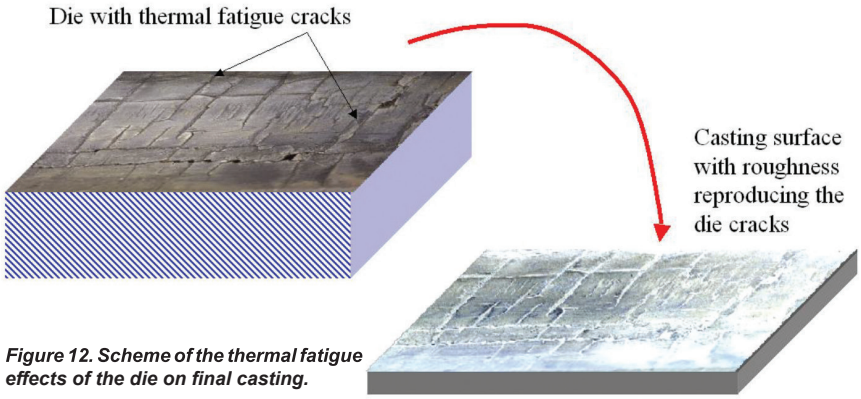


*Figure 12. Scheme of the thermal fatigue effects of the die on final casting.*

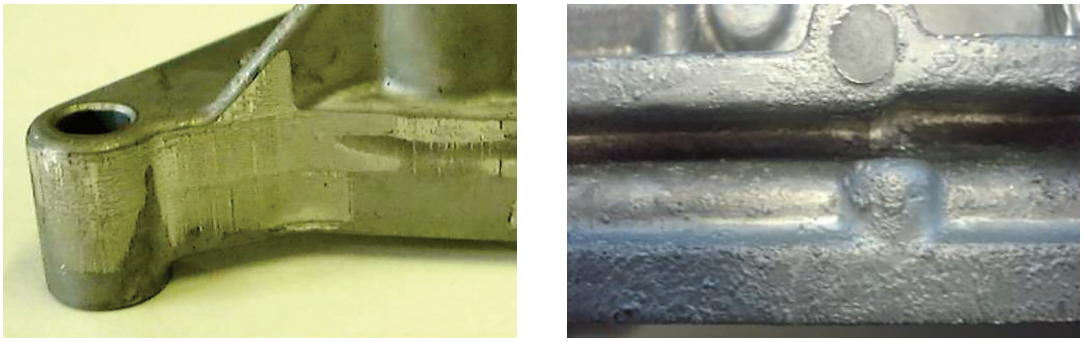

(a) (b)

*Figure 13. Macrographs of (a) ejection marks and (b) casting produced using a corroded die.*

## Geometrical Defects and Imperfections

Geometrical defects cause non-compliance to designed shape in terms of lack or excess of material and out of tolerances. This class of defects includes incompleteness, flash and deformation.

*Incompleteness* (C1.1 in Table 3) shows a lack of material in the casting with respect to the designed geometry. The incomplete filling of the die cavity is related to an excessively high viscosity of the melt.[29]

*Flash* (C2.1 in Table 3) is an excess of material on the casting corresponding to melt infiltration into the thin gap between die parts (Figure 14). This defect is caused by an insufficient clamping force of the machine, which cannot counterbalance alloy pressure.[36]

*Deformation* (C3.1 in Table 3) consists of a geometrical non-conformity of the casting to its foreseen geometry due to thermal contraction during cooling. This defect is more evident in castings ejected from the die at high temperature or having high thickness variability.

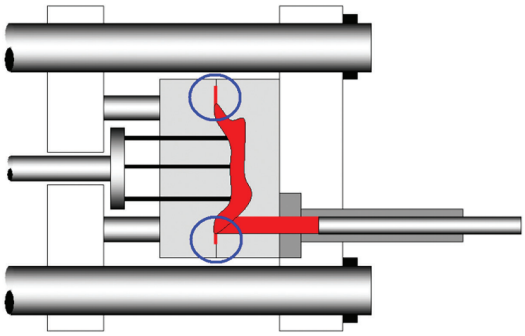

*Figure 14. Image showing flashes' formation.*

## Conclusions

In the present paper, a new classification of defects and imperfections for Al alloy castings has been presented. Five categories of internal and surface defects in castings have been identified: shrinkage defects, gas-related defects, filling-related defects, undesired phases and thermal contraction defects. Briefly, shrinkage defects are macro- or interdendritic

cavities due to the volume contraction during solidification, while gas-related defects are spherical or elongated cavities characterized by smooth surface and caused by entrapment of air, hydrogen, vapor or lubricant/die release agent. Filling-related defects result from the interaction between melt flows at different temperature, while undesired phases are non-metallic phases, such as oxides, pieces of refractory and dross, which come from the interaction between melt and environment. Finally, thermal contraction defects are cracks due to the casting contraction constrained by the die or already solidified material.

Another class of defects is the metal-die interaction defects, which are only surface defects and appear as unsuitable surface conditions of the castings caused by the interaction between metal and die (e.g. soldering or thermal fatigue). Lastly, geometrical defects result in excess/lack of material or geometrical non-conformity of the casting to its designed shape.

Since defects are always present in foundry products and knowledge of them (in terms of morphology, size, causes, etc.) represents the first step for understanding their admissibility, the proposal of this new classification of defects and imperfections is of significant importance. The classification will allow all the actors of the design and manufacturing chain to adopt a common "technical language," which is fundamental for a correct approach to quality control and improvement. This new classification also will offer the opportunity to better understand the factors affecting product quality, providing the opportunity to perform corrective actions in order to reduce/eliminate defects.

## Acknowledgements

The Authors would like to acknowledge the financing of the European Project StaCast (New Quality and Design Standards for Aluminum Alloys Cast Products - FP7-NMP-2012-CSA-6, Grant n. 319188). The StaCast project refers to University of Padova (Italy), Aalen University (Germany), Norwegian University of Science and Technology (Norway), Italian Association of Metallurgy (Italy), Assomet Services (Italy), and Federation of Aluminum Consumers in Europe (Brussels).

This paper presents the main key-issues of the CEN Technical Report, which has been elaborated on defects and imperfections classification of Al alloys approved by CEN Technical Committee 132 (Aluminum and its alloy).

## REFERENCES

1. Cocks, D.L., "A Proposed Simple Qualitative Classification for Die-Casting Defects," Proc. Die-casting Conference, Montreaux, pp. 19/1-19/15 (1996).
2. Campbell, J., Harding, R.A., "Casting Technology," TALAT 2.0 CD-ROM, EAA, Brussels (2000).
3. Campbell, J., "Castings," Elsevier Science Ltd., Oxford (2003).
4. Walkington, W.G., "Die Casting Defects – Causes and Solutions," North American Die Casting Association (1997).
5. European Standard for products made from aluminum & aluminum alloys "EN 12258-1:2012" Standard (2012).
6. Gariboldi, E., Bonollo, F., Rosso, M., "Proposal of a Classification of Defects of High-Pressure Diecast Products," *La Metallurgia Italiana*, vol. 99, p. 39 (2007).
7. Flemings, M.C., "Solidification Processing," McGraw-Hill, NY (1974).
8. "ASM Metals Handbook," 10th ed., vol. 15, "Casting," ASM - Metals Park, Ohio (1990).
9. Di Russo, E., "Metallographic Atlas of Al Foundry Alloys," Edimet, Brescia (1991).
10. Brown, J.R., "Non-Ferrous Foundryman's Handbook," Butterworth, Oxford (1999).
11. Kubo, K., Pehlke, R.D., "Mathematical Modeling of Porosity Formation in Solidification," *Metall. Trans. B*, vol. 16, pp. 359-366 (1985).
12. Timelli, G., Bonollo, F., "Microstructure, Defects and Properties in Aluminum Alloys Castings: A Review," Proc. Int. Conf. Aluminium Two Thousand, Firenze (2007).
13. Lee, P.D., Chirazi, A., See, D., "Modeling Microporosity in Aluminum-Silicon Alloys: A Review," *J. Light Met.,* vol. 1, issue 1, pp. 15-30 (2001).
14. Lee, Y.W., Chang, E., Chieu, C.F., "Modeling of Feeding Behavior of Solidifying Al-7Si-0.3Mg Alloy Plate Casting," *Metall. Trans. B*, vol. 21, issue 4, pp. 715-722 (1990).
15. Mathiesen, R.H., Arnberg, L., Ramsoskar, K., "Time Resolved X-Ray Imaging of Aluminum Alloy Solidification Processes," *Metall. Mat. Trans B*, vol. 33, issue 4, pp. 613-623 (2002).
16. Anson, J.P., Gruzleski, J.E., "The Quantitative Discrimination between Shrinkage and Gas Microporosity in Cast Aluminum Alloys Using Spatial Data Analysis," *Mater. Charact.,* vol. 43, issue 5, pp. 319-335 (1999).
17. Shin, T.-S., Huang, L.-W., Chen, Y.-J., "Relative Porosity in Aluminium and Aluminium Alloys," *Int. J. Cast Met. Res*., vol. 18, pp. 301-308 (2005).
18. Shang, L.H., Paray, F., Gruzleski, J.E., Bergeron, S., Mercadante, C., Loong, C.A., "Prediction of Microporosity in Al-Si Castings in Low Pressure Permanent Mould Casting Using Criteria Functions," *Int. J. Cast Metals Res*., vol. 17, pp. 193-200 (2004).
19. Wang, Q.G., Apelian, D., Lados, D.A., "Fatigue Behaviour of A356-T6 Aluminum Cast Alloys. Part I. Effect of Casting Defects," *J. Light Met*., vol. 1, issue 1, pp. 73-84 (2001).
20. Wang, Q.G., Apelian, D., Lados, D.A., "Fatigue Behaviour of A356/357 Aluminum Cast Alloys. Part II - Effect of Microstructural Constituents," *J. Light Met.,* vol. 1, issue 1, pp. 85-97 (2001).
21. Francis, J.A., Cantin, G.M.D., "The Role of Defects in the Fracture of an Al-Si-Mg Cast Alloy," *Mater. Sci.*

*Eng. A*, vol. 407, issue 1-2, pp. 322-329 (2005).
22. Akhtar, S., Arnberg, L., Di Sabatino, M., Timelli, G., Bonollo, F., "A Comparative Study of Defects and Mechanical Properties in High Pressure Die Cast and Gravity Die Cast Aluminium Alloys," *Int. Foundry Research*, issue 2, pp. 36-48 (2009).
23. Merlin, M., Timelli, G., Bonollo, F., Garagnani, G.L., "Impact Behaviour of A356 alloy for Low-Pressure Die Casting Automotive Wheels," *J. Mater. Process. Technol.,* vol. 209, issue 2, pp. 1060-1073 (2009).
24. Dai, X., Yang, X., Campbell, J., Wood, J., "Effects of Runner System Design on the Mechanical Strength of Al-7Si-Mg Alloy Castings," *Mater. Sci. Eng. A*, vol. 354, issues 1-2, pp. 315-325 (2003).
25. Cáceres, C.H., Selling, B.I., "Casting Defects and the Tensile Properties of an Al-Si-Mg Alloy", *Mater. Sci. Eng. A*, vol. 220, pp. 109-116 (1996).
26. Avalle, M., Belingardi, G., Cavatorta, M.P., Doglione, R., "Casting Defects and Fatigue Strength of a Die Cast Aluminium Alloy: A Comparison Between Standard Specimens and Production Components," *Int. J. Fatigue*, vol. 24, pp. 1-9 (2002).
27. Cáceres, C.H., "A Phenomenological Approach to the Quality Index of Al-Si-Mg Casting Alloys," *Int. J. Cast Metals Res*., vol. 12, pp. 367-375 (2000).
28. Cáceres, C.H., "A Rationale for the Quality Index of Al-Si-Mg Casting Alloys," *Int. J. Cast Metals Res*., vol. 12, pp. 385-391 (2000).
29. Verran, G.O., Mendes, R.P.K., Rossi, M.A., "Influence of Injection Parameters on Defects Formation in Die Casting Al12Si1,3Cu Alloy: Experimental Results and Numeric Simulation," *J. Mater. Process. Technol*., vol. 179, pp. 190-195 (2006).
30. Campbell, J., "Materials Perspective, Entrainment Defects," *Mater. Sci. Technol.,* vol. 22, no. 2, pp. 132-136 (2006).
31. Faura, F., López, J., Hernández, J., "On the Optimum Plunger Acceleration Law in the Slow Shot Phase of Pressure Die Casting Machines," *Int. J. Mach. Tools Manuf*., vol. 41, issue 2, pp. 173-191 (2001).
32. Timelli, G., Bonollo, F., "Quality Mapping of Aluminium Alloy Diecastings," *Metall. Science and Technol*., vol. 26, issue 1, pp. 2-8 (2008).
33. Timelli, G., Bonollo, F., Cupitò, G., "The Impact of Defects on the Quality of Aluminium Alloys Die Castings," *ATA – Ingegneria dell'autoveicolo*, 62 (1/2), pp. 12-19 (2009).
34. Yi, J.Z., "Statistical Modeling of Microstructure and Defect Population Effects on the Fatigue Performance of Cast A356-T6 Automotive Components," *Mat. Sci. Eng*., vol. 432, issues 1-2, pp. 59-68 (2006).
35. Wang, Q.G., "Oxide Films, Pores and the Fatigue Lives of Cast Aluminum Alloys," *Metall. Mater. Trans. B*., vol. 37, issue 6, pp. 887-895 (2006).
36. American Foundry Society, "International Atlas of Casting Defects," pp. 81-87 (1999).
37. Moores, A.W., et al. "New Device for the Determination of Hydrogen Concentration in Aluminum Alloys," *AFS Transactions*, vol. 113, pp. 265-274 (2005).
38. Marcolongo, P., Evans, J.W., Steingart, D.A., Bonollo, F., "New Probe to Detect Gas Bubbles – Part 1," *Pressocolata e Tecniche Fusorie*, 2, pp. 117-121 (2007).
39. Marcolongo, P., Evans, J.W., Steingart, D. ., Bonollo, F., "New Probe to Detect Gas Bubbles – Part 2," *Pressocolata e Tecniche Fusorie*, 2, pp. 96-101 (2007).
40. Atwood, R.C., "Diffusion-Controlled Growth of Hydrogen Pores in Al-Si Castings: In Situ Observation and Modelling," *Acta Mater*., vol. 48, issue 2, pp. 405-417 (2000).
41. Chen, X.G., Gruzleski, J.E., "Influence of Melt Cleanliness on Pore Formation in Aluminium-Silicon Alloys," *Int. J. Cast Metals Res*., vol. 9, pp. 17-26 (1996).
42. Yang, X., Huang, X., Dai, X., Campbell, J., Tatler, J., "Numerical Modelling of Entrainment of Oxide Film Defects in Filling of Aluminium Alloy Castings," *Int. J. Cast Metals Res*., vol. 17, pp. 321-331 (2004).
43. Dai, X., Yang, X., Campbell, J., Wood, J., "Influence of Oxide Film Defects Generated in Filling on Mechanical Strength of Aluminium Alloy Castings," *Mater. Sci. Technol.,* vol. 20, issue 4, pp. 505-513 (2004).
44. Fox, S., Campbell, J., "Visualisation of Oxide Film Defects During Solidification of Aluminium Alloys," *Scripta Mater*., vol. 43, issue 10, pp. 881-886 (2000).
45. Dispinar, D., Campbell, J., "Use of Bifilm Index as an Assessment of Liquid Metal Quality," *Int. J. Cast Metals Res.,* vol. 19, pp. 5-17 (2006).
46. Campbell, J., "An Overview of the Effects of Bifilms on the Structure and Properties of Cast Alloys," *Metall. and Mater. Trans. B*, vol. 37, issue 6, pp. 857-863 (2006).
47. Espinoza-Cuadra, J., Garcıa-Garcıa, G., Mancha-Molinar, H., "Influence of Defects on Strength of Industrial Aluminum Alloy Al–Si 319," *Materials & Design*, vol. 28, issue 3, pp. 1038-1044 (2007).
48. Aziz Ahamed, A.K.M., Kato, H., Kageyama, K., Komazaki, T., "Acoustic Visualization of Cold Flakes and Crack Propagation in Aluminum Alloy Die-Cast Plate," *Mater. Sci. Eng*., *A*, vol. 423, issues 1-2, pp. 313-323 (2006).
49. Liu, F., Samuel, F.H., "Effect of Inclusions on the Tensile Properties of Al-7%Si-0.35% Mg (A356.2) Aluminium Casting Alloy," *J. Mat. Sci*., vol. 33, pp. 2269-2281 (1998).
50. Seniw, M., Conley, J., Fine, M., "The Effect of Microscopic Inclusion Locations and Silicon Segregation on Fatigue Lifetimes of Aluminum Alloy A356 Castings," *Mat. Sci. Eng., A*, vol. 285, pp. 43-48 (2000).
51. Wang, L., Makhlouf, M., Apelian, D., "Aluminum Die-Casting Alloys - Alloy Composition, Microstructure, and Properties/Performance Relationship," *Int. Materials Review*, vol. 40, pp. 221-238 (1995).

52. Timelli, G., Lohne, O., Arnberg, L., Laukli, H.I., "Effect of Solution Heat Treatments on the Microstructure and Mechanical Properties of a Die-Cast AlSi$_7$MgMn Alloy," *Metall. Mater. Trans. A*, vol. 39, issue 7, pp. 1747-1758 (2008).
53. Battle, T.P., "Mathematical Modelling of Solute Segregation in Solidifying Materials," *Int. Mater. Rev.*, vol. 37, issue 1, pp. 249-270 (1992).
54. Farupi, J., Drezet, J.M., Rappaz, M., "In Situ Observation of Hot Tearing Formation in Succilonitrile-Acetone," *Acta Mater*. vol. 49, issue 7, pp. 1261-1269 (2001).
55. Yan, X., Lin, J.C., "Prediction of Hot Tearing Tendency for Multicomponent Aluminum Alloys," *Metall. And Mater. Trans. B*., vol. 37, issue 6, pp. 913-918 (2006).
56. Knuutinen, A., Nogita, K., McDonald, S.D., Dahle, A.K., "Porosity Formation in Aluminium Alloy A356 Modified with Ba, Ca, Y and Yb," *J. Light Metals*, vol. 1, issue 4, pp. 241-249 (2001).
57. Niu, X.P., Hua, B.H., Pinwilla, I., Lib, H., "Vacuum Assisted High Pressure Die Casting of Aluminium Alloys," *J. Mater. Process. Technol.,* vol. 105, pp. 119-127 (2000).
58. Kosec, B., Kosec, L., Kopac, J., "Analysis of Casting Die Failures," *Eng. Failure Analysis*, vol. 8, issue 4, pp. 355-359 (2001).
59. Chen, Z.W., Jahedi, M.Z., "Die Erosion and its Effect on Soldering Formation in High Pressure Die Casting of Aluminium Alloys," *Mater. Des.,* vol. 20, issue 6, pp. 303-309 (1999).
60. Mitterer, C., Holler, F., Üstel, F., Heim, D., "Application of Hard Coatings in Aluminium Die Casting - Soldering, Erosion and Thermal Fatigue Behaviour," *Surf. Coat. Technol*., vol. 125, issues 1-3, pp. 233-239 (2000).
61. Gulizia, S., Jahedi, M.Z., Doyle, E.D., "Performance Evaluation of PVD Coatings for High Pressure Die Casting," *Surf. Coat. Technol*., vol. 140, issue 3, pp. 200-205 (2001).
62. Domkin, K., Hattel, J.H., Thorborg, J., "Modeling of High Temperature- and Diffusion-Controlled Die Soldering in Aluminum High Pressure Die Casting," *J. Mater. Process. Technol*., vol. 209, issue 8, pp. 4051-4061 (2009).
63. Zhu, H., Guo, J., Ji, J., "Experimental Study and Theoretical Analysis on Die Soldering in Aluminum Die Casting," *J. Mater. Process. Technol*., vol. 123, issue 2, pp. 229-235 (2002).
64. Joshi, V., Srivastava, A., Shivpuri, R., "Intermetallic Formation and its Relation to Interface Mass Loss and Tribology in Die Casting Dies," *Wear*, vol. 256, issues 11-12, pp. 1232-1235 (2004).
65. Tentardini, E.K., et al., "Soldering Mechanisms in Materials and Coatings for Aluminum Die Casting," *Surf. Coat. Technol*., vol. 202, issue 16, pp. 3764-3771 (2008).
66. Zhu, Y., Schwam, D., Wallace, J.F., Birceanu, S., "Evaluation of Soldering, Washout and Thermal Fatigue Resistance of Advanced Metal Materials for Aluminum Die-Casting Dies," *Mater. Sci. Eng., A,* vol. 379, issues 1-2, pp. 420-431 (2004).
67. Shankar, S., Apelian, D., "Die Soldering: Mechanism of the Interface Reaction between Molten Aluminum Alloy and Tool Steel," *Metall. Mater. Trans. B*, vol. 33, pp. 465-476 (2002).
68. Sundqvist, M., Hogmark, S., "The Mechanisms of Erosive Wear of Die Casting Dies for Aluminium," *Proceedings of the Int. European Conf. on Tooling Materials*, pp. 453-466 (1992).
69. Bernacchi, E., Ferrero, A., Gariboldi, G., Korovkin, A., Pontini, G., "PVD Coatings in Aluminium Die Casting Dies and Steel Forming Tools," *Metall. Sci. and Tech.,* vol. 14, issue 1, pp. 3-11 (1996).
70. Bucci, M., "Analysis of Defects in Machined High-Pressure Die-Castings of AlSi12Cu2Fe Alloy," MS thesis, University of Padova (1998).
71. Persson, A., Hogmark, S., Bergstrom, J., "Failure Modes in Field-Tested Die Casting Dies," *J. Mater. Process. Technol*., vol. 148, pp. 108-118 (2004).

## Technical Review & Discussion

### New Classification of Defects and Imperfections For Aluminum Alloy Castings

*Elena Fiorese, Franco Bonollo and Giulio Timelli*
*University of Padova, Vicenza, Italy*
*Lars Arnberg, Norwegian University of Science and Technology, Trondheim, Norway*
*Elisabetta Gariboldi, Polytechnic of Milano, Milano, Italy*

**Reviewer:** Regarding hydrogen porosity, it would be useful, especially for the high-pressure die casting community, to explain the effects of high pressure of the solidifying melt on increasing the solubility of nascent hydrogen in the remaining melt and on drastically reducing the size of forming molecular gas pores according to the gas laws.

***Authors:*** *Porosity in Al alloys resulting from hydrogen is a well-known problem in solidification processes. It results from the fact that hydrogen dissolves well in the liquid but its solubility decreases significantly in the solid. During solidification, hydrogen is segregated to the liquid ahead of the solidification front. Usually gas bubbles form when the partial pressure in the liquid exceeds the atmospheric pressure according to the Sievert's law. In high-pressure die casting, this pressure should be much higher. Pores form when the gas bubbles are caught by the solidification front.*

# INFLUENCE OF INJECTION PARAMETERS ON THE POROSITY AND TENSILE PROPERTIES OF HIGH-PRESSURE DIE CAST Al-Si ALLOYS: A REVIEW

**Anilchandra R. Adamane, Lars Arnberg**
Department of Materials Science and Engineering,
Norwegian University of Science and Technology (NTNU), Trondheim, Norway

**Elena Fiorese, Giulio Timelli, Franco Bonollo**
University of Padova, Department of Management and Engineering, Vicenza, Italy



## Abstract

*Aluminum-Silicon alloys are the most extensively used Al foundry alloys and are widely used in high-pressure die casting (HPDC) of automotive components. Several process parameters need to be controlled during HPDC in order to obtain sound and reliable castings. Among the different process variables, the determination and control of the injection parameters, such as the gate velocity and intensification pressure (IP), remain a key requirement throughout the HPDC process. This work critically reviews the effects of the injection parameters on the porosity and tensile properties of the die castings. The results of the literature review are summarized and optimal values for the gate velocity and IP are suggested.*

***Keywords:*** *foundry aluminum alloys, high-pressure die casting, injection parameters, porosity, tensile properties, HPDC*

## Introduction

High-pressure die casting (HPDC) is a cost-effective process for the production of castings in large quantities and with high dimensional accuracy. Very high flow rates can be achieved inside the die cavity and this requires careful casting design. The main disadvantage of HPDC is the entrapment of gas and oxides due to the turbulent flow of metal during the filling phase, resulting in porosity and deterioration of the casting quality. In cold chamber HPDC, the molten metal poured into the shot sleeve is pushed into the die cavity using a hydraulic piston-cylinder arrangement, schematically shown in Fig. 1. The different valves and gas accumulators (shown in Fig. 1 and described in Table 1) allow the fine control of the plunger's movements. A detailed description of the injection system is given elsewhere.[1]

The filling of the die cavity through the plunger motion takes place in three continuous stages, which are illustrated in Fig. 2a. The build-up of the pressure, the plunger's displacement and velocity, corresponding to the different stages, are depicted in Fig. 2b.

A brief description of the process stages is as follows:[2]

Stage I. The molten metal fills the shot sleeve and the plunger begins to move at a low velocity to avoid turbulence. The velocity of the plunger in this stage is represented as $v_{PI}$.

Stage II. The filling of the die cavity is done at high velocity to avoid premature solidification at the gate (also called the ingate) and incomplete castings. The velocity of the plunger in this stage is represented as $v_{PII}$ and the corresponding velocity of the melt at the gate is called gate velocity, $v_g$. The transition from Stage I to Stage II is termed as the *switch point* or *change over position* (COP).

Stage III. High pressure (also called *intensification pressure* or IP) is applied on the molten metal once the die cavity is full.

The Al-Si alloys are the most commonly used alloys for HPDC automotive components and the effect of Si concentration on the strength and ductility is evident from Fig. 3. However, it is well known how, in addition to the chemical composition, the quality or soundness of castings govern the strength of a cast material (Fig. 4).[4,5] This implies that higher strength values could be obtained from a material by controlling the casting parameters. Defects arising from the metalcasting process will determine the final quality of castings. Generally, casting defects are very difficult to be completely eliminated (i.e., zero-defect casting).

Most of the available literature on HPDC of Al-Si alloys focuses on the casting parameters that influence the microstructure and tensile behavior, particularly the variables regarding the injection phase. The velocity of the molten metal at the gate (gate velocity) and the IP are the main

injection parameters established on the locking force of the HPDC machine. Further, the dimensions of the gate and runners are strictly related to these injection parameters. Other important casting parameters, frequently reported in the literature, are the die temperature and the temperature of the molten metal inside the shot sleeve. For instance, the die temperature, generally set up in a range between 200-230°C (392-446°F),[6,7] is a critical variable that determines the cooling rate of the casting and the soldering phenomena. Both the thermal history of the molten metal in the shot sleeve and the piston velocity affect the melt fluidity, the cavity filling, the final microstructure and mechanical

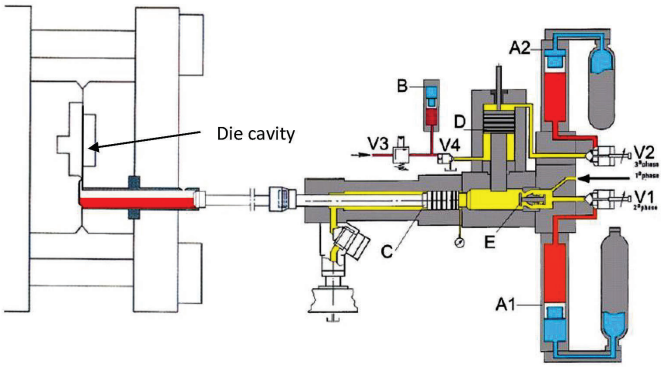


*Figure 1. Schematic illustration of hydraulic injection system.*[1]

*Table 1. Description of Various Parts of the HPDC Set-Up Shown in Fig. 1*

| | |
|---|---|
| A1 | Gas accumulator to control the *Stage II* |
| A2 | Gas accumulator to control the *Stage III* |
| B | Counter-pressure accumulator |
| C | Plunger |
| D | Plunger for the *intensification pressure* |
| E | Back-pressure valve |
| V1 | Flow valve to control the *Stage II* |
| V2 | Flow valve to control the *Stage III* |
| V3 | Pressure-relief valve |
| V4 | Counter-pressure flow valve |

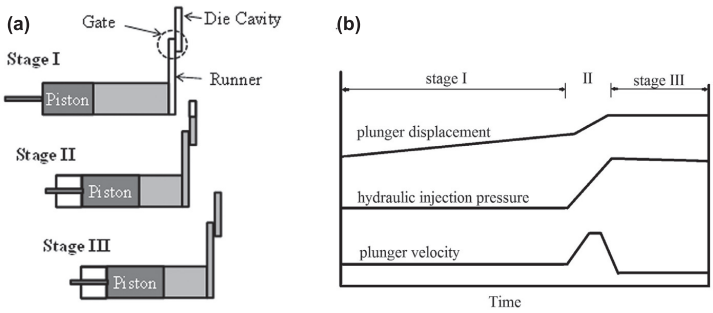


*Figure 2 (a) Schematic representation of the plunger movement during HPDC and (b) the corresponding change in velocity and pressure at different stages.*

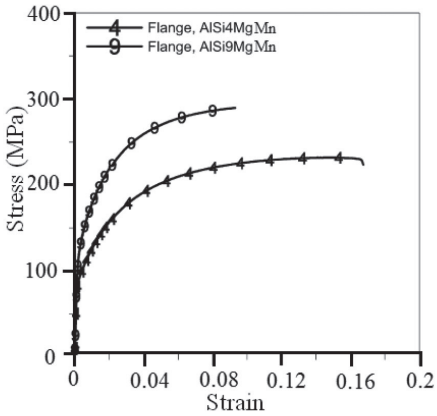


*Figure 3. Engineering stress-strain curves of high pressure die-cast AlSi4MgMn and AlSi9MgMn alloys.*[3]

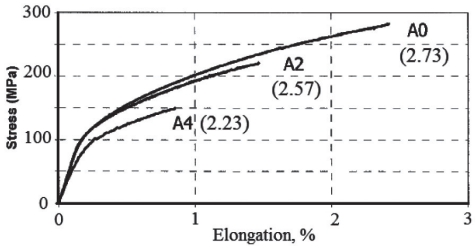


*Figure 4. Tensile stress-strain curves of three different AlSi9Cu3(Fe) castings with density values indicated within the parentheses (g cm$^{-3}$).*[4] *Lower density castings show reduced strength properties owing to higher casting defects.*

properties of the casting.[8-10] Although the design of vents and overflows in a die casting is rarely discussed in the literature, it constitutes an important die parameter that can influence the casting quality. Apart from few suggestions on vent design[11] there is hardly any work available relating the vent design to the porosity distribution or the tensile properties of the castings. Most of these parameters are interrelated and can be optimized by using process numerical simulation softwares and algorithms. In the present work, the influence of the injection parameters on the porosity and tensile properties of HPDC Al-Si alloys are reviewed and discussed.

## Effects of Gate Velocity

The melt velocity is one of the most important features controlling the casting quality in HPDC. The velocity at the gate determines the flow contour within the die cavity and is related to the runner-gate type, gate dimension and the geometrical profile of the cavity. Its influence on the porosity and subsequently on the tensile strength properties will be discussed in the following paragraphs.

## Porosity

Jian and Wu[12] experimentally showed that the cavity filling time significantly reduces with increasing gate velocity, to a certain extent. While excessively high gate velocity may worsen the surface finish and increase the porosity caused by gas entrapment. On the contrary, Hartmann et al. showed that the porosity content linearly decreases with the cavity filling time and this is dependent on the casting thickness.[13] In order to clarify this contrast, Karban tried to summarize the results of several scientific works and found that the majority of the works agreed that higher melt velocities increased porosity, though few works indicated the contrary and a few others reported the presence of an optimal melt velocity in minimizing porosity.[14] Karban's work itself showed that a plunger velocity between 1.7 and 3.4 m $s^{-1}$ (5.6 and 11.2 ft $s^{-1}$) produced less porosity, therefore supporting the viewpoint of the presence of an optimal velocity in HPDC. Low gate velocity could lead to early solidification at the gates thereby reducing the effective gate area and decreasing the ratio of actual flow rate (effective gate area) to the ideal flow rate (theoretical gate area) ($C_d$).[15] Niu et al. showed that by doubling the gate velocity, from 30 to 60 m $s^{-1}$, the gate freezing time could be increased by 20 ms.[16] The $C_d$ varies significantly by changing the gate velocity which in turn influences the porosity content.[13] Gunasegaram et al. showed that the percentage of smaller pores (< 20µm) increased with gate velocity, from 26 to 82 m $s^{-1}$ (~85 to 269 ft $s^{-1}$), while the larger pores (> 100 µm) were almost eliminated at 82 m $s^{-1}$ (269 ft $s^{-1}$) though velocity higher than 48 m $s^{-1}$ (157.5 ft $s^{-1}$) could not significantly reduce the overall porosity content (Fig.5).[17] The porosity volume fraction was measured from the gauge length of the tensile test specimen which is argued as more appropriate compared to measurements made from the entire casting, called bulk pore fraction elsewhere.[18] However, Ghomashchi[19] observed that the size of the porosity decreases with the increase in the gate velocity to a certain value (~55 m $s^{-1}$, equivalent to ~180 ft $s^{-1}$) beyond which the size increases. Nevertheless, the overall porosity content was found to decrease with an increase in the velocity (Fig. 5). The author observed that the porosity content was minimum near the gates and maximum near the overflows.[20]

## Tensile Strength Properties

Figure 6 shows the increase in strength and ductility of die cast CA 313 alloy (equivalent to A380 alloy) with an increase in gate velocity.[17] The authors attribute it to the increase in density and reduction in porosity. Further, it is shown that the scatter in the strength values decreases with increasing melt velocity, therefore suggesting higher repeatability in the HPDC process. Lumley et al. also reported improvement in tensile strength properties with an increase in gate velocity.[21] Figure 7 summarizes the influence of gate velocity on the tensile properties from different works. Timelli and Bonollo, experimented with different plunger velocities and maintained the IP constant, showed that a higher gate velocity yielded better tensile properties (Fig. 8).[22,23] Among the P2 and P4 processes,

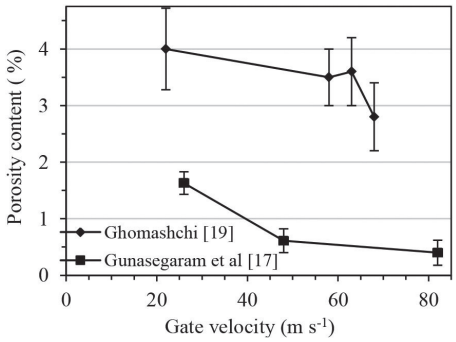


***Figure 5. Change of porosity content with different gate velocity in HPDC.***

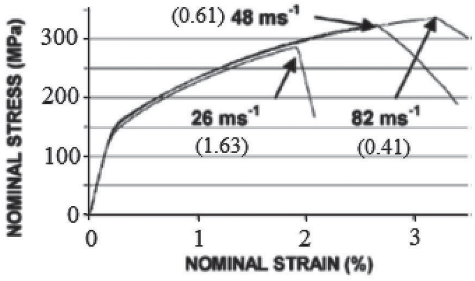


***Figure 6. Tensile test curves of specimens cast with three different gate velocities: porosity content (%) are also indicated in the brackets.[17]***

P2 with higher $v_{pII}$ resulted in lower filling time and better tensile properties as shown in Fig. 8.

It is clear from the figure that the switch point was varied in all the experimental processes. Although Gunasegaram et al.[24] did not report a significant change in tensile properties with the change in switch point, it is indeed a critical parameter in reducing turbulence and the filling time. Overall, it appears that higher gate velocity improves the tensile strength properties in die cast Al-Si alloys. Several publications on die cast Mg alloys also report similar conclusion.[25,26] However, for minimizing the phenomena of die erosion, related to high melt velocity, diecasters generally maintain the gate velocities less than 40 m $s^{-1}$ (131 ft $s^{-1}$).[27]

## Influence of Intensification Pressure

Intensification pressure is applied once the die cavity is completely filled to limit the formation of porosity due to solidification shrinkage, gas evolution and the expansion of entrapped air, improving the strength properties of the casting.[14,28,29] The importance of IP in HPDC is discussed in the works of Schaffer and Laukli[30] and Otarawanna et al.[31,32] by using AlSi3MgMn alloys. The common conclusion is that high IP (61 MPa) significantly reduces the porosity content in the casting, as shown in Fig. 9a and 9b. Otarawanna et al. highlight the importance of using the right combination of gate thickness and IP in achieving minimum porosity content in HPDC, and is represented graphically in Fig. 9b.[31] Another striking feature in the microstructure (Fig. 9a) is the presence of shear bands through the gate leading into the casting which is believed to be related to high IP. Probably, high IP leads to localized deformation resulting in dilatant shear banding, not visible at lower IP.

Verran et al. tried different values of melt velocity and IP, using the design of experiments (DOE) methodology, to cast a double cylinder cover of AlSi12Cu1.3 alloy with the 'Best' density value.[33,34] The authors showed that, for a given value of $v_{pI}$ and IP, lower $v_{pII}$ generally results in higher density values

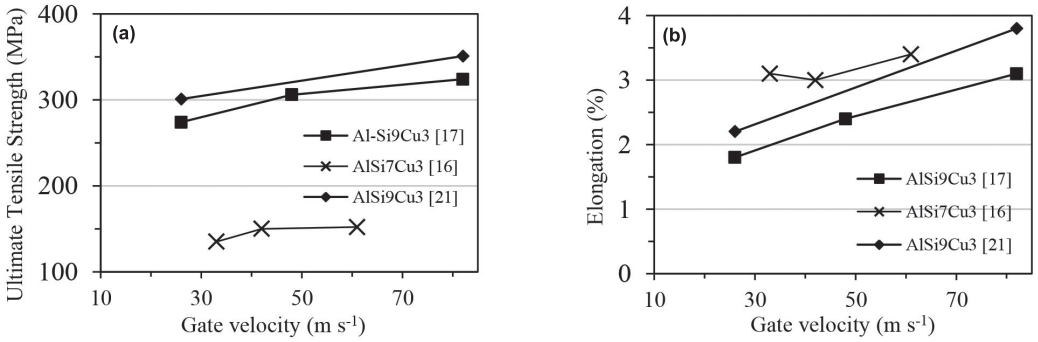


*Figure 7. Effect of gate velocity on the tensile properties of die cast Al-Si alloys.*

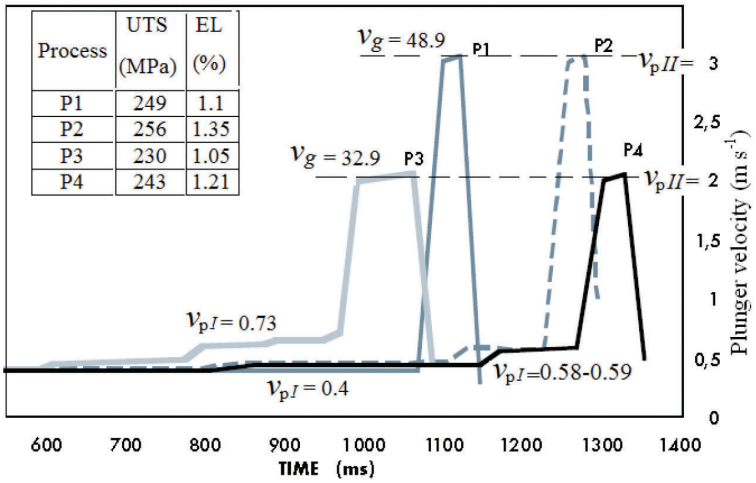


*Figure 8. Plot depicting the effect of varying plunger velocity on the tensile properties of Al-9Si alloy equivalent to US A380 aluminum alloy.*[22,23]

or lower porosity. For example at 0.27 m $s^{-1}$ (0.89 ft $s^{-1}$) and 15 MPa of $v_{pI}$ and IP respectively, 2.62 m $s^{-1}$ (8.6 ft $s^{-1}$) of $v_{pII}$ resulted in a lower density value of 2.658 g $cm^{-3}$ (165.934 lb $ft^{-3}$) as compared to 2.673 g $cm^{-3}$ (166.87 lb $ft^{-3}$) at 1.34 m $s^{-1}$ (Fig. 10). Figure 11 shows the quality of the cylinder cover casting, in terms of visible porosity, under two extreme density values highlighted in Fig. 10. Overall, the density increases with an increase in IP. This argument was further justified by Niu et al.[16] who showed that higher IP would be more effective in controlling porosity than melt velocity. For instance, gate freezing time could be increased by ~25 ms by doubling the gate velocity from 33 to 61 m $s^{-1}$ (108.3 to 200 ft $s^{-1}$) (Fig. 12a) as compared to about 70 ms with doubling the IP from 39 MPa to 79 MPa (Fig. 12b), for a particular value of IP and gate velocity respectively. Although higher IP improves the soundness of the castings, the value is limited by machine power.[35]

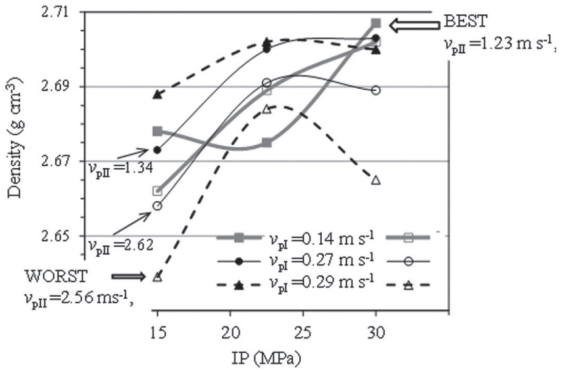


*Figure 10. Density as a function of different IP levels: the curves refer to different injection plunger velocities.*

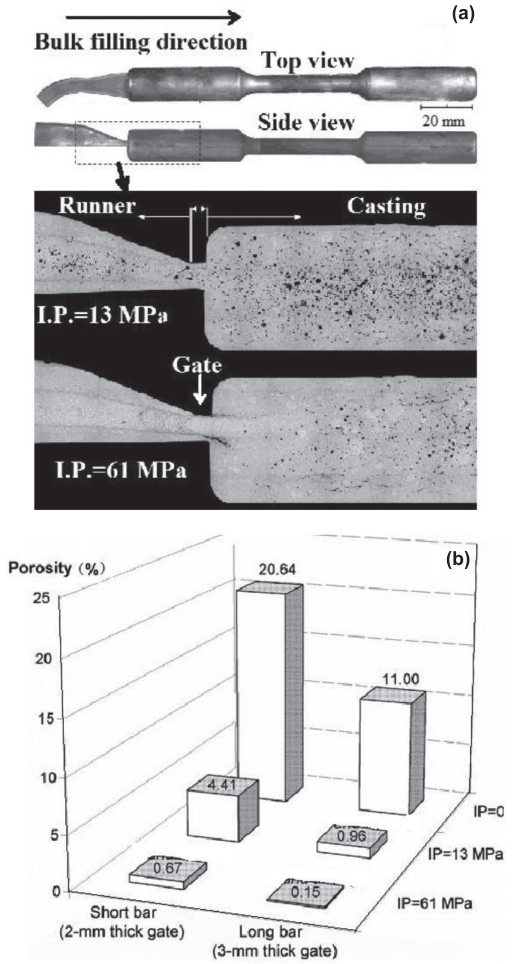


*Figure. 9 Effect of different IP on the (a) microstructure of the die castings[30] and (b) percentage porosity.[31]*

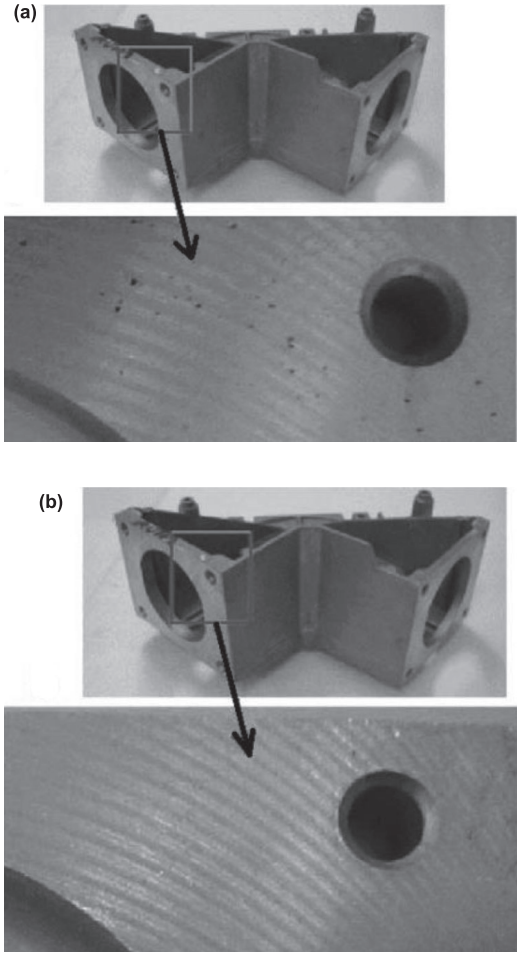


*Figure 11. Photographs showing the double cylinder cover casting under Worst and (b) Best density values.[33]*

## Selection of Runners and Gates

The melt flowing through the runner enters the mold or the die cavity through the gate (Fig. 2a). The design of the runner-gate system is critical in controlling the flow contour which subsequently affects the quality of the casting. Four different types of runner-gate systems namely: Linear type, Fan type, T-shaped and Split type, shown in Fig. 13, were examined in detail by Itamura et al. using a numerical approach.[36] The nature of the die cavity filling at different injection velocities, in the range of 0.5 to 10 m $s^{-1}$ (1.64 to 32.8 ft $s^{-1}$), was analyzed for the different runner-gate combinations. The authors showed that the combination of injection velocity and runner-gate arrangement could definitely change the flow contour.

Simulation results from the work of Zhao et al.[37] showed that in the fan type gate, the velocity of the incoming molten metal is higher along the side walls of the die cavity (Fig. 14a) than at the centerline; therefore, resulting in the formation of a cavity of gas entrapped by molten metal (Fig. 14b), which subsequently will result in air/gas porosity located in the regions '1' and '2' (Fig. 14c) more than in the surroundings. The porosity measurements and the tensile properties carried out at various locations on the casting, shown in Fig. 15, highlight these observations. Specimens from location '1' and '2', (i.e. far from the gate), show poor strength and ductility, whereas from location '6', closer to the gate, the properties are better. Although the high velocity along the side walls seems to be attributed to the lubrication process in HPDC, the work of Zhao et al. clearly indicates the limita-

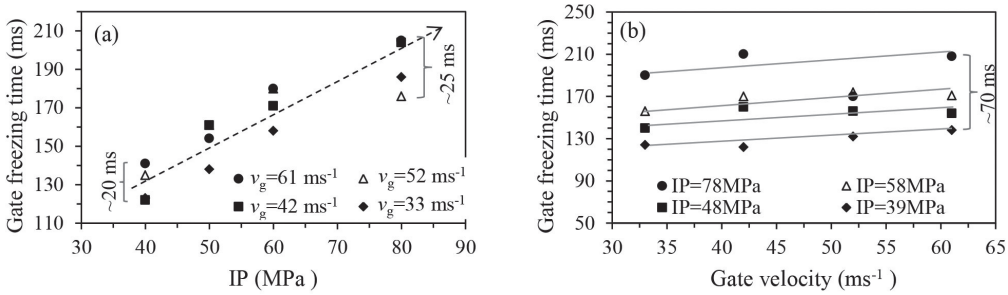


***Figure 12. Effect of (a) intensification pressure and (b) gate velocity, on the gate freezing time.***[16]

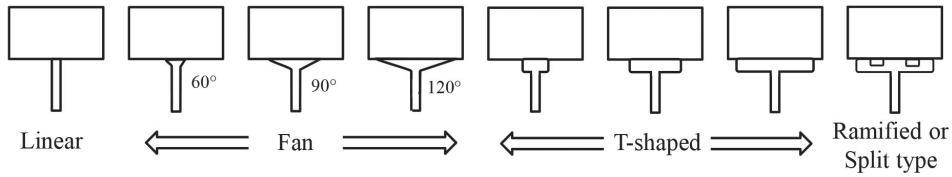


***Figure 13. Different types of runner-gate systems used by Itamura et al.***[36] ***The gate angle in the Fan-type and the gate width in the T-shaped systems were varied.***

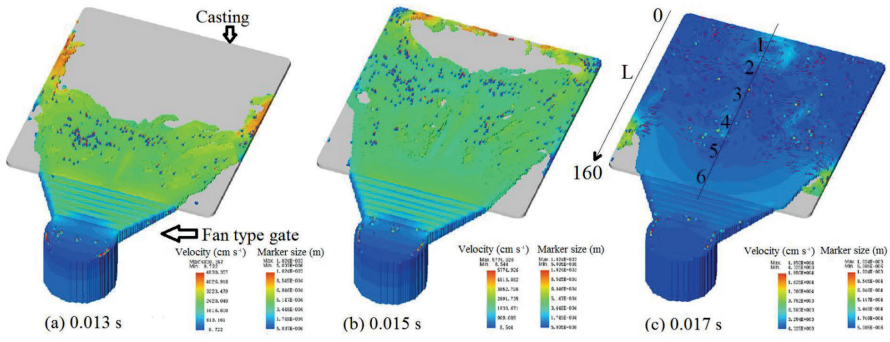


***Figure 14. The simulation results of melt flow velocity and gas entrapment (represented by marker size) at different time of injection. Markers with different colors indicate entrapped gas with different size. Sampling location for tensile and porosity measurements is indicated in (c).***[37]

tions of the fan type gate for the analyzed diecasting geometry. Ghomashchi[20] reached similar conclusions regarding minimum porosity content near the gate and maximum close to the overflows for a similar fan-type gate.

Kim et al. experimentally tested three of the previously four gating systems, namely finger-, tangential- and split-type as shown in Fig. 16, by using an ADC 12 alloy (equivalent to US A384).[38] It has been shown that the split type was the best amongst all the three from the point of view of flow pattern, temperature distribution during filling and soundness of casting. On the contrary, the work of Dargusch et al.[39] referred to an A413 diecasting alloy showed that, among the three gate types shown in Fig. 17, the tangential gate delivery system was the most efficient in terms of uniform filling of the molten metal, less turbulence and compact die size. Another advantage of the tangential system, which is limited or absent in the other gate types, is the possibility of directing the metal flow. Further, the distance between the biscuit and the gate is reduced in tangential type (Fig. 17c): this decreases the melt flow-length resulting in lower heat loss during filling and saving cost. Thus, it could be concluded that every diecasting geometry can be associated with its own filling time, filling velocity, and its own gating system. Selecting the best combination minimizes defects and improves productivity.

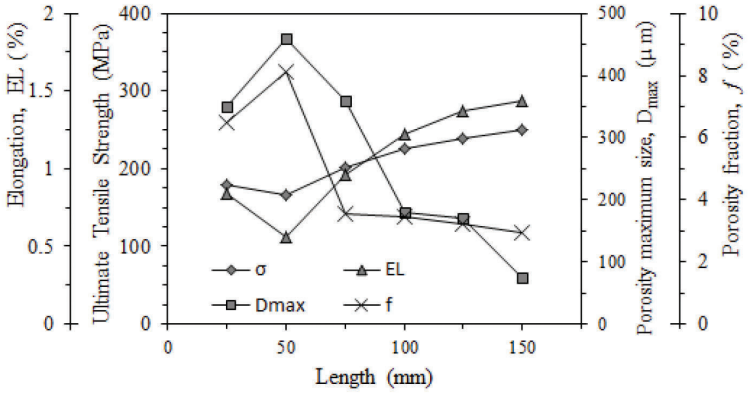


***Figure 15. Tensile properties and porosity measurements made at different locations along the length of the casting (L) as shown in Fig. 13c .[37]***

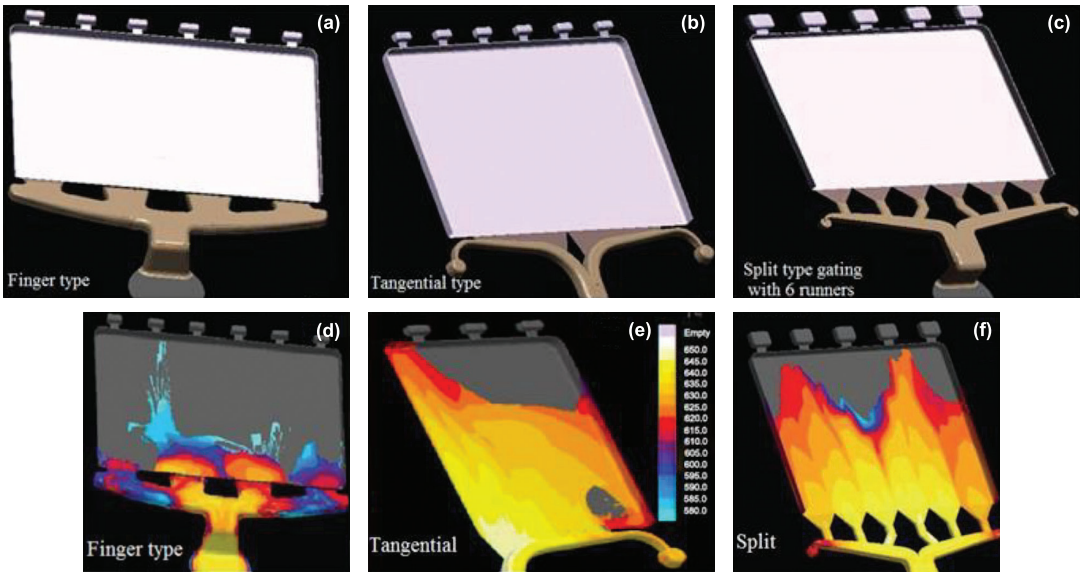


***Figure 16. (a,b,c) Schematic of the three gate types along with the corresponding (d,e,f) temperature distribution during die filling.[38]***

Generally, the casting dimensions are known and therefore the die design could be virtually modeled to fix the casting parameters, such as the injection parameters and design of the runner-gate systems, vents and overflows. The capacity of the HPDC machine, known by its force (F), should be taken into consideration while optimizing the parameters. The locking force ($F_m$) is the force that resists the mold opening at the end of Stage III and is proportional to the metal pressure ($P_m$) inside the total projected area (A) of the die in the parting plane including the casting, runner, biscuit and the overflows as shown schematically in Fig. 18. Therefore, the capacity of the machine must be higher than the locking force in order to open the dies at the end of the operation and may be represented as follows:

$$F > F_m = P_m \cdot A \qquad \text{Eqn. 1}$$

Considering the maximum pressure, approximately equal to the IP, that could be applied in the process and the most suitable runner-gate system for a defined casting geometry, the injection parameters can be inter-related using the following relationships:[40]

$$v_g = C_d \cdot \sqrt{\frac{P_m \cdot 2g}{\rho}} \qquad \text{Eqn. 2}$$

$$v_{PII} = Q \cdot \frac{4}{\pi \cdot D^2} \qquad \text{Eqn. 3}$$

$$Q = A_g \cdot v_g \qquad \text{Eqn. 4}$$

The coefficient of discharge ($C_d$), previously described, is a fraction which indicates the effective area that is available at the gate during the metal flow and is generally found to be between 0.6 to 0.8 in aluminum alloys depending on the streamlined runner systems.[41] It may be observed that for a constant flow rate, $Q$, the velocity at the gate ($v_g$) is inversely proportional to gate area ($A_g$); therefore, in order to have high gate velocities, thin gates are designed, generally between 0.5 and 3 mm (~0.02 and 0.118 inch),[42-45] giving the castings an added advantage of avoiding part distortion or breakout during post-casting operations such as trimming.[46] However, it would be challenging to prevent early solidification of the melt in the thin gates, which could be detrimental to the casting quality. Further, the cavity filling time ($t_{fill}$), which indicates how quickly a casting could be filled, is related to the '$v_g$' and '$A_g$', for a known volume of casting or the molten metal flow though the gate, $V$, as follows:

$$t_{fill} = \frac{V}{A_g \cdot v_g} \qquad \text{Eqn. 5}$$

The temperature of the molten metal ($T_m$) and the die ($T_d$) are the two important parameters that have to be considered while calculating the '$t_{fill}$' and are inter-related as follows:[40]

$$t_{fill} = K\left(\frac{T_m - T_f + f_s \cdot Z}{T_f - T_d}\right)S \qquad \text{Eqn. 6}$$

where, '$K$' is the empirically derived constant related to the thermal conductivity of the die steel, '$T_f$' is the liquidus temperature of the metal, '$f_s$' is the fraction solid formed during the filling stage in %, '$Z$' is a conversion factor from °C to % and '$S$' is the characteristic wall thickness of the casting.

## Conclusions

The present work critically reviews the effect of injection parameters on the porosity and tensile properties of Al-Si alloy high pressure die castings. The following are the salient observations:

- Higher values of gate velocity and intensification pressure reduce porosity and increase tensile properties. However, practical conditions such as die erosion and the capacity of the machine impose limitations.
- Thin gates (between 1 to 3 mm [0.039 to 0.118 inch]) and high gate velocities are critical in avoiding early solidification. In order to overcome turbu-

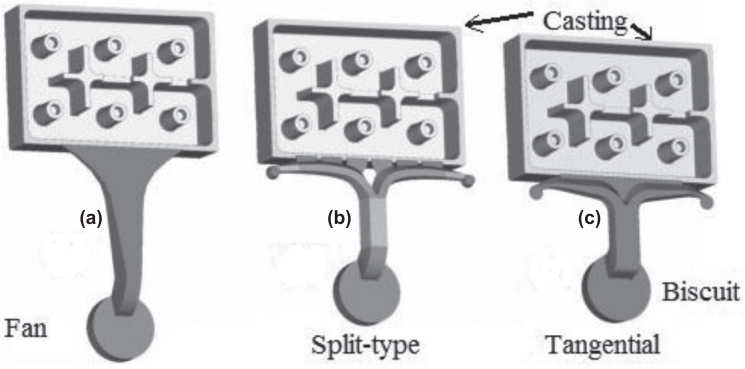


*Figure 17. Runner-gate systems investigated by Dargush et al.[39]*

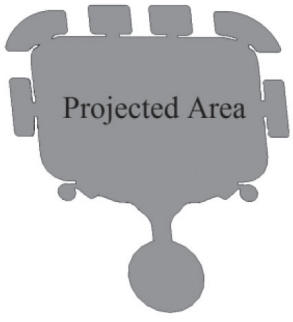


*Figure 18. Projected area of the die in the parting surface.*

lence, the velocity of the plunger in Stage I should be approximately 10 times lesser than the velocity in Stage II.

- Selecting the ideal runner-gate system is crucial and is strictly dependent on the casting geometry. The best system would bring about a uniformity in filling; concomitantly, reducing the turbulence, filling time and the melt flow length.


## Acknowledgements

This work was developed with the financial support of the European Project StaCast (New Quality and Design Standards for Aluminium Alloys Cast Products, FP7-NMP-2012-CSA-6, project n. 319188). The authors would like to acknowledge the skillful contribution of all the partners.


## List of Symbols

$P_m$ = metal pressure
$\rho$ = metal density
$g$ = gravitational constant
$v_g$ = gate velocity
$v_{pI}$ = velocity of the melt in stage I
$v_{pII}$ = velocity of the melt in stage II
$D$ = plunger diameter
$C_d$ = coefficient of discharge
$F$ = force
$A$ = projected area of the die in the parting plane
$A_g$ = total gate area
$Q$ = metal flow rate
$IP$ = intensification pressure
$t_{fill}$ = cavity filling time
$V$ = volume of the casting
$T_m$ = temperature of the molten metal
$T_d$ = die surface temperature just before the shot
K = empirically derived constant related to the thermal conductivity of the die steel
$T_f$ = liquidus temperature of the metal
$f_s$ = % fraction solid formed during the filling stage
Z = conversion factor from °C to %
S = characteristic wall thickness of the casting

## REFERENCES


1. Benini, A., "High-Pressure Die-Casting Technology – Casting Process and Machines Through the Analysis of Some Case Histories," Brochure of Italpresse (BS - Italy) (2009).
2. Vinarick, E.J., "Die Casting Processes," John Wiley & Sons Inc., NJ, USA (2003).
3. Dørum, C., Laukli, H.I., Hopperstad, O.S., Langseth, M., "Structural Behaviour of Al–Si Die-castings: Experiments and Numerical Simulations," *European Journal of Mechanics - A/Solids*, vol. 28, issue 1, pp. 1–13 (2009).
4. Avalle, M., Belingardi, G., Cavatorta, M. P., Doglione, R., "Static and Fatigue Strength of a Die Cast Aluminium Alloy under Different Feeding Conditions," *Proceedings of the Institution of Mechanical Engineers, Part L: Journal of Materials Design and Applications*, pp. 25-30 (2002).
5. Avalle, M., Belingardi, G., Cavatorta, M.P., Doglione, R., "Casting Defects and Fatigue Strength of a Die Cast Aluminium Alloy: A Comparison Between Standard Specimens and Production Components," *Int. J. Fatigue*, vol. 24, pp. 1–9 (2002).
6. Srivastava, M.C., "High Pressure Die Casting of Aluminium and Magnesium Alloys," Ph.D.Thesis, NTNU-Norway, 2009:207 (2009).
7. Kotadia, H.R., Babu, N.H., Zhang, H., Arumuganathar, S., Fan, Z., "Solidification Behavior of Intensively Sheared Hypoeutectic Al-Si Alloy Liquid," *Metall. Mater. Trans. A,* vol. 42, pp. 1117-1126 (2011).
8. Joshi, V., Srivastava, A., Shivpuri, R., Rolinski, E., "Investigating Ion Nitriding for the Reduction of Dissolution and Soldering in Die-casting Shot Sleeves," *Surf. Coat. Technol.,* vol. 163–164, pp. 668–673 (2003).
9. Helenius, R., Lohne, O., Arnberg, L., Laukli, H.I.,"The Heat Transfer During Filling of a High-Pressure Die-casting Shot Sleeve," *Mater. Sci. Eng., A,* vol. 413–414, pp. 52–55 (2005).
10. Verran, G.O., Mendes, R.P.K., Rossi, M.A., "Influence of Injection Parameters on Defects Formation in Die Casting Al12Si1,3Cu Alloy: Experimental Results and Numeric Simulation," *J. Mater. Process. Technol.,* vol. 179, pp. 190–195 (2006).
11. Ward, M., "Gating Manual," NADCA, USA (2006).
12. Jian, X., Wu, G., "An Experimental Investigation on the Flow Behavior of Liquid Aluminium Inside Pressure Die-casting Dies Using High-Speed Photography," SPIE Proceedings, vol. 1358, *19th International Congress on High-Speed Photography and Photonics*, pp. 1237-1244 (1990).
13. Hartmann, G.C., Chadwick, G., Lindeberg, B., "Process Analysis, Computer Modelling and Production Development of High Pressure Die Casting," EUR 15230EN (1995).
14. Karban, R., "The Effects of Intensification Pressure, Gate Velocity, and Intermediate Shot Velocity on the Internal Quality of Aluminum Die Castings," PhD thesis, Purdue University, West Lafayette, IN, USA (2000).
15. Davis, A.J., Robinson, P.M., "Production of Aluminum Die Castings Using a Fan Gate, Part 2. The Effect of Flow Conditions at the Gate on Casting Quality," *Trans. Society of Diecasting Engineers*, Paper No. G-T75-122, Detroit, MI, USA (1975).
16. Niu, X.P., Tong, K.K., Hu, B.H., Pinwill, I., "Cavity Pressure Sensor Study of the Gate Freezing Behaviour in Aluminium High Pressure Die Casting," *Int. J. Cast Met. Res.,* vol. 11, pp. 105–112 (1998).
17. Gunasegaram, D.R., Finnin, B.R., Polivka, F.B., "Melt Flow Velocity in High Pressure Die Casting: Its Effect on Microstructure and Mechanical Properties in an Al–Si Alloy," *Mater. Sci. Technol.,* vol. 23, pp. 847-856 (2007).

18. Caceres, C.H., Selling, B.I., "Casting Defects and the Tensile Properties of an Al-Si-Mg Alloy," *Mater. Sci. Eng. A*, vol. 220, pp. 109-116 (1996).
19. Ghomashchi, M.R., "High-Pressure Die Casting: Effect of Fluid Flow on the Microstructure of LM24 Die-Casting Alloy," *J. Mater. Process. Technol.,* vol. 52, pp. 193–206 (1995).
20. Ghomashchi, R., *Proceedings of the 9th International Conference on Aluminium Alloys* (ed. J. F. Nie et al.), Melbourne, Institute of Materials Engineering Australasia Ltd. pp.1290–1296 (2004).
21. Lumley, R., Deeva, N., Gershenzon, M., "An Evaluation of Quality Parameters for High Pressure Die Castings," *Int. J. of Metalcasting*, vol. 5, issue 3, pp. 37-56 (2011).
22. Timelli, G., Bonollo, F., "Quality Mapping of Aluminium Alloy Diecastings," *Metallurgical Science and Technology*, vol. 26, no.1, pp. 2-8 (2008).
23. Timelli, G., "Constitutive and Stochastic Models to Predict the Effect of Casting Defects on the Mechanical Properties of High Pressure Die Cast AlSi9Cu3(Fe) Alloys," *Metallurgical Science and Technology*, vol. 28, no. 2, pp. 9-17 (2010).
24. Gunasegaram, D.R., Givord, M., O'Donnel, R.G., Finnin, B.R., "Improvements Engineered in UTS and Elongation of Aluminum Alloy High Pressure Die Castings Through the Alteration of Runner Geometry and Plunger Velocity," *Mater. Sci. Eng., A,* vol. 559, pp 276-286 (2013).
25. Pitsaris, C., Savage, G., Abbott, T., Proc. 22nd NADCA International Die Casting Cong., Indianapolis, IN, USA, pp.195-203 (2003).
26. Klein, F., Proc. 51st Annual World Magnesium Conf., Berlin, Germany, Inter. Magnesium Association (USA), pp. 35-43 (1994).
27. Herman, E.A., "Gating Die Casting Dies," NADCA, Rosemont, IL, pp. 1-3 and 73-93 (1996).
28. Dargusch, M.S., Wang, G., Schauer, N., Dinnis, C.M., Savage, G., "Manufacture of High Pressure Die-Cast Radio Frequency Filter Bodies," *Int. J. Cast Met. Res.,* vol. 18, issue 1, pp. 47-54 (2005).
29. Dargusch, M.S., Dour, G., Schauer, N., Dinnis, C.M., Savage, G., "The Influence of Pressure During Solidification of High Pressure Die Cast Aluminium Telecommunications Components," *J. Mater. Process. Technol.,* vol. 180, pp. 37-43 (2006).
30. Schaffer, P.L., Laukli, H.I., "Recent Developments in Aluminum High Pressure Die Castings," *Die Casting Engineer*, pp. 20-22 (May 2012).
31. Otarawanna, S., Laukli, H.I., Gourlay, C.M., Dahle, A.K., "Feeding Mechanisms in High-Pressure Die Castings," *Metall. Mater. Trans. A*, vol. 41, pp. 1836-1846 (2010).
32. Otarawanna, S., Gourlay, C.M., Laukli, H.I., Dahle, A.K., "Microstructure Formation in AlSi4MgMn and AlMg5Si2Mn High-Pressure Die Castings," *Metall. Mater. Trans. A*, vol. 40, pp. 1645-1659 (2009).
33. Verran, G.O., Mendes, R.P.K., Rossi, M.A., "Influence of Injection Parameters on Defects Formation in Die Casting Al12Si1,3Cu Alloy: Experimental Results and Numeric Simulation," *J. Mater. Process. Technol.,* vol. 179, pp. 190–195 (2006).
34. Verran, G.O., Mendes, R.P.K., Valentina, L.V.O.D., "DOE Applied to Optimization of Aluminum Alloy Die Castings," *J. Mater. Process. Technol.,* vol. 200, pp. 120–125 (2008).
35. Herman, E., "Searching for the Perfect Gate Velocity," *Die Casting Engineer*, pp. 58-61 (March 2004).
36. Itamura, M., Murakami, K., Harada, T., Tanaka, M., Yamamoto, N., "Effect of Runner Design on Metal Flow Into Cavity," *Int. J. Cast Met. Res.,* vol. 15, pp. 167-172 (2002).
37. Zhao, H.D., Wang, F., Li, Y.Y., Xia, W., "Experimental and Numerical Analysis of Gas Entrapment Defects in Plate ADC12 Die Castings," *J. Mater. Process. Technol.,* vol. 209, pp. 4537-4542 (2009).
38. Kim, Y.C., Kang, C.S., Cho, J.I., Jeong, C.Y., Choi, S.W., Hong, S.K., "Die Casting Mold Design of the Thin-walled Aluminum Case by Computational Solidification Simulation," *J. Mater. Sci. Technol.,* vol. 24 (3), pp. 383-388 (2008).
39. Dargusch, M.S., Wang, G., Schauer, N., Dinnis, C.M., Savage, G., "Manufacture of High Pressure Die-cast Radio Frequency Filter Bodies," *Int. J. Cast Met. Res.*, vol. 18, pp. 47–53 (2005).
40. Ward, M., "Gating Manual," NADCA, USA, (2006).
41. Herman, E., "Searching for the Perfect Gate Velocity," *Die Casting Engineer*, pp. 58-61 (March 2004).
42. Kim, C.H., Kwon, T.H., "A Runner–Gate Design System for Die Casting," *Mater. Manuf. Processes,* vol. 16 (6), pp. 789-801 (2001).
43. Lin, C.B., Ma, C.L., Chung, Y.W., "Microstructure of A380–SiC(p) Composites for Die Casting," *J. Mater. Process. Technol.,* vol. 48, pp. 236–246 (1998).
44. Chen, Z.W., "Skin Solidification During High Pressure Die Casting of Al–11Si–2Cu–1Fe Alloy," *Mater. Sci. Eng., A,* vol. 348, pp. 145-153 (2003).
45. Ji, S., Wang, Y., Watson, D., Fan, Z., "Microstructural Evolution and Solidification Behavior of Al-Mg-Si Alloy in High-Pressure Die Casting," *Metall. Mater. Trans. A,* vol. 44, pp. 3185-3197 (2013).
46. Niu, X.P., Tong, K.K., Hu, B.H., Pinwill, I., "Cavity Pressure Sensor Study of the Gate Freezing Behaviour in Aluminium High Pressure Die Casting," *Int. J. Cast Met. Res.,* vol. 11, pp. 105–112 (1998).

## Influence Of Injection Parameters On The Porosity And Tensile Properties Of High-Pressure Die Cast Al-Si Alloys: A Review

*Anilchandra R. Adamane, Lars Arnberg*
*Norwegian University of Science and Technology, Trondheim, Norway*
*Elena Fiorese, Giulio Timelli, Franco Bonollo*
*University of Padova, Vicenza, Italy*

**Reviewer:** The paper states that higher gate velocities usually correlate with sounder castings, however, my experience has been that it is not higher velocity per se that benefits casting soundness, but rather it is shorter cavity fill time. The shorter cavity fill time means higher terminal pressure, which is of great benefit in immediate compression of entrapped gas pores. Shorter cavity fill time can be achieved without increasing gate velocity if slightly larger gates are used (but not so thick as to not snap free without distorting the cast part). The benefit of timely intensification pressure is also largely to compress entrapped cavity gasses (the principal source of pores in high-pressure die castings) to smaller size, although for a very short time (ms) intensification might also collapse/compress the alpha structure and force movement of the still-molten eutectic into areas nearby the gates (thus the often-observed microstructure striations seen in and near the gates. Can the authors elaborate further on this?

***Authors:*** *The authors agree with the reviewer's comment that shorter cavity filling time per se would be more beneficial in obtaining sound castings than higher melt velocity at gates. As suggested by the North American Die Association [Product Design for Die Casting, NADCA, 2009], during the design process of a diecast component, the filling time can be preliminary estimated by taking into account the average wall thickness of the casting and the mean die temperature. These variables are critical in the premature freezing of molten metal during the filling stage. Actually, there exist empirical tables, diagrams and nomograms where a designer can decide a-priori the filling time of the die cavity. This approach does not consider the initial temperature of the metal as an input variable, which is contrary established according to the standard foundry practice,* i.e. *minimum allowed temperature to increases the die life.*

*An alternative approach takes into account the metal temperature according to the following equation*

$$t_{fill} = k\left(\frac{T_{metal} - T_{min} + f_s \cdot Z}{T_{min} - T_{die}}\right)s$$

*Therefore, it is possible to correlate the filling time '$t_{fill}$' with the gate velocity '$v_g$' according to the following equation*

$$t_{fill} = \frac{V}{A_g \cdot v_g}$$

*Upon "machining" the gate area in the die, the variable that can be varied for practical reasons and production requirements is the gate velocity, which is the common parameter of discussion in the literature. The above two equations have been included as Equations 5 and 6 in the revised manuscript.*

# Process parameters affecting quality of high-pressure die-cast Al-Si alloy

Elena Fiorese, Franco Bonollo

University of Padova
Department of Management and Engineering
Stradella S. Nicola 3
I-36100 Vicenza, Italy

**Keywords:** Al-Si alloy, high-pressure die-casting, process parameters, quality

## Abstract

In the last years, aluminium alloys have become more and more relevant because of their low density, coupled with good mechanical and corrosion properties. Different processes are available for the production of aluminium alloy components, but a very significant role is played by foundry processes. However, defects and imperfections are physiologically generated by foundry techniques, as a result of the process itself, of the alloy properties and of the die design. Particularly, high-pressure die-casting (HPDC) is considered a “defect generating process”, since an average of 5-10 % scrap is typically generated by this process. Several process parameters need to be controlled in order to obtain sound and reliable castings. Among the different process variables, the determination and control of the injection parameters remain a key requirement throughout the HPDC process.

In this work, a statistically significant sample of castings in AlSi9Cu3(Fe) alloy has been manufactured through different injection parameters in order to identify the most relevant process parameters and estimate their correlations with the quality of the casting. In particular, the plunger I and II phase velocities ($v_1$ and $v_2$), the switch point between two phases (SW) and the intensification pressure (IP) have been varied randomly in accordance to the Design of Experiment methodology. The static mechanical properties of the castings have been measured using the bending test. Furthermore, the castings have been analysed by X-rays and their percentage of porosity has been estimated by means of image analysis software. Some novel aggregate parameters, representing a measure of the mechanical energy related to the plunger motion and the thermal energy exchanged with the die have been extracted from the plunger displacement curves and from thermocouple signals. The application of statistical concepts, methods and models demonstrates that these novel parameters allow explaining and forecasting both the mechanical properties and the porosity, and therefore the overall quality of the castings.

# 1 Introduction

High-pressure die-casting (HPDC) is a cost-effective process for the production of castings in large quantities and with high dimensional accuracy. Very high flow rates can be achieved inside the die cavity and this requires careful design of the casting. The main disadvantage of HPDC is the entrapment of gas and oxides due to the turbulent flow of metal during the filling phase, resulting in porosity and deterioration of the casting quality [1].

In cold chamber HPDC, the molten metal poured into the shot sleeve is pushed into the die cavity using a hydraulic piston-cylinder arrangement. The filling of the die cavity through the plunger motion and the solidification of the casting take place in three continuous phases, which are briefly described below [2].

- Phase I. The molten metal fills up the shot sleeve and the plunger begins to move at a low velocity to avoid turbulence. The velocity of the plunger in this phase is called $v_1$.
- Phase II. The filling of the die cavity is performed at high velocity to avoid premature solidification at the gate and incomplete castings. The velocity of the plunger in this phase is called $v_2$ and the corresponding velocity of the melt at the gate is called gate velocity, $v_g$. The transition from phase I to phase II is termed as switch position (SW).
- Phase III. Intensification pressure (IP), is applied on the molten metal once the die cavity is full to limit the formation of shrinkage porosity and the expansion of entrapped air.

HPDC is considered a “defect generating process”, since an average of 5-10 % scrap is typically generated by this process. Several process variables, especially the injection parameters, need to be controlled in order to obtain sound and reliable castings. Ghomashchi [3] and Gunasegaram et al. [4-5] have experimented that the percentage of porosity may decrease by increasing the gate velocity. Moreover, Gunasegaram [4-5], Lumley [6] and Fiorese et al. [7] have shown that the tensile mechanical properties can improve by increasing the gate velocity, and then the II phase velocity, due to the reduced porosity. Otarawanna et al. [8-9] have demonstrated that enhancing the intensification pressure, the porosity drops down and the mechanical properties consequently increase. Therefore, some correlations between process parameters and quality of castings already exist in literature. Nevertheless, the gap in knowledge is evident, as the existing results are fragmented, partial, sometimes conflicting and without any statistical basis.

The aim of the present work is to find the process parameters affecting the quality of high-pressure die-cast Al-Si alloy through a systematic experimental approach. In section 2 of the paper, the experimental procedure is presented. In particular, casting experiment, shot profile recordings, radiographic and bending testing are described. In section 3, a novel approach based on numerical processing of signals and statistical analysis is proposed. This approach permits identifying some significant correlations between process and quality of the castings. In section 4, conclusions from this work are drawn.

# 2 Experimental procedure

## 2.1 Casting experiment

For research purposes, a die for manufacturing horseshoe-shaped castings of aluminium alloy has been designed and realized in the frame of European Music project (MUlti-layers control & cognitive System to drive metal and plastic production line for Injected Components, N. 314145).

The castings have been manufactured using a Italpresse cold chamber die-casting machine with locking force 7500 kN, shot chamber length 0.482 m and diameter 0.080 m. The fill fraction of the shot sleeve was kept constant at 0.40. The furnace was set to 705 °C, while the pouring temperature was approximately 45 °C lower. The temperature of the die was kept constant by a thermoregulation system. The temperature of the oil cooling channels was set to 245 °C for the moving half of the die, and to 235 °C for the fixed half; the flow, for each channel of both die parts, was set to 1 l/s. Moreover, automatic spraying and blowing process were performed in order to properly cool down the die material and aid the release of the casting after its complete solidification. The shot sleeve and the die were preheated before the experimental campaign and reached a quasi-steady state temperature after some shots. The whole cycle, including injection, die opening and closing, casting ejection, spraying and blowing lasted approximately 70 s. The total weight of each casting obtained, including the runners, gating and overflow system was approximately 2000 g.

In the present work an EN AB-46000 aluminium alloy (European designation, equivalent to the US designation A380), according UNI EN 1706, with the composition reported in table 1, was cast. This alloy has a liquidus-solidus temperature range of approximately 593-538 °C [10].

Table 1: Chemical composition of the casting alloy (wt. %)

| Alloy | Si | Fe | Cu | Mn | Mg | Cr | Ni | Zn | Al |
|---|---|---|---|---|---|---|---|---|---|
| EN AB-46000 | 10.40 | 0.82 | 2.95 | 0.55 | 0.15 | 0.15 | 0.55 | 1.2 | bal. |

A Design of Experiments (DoE) has been planned and applied, which provided to change the plunger I and II phase velocities ($v_1$ and $v_2$), the switch position between two phases (SW), and the III phase intensification pressure (IP). Each independent variable, called factor, has been analysed within a specific range of variation. The factors, with their lower and upper levels of observation, are given in table 2. A factorial experiment has been performed, i.e. in each complete replicate of the experiment all possible combinations of the levels of the factors were investigated. Factorial designs are frequently used in experiments involving several factors where it is necessary to study the joint effect of the factors on a response. The most important of the factorial designs is that of k factors, each at only two levels: a complete replicate of such a design requires $2^k$ observations [11]. By considering four factors and two levels for each factor, a total of 16 designs were needed. However, a central design has been added to these series in order to improve the precision of the experiment and check its repeatability, by leading to 32 designs. Therefore, a statistically significant sample has been manufactured, that means from 3 to 7 castings for each of 32 designs.

Table 2: Factors with their different levels of observation

| Factor | Low level | High level |
|---|---|---|
| $v_1$ (m/s) | 0.2 | 0.8 |
| $v_2$ (m/s) | 1.5 | 4.0 |
| SW (m) | 0.3 | 0.35 |
| IP (MPa) | 50 | 100 |

## 2.2 Shot profile recordings, radiographic and bending testing

During the experimental campaign, each casting was documented with its shot profile, corresponding to the plunger displacement curve. Temperature measurements were executed during the whole cycle using a thermocouple mounted in the die in the middle of the stepped wedge.

The stepped wedge is a zone of the casting with dimensions: 0.059 m width, thickness ranging from 0.001 m through 0.003 m, and 0.2 m length (figure 1). The stepped wedge of the casting has been chosen for porosity measurements, as it is the most critical zone and emphasizes the difference in quality level of the castings obtained by different process parameters. The stepped wedges has been analysed by a macro-focus X-ray equipment and their percentage of porosity has been estimated by means of an image analysis software. The average settings for the X-ray analyses of the stepped wedge were 60 kV and 1.5 mA.

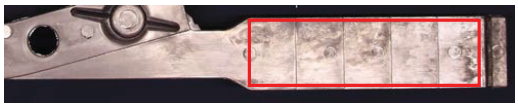

Figure 1: Position of specimen for radiographic testing in the stepped wedge of the casting

Bending test specimens were trimmed from the flat appendixes of the casting (figure 2). Four specimens for each casting were drawn with dimensions: 0.04 m width, 0.002 m thickness and 0.06 m length. The three-point bending test has been carried out with displacement control 4 mm/min and rating force 10 kN. Experimental data have been collected and processed to provide peak loads (kN) of the specimens.

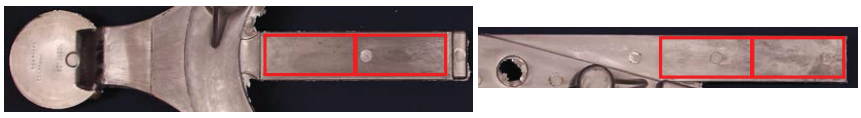

Figure 2: Position of specimens for bending testing in the appendixes of the casting

# 3 Results and discussion

## 3.1 Novel aggregate process parameters

Extraction of data or information from the plunger displacement and temperature signals constitutes a fundamental step for identifying some significant correlations between process parameters and quality of the castings. A simplistic approach consists in extracting some instantaneous or maximum values from the plunger displacement curves and temperature signals. Such approach is as simple as ineffective in finding statistically significant correlations between process and quality of the castings. For this reason, a new approach based on aggregate parameters has been developed and proposed.

The new aggregate parameters extracted from the sensor curves have the characteristics described below.

- They should represent the physical phenomena affecting the filling of the die and the solidification of the casting.
- They do not belong to just the set of physical variables that were directly measured by the sensors, i.e. position or temperature.
- Being the filling of the die and the solidification of the casting an “integral process”, these variables should represent the time history of the phenomenon, rather than just some instants. Therefore, they have an integral nature.

In accordance with the first of the three requirements previously defined, the variables should represent the mechanical energy transmitted to the melt by the plunger, or the thermal energy exchanged with the die. To enlarge the set of data available and, therefore, to provide a more exhaustive explanation of the phenomena, the measured values provided by the sensors have been numerically processed to extract some new signals, as stated in the second of the three requirements previously defined. Clearly, the availability of effective and reliable numerical schemes to perform signal processing is of primary importance and allows reducing the number of sensors to be employed, e.g. by avoiding speed or acceleration direct measurements.

In particular, the plunger speed and acceleration have been estimated through numerical differentiation of the measured plunger position. Indeed, both these variables are of interest for this analysis in order to investigate the mechanical energy. As for the speed, its effect on porosity and tensile strength has been briefly discussed in literature, as mentioned in the Introduction, although no thorough investigation has been proposed. In contrast, since acceleration measurements are usually not provided, the effect of acceleration has never been studied, unless vibrocasting process is performed [12]. On the other hand, however, acceleration represents the inertial forces and it should be therefore accounted for.

In order to perform accurate estimation of these variables, by reducing the high-frequency noise usually introduced by numerical derivation [13], an improved 7th order Lanczos low-noise differentiator has been adopted, in accordance with the following scheme:

$$v(k) = \frac{3p(k+3) + 2p(k+2) + p(k+1) - 3p(k-3) - 2p(k-2) - p(k-1)}{28\,\Delta t} \quad (1)$$

where *v(k)* and *p(k)* denote the k-th sample of, respectively, the estimated speed and the measured position at time $k\Delta t$, with $\Delta t$ the sample time. Obvious extension of equation (1) is adopted to estimate acceleration *a(k)*. Such a scheme has been applied, in a non-causal way, since it trades off very effectively between the need of smoothing the numerical noise, while ensuring accurate estimation of the signal peaks with small computational effort [13]. Additionally, if it is implemented in a causal way by just considering previous samples, it can be implemented on-line to perform real-time control of the process with negligible time delay.

In figure 3, the measured position, and the computed speed and acceleration of the plunger of an arbitrary casting, assumed as an example, have been represented.

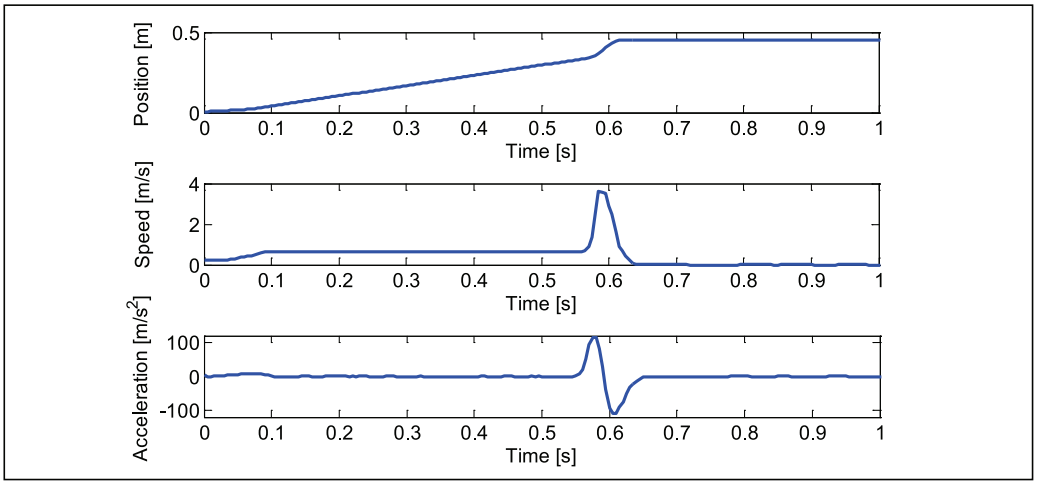


Figure 3: Example of position, speed and acceleration of the plunger during the process

To account for the integral nature of the HPDC process, whose final outcome is expected to depend on the whole process (or on some time intervals), rather than just some instants, integral values of some variables computed over different time intervals are considered, according to the third of the three abovementioned requirements. This is translated, in practice, into the computation of average values or of energy.

### 3.1.1 Parameter representative of the energy associated to the flow forces: $E_f$

Two meaningful variables have been selected to represent the effect of the mechanical power (or energy), and validated through a thorough statistical analysis, which is reported in section 3.2.

The first influential aggregate variable is a parameter representative of the energy associated to the flow forces, due to the contact between the melt and the die or some solid particles, such as oxides or inclusions, which are known to be preferential nucleation sites for porosity. Flow forces are proportional to the square velocity [14] and therefore the energy, i.e. the integral over time of the power, is proportional to the integral of the cubic velocity. To account for the whole process of filling of the die, integration of the cubic velocity has been performed over both the I and the II phases, i.e. from time *0* to time *t_end_II*:

$$E_f = \int_0^{t\_end\_II} v(t)^3 \, dt \tag{2}$$

The computation of the integrals has been performed numerically with the trapezoidal rule, in accordance with the following recursive scheme, with $E_f = E_f\left(\frac{t\_end\_II}{\Delta t}\right)$:

$$E_f(k) = E_f(k-1) + \Delta t \frac{v(k)^3 + v(k-1)^3}{2} \quad \left(k = 1, \ldots, \frac{t\_end\_II}{\Delta t}\right) \tag{3}$$

where $E_f(k)$ is the integral value at time $k\Delta t$, while $v(k)^3$ is the signal to be integrated. Such a scheme has been adopted to ensure negligible signal drift, due to the unavoidable low-frequency noise usually introduced by numerical integration schemes [15].

A second physical interpretation can be given to this parameter, according to Bernoulli principle. Indeed, $E_f(k)$ can be seen as a meaningful measure of the energy associated to the pressure forces, since the pressure variation is related to the square velocity.

Besides having two different and significant physical interpretations, this parameter deserves a mathematical interpretation, in accordance with some works proposed in the literature showing that the II phase speed has more influence compared with the one of I phase [4-5,7]. The presence of the cubic exponent in the integral, as assumed in the novel parameter here proposed, gives higher weight to the higher speed values. The proposed parameter is therefore significantly affected by the peak speed and by the II phase speed, but also accounts for the I phase.

### 3.1.2 Root mean square acceleration: $a_{RMS}$

The second influential aggregate variable assumed is the root mean square (RMS) acceleration in the II phase, i.e. from time *t_end_I* to time *t_end_II*:

$$a_{RMS} = \sqrt{\frac{\int_{t\_end\_I}^{t\_end\_II} a(t)^2 dt}{t\_end\_II - t\_end\_I}} \tag{4}$$

In practice, this parameter represents the average value of the inertial forces related to the plunger motion.

### 3.1.3 Parameter representative of the thermal energy: $E_t$

Besides being affected by kinetic variables, as the speed and acceleration, and the related aggregate parameters, the effect of the temperature can be also accounted for in the model to be developed.

Once again, to account for the abovementioned integral nature of the process, the integral value of the signals of the thermocouple mounted in the die have been computed. In figure 4, an example of the signal measured by the thermocouple mounted in the die is shown.

Another parameter has been therefore defined and numerically computed as the integral of the temperature in the II phase, i.e. from time *t_end_I* to time *t_end_II*. This aggregate variable, referred to as $E_t$, represents in practice, the thermal energy exchanged between the melt and the die in the solidification of the casting during the filling of the die, by considering the presence of a system with outflow [16]:

$$E_t = \int_{t\_end\_I}^{t\_end\_II} T(t)dt \tag{5}$$

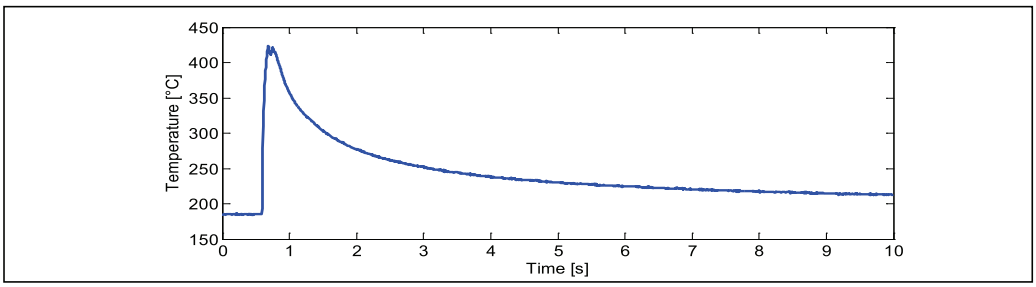


Figure 4: Example of signal measured by the thermocouple mounted in the die

## 3.2 Statistical analysis

The application of statistical concepts, methods and models has been employed in this section to demonstrate that these novel process parameters allow explaining and forecasting both the static mechanical properties and the porosity, and therefore the overall quality of the castings.

### 3.2.1 Correlations between process and static mechanical properties

In order to find some statistically significant correlations between aggregate process parameters and mechanical properties measured in the appendixes of the castings (figure 2), both exploratory and confirmatory analyses have been carried out.

The exploratory analysis includes summary statistics (i.e. minimum, maximum, median, 25$^{th}$ percentile, 75$^{th}$ percentile, mean and standard deviation) and graphical displays of the data, such as boxplots, without making any assumption on distributions or models [17].

The castings have been discriminated in two groups on the basis of their peak load, to analyse the summary statistics of the two most influential process parameters for two groups, i.e. $a_{RMS}$ and $E_t$. The other parameter, i.e. $E_f$, has a weaker correlation and therefore is not reported here for brevity. The first group collects the castings with peak load lower or equal to 1.1 kN (see table 3), while the second one those with peak load greater than this value (see table 4). The threshold of 1.1 kN corresponds to the median value of all the measured peak loads.

Table 3: Summary statistics of the parameters for castings with peak load ≤ 1.1 kN

| Parameter | Min | 1st Qu. | Median | 3rd Qu. | Max | Mean | St. dev. |
|---|---|---|---|---|---|---|---|
| $a_{RMS}$ $[m/s^2]$ | 17.11 | 21.84 | 36.09 | 46.36 | 64.57 | 34.80 | 12.50 |
| $E_t$ $[°Cs]$ | 7.21 | 8.62 | 9.30 | 9.94 | 13.12 | 9.27 | 1.10 |

Table 4: Summary statistics of the parameters for castings with peak load > 1.1 kN

| Parameter | Min | 1st Qu. | Median | 3rd Qu. | Max | Mean | St. dev. |
|---|---|---|---|---|---|---|---|
| $a_{RMS}$ $[m/s^2]$ | 29.78 | 51.32 | 65.73 | 71.46 | 80.59 | 60.23 | 14.70 |
| $E_t$ $[°Cs]$ | 3.75 | 6.87 | 7.76 | 8.22 | 10.50 | 7.47 | 1.42 |

The boxplots of these two process parameters for the two groups of castings are represented in figure 5. This figure highlights that the $a_{RMS}$ and the $E_t$ significantly affect the peak load of the castings (referred to as $PL$), since the interquartile ranges of the two groups are markedly distinct. This fact is corroborated for the $a_{RMS}$ by figure 6, which plots the exponential of the median peak load (called $PL_{median}$) against this parameter. The graph of $E_t$ has been omitted for brevity. The median value has been calculated between the peak loads of the four bending test specimens obtained from each casting. Indeed, the median value is more representative than the mean in the presence of outliers, due to random and uncontrolled exogenous factors. The fitting models for these two parameters approximate the data distribution with correlation coefficients, respectively, equal to 0.66 and 0.51. Although these values do not approach the ideal target of 1, they should be assumed as satisfactory, since they have been computed through a relevant number of samples, and in the presence of the unavoidable uncertainty and disturbance of exogenous factors, affecting this process.

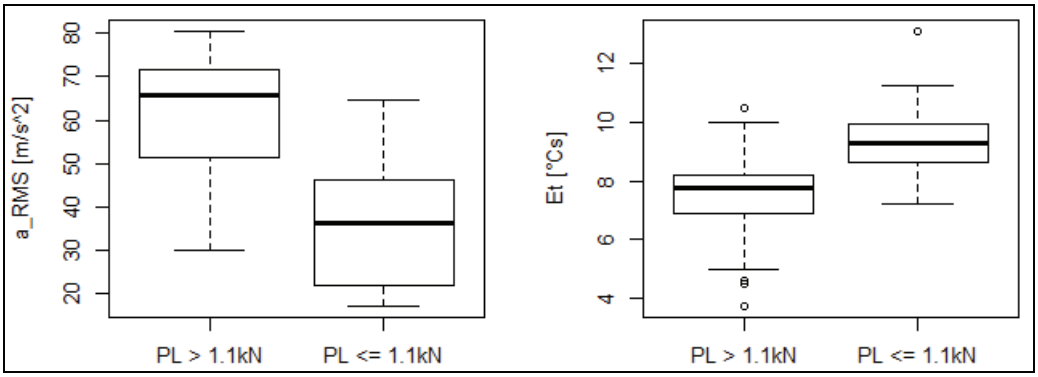


Figure 5: Boxplots of $a_{RMS}$ and $E_t$ parameters for the two groups of castings

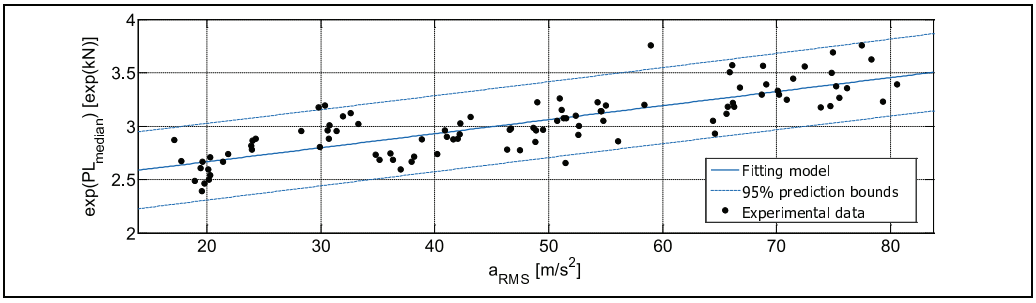


Figure 6: Plot of the exponential of the median peak load ($PL_{median}$) against $a_{RMS}$ ($R^2 = 0.66$)

The results of the exploratory analysis have been also confirmed through the application of the formal statistical methods performed through the confirmatory analysis. In particular, in order to draw conclusions about the population and by taking advantage of the large size of the sample investigated, t-tests and regression models have been developed. T-tests executed on $a_{RMS}$ and $E_t$ demonstrate that there is true difference in means between the two groups of castings with 95 % confidence interval and the p-values are $8.4e^{-15}$ and $4.2e^{-10}$, respectively. The p-value measures the evidence that there is true difference in means between the two groups of castings: the smaller the p-value (particularly less than 0.05), the stronger the evidence [17]. In contrast, the t-test carried out on $E_f$ has shown that there is a weaker difference, and therefore a weaker correlation. Nevertheless, it is worth noticing that the t-test may fail if the difference in means between the two groups is small [17], as it is the case of $E_f$.

In order to provide a more complete description of the complex phenomenon investigated, a multivariable regression model has been developed, including all the three parameters discussed. A regression model approximates the relationship between a response and a set of predictors (covariates). In other words, a regression model attempts to partially explain the variation in the response by predictors/covariates [18-19]. In this case, the response is the exponential of the $PL_{median}$ (median peak load), while the predictors are the three novel process parameters $E_f$, $a_{RMS}$ and $E_t$. An exponential model has been assumed since exponential functions have asymptotic behaviours, which are reasonable and prevent from the wrong prediction of infinite values of the peak load, as linear models do. The inclusion of the parameter $E_f$ in the regression model, besides the most influential ones $a_{RMS}$ and $E_t$, allows further improving the model correctness, by leading to an overall 0.68 correlation coefficient, which is once again highly satisfactory. The final model obtained is therefore the following one:

$$\exp(PL_{median}) = \beta_0 + \beta_1 E_f + \beta_2 a_{RMS} + \beta_3 E_t \quad (6)$$

The fitted coefficients for the alloy investigated are the following ones: $\beta_0 = 2.10$; $\beta_1 = -0.03$; $\beta_2 = 0.01$ and $\beta_3 = -0.05$. The diagnostic plots (figure 7) highlight that this model fits the data well, because the residual plot does not show any pattern, and the QQ plot shows normality since its points do not deviate from a straight-line [18]. The conclusions are reliable and convincing, as the results from exploratory and confirmatory analyses agree.

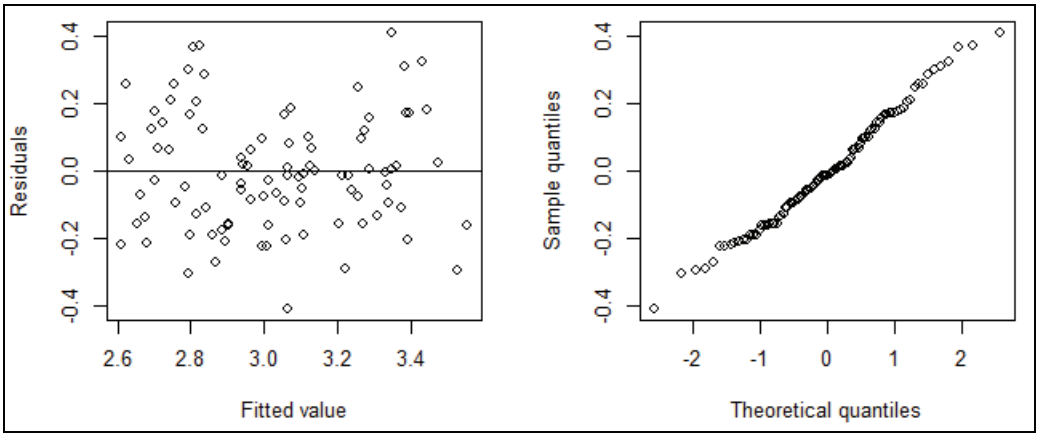


Figure 7: Residual plot and QQ plot for the model in equation (6)

Just to allow a graphical representation, the model in equation 6 has been projected in the two dimensional set of the two independent variables $a_{RMS}$ and $E_t$, and then represented in figure 8. It can be seen how the plane of the regression model fits very effectively the experimental data.

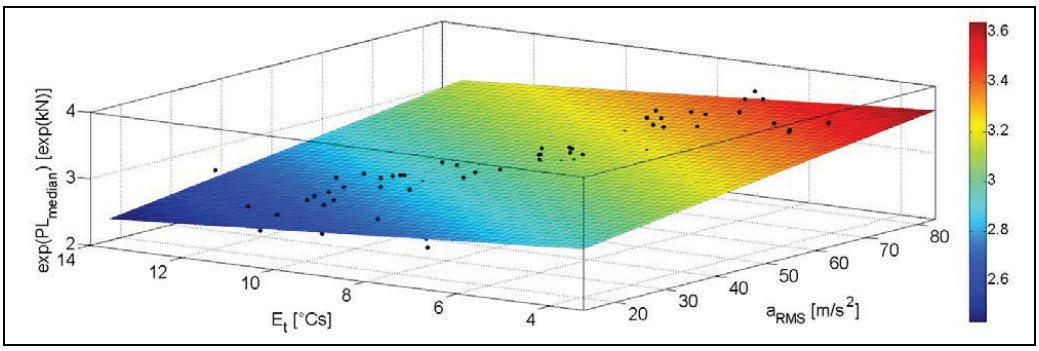


Figure 8: Three-dimensional projection of the model in equation (6)

### 3.2.2 Correlations between process and porosity

In order to find some statistically significant correlations between aggregate process parameters and porosity measured in the stepped wedge of the castings (figure 1), the same analyses of section 3.2.1 have been replicated for the porosity.

The castings have been discriminated in two groups on the basis of their percentage of porosity, to analyse the summary statistics of the three novel process parameters for two groups. The first group collects the castings with percentage of porosity lower or equal to 2 % (see table 5), while the second one those with porosity greater than this value (see table 6). Based on a common practice, a threshold of 2 % porosity has been chosen to discriminate sound and poor castings.

Table 5: Summary statistics of the parameters for castings with 2 % porosity or lower

| Parameter | Min | 1st Qu. | Median | 3rd Qu. | Max | Mean | St. dev. |
|---|---|---|---|---|---|---|---|
| $E_f\,[m^3/s^2]$ | 0.29 | 0.86 | 1.09 | 1.29 | 2.09 | 1.09 | 0.39 |
| $a_{RMS}\,[m/s^2]$ | 19.41 | 50.85 | 56.09 | 70.55 | 80.59 | 58.95 | 13.68 |
| $E_t\,[°Cs]$ | 4.61 | 7.14 | 7.97 | 8.33 | 10.15 | 7.75 | 1.16 |

Table 6: Summary statistics of the parameters for castings with more than 2 % porosity

| Parameter | Min | 1st Qu. | Median | 3rd Qu. | Max | Mean | St. dev. |
|---|---|---|---|---|---|---|---|
| $E_f\,[m^3/s^2]$ | 0.20 | 0.37 | 0.49 | 0.75 | 2.01 | 0.68 | 0.51 |
| $a_{RMS}\,[m/s^2]$ | 17.11 | 21.06 | 29.07 | 40.82 | 68.79 | 34.05 | 16.98 |
| $E_t\,[°Cs]$ | 3.75 | 8.05 | 9.41 | 10.07 | 13.12 | 8.89 | 2.00 |

The boxplots of two of the three process parameters for the two groups of castings are represented in figure 9. This figure highlights that the $a_{RMS}$ significantly affects the porosity of the castings (referred to as *Por*), since the interquartile ranges of the two groups are markedly distinct. This fact is confirmed by figure 10, which plots the natural logarithm of the porosity against such a parameter, in order to represent an exponential effect of the RMS acceleration on the porosity. The fitting model approximates the data distribution with correlation coefficient equal to 0.63. Once again, this value can be assumed as satisfactory. The boxplots of the other two variables show a weaker correlation, in particular the one of $E_t$ which has been therefore omitted for brevity.

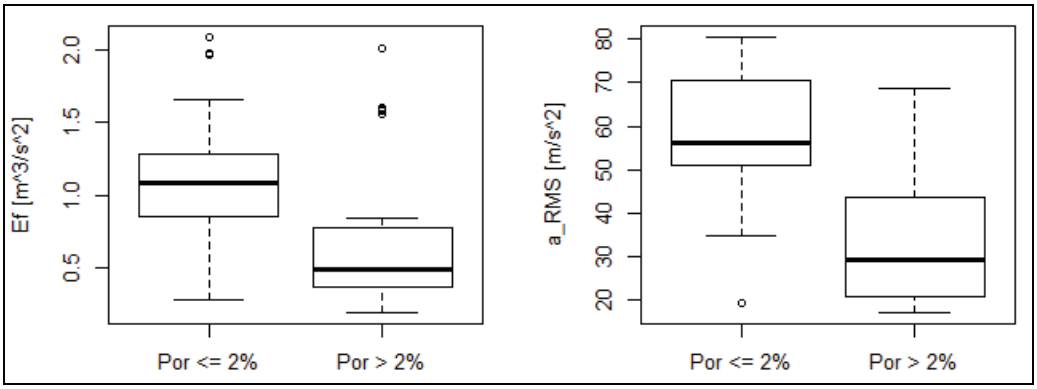


Figure 9: Boxplots of $E_f$ and $a_{RMS}$ parameters for the two groups of castings

The results of the exploratory analysis have been also confirmed through the application of the formal statistical methods performed through the confirmatory analysis. T-tests performed on $E_f$, $a_{RMS}$ and $E_t$ demonstrate that there is true difference in means between the sound and poor castings with 95 % confidence interval and the p-values are, respectively, $5.4e^{-4}$, $2.8e^{-08}$ and $8.5e^{-3}$.

Indeed, taking into account both $E_f$ and $E_t$ in a multivariable model allows improving the model correctness, by leading to a 0.73 correlation coefficient, which is once again highly satisfactory. The final model obtained is therefore the following one:

$$\log(Por) = \gamma_0 + \gamma_1 E_f + \gamma_2 a_{RMS} + \gamma_3 E_t \quad (7)$$

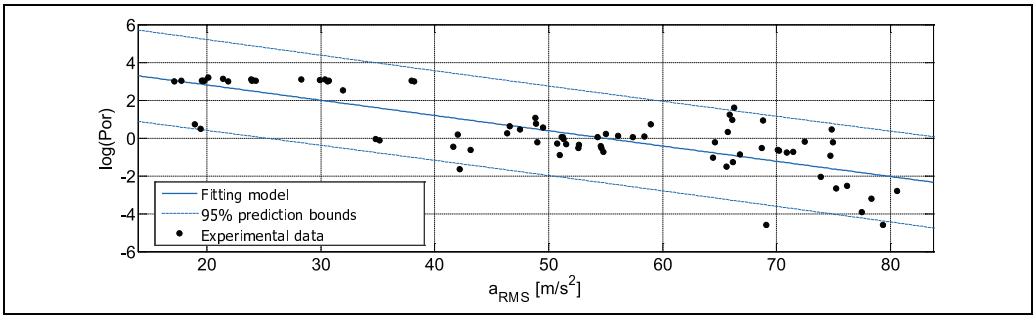


Figure 10: Plot of the natural logarithm of the porosity (*log(Por)*) against the $a_{RMS}$ ($R^2 = 0.63$)

The fitted coefficients for the alloy investigated are the following ones: $\gamma_0 = 1.94$; $\gamma_1 = 2.92$; $\gamma_2 = -0.13$ and $\gamma_3 = 0.26$. The diagnostic plots of this model are similar to those in figure 7, and show that this model fits, once again, the experimental data well. Since the results from exploratory and confirmatory analyses agree, the conclusions are reliable and convincing.

Just to allow a graphical representation, the model in equation 7 has been projected in the two dimensional set of the two independent variables $a_{RMS}$ and $E_f$, and then represented in figure 11. Also in this case, the plane of the regression model fits very effectively the experimental data.

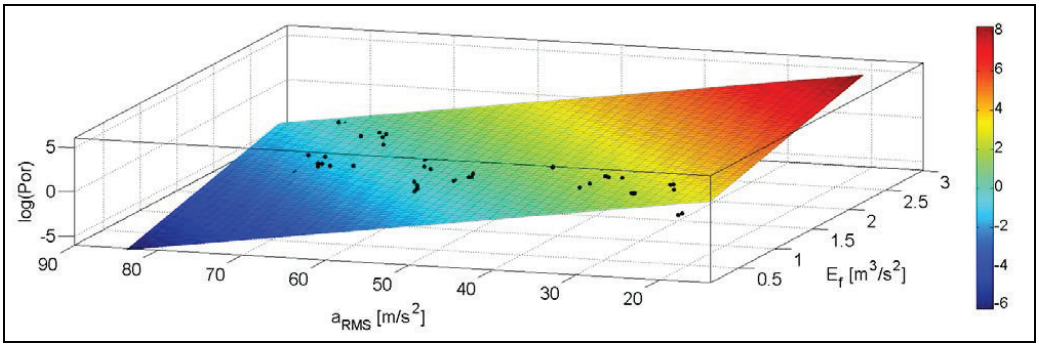


Figure 11: Three-dimensional projection of the model in equation (7)

# 4 Conclusions

The aim of the present work is to find the process parameters affecting the quality of high-pressure die-cast Al-Si alloys through a systematic experimental approach. Extraction of information from the plunger displacement and temperature signals constitutes a fundamental step for achieving this target. Since the traditional approach, consisting in the extraction of some instantaneous or maximum values of directly measured variables, has been proved to be too rough and ineffective, an approach based on some newly defined aggregate process parameters has been developed and pro-

posed. In particular, given the integral nature of the process, parameters accounting for the whole process or for some significant time intervals in terms of energy or mean values, have been computed. Some influential parameters has been identified and demonstrated through a large experimental campaign. Both the static mechanical properties and the porosity, measured in different regions of the castings, have been related to three parameters:

- $E_f$, representing both the energy associated to the flow forces, due to the contact between the melt and the die or some solid particles (such as oxides or inclusions), and the energy of the fluid pressure forces;
- $a_{RMS}$, which is the root mean square plunger acceleration and represents the average value of inertial forces related to the plunger motion;
- $E_t$, representing the thermal energy exchanged between the melt and the die in the solidification of the casting during the filling of the die.

The application of statistical concepts, methods and models has demonstrated that these novel process parameters allow explaining and forecasting the overall quality of the castings. In particular, an exponential model has been assumed for the mechanical behaviour, while a logarithmic one for the porosity. Both these models show $E_f$, $a_{RMS}$ and $E_t$ as predictors, and have good correlation coefficients, respectively, 0.68 and 0.73. Although these values do not approach the ideal target of 1, they are satisfactory, since they have been computed through a relevant number of samples, whose large size exacerbates the process variance, due to the unavoidable uncertainty and disturbance of the uncontrollable and casual exogenous factors usually affecting the high-pressure die-casting process.

## Acknowledgement

The Authors would like to acknowledge the financing of the European MUSIC Project (N. 314145), the contribution of the Partners EnginSoft, GTA, Saen, Electronics and of the DTG Collaborators Giulio Timelli, Giacomo Mazzacavallo, Enrico Della Rovere, Giorgio Kral, Eleonora Battaglia, Ilaria Tonello, Margherita Calcinai.

## References

[1] ADAMANE A.R., ARNBERG L., FIORESE E., TIMELLI G., BONOLLO F. (2015): Influence of injection parameters on the porosity and tensile properties of high-pressure die cast Al-Si alloys: a review – International Journal of Metalcasting, Vol. 9, N. 1: 43-53

[2] VINARCIK E.J. (2003): High integrity die casting processes – John Wiley & Sons, Inc., NY

[3] GHOMASHCHI M.R. (1995): High-pressure die casting: effect of fluid flow on the microstructure of LM24 die-casting alloy – Journal of Materials Processing Technology, Vol. 52, N. 2: 193-206

[4] GUNASEGARAM D.R., FINNIN B.R., POLIVKA F.B. (2007): Melt flow velocity in high pressure die casting: its effect on microstructure and mechanical properties in an Al-Si alloy – Materials Science and Technology, Vol. 23, N. 7: 847-856

[5] GUNASEGARAM D.R., GIVORD M., O'DONNELL R.G., FINNIN B.R. (2013): Improvements engineered in UTS and elongation of aluminum alloy high pressure die castings through the alteration of runner geometry and plunger velocity – Materials Science and Engineering A, Vol. 559: 276-286

[6] LUMLEY R., DEEVA N., GERSHENZON M. (2011): An evaluation of quality parameters for high pressure die castings – International Journal of Metalcasting/Summer: 37-56

[7] FIORESE E., TIMELLI G., KALLIEN L., LEIS W., TONN B. (2013): Hypereutectic Al alloys die-cast at semi-solid state – 8th international congress Aluminium 2000, Milano, Italy

[8] OTARAWANNA S., GOURLAY C.M., LAUKLI H.I., DAHLE A.K. (2009): Microstructure formation in AlSi4MgMn and AlMg5Si2Mn high-pressure die castings – Metallurgical and Materials Transactions A, Vol. 40A: 1645-1659

[9] OTARAWANNA S., LAUKLI H.I., GOURLAY C.M., DAHLE A.K. (2010): Feeding mechanisms in high-pressure die castings – Metallurgical and Materials Transactions A, Vol. 41: 1836-1846

[10] AMERICAN SOCIETY OF METALS (1991): Casting ASM Handbook, 15 – ASM International, Materials Park, Ohio

[11] MONTGOMERY D.C. (2012): Design and Analysis of Experiments – John Wiley & Sons, Inc., New York

[12] WU S., XIE L., ZHAO J., NAKAE H. (2008): Formation of non-dendritic microstructure of semi-solid aluminum alloy under vibration – Scripta Materialia, Vol. 58: 556-559

[13] PALOMBA I., RICHIEDEI D., TREVISANI A. (2014): Nonlinear kinematic state estimation in rigid-link multibody systems by spherical simplex sigma point unscented Kalman filters (ID 256) – Proceedings of 26th International Conference on Noise and Vibration Engineering (ISMA): 2899-2914, Leuven, Belgium

[14] MERRITT H.E. (1967): Hydraulic control systems – John Wiley & Sons, Inc., New York

[15] BOSCHETTI G., CARACCIOLO R., RICHIEDEI D., TREVISANI A. (2013): Model-based dynamic compensation of load cell response in weighting machines affected by environmental vibrations – Mechanical Systems and Signal Processing, Vol. 34: 116-130

[16] CAVALLINI A., MATTAROLO L. (1990): Termodinamica applicata – CLEUP

[17] MONTGOMERY D.C., RUNGER G.C. (1994): Applied statistics and probability for engineers – John Wiley & Sons, New York

[18] WU L. (2009): Mixed effects models for complex data – Chapman and Hall/CRC

[19] FARAWAY J.J (2004): Linear models with R – Chapman and Hall/CRC

# Analytical computation of the plunger kinematic parameters affecting quality in HPDC

Elena Fiorese, Dario Richiedei, Franco Bonollo

University of Padova, Department of Management and Engineering – DTG

Vicenza, Italy

Email: **fiorese@gest.unipd.it, dario.richiedei@unipd.it, bonollo@gest.unipd.it**

## Summary

High Pressure Die Casting (HPDC) is one of the most used process for manufacturing Al alloy components, thanks to its high production rate. Nevertheless, HPDC is considered a "defect generating process", due to high scrap percentage usually detected. Thus, the identification and the computation of the parameters affecting quality of castings is the challenge towards an efficient and effective production.

In their previous work, the Authors have found and statistically validated a novel parameter explaining and forecasting both static mechanical properties and porosity of the castings. Such a parameter, defined as the Root Mean Square value of the plunger acceleration in the second phase, represents a measure of the average force transmitted by the plunger to the melt, and has been proved to be more effective than speed in predicting the casting quality. In order to provide a tool for the practical use of this novel and effective approach, this work proposes an analytical method for computing this influential parameter, starting from the plunger displacement curve or just some notable points. The method formulation takes advantage of the analytical development of the typical motion primitive adopted for this kind of process. Hence, the optimization of the process can be achieved by selecting in advance the characteristic of the most suitable motion profile of the plunger that allows improving the quality of castings.

Besides the theoretical formulation, experimental validation is provided to demonstrate the correctness of the proposed parameter and of the analytical approach, as well as its ease of implementation that makes it suitable for being used in industrial manufacturing plants.

## Keywords

Al-Si alloy, High Pressure Die Casting, process parameters, plunger displacement curve, quality optimization

# 1. Introduction and state of the art

High Pressure Die Casting (HPDC) is a manufacturing process widely employed for the production of castings in large quantities and with high dimensional accuracy. In cold chamber HPDC, the molten metal poured into the shot sleeve is pushed into the die cavity through a servo-controlled hydraulic cylinder driving the plunger. The process of filling of the die cavity and the solidification of the casting is performed in three phases [1]. In the first phase (also called slow shot phase), the molten metal fills up the shot sleeve and the plunger begins to move at a low and usually constant speed. In the second phase (also called fast shot phase), the filling of the die cavity is performed at higher and time-varying velocity. Finally, once the die cavity is filled and the plunger has almost reached the final position, the intensification pressure is applied on the molten metal, to prevent the formation of shrinkage porosity and the expansion of entrapped air (third phase).

HPDC is still a "defect generating process", since an average of 5-10% scrap is typically manufactured by this process. Indeed, entrapment of oxides and gas during the filling phase might result in porosity and therefore deterioration of the overall casting quality, in the case of wrong selection of the process parameters or of bad design of the casting die [1].

Among the approaches to optimize HPDC, several works in the literature focus on the effect of the plunger motion, by analyzing the impact of some representative kinematic parameters of the plunger (such as speed) which are related to the motion of the servo-controlled cylinder. Some papers focus on the first phase, by investigating the effect of the plunger speed and the volume of trapped air [2-4]. Indeed, the amount of air trapped during the slow phase is a considerable contribution on the overall trapped air that causes porosity in the casting. Nevertheless, the sole investigation of the first phase neglects the positive effects due to the high forces exerted by the plunger to the melt in the second phase, which may produce for instance bubble collapsing and oxide fragmenting. This idea is consistent with those proposed in [5] and [6], which show that the tensile mechanical properties improve by increasing the gate velocity in the second phase, due to porosity reduction.

This brief review of the state of the art shows that some correlations between process parameters and quality of castings already exist in the previous literature, although the available results are sometimes fragmented or conflicting. As a matter of the fact, these works usually take into account instantaneous values of the speed, such as just the maximum value. In contrast, they neglect the analysis of the time history of the speed and of its rate of variation. The definition of reliable criteria for tuning the injection parameters, in order to obtain sound and reliable castings, is therefore still an open and challenging issue.

Since the final outcome of HPDC process is expected to depend on the whole process (or on some relevant time intervals) rather than just some instants, the use of a parameter taken from the time history of the plunger displacement curve is more reasonable than assuming some characteristic values of just some instants. In mathematical terms, since the filling of the die cavity and the solidification of the casting are integral processes, any parameter suitable for explaining and forecasting the casting quality should have a similar integral mathematical nature. In this way, the parameters would allow representing the time history of the phenomenon over some proper intervals. This is, basically, the logical justification beneath the use of parameters obtained by integrating the plunger motion time histories, such as energy or average values. By taking advantage of this idea, in their recent work [7], the Authors have proposed and validated with experimental activity and thorough statistical analysis the use of some novel parameters, based on numerically processing and integration of some measurements recorded during the process. Their use, through non-linear fitting models, has allowed explaining and forecasting effectively both the static mechanical properties and the porosity of the castings. Among these parameters, the most influential one has been proved to be

the Root Mean Square (RMS) plunger acceleration in the second phase, denoted $a_{RMS}$ and defined as follows:

$$a_{RMS} = \sqrt{\frac{\int_{t_{SW}}^{T} \ddot{x}(t)^2 dt}{T_2}} \quad (1)$$

In Equation (1), $t$ is the time, $x(t)$ denotes the plunger displacement (and hence $\ddot{x}$ $(t)$the acceleration), $T_2$ is the duration of phase 2, which begins at $t = t_{SW}$ (the so-called switching time) and ends at $t = T$ (i.e. the motion time). This parameter represents the average value of the inertial forces of the plunger over the interval of integration (for a unitary mass). In practice, by expressing the Newtonian equilibrium of the plunger, it is evident that acceleration is a measure of the force transmitted to the melt by the plunger during the second phase, which has been often recognized in the literature as the phase most affecting the final outcome. The higher the RMS acceleration, the lower is the porosity and the higher is the tensile strength, since higher accelerations mean higher forces that strive against porosity and oxides.

In the previous work [7], the use of this parameter has been firstly proposed and then applied by computing acceleration through numerical derivation of the measured plunger position. A different approach is instead proposed in this work, where an analytical method for computing this parameter is proposed starting from some notable points extracted from the plunger displacement curve.

As a matter of the fact, the availability of some algebraic formulas will allow the straightforward method application in optimizing the HPDC process by selecting the most suitable plunger motion profile. The method here proposed is therefore well suited for being used also by practitioners in the manufacturing field. Additionally, these analytical equations allow better understanding how other well-known process parameters usually adopted by practitioners, such as speed and time, contribute to the final outcome.

Besides the theoretical explanation of the method, the paper proposes the experimental application and assessment of the method. Compared with the previous work [7], different alloy, die and injection machine are employed, to provide further experimental evidence of the correctness of the suggested parameter.

## 2. Analytical computation of the RMS acceleration

In order to obtain an analytical expression of the RMS acceleration in the second phase, the typical HPDC cycle is considered, which includes the constant-speed phase (denoted phase 1) and the high-speed phase (denoted phase 2). Additionally, the initial transient phase to reach the constant speed is accounted for, and denoted phase 0.

The following motion primitives are assumed for the displacement curve: a parabolic blend (i.e. a speed ramp) in the phase 0, a ramp (i.e. constant speed) in the phase 1, and finally a 5$^{th}$ degree polynomial in the phase 2. A sample curve is also shown in Figure 1. Several considerations justify using a 5$^{th}$ degree polynomial displacement curve. First of all, it is in practice frequently adopted in HDPC processes. Secondly, it represents a motion profile that is feasible and consistent with the physic nature of the system, with continuous speed and acceleration curves. Finally, 5$^{th}$ degree polynomial displacement curve can also effectively approximate other motion profiles.

This cycle should be regarded as the “standard cycle”, which represents the vast majority of the HDPC processes. In the case of small modifications of the cycle occur, the proposed approach keeps on representing correctly the relative ranking of the RMS acceleration between different sets of

process parameters, with just an approximation of the absolute magnitude. Nonetheless, the analytical approach herein proposed can be easily developed for arbitrary processes, once that their motion primitives are known. The method is hence a general approach.

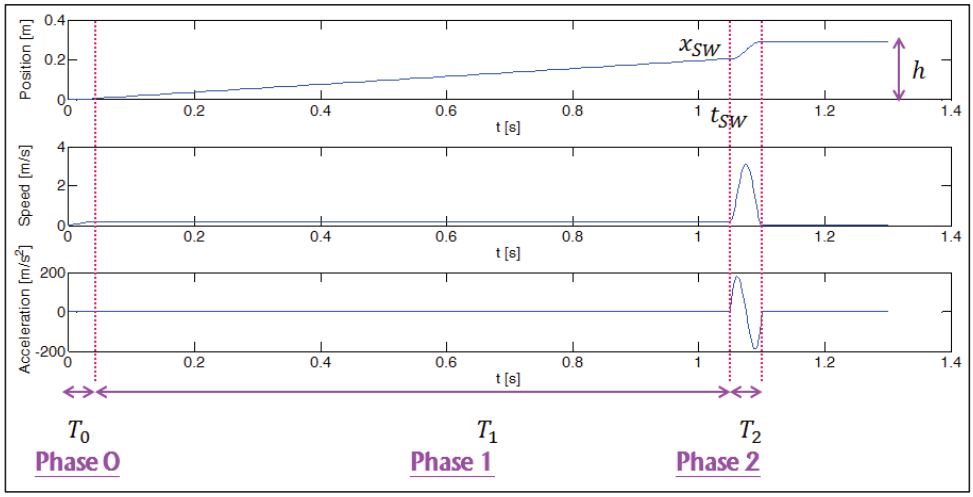


*Figure 1: Example of position, speed and acceleration of the plunger during the process*

## 2.1. Parameter computation

The analytical integration of the squared acceleration obtained by Equation (1) and the algebraic manipulation of the results, lead to two equivalent formulations of $a_{RMS}$.

The first formulation highlights the absolute value of the duration of the three phases, namely $T_0, T_1, T_2$ on $a_{RMS}$ (where $v_1$ is the constant speed in phase 1):

$$a_{RMS} = \sqrt{\frac{30(T_0 v_1 + 2T_1 v_1 - 2h)^2}{7T_2^4} + \frac{60v_1(T_0 v_1 + 2T_1 v_1 - 2h)}{7T_2^3} + \frac{192v_1^2}{35T_2^2}} \quad (2)$$

A different formulation can be obtained by making explicit the overall plunger displacement $h$, and the switching position $x_{SW}$, as it is often done in foundries:

$$a_{RMS} = \sqrt{\frac{120(h - x_{SW})^2}{7T_2^4} - \frac{120v_1(h - x_{SW})}{7T_2^3} + \frac{192v_1^2}{35T_2^2}} \quad (3)$$

On the one hand, these two analytical equations are a powerful and practical tool for optimizing the process by choosing in advance the best plunger motion parameters to improve the quality of castings. On the other, they allow better understanding how the parameter $a_{RMS}$, calculated numerically in the previous work [7], is related in a complicate and non-linear way to well-known parameters such as $v_1, x_{SW}, T_2$, usually adopted in foundries by practitioners. Finally, analytical equations allow easily predicting $a_{RMS}$ and therefore the casting quality by reconstructing plunger motion curves from some notable points or simple information, without the need of additional sensors recording the displacement time history.

### 2.2. Formula explanation and sensitivity analysis

Sensitivity analysis of the equation allows better understanding the complicate relation and proves that just one parameter is not sufficient to explain the casting quality. This fact explains the presence of conflicting results often proposed in literature when just one parameter is accounted for, as discussed in the Introduction.

In the following subsections a sensitivity analysis is proposed by discussing the impact of the modification of one parameter in the resulting RMS acceleration. Clearly, the modification of just one or two parameters is not sufficient to explain the final outcome, since the mutual effect of all the parameters should be accounted for. Indeed, different combinations of all these parameters, with different values of each single parameter, may lead to the same casting quality since they lead to the same value of $a_{RMS}$.

#### 2.2.1. Effect of the first phase speed and duration

The analysis of Equations (2) and (3), and of the partial derivative $da_{RMS}/dv_1$ reveals that $a_{RMS}$ decreases by increasing $v_1$, with a quasi-constant rate (if all the other parameters are unchanged). This is due to the reduced residual space to cover in the phase 2, which imposes smaller acceleration.

The same reason justifies the similar linear effect of $T_1$ and of $x_{SW}$. Indeed $a_{RMS}$ decreases linearly by increasing either the duration of the first phase or the switching position between phases 1 and 2.

#### 2.2.2. Effect of the overall motion time

Reducing the motion time $T$, by keeping the same partitioning between the three phases (i.e. the same ratios $T_0/T_2, T_1/T_2$), makes $a_{RMS}$ increasing almost quadratically, as it can be noticed by developing the partial derivative $da_{RMS}/dT$.

#### 2.2.3. Effect of the second phase duration

The study of the partial derivative $da_{RMS}/dT_2$ shows the effect of a variation of the duration of the second phase. It clearly shows that $a_{RMS}$ increases quadratically by decreasing $T_2$, and by keeping fixed the other parameters. This is the parameter that mainly affect $a_{RMS}$, and hence should be properly selected in order to improve the quality of castings. On the other hand, the duration of the second phase is limited by a lower bound, which hence sets an upper bound of the achievable acceleration, due to acceleration (force) and speed (flow) constraints of the hydraulic injection machine [8].

## 3. Method experimental application

### 3.1. Experiment description

In the present work, an AlSi12(Fe) Sr-modified alloy was cast, corresponding to the EN AC-44300 modified aluminium alloy. The die adopted is shown in Figure 2, and it is the one developed within the frame of NADIA project (New Automotive components Designed for and manufactured by Intelligent processing of light Alloys, EU IPs-SMEs, Contract n. 026563-2, 2006-2010). Such a die has been recently included in CEN/TR 16748:2014 [9] as reference die, since it has been carefully designed and optimized to maximize the process quality by reducing the scrap percentage, and hence to reduce variance of the casting mechanical properties over a wide range of process parameters.

Castings were manufactured in accordance with a planned Design of Experiments, based on ensuring a wide range of feasible values of the parameter $a_{RMS}$ from about 20 to 180 m/s$^2$, by changing the

plunger velocity of the first phase (i.e. $v_1$), the maximum speed in the second phase (called $v_2$) and the switching position between the two phases (i.e. $x_{SW}$) within a specific range of variation (see Table 1). Exactly 6 samples were manufactured for each combination of parameters.

Tensile test bars with circular cross section, 6 mm diameter and 32.5 mm gauge length were extracted from the castings and tested without machining, by means of a tensile testing machine.

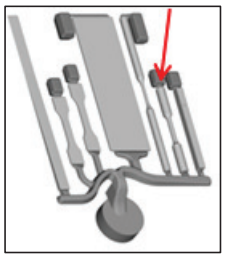

*Figure 2: Geometry of the casting manufactured during the experimental campaign*

| Factor | Low level | High level | Discretization |
|---|---|---|---|
| $v_1$, first phase speed (m/s) | 0.08 | 0.42 | 0.17 |
| $v_2$, second phase maximum speed (m/s) | 2.00 | 3.20 | 0.60 |
| $x_{SW}$, switching position (mm) | 215 | 230 | 15 |

*Table 1: Control factors with lower and upper levels of observation, and discretization values*

## 3.2. Results of the method application

The computation of the RMS acceleration has been performed on the basis of the actual values provided in the control and interface panel of the machine (i.e. $v_1, x_{SW}, T_2$) and on the basis of the Equation (3) proposed. In accordance with the model described in [7], the following relation has been assumed to fit the experimental data:

$$\sigma = \alpha + \beta \, log(a_{RMS}) \tag{4}$$

where $\sigma$ represents the measured tensile properties (i.e. the ultimate and the yield strengths), while $\alpha$ and $\beta$ are two scalar coefficients computed through data fitting. The use of the natural logarithm is justified by the decreasing rate of growth of $\sigma$ for increasing accelerations, compared with that of a linear model.

The results of the application of the least-squares fitting model are shown in Figures 3 and 4 for, respectively, the yield stress and the ultimate tensile stress of the same specimens (the central lines are the fitting models, while the upper and lower bound lines are the 95% confidence intervals). The fitting models for these two casting properties approximate the data distribution with $R^2$ correlation coefficients equal to 0.65 and 0.58, respectively, as it can be expected by the presence of evident trends in the two figures. Both these coefficients are highly satisfactory, by considering the relevant number of samples and the unavoidable presence of uncertainty. These results confirm that the RMS acceleration in the second phase, computed through the analytical model proposed in this work, allows explaining and predicting effectively the static mechanical properties of the castings.

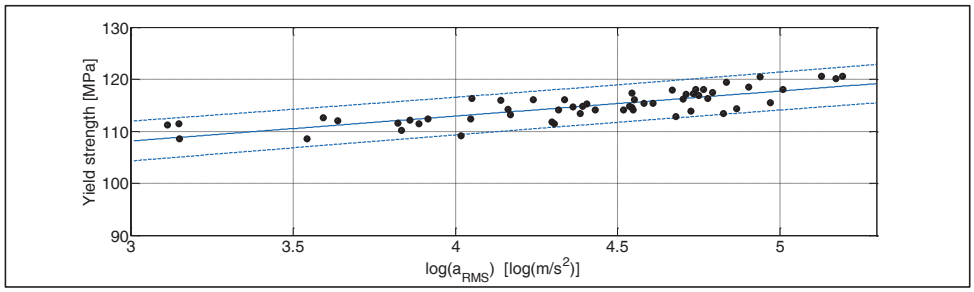


*Figure 3: Correlation between process parameter and yield strength of the castings*

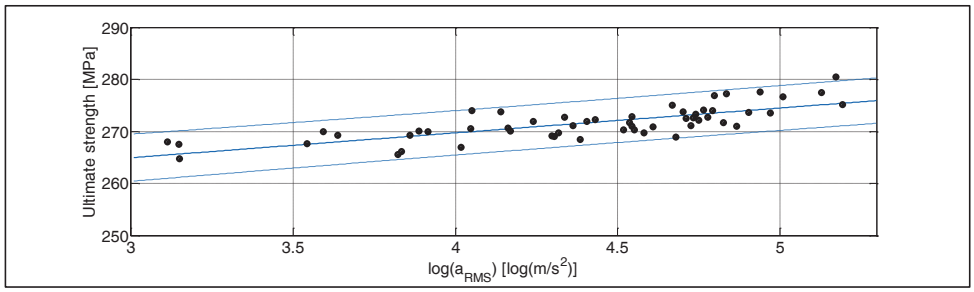


*Figure 4: Correlation between process parameter and ultimate strength of the castings*

## 4. Conclusions

This paper proposes and validates experimentally a method for explaining and predicting the tensile properties of die castings as a function of the time history of the plunger displacement curve, thus overcoming the limitations of the traditional approaches based on the extraction of some instantaneous values of directly measured process parameters.

Besides showing the correctness of the use of the RMS acceleration in the second phase to represent the static mechanical properties, some analytical formuations of such an effective parameter are proposed. On the one hand, these equations explain the relation between the RMS acceleration and the instantaneous or constant parameters usually adopted by practitioners in foundries. On the other, the suggested equations are a straightforward tool to optimize the HPDC process by selecting, in advance, the proper plunger motion profile, that assures higher accelerations and therefore higher mechanical strength.

The experimental results reported corroborate the effectiveness of the proposed method. Compared with the previous work of the Authors, different alloy, die and injection machine are employed, to provide further experimental evidence of the correctness of the suggested parameter.

Future investigations will be devoted to include explicitly some feasibility constraints within the selection of the suitable plunger motion profile.

## Acknowledgements

The Authors would like to acknowledge the financing of the European MUSIC Project (MUlti-layers control & cognitive System to drive metal and plastic production line for Injected Components, N. 314145). Moreover, the Authors would like to acknowledge the contribution to the experimental activity given by Saen, Raffmetal, and the DTG Collaborators Eleonora Battaglia and Giacomo Mazzacavallo.

## References

[1] Adamane A.R., Arnberg L., Fiorese E., Timelli G., Bonollo F.: “Influence of injection parameters on the porosity and tensile properties of high-pressure die cast Al-Si alloys: a review”, International Journal of Metalcasting, Vol. 9, No. 1, 2015, pp. 43-53

[2] Garber L.W.: “Theoretical analysis and experimental observation of air entrapment during cold chamber filling”, Die Casting Engineer, Vol. 26, No. 3, 1982, pp. 14-22

[3] Zamora R., Faura F., López J., Hernández J.: “Experimental verification of numerical predictions for the optimum plunger speed in the slow phase of a high-pressure die casting machine”, International Journal of Advanced Manufacturing Technology, Vol. 33, 2007, pp. 266-276

[4] Nikroo A.J., Akhlaghi M., Najafabadi M.A.: “Simulation and analysis of flow in the injection chamber of die casting machine during the slow shot phase”, International Journal of Advanced Manufacturing Technology, Vol. 41, 2009, pp. 31-41

[5] Gunasegaram D.R., Finnin B.R., Polivka F.B.: “Melt flow velocity in high pressure die casting: its effect on microstructure and mechanical properties in an Al–Si alloy”, Materials Science and Technology, Vol. 23, No. 7, 2007, pp. 847-856

[6] Lumley R., Deeva N., Gershenzon M.: “An evaluation of quality parameters for high pressure die castings”, International Journal of Metalcasting/Summer, 2011, pp. 37-56

[7] Fiorese E., Bonollo F.: “Process parameters affecting quality of high-pressure die-cast Al-Si alloy”, Proceedings of EMC 2015 (European Metallurgical Conference), Düsseldorf, Germany, Vol. 1 2015, pp. 261-276. ISBN 978-3-940276-61-2

[8] Richiedei D.: “Synchronous motion control of dual-cylinder electrohydraulic actuators through a non-time based scheme”, Journal of Control Engineering and Applied Informatics, Vol.14, No.4, 2012, pp. 80-89

[9] CEN/TR 16748: “Aluminium and aluminium alloys – Mechanical potential of Al-Si alloys for high pressure, low pressure and gravity die casting”, 2014, pp. 1-21

# *Acknowledgements*

*The Author is immensely grateful to the following peoples and would like to acknowledge their significant contribution to the core of this Ph. D. Thesis:*

- Franco Bonollo (Department of Management and Engineering, University of Padova, Italy) for his valuable comments and precious suggestions to the improvement of the overall quality of this work;
- Giacomo Mazzacavallo, Enrico Della Rovere and Eleonora Battaglia (Department of Management and Engineering, University of Padova, Italy) for their kind contribution to the experimental activity and laboratory support;
- Dario Richiedei (Department of Management and Engineering, University of Padova, Italy) for his significant contribution to the analytical modelling and inter-disciplinary view;
- Lothar Kallien and Martina Winkler (Aalen University of Applied Sciences, Aalen, Germany) for having readily collaborated in the experimental activity carried out in Germany.

*The Author would like to acknowledge the following peoples for their contribution to the drawing up of the cited CEN Technical Reports:*

- Giulio Timelli (Department of Management and Engineering, University of Padova, Italy) also for his kind support during the Bachelor/Master Theses, which were preliminary for the Ph. D. programme;
- Giorgio Kral (Department of Management and Engineering, University of Padova, Italy) for his support during the survey addressed to the European foundries;
- Lars Arnberg and Anilchandra Adamane (Norwegian University of Science and Technology, Trondheim, Norway) for having kindly guested the Author during her staying in Norway.

*The Author would like to acknowledge all the Partners and the financing support of the European Projects for giving the opportunity to develop this work:*

- MUSIC (MUlti-layers control & cognitive System to drive metal and plastic production line for Injected Components, N. 314145);
- StaCast (New quality and design STAndards for aluminium alloys CAST products, N. 319188).

*Finally, I would like to thanks my family, friends, research group, colleagues and all the affectionate peoples for their affective and moral support during this challenging path towards the sun behind hill.*